frontiers | Research Topics

Exploiting genetics and genomics to improve the understanding of eye diseases

Edited by
Denis Plotnikov, Jeremy Guggenheim
and Xiaoyi Raymond Gao

Published in
Frontiers in Genetics
Frontiers in Pediatrics

ISSN 1664-8714
ISBN 978-2-8325-3838-8
DOI 10.3389/978-2-8325-3838-8

About Frontiers

Frontiers is more than just an open access publisher of scholarly articles: it is a pioneering approach to the world of academia, radically improving the way scholarly research is managed. The grand vision of Frontiers is a world where all people have an equal opportunity to seek, share and generate knowledge. Frontiers provides immediate and permanent online open access to all its publications, but this alone is not enough to realize our grand goals.

Frontiers journal series

The Frontiers journal series is a multi-tier and interdisciplinary set of open-access, online journals, promising a paradigm shift from the current review, selection and dissemination processes in academic publishing. All Frontiers journals are driven by researchers for researchers; therefore, they constitute a service to the scholarly community. At the same time, the *Frontiers journal series* operates on a revolutionary invention, the tiered publishing system, initially addressing specific communities of scholars, and gradually climbing up to broader public understanding, thus serving the interests of the lay society, too.

Dedication to quality

Each Frontiers article is a landmark of the highest quality, thanks to genuinely collaborative interactions between authors and review editors, who include some of the world's best academicians. Research must be certified by peers before entering a stream of knowledge that may eventually reach the public - and shape society; therefore, Frontiers only applies the most rigorous and unbiased reviews. Frontiers revolutionizes research publishing by freely delivering the most outstanding research, evaluated with no bias from both the academic and social point of view. By applying the most advanced information technologies, Frontiers is catapulting scholarly publishing into a new generation.

What are Frontiers Research Topics?

Frontiers Research Topics are very popular trademarks of the *Frontiers journals series*: they are collections of at least ten articles, all centered on a particular subject. With their unique mix of varied contributions from Original Research to Review Articles, Frontiers Research Topics unify the most influential researchers, the latest key findings and historical advances in a hot research area.

Find out more on how to host your own Frontiers Research Topic or contribute to one as an author by contacting the Frontiers editorial office: frontiersin.org/about/contact

Exploiting genetics and genomics to improve the understanding of eye diseases

Topic editors

Denis Plotnikov — Kazan State Medical University, Russia

Jeremy Guggenheim — Cardiff University, United Kingdom

Xiaoyi Raymond Gao — The Ohio State University, United States

Citation

Plotnikov, D., Guggenheim, J., Gao, X. R., eds. (2023). *Exploiting genetics and genomics to improve the understanding of eye diseases*. Lausanne: Frontiers Media SA. doi: 10.3389/978-2-8325-3838-8

Table of contents

frontiers | Frontiers in Genetics

TYPE Editorial
PUBLISHED 18 October 2023
DOI 10.3389/fgene.2023.1308071

OPEN ACCESS

EDITED AND REVIEWED BY
Jordi Pérez-Tur,
Spanish National Research Council (CSIC), Spain

*CORRESPONDENCE
Denis Plotnikov,
denis.plotnikov@kazangmu.ru

RECEIVED 05 October 2023
ACCEPTED 10 October 2023
PUBLISHED 18 October 2023

CITATION
Plotnikov D, Guggenheim JA and Gao XR (2023), Editorial: Exploiting genetics and genomics to improve the understanding of eye diseases.
Front. Genet. 14:1308071.
doi: 10.3389/fgene.2023.1308071

Editorial: Exploiting genetics and genomics to improve the understanding of eye diseases

Denis Plotnikov[1]*, Jeremy A. Guggenheim[2] and Xiaoyi Raymond Gao[3,4,5]

[1]Central Research Laboratory, Kazan State Medical University, Kazan, Russia, [2]School of Optometry and Vision Sciences, Cardiff University, Cardiff, United Kingdom, [3]Department of Ophthalmology and Visual Sciences, The Ohio State University, Columbus, OH, United States, [4]Department of Biomedical Informatics, The Ohio State University, Columbus, OH, United States, [5]Division of Human Genetics, The Ohio State University, Columbus, OH, United States

KEYWORDS

genetics, genomics, GWAS, ophthalmology, genes

Editorial on the Research Topic
Exploiting genetics and genomics to improve the understanding of eye diseases

Eye diseases impose a significant global health burden, affecting millions across diverse demographics. Common conditions such as age-related macular degeneration, glaucoma, and diabetic retinopathy, along with less prevalent hereditary disorders like retinitis pigmentosa and congenital cataracts, impair vision and impact quality of life and productivity. Advances in genetics and genomics have transformed the landscape of eye disease research. Traditional diagnostic methods and treatments are being augmented, and in some cases, replaced, by cutting-edge genomic technologies. Genomic research has not only facilitated the identification of disease-associated genetic variants but has also paved the way for innovative therapeutic approaches, such as gene editing and gene therapies. This Research Topic provides an insight into how genetics and genomics are reshaping the field of ophthalmology, offering new avenues for understanding, diagnosing, and treating eye diseases.

The articles in this Research Topic can be broadly classified in following groups: A review article summarizing recent progress in genome-wide association studies of intraocular pressure, two high-quality case reports, and a series of cutting-edge research articles covering a wide range of topics.

Glaucoma remains a leading cause of global irreversible blindness. In the review article by Gao et al. the focus was on intraocular pressure (IOP), which is the only known modifiable risk factor for glaucoma. Genome-wide association studies (GWASs), primarily conducted in European and Asian ancestries, have revealed over 190 genetic loci associated with IOP. Most of these loci were identified through common variants. These findings have led to the development of polygenic scores (PGS) for predicting IOP and glaucoma risk. Recent large-scale exome-wide association studies (ExWAS) have successfully identified rare variants in 40 novel genes, some being noteworthy drug targets for clinical treatment. However, since the majority of GWASs have been conducted in individuals of European descent, limited information exists currently about underrepresented populations such as Latinos and Africans. Current PGSs perform very well in European populations, but the PGS

"portability gap" has the potential to create or worsen existing health disparities. Efforts to increase diversity in GWASs, such as the All of Us research program in the United States, aim to address this imbalance. The future of IOP GWASs may involve whole-genome sequencing approaches, aided by advancements in artificial intelligence, leading to personalized genetic applications in prevention, diagnosis, and treatment across diverse patient backgrounds.

In the first of the two case reports in this Research Topic, Chen and Lu report on the AB variant GM2 gangliosidosis, an exceptionally rare autosomal recessive lysosomal storage disease, described in a 7-month-old infant from China. The child presented with nystagmus, and ophthalmic examinations revealed a distinctive cherry-red spot surrounded by a whitish infiltrate around the macula. Optical coherence tomography (OCT) revealed abnormal thickening and increased reflectivity in inner retinal layers. Genetic testing confirmed a homozygous deletion in the *GM2A* gene's exon 2, leading to the diagnosis of AB variant GM2 gangliosidosis. This case, the first reported in China, underscores the pivotal role of ophthalmic examinations in early disease detection. The cherry-red spots observed were distinct from those caused by central retinal artery occlusion and were accompanied by unique OCT findings, providing valuable clinical insights into this rare disease's ocular manifestations. In the case report by Peng et al., a novel frameshift variant (c.394delG, p.V132Sfs*15) within the *CRYGC* gene was identified in a patient with congenital cataract, contributing to our understanding of the genetic basis of congenital cataracts in the Chinese population. The research utilized whole-exome sequencing to pinpoint the genetic defect in a patient lacking a family history of the condition. This rapid and accurate genetic diagnosis proved invaluable in guiding clinical decisions and ensuring timely intervention, highlighting the importance of genetic testing in pediatric cases. The identified variant disrupted a critical region of the *CRYGC* gene, shedding light on the structural changes responsible for congenital cataracts. This study adds to the growing body of knowledge about the genetic diversity underlying cataract disorders and emphasizes the significance of precise genetic diagnoses in pediatric ophthalmology.

Two brief research reports in this Research Topic highlighted the role, first, of DNA methylation in microRNA (miRNA) genes in patients with high myopia (HM), and, second, the role of the polymorphisms rs2472493 in *ABCA1* and rs7636836 in *FNDC3B* in pseudoexfoliation glaucoma (PXG) and primary angle-closure glaucoma (PACG). Swierkowska et al. observed specific methylation patterns in miRNA genes associated with HM. The study highlighted differential methylation levels in CG dinucleotides located in the promoter regions of several miRNA genes, including *MIR3621*, *MIR34C*, *MIR423* (with increased methylation) and *MIR1178*, *MIRLET7A2*, *MIR885*, *MIR548I3*, *MIR6854*, *MIR675*, *MIRLET7C*, *MIR99A* (with reduced methylation). These findings implicate potential disruption in the regulation of miRNA expression in the pathogenesis of HM. Additionally, the study linked these differentially-methylated miRNA genes to target genes associated with eye-related biological pathways, providing insights into the molecular mechanisms underlying HM. While the study was conducted on blood samples, it offers promising directions for further research into non-invasive diagnostic biomarkers for HM. Kondkar et al. reported an in-depth analysis of two gene polymorphisms, rs2472493 in *ABCA1* and rs7636836 in *FNDC3B*, previously linked to primary open-angle glaucoma (POAG). The study included 442 subjects, comprising healthy controls, and patients with PACG or PXG. While overall associations were not significant, the rs7636836[T] allele was associated with an increased risk of PXG in males. Additionally, a combination of alleles (G-T) was associated with increased PACG risk. Further research in larger, more diverse cohorts would help to clarify the clinical impact of these findings and pave the way for additional gene-gene and gene-environment interaction analyses in patients with glaucoma.

Eight original research papers employed diverse methods to offer new insights into the development of different eye conditions. A GWAS of color vision defects in isolated Silk Road communities, conducted by Nardone et al., identified potential genetic associations for both Deutan-Protan (DP) and Tritan (TR) traits. For DP, the genes *PIWIL4*, *MBD2*, and *NTN1* were highlighted as candidates linked to retinal health and visual signal transmission. TR traits were associated with the *VPS54*, *IQGAP1*, *NMB*, and *MC5R* genes, highlighting potential roles in RPE regulation, cone imbalances, and lacrimal gland function. In their extensive study, Jiang et al. conducted a GWAS in a sample of 19,420 adults from diverse ethnic backgrounds to explore the genetic underpinnings of ocular axial length (AL), a clinical feature of myopia. They identified 16 genomic loci associated with AL, including five novel discoveries. The loci associated with AL were also significantly associated with spherical equivalent refractive error (SER) and myopia; moreover, genetic correlations between AL, SER, and myopia were found, suggesting shared genetic etiology. The study highlighted potential candidate genes such as *SLC25A12*, *BMP3*, *RGR*, *RBFOX1*, and *MYO5B*, shedding light on their roles in visual function and eye development. The research also unveiled a genome-wide association at the *PRSS56* gene locus, a gene associated with ocular axial growth, in individuals of European ancestry. While the study focused only on common variants, it provided valuable data for elucidating the role of axial elongation in myopia development.

Yu et al. reported a detailed study of patients with congenital insensitivity to pain (CIP) associated with *PRDM12* mutations. They observed a range of manifestations, including pain insensitivity, self-mutilation, facial and limb defects, and recurrent infections. Remarkably, nearly every patient exhibited some degree of corneal injury, highlighting the significance of monitoring eye symptoms. The importance of early diagnosis and treatment were stressed, especially considering the challenge of managing corneal issues in CIP patients. While corneal transplantation is a potential treatment, it necessitates careful evaluation due to patients' overall health and possible post-surgical complications. This research underscores the critical need for attentive eye care and customized treatments for individuals affected by *PRDM12*-related CIP. In their study, Chen et al. investigated the molecular basis of oculocutaneous albinism (OCA) in two families, aiming to facilitate prenatal diagnosis. They identified distinct mutations in the *TYR*, *TYRP1*, and *SLC45A2* genes. In one family, a patient exhibited OCA2 with Prader-Willi Syndrome due to a novel paternal deletion and a pathogenic mutation in the maternal chromosome. Prenatal diagnosis for this family revealed a carrier fetus. In another family, a patient was diagnosed with OCA2 and

Angelman Syndrome due to a maternal deletion and a novel pathogenic mutation in the paternal chromosome. These findings expand our understanding of OCA-related mutations, emphasizing the importance of precise molecular classification for genetic counseling and early intervention in these cases.

Zhou et al. examined the pathogenic effects of *MYOC* gene mutations in patients with POAG. By analyzing specific myocilin (*MYOC*) variants, the research revealed genotype-phenotype links relating to the structure and function of this critical protein, including its secretion, subcellular localization, and potential role in autophagy and oxidative stress. The study found that secretion defects, often related to steric clash alterations, were closely linked to the pathogenicity of *MYOC* variants. Mutant forms of myocilin with reduced levels of secretion were found to accumulate in the endoplasmic reticulum, disrupting autophagy and increasing oxidative stress. The research provided an exciting example of how human genetics can lead to improved understanding of disease mechanisms, here shedding light on the pathophysiology of POAG.

A Chinese family with congenital retinoschisis was investigated using whole-exome sequencing and comprehensive clinical examination by Wang et al. A novel splice site mutation (RS1.c.53-1G>A) was identified in the *RS1* gene, suggesting potential for gene therapy and enhancing our understanding of this highly debilitating X-linked retinal disorder. Meanwhile, Tan et al. investigated two Chinese pedigrees with pigmentary glaucoma (PG). This revealed novel, compound heterozygous variants in the *CPAMD8* gene. The variants were classified as damaging or deleterious based on bioinformatics analysis. The autosomal recessive nature of disease transmission in these pedigrees and the strong evidence for a role of *CPAMD8* variants in pigment dispersion syndrome/pigmentary glaucoma were notable findings. Additionally, the study emphasized the need for further research to explore the role of *CPAMD8* in iris stromal abnormalities and immunological factors in the development of pigmentary glaucoma.

In a tour-de-force multiomics study, Jiang et al. explored the genetic determinants of corneal resistance factor (CRF), a key index of corneal biomechanics that is relevant to diseases including keratoconus and to ocular surgical procedures such as corneal transplantation. The researchers began by fine-mapping GWAS loci for CRF, which yielded credible sets comprising 181 signals. Leveraging gene expression data for non-eye tissues from the Genotype-Tissue Expression (GTEx) portal and single cell transcriptomics datasets from cornea, limbus and conjunctiva, the authors found that more than 25% of CRF and GTEx signals were shared. As well as indicating the potential involvement of corneal stromal cells and limbal cells, the research strongly suggested key roles for genes impacting extracellular matrix composition, mechanosensing, and signaling. Colocalization analysis of GWAS signals for CRF and keratoconus further strengthened the clinical relevance of the findings. This work emphasized the importance of considering the tissue-specific context in which genetic variants exert their effects, elegantly demonstrating how this approach can uncover potential therapeutic targets for corneal disorders.

Author contributions

DP: Writing–original draft. JG: Writing–review and editing. XG: Writing–review and editing.

Conflict of interest

The authors declare that the research was conducted in the absence of any commercial or financial relationships that could be construed as a potential conflict of interest.

Publisher's note

frontiers | Frontiers in Genetics

CASE REPORT
published: 27 May 2022
doi: 10.3389/fgene.2022.866246

Case Report: A *de novo* Variant of *CRYGC* Gene Associated With Congenital Cataract and Microphthalmia

Yu Peng[1†], *Yu Zheng*[2†], *Zifeng Deng*[3], *Shuju Zhang*[2], *Yilan Tan*[3], *Zhengmao Hu*[4], *Lijuan Tao*[3*] *and Yulin Luo*[3*]

[1]Department of Ophthalmology & Pediatrics Research Institute of Hunan Province, Hunan Children's Hospital, Changsha, China, [2]Pediatrics Research Institute of Hunan Province, Hunan Children's Hospital, Changsha, China, [3]Department of Ophthalmology, Hunan Children's Hospital, Changsha, China, [4]Center for Medical Genetics & Hunan Key Laboratory of Medical Genetics, School of Life Sciences, Central South University, Changsha, China

OPEN ACCESS

Edited by:
Zi-Bing Jin,
Capital Medical University, China

Reviewed by:
Abhinav Jain,
Council of Scientific and Industrial Research (CSIR), India
Emilia Severin,
Carol Davila University of Medicine and Pharmacy, Romania

***Correspondence:**
Yulin Luo
luoyulin2000@126.com
Lijuan Tao
hnetyy1221@163.com

[†]*These authors have contributed equally to this work*

Specialty section:
This article was submitted to Genetics of Common and Rare Diseases, a section of the journal Frontiers in Genetics

Received: *31 January 2022*
Accepted: *11 May 2022*
Published: *27 May 2022*

Citation:
Peng Y, Zheng Y, Deng Z, Zhang S, Tan Y, Hu Z, Tao L and Luo Y (2022) Case Report: A de novo Variant of CRYGC Gene Associated With Congenital Cataract and Microphthalmia. Front. Genet. 13:866246. doi: 10.3389/fgene.2022.866246

Background: Congenital cataract is one of the most common causes of blindness in children. A rapid and accurate genetic diagnosis benefit the patients in the pediatric department. The current study aims to identify the genetic defects in a congenital cataract patient without a family history.

Case presentation: A congenital cataract patient with microphthalmia and nystagmus was recruited for this study. Trio-based whole-exome sequencing revealed a *de novo* variant (c.394delG, p.V132Sfs*15) in *CRYGC* gene. According to the American College of Medical Genetics and Genomics (ACMG) criteria, the variant could be annontated as pathogenic.

Conclusion: Our findings provide new knowledge of the variant spectrum of *CRYGC* gene and are essential for understanding the heterogeneity of cataracts in the Chinese population.

Keywords: congenital cataract, crystallin, *CRYGC*, microphthalmia, whole-exome sequencing

BACKGROUND

Congenital cataract is visible at birth or during the first decade of life; it is usually diagnosed by red light reflex, ophthalmoscopy examination and ocular color doppler ultrasound. Congenital cataract is one of the most common causes of blindness in children, with an estimated prevalence of 1–6 cases per 10,000 live births (Santana and Waiswo, 2011). About 8.3%–25% of congenital cataract cases present Mendelian inheritance; autosomal dominant inheritance pattern is the most common, but autosomal recessive and X-linked patterns have also been reported (Merin and Crawford, 1971; Francois, 1982; Zhong et al., 2017).

Inherited cataracts are genetically heterogeneous. With the development of WGS techniques, more and more cataract-related genes have been mapped and identified. So far, there are at least 49 loci and 37 genes have been identified for inherited isolated forms of cataracts according to OMIM (https://www.ncbi.nlm.nih.gov/omim/). These genes can be roughly grouped into four categories: crystallins, membrane proteins, cytoskeletal proteins, and DNA/RNA-banding proteins (Shiels and Hejtmanick, 2015). Crystallins are a kind of water-soluble protein that compose about 90% of lenticular protein mass and maintain the transparency of the lens (Hoehenwarter et al., 2006). They

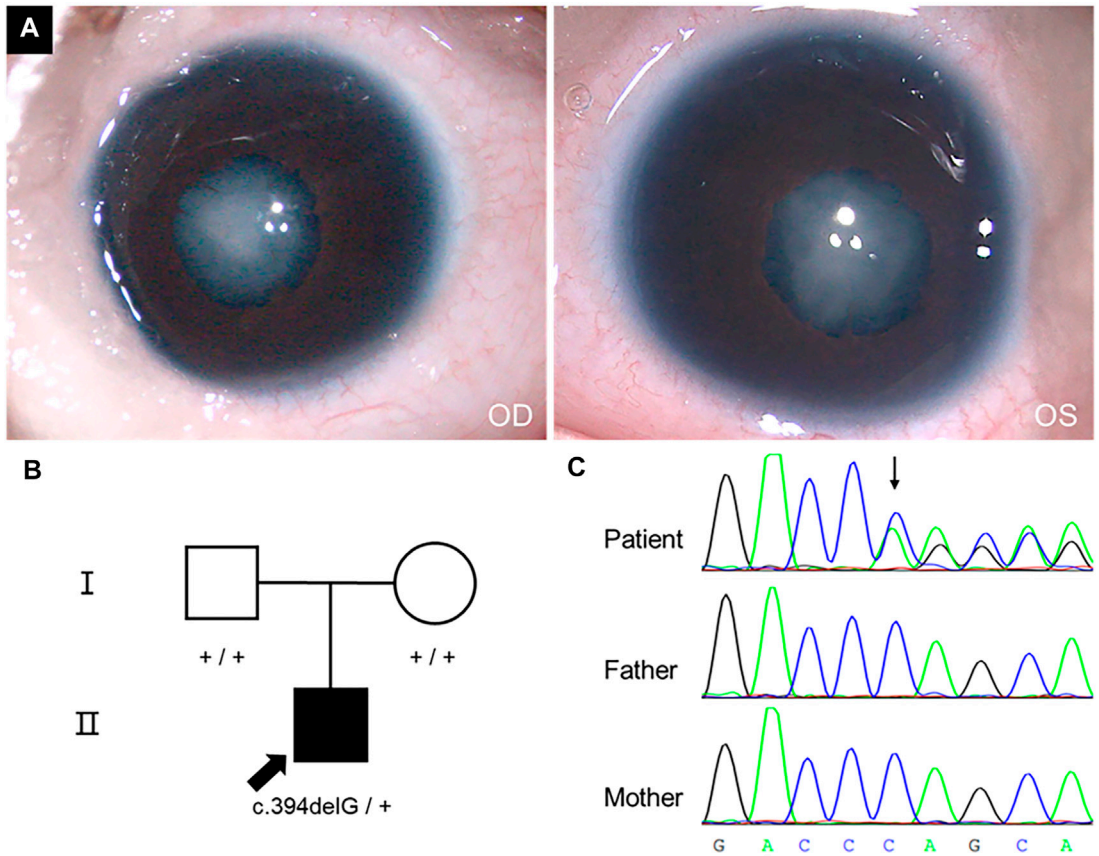

FIGURE 1 | Phenotype, pedigree, and Sanger sequencing results. **(A)** Cataract phenotype and pupils with irregular borders of the proband were shown. **(B)** The pedigree of a congenital cataract trios family. **(C)** c.394delG variant in *CRYGC* gene.

are divided into three major classes, α-, β-, and γ-crystallins. The α-crystallins belong to the small heat shock protein (HSP20) family, accounting for up to 50% of the total soluble protein of the lens (Bhat, 2003). Furthermore, they act as chaperones by binding partially unfolded lens βγ-crystallins to prevent their aggregation and thus maintain the transparency of the lens (Bhat, 2003). The βγ-crystallins are a superfamily of proteins with a "Greek key" motif unit base. Generally, the βγ-crystallins are supposed to be the essential structural proteins of the lens, but their exact function is still not fully understood (Jaenicke and Slingsby, 2001; Bhat, 2003; Slingsby and Wistow, 2014). Human γ-crystallins include six Cryg genes (*CRYGA*, *CRYGB*, *CRYGC*, *CRYGD*, *CRYGN*, and *CRYGS*); among them, variants of *CRYGC*, *CRYGD*, *CRYGS*, and *CRYGB* have been reported to be associated with congenital cataract (Heon et al., 1999; Stephan et al., 1999; Sun et al., 2005; AlFadhli et al., 2012).

In this study, a novel 1-bp deletion (c.394delG) in *CRYGC* gene was detected in a congenital cataract patient by trio-based whole-exome sequencing.

Case Presentation

The patient was examined at three months old because the pupil area of both eyes was found to be white for 15 days. He had poor light tracing reactions and no family history of cataracts. An ophthalmological exam revealed bilateral phacoscotasmus (C5), shallow anterior chamber, persistent pupillary membrane, invisible fundus, and nystagmus (**Figure 1A**). His corneas were transparent and had a diameter of 7.5 mm. The axial lengths of his eyes were 15.13 mm (OD) and 15.05 mm (OS), respectively. The intraocular pressures (IOP) were 10.2 mmHg (OD) and 14.0 mmHg (OS). Ultrasonography showed no alterations other than the opacified lens and reduced axial lengths.

A diagnosis of total cataracts and bilateral microphthalmia was made. Vitrectomy and lensectomy *via* anterior approach, posterior capsulorhexis, and peripheral iridectomy were performed on his both eyes. On postoperative one day, the IOP of the patient was 11 and 13 mmHg in the right and left eyes, respectively. Levofloxacin eye drops, tobramycin and dexamethasone eye drops, and tropicamide phenylephrine eye drops were used four times per day. 1 month after surgery, refractive correction in diopters (dpt) was +22.00 dpt −1.00 × 180 for the right eye and +22.00 dpt −1.00 × 180 for the left eye with spectacles. At the same time, the patient began amblyopia training under the guidance of doctors and parents.

METHODS

Genomic DNA Preparation

DNA was isolated from peripheral blood using DNA Isolation Kit (Blood DNA Kit V2, CW2553). Concentrations were determined on a Qubit fluorometer (Invitrogen, Q33216) using Qubit dsDNA HS Assay Kit (Invitrogen, Q32851). Agarose gel (1%) electrophoresis was performed for quality control.

Whole-Exome Sequencing

1 μg of the isolated DNA was sheared into about 200 bp sized fragments using Bioruptor UCD-200 (Diagenode). 3 μl of the sheared DNA was electrophoresed in a 2% agarose gel to confirm the presence of fragments of the desired size range. DNA libraries were prepared with KAPA Library Preparation Kit (Kapa Biosystems, KR0453) following the manufacturer's instructions. The libraries were estimated with Qubit dsDNA HS Assay kit (Invitrogen, Q32851). The hybridization of pooled libraries to the capture probes and remove non-hybridized library molecules were carried out by Agilent SureSelectXT2 Target Enrichment System. DNA libraries were sequenced on the Illumina Novaseq. 6000 platform (Illumina, San Diego, CA, United States) as paired-end 150-bp reads. Sample dilution, flowcell loading and sequencing were performed according to the Illumina specifications. Each sample yielded more than 10 Gb of raw data; over 95% of bases had a Phred quality score >20. The mean coverage was ×100 of the genome and the minimum coverage of ×10 was about 99%.

Data Analysis

FastQC (http://www.bioinformatics.babraham.ac.uk/projects/fastqc/) tool was used to evaluate reads quality, and our in-house script was used to filter low-quality reads. The sequenced raw reads in FastQ file format were preprocessed using Trim Galore (version 0.6.4, http://www.bioinformatics.babraham.ac.uk/projects/trim_galore/) to remove adapter-contaminated ends and low-quality bases with Phred scores < 20. Reads with > 5N bases, > 40% low-quality bases, or trimmed lengths < 30 bp were also removed. Subsequently, the quality passed reads were subsequently mapped to the human reference sequence (version: hg19) by alignment tool Burrows Wheeler Aligner (BWA, v0.7.17) (Li and Durbin, 2009). SNPs and small InDels were generated with Genome Analysis Toolkit (GATK, v3.8) (McKenna et al., 2010). The parent-child relationship was identified by King software (v2.2.7) (Manichaikul et al., 2010) to confirm the *de novo* variant.

Sanger Sequencing

Sanger sequencing was used to validate the variant through the filtering procedures. Primers were designed by the Primer3 program (http://frodo.wi.mit.edu/).

RESULT

WES yielded 14.7, 10.3, and 13.2 Gb data from genomes of proband, father, and mother, respectively. Totally, 17,823 nonsynonymous SNVs and 549 Indels were identified. Considering the patient has no family history, we checked *de novo* variants and recessive inherit variants at first. We identified 93 recessive inherit variants (including homozygous and compound heterozygous variants, Max MAF < 0.05), involving 54 genes. But none of these genes was associated with cataracts. In addition, there were 24 *de novo* variants (Max MAF < 0.005) involving 19 genes in the proband. A *de novo* frameshift variant c.394delG (hg19: chr2:208993058) was identified in *CRYGC* gene (NM_020989) through our filter pipeline. The variant would cause a frameshift from the 132nd codon and prematurely terminate at the 147th codon if a mutant protein was produced (p.V132Sfs*15). Sanger sequencing confirmed that the variant is heterozygous in the proband but absent from his parents (**Figure 1C**). The relationships between the three samples were confirmed (**Supplementary Table S1**). Furthermore, the variant was absent in the gnomAD exomes or genomes (http://gnomad.broadinstitute.org). Therefore, the c.394delG variant could be categorised as pathogenic according to the American College of Medical Genetics and Genomics (ACMG) criteria (Richards et al., 2015) (PVS1+PS2+PM2).

DISCUSSION

To date, a total of 32 variants in *CRYGC* gene have been reported to be associated with congenital cataract (Heon et al., 1999; Ren et al., 2000; Santhiya et al., 2002; Gonzalez-Huerta et al., 2007; Devi et al., 2008; Yao et al., 2008; Zhang et al., 2009; Kumar et al., 2011; Guo et al., 2012; Li et al., 2012; Kondo et al., 2013; Reis et al., 2013; Gillespie et al., 2014; Prokudin et al., 2014; Li et al., 2016; Ma et al., 2016; Patel et al., 2017; Sun et al., 2017; Zhong et al., 2017; Astiazaran et al., 2018; Li et al., 2018; Zhang et al., 2019; Zhuang et al., 2019; Berry et al., 2020; Taylan Sekeroglu et al., 2020; Fernandez-Alcalde et al., 2021; Karahan et al., 2021; Rechsteiner et al., 2021), but there were few reports about the *de novo* mutations. In 2017, Zhong et al. reported a frameshift mutation (p.Asp65ThrfsX38) which might be *de novo* (Zhong et al., 2017). In 2021, Rechsteiner et al. reported a *de novo* mutation p.Glu107GlyfsX56, which causes cataracts and microphthalmia (Rechsteiner et al., 2021), and Fernández-Alcalde et al. reported a *de novo* mutation p.Leu145GlyfsX5 (Fernandez-Alcalde et al., 2021). In the present study, a *de novo* frameshift variant (c.394delG, p.V132Sfs*15) was identified in *CRYGC* gene as the cause of a patient with congenital cataract and microphthalmia.

CRYGC has a two-domain beta-structure, folded into four similar Greek key motifs (GKM); like all γ-crystallins, it has the highest intrachain symmetry (Blundell et al., 1981). The high degree of symmetry may contribute to the stability of γ-crystallins (Blundell et al., 1981). *CRYGC* variants in GKMs may disrupt the symmetrical structure, which changes the intra- or inter-molecular interactions, possibly leading to destabilisation and aggregation, respectively (Zhong et al., 2017). The variant p.V132Sfs*15 occurred at the beginning of GKM4 (129-171aa), leading to a frameshift and premature termination, disrupting the entire GKM4.

According to Cat-Map (Shiels et al., 2010) (https://cat-map.wustl.edu/, last updated on October 2021), the most common phenotype caused by *CRYGC* variants was nuclear cataracts, followed by lamellar and pulverulent cataracts. The missense variants p.F6S and p.R168W had been reported to be associated with either nuclear or lamellar

cataracts (Santhiya et al., 2002; Gonzalez-Huerta et al., 2007; Devi et al., 2008; Astiazaran et al., 2018). It seems that there was no particular connection between cataract phenotypes and variant sites. Inherited cataracts could be isolated or associated with other ocular signs, including microcornea/microphthalmia, eye movement disorders (nystagmus, strabismus, amblyopia), or refractive errors. There 15 variants were reported to cause cataracts and additional ocular signs among all the 32 reported *CRYGC* variants. Microcornea was the most common additional ocular sign (Zhang et al., 2009; Guo et al., 2012; Reis et al., 2013; Patel et al., 2017; Sun et al., 2017; Zhong et al., 2017; Rechsteiner et al., 2021). The phenotypic heterogeneity could be due to unidentified modifier genes (Astiazaran et al., 2018) or some unknown mechanisms in which CRYGC takes part during eye development. For example, proteomics research showed that the CRYGC and some other crystallins are highly expressed in the human cornea (Subbannayya et al., 2020), indicating that these genes might involve in the cornea morphogenesis and transparency.

Next-generation DNA sequencing technologies could identify the precise genetic cause in about 45%–75% of congenital cataract families. For example, testing of WES in 11 cataract families by Kandaswamy et al. determined a genetic cause in 6 families (55%) (Kandaswamy et al., 2020). A recent study on inherited eye diseases found that WGS (through 100,000 Genomes Project) had a diagnostic yield of 44.7% (17/38) for congenital cataract families (Jackson et al., 2020). In the past few years, it has been reported that testing of a targeted gene panel (115 genes) in 36 bilateral cataracts patients identified a genetic cause in 75% of cases (Gillespie et al., 2014). However, another research using the same panel established a genetic diagnosis in 50% of congenital cataract cases (Lenassi et al., 2020). A rapid and accurate genetic diagnosis in the pediatric department helps patients understand their cause of disease, make clinical decisions, carry on the instruction for procreation, or even look for therapeutic schemes. In the current study, a genetic cause was identified in a three-month-old congenital cataract patient. He underwent cataract surgery immediately after diagnosis and had a good prognosis.

CONCLUSION

In conclusion, we have identified a novel frameshift variant, c.394delG, p.V132Sfs*15, within the *CRYGC* gene in a congenital cataract boy. Our findings provide new knowledge of the variant spectrum of *CRYGC* and are essential for understanding the heterogeneity of cataracts in the Chinese population.

DATA AVAILABILITY STATEMENT

The datasets presented in this study can be found in online repositories. The names of the repository/repositories and accession number(s) can be found below: (BankIt2557536 BSeq#1 OM912449).

ETHICS STATEMENT

The study was approved by the Ethics Committee of Hunan Children's Hospital. Written informed consent to participate in this study was provided by the participants' legal guardian/next of kin.

AUTHOR CONTRIBUTIONS

YL and LT: supervision and resources acquisition. YP: original manuscript writing and editing, data analysis. YZ and SZ: methodology and validation. YL: sample collection and clinical data curation and validation. ZD and YT: methodology and resources collection. YP and ZH: manuscript review and editing. All authors read and approved the final manuscript.

FUNDING

This work was supported by the Hunan Province Natural Science Foundation of China (Grant number: 2020JJ8076, 2020JJ8005); The Health Commission Science Research Project of Hunan Province (Grant Number: 202107021955).

ACKNOWLEDGMENTS

The authors greatly thank the patient and his parents who participated in this study.

SUPPLEMENTARY MATERIAL

The Supplementary Material for this article can be found online at: https://www.frontiersin.org/articles/10.3389/fgene.2022.866246/full#supplementary-material

REFERENCES

AlFadhli, S., Abdelmoaty, S., Al-Hajeri, A., Behbehani, A., and Alkuraya, F. (2012). Novel Crystallin Gamma B Mutations in a Kuwaiti Family with Autosomal Dominant Congenital Cataracts Reveal Genetic and Clinical Heterogeneity. *Mol. Vis.* 18, 2931–2936.

Astiazarán, M. C., García-Montaño, L. A., Sánchez-Moreno, F., Matiz-Moreno, H., and Zenteno, J. C. (2018). Next Generation Sequencing-Based Molecular Diagnosis in Familial Congenital Cataract Expands the Mutational Spectrum in Known Congenital Cataract Genes. *Am. J. Med. Genet.* 176, 2637–2645. doi:10.1002/ajmg.a.40524

Berry, V., Ionides, A., Pontikos, N., Georgiou, M., Yu, J., and Ocaka, L. A. (2020). The Genetic Landscape of Crystallins in Congenital Cataract. *Orphanet J. Rare Dis.* 15, 333. doi:10.1186/s13023-020-01613-3

Bhat, S. P. (2003). Crystallins, Genes and Cataract. *Prog. Drug Res.* 60, 205–262. doi:10.1007/978-3-0348-8012-1_7

Blundell, T., Lindley, P., Miller, L., Moss, D., Slingsby, C., Tickle, I., et al. (1981). The Molecular Structure and Stability of the Eye Lens: X-Ray Analysis of Gamma-Crystallin II. *Nature.* 289, 771–777. doi:10.1038/289771a0

Devi, R. R., Yao, W., Vijayalakshmi, P., Sergeev, Y. V., Sundaresan, P., and Hejtmancik, J. F. (2008). Crystallin Gene Mutations in Indian Families with Inherited Pediatric Cataract. *Mol. Vis.* 14, 1157–1170.

Fernandez-Alcalde, C., Nieves-Moreno, M., Noval, S., Peralta, J. M., Montano, V. E. F., Del Pozo, A., et al. (2021). Molecular and Genetic Mechanism of Non-syndromic Congenital Cataracts. *Genes. (Basel).* 12 (4), 580. doi:10.3390/genes12040580

Francois, J. (1982). Genetics of Cataract. *Ophthalmologica* 184, 61–71. doi:10.1159/000309186

Gillespie, R. L., O'Sullivan, J., Ashworth, J., Bhaskar, S., Williams, S., Biswas, S., et al. (2014). Personalized Diagnosis and Management of Congenital Cataract by Next-Generation Sequencing. *Ophthalmology.* 121, 2124–2137. e1-2. doi:10.1016/j.ophtha.2014.06.006

Gonzalez-Huerta, L. M., Messina-Baas, O. M., and Cuevas-Covarrubias, S. A. (2007). A Family with Autosomal Dominant Primary Congenital Cataract Associated with a CRYGC Mutation: Evidence of Clinical Heterogeneity. *Mol. Vis.* 13, 1333–1338.

Guo, Y., Su, D., Li, Q., Yang, Z., Ma, Z., Ma, X., et al. (2012). A Nonsense Mutation of CRYGC Associated with Autosomal Dominant Congenital Nuclear Cataracts and Microcornea in a Chinese Pedigree. *Mol. Vis.* 18, 1874–1880.

Heon, E., Priston, M., Schorderet, D. F., Billingsley, G. D., Girard, P. O., Lubsen, N., et al. (1999). The Gamma-Crystallins and Human Cataracts: a Puzzle Made Clearer. *Am. J. Hum. Genet.* 65, 1261–1267. doi:10.1086/302619

Hoehenwarter, W., Klose, J., and Jungblut, P. R. (2006). Eye Lens Proteomics. *Amino Acids.* 30, 369–389. doi:10.1007/s00726-005-0283-9

Jackson, D., Malka, S., Harding, P., Palma, J., Dunbar, H., and Moosajee, M. (2020). Molecular Diagnostic Challenges for Non-retinal Developmental Eye Disorders in the United Kingdom. *Am. J. Med. Genet. C Semin. Med. Genet.* 184, 578–589. doi:10.1002/ajmg.c.31837

Jaenicke, R., and Slingsby, C. (2001). Lens Crystallins and Their Microbial Homologs: Structure, Stability, and Function. *Crit. Rev. Biochem. Mol. Biol.* 36, 435–499. doi:10.1080/20014091074237

Kandaswamy, D. K., Prakash, M. V. S., Graw, J., Koller, S., Magyar, I., Tiwari, A., et al. (2020). Application of WES towards Molecular Investigation of Congenital Cataracts: Identification of Novel Alleles and Genes in a Hospital-Based Cohort of South India. *Int. J. Mol. Sci.* 21, 9569. doi:10.3390/ijms21249569

Karahan, M., Demirtas, A. A., Erdem, S., Ava, S., Tekes, S., and Keklikci, U. (2021). Crystalline Gene Mutations in Turkish Children with Congenital Cataracts. *Int. Ophthalmol.* 41, 2847–2852. doi:10.1007/s10792-021-01843-9

Kondo, Y., Saitsu, H., Miyamoto, T., Lee, B. J., Nishiyama, K., Nakashima, M., et al. (2013). Pathogenic Mutations in Two Families with Congenital Cataract Identified with Whole-Exome Sequencing. *Mol. Vis.* 19, 384–389.

Kumar, M., Agarwal, T., Khokhar, S., Kumar, M., Kaur, P., Roy, T. S., et al. (2011). Mutation Screening and Genotype Phenotype Correlation of Alpha-Crystallin, Gamma-Crystallin and GJA8 Gene in Congenital Cataract. *Mol. Vis.* 17, 693–707.

Lenassi, E., Clayton-Smith, J., Douzgou, S., Ramsden, S. C., Ingram, S., Hall, G., et al. (2020). Clinical Utility of Genetic Testing in 201 Preschool Children with Inherited Eye Disorders. *Genet. Med.* 22, 745–751. doi:10.1038/s41436-019-0722-8

Li, D., Wang, S., Ye, H., Tang, Y., Qiu, X., Fan, Q., et al. (2016). Distribution of Gene Mutations in Sporadic Congenital Cataract in a Han Chinese Population. *Mol. Vis.* 22, 589–598.

Li, H., and Durbin, R. (2009). Fast and Accurate Short Read Alignment with Burrows-Wheeler Transform. *Bioinformatics* 25, 1754–1760. doi:10.1093/bioinformatics/btp324

Li, J., Leng, Y., Han, S., Yan, L., Lu, C., Luo, Y., et al. (2018). Clinical and Genetic Characteristics of Chinese Patients with Familial or Sporadic Pediatric Cataract. *Orphanet J. Rare Dis.* 13, 94. doi:10.1186/s13023-018-0828-0

Li, X. Q., Cai, H. C., Zhou, S. Y., Yang, J. H., Xi, Y. B., Gao, X. B., et al. (2012). A Novel Mutation Impairing the Tertiary Structure and Stability of gammaC-Crystallin (CRYGC) Leads to Cataract Formation in Humans and Zebrafish Lens. *Hum. Mutat.* 33, 391–401. doi:10.1002/humu.21648

Ma, A. S., Grigg, J. R., Ho, G., Prokudin, I., Farnsworth, E., Holman, K., et al. (2016). Sporadic and Familial Congenital Cataracts: Mutational Spectrum and New Diagnoses Using Next-Generation Sequencing. *Hum. Mutat.* 37, 371–384. doi:10.1002/humu.22948

Manichaikul, A., Mychaleckyj, J. C., Rich, S. S., Daly, K., Sale, M., and Chen, W. M. (2010). Robust Relationship Inference in Genome-wide Association Studies. *Bioinformatics.* 26, 2867–2873. doi:10.1093/bioinformatics/btq559

McKenna, A., Hanna, M., Banks, E., Sivachenko, A., Cibulskis, K., Kernytsky, A., et al. (2010). The Genome Analysis Toolkit: a MapReduce Framework for Analyzing Next-Generation DNA Sequencing Data. *Genome Res.* 20, 1297–1303. doi:10.1101/gr.107524.110

Merin, S., and Crawford, J. S. (1971). The Etiology of Congenital Cataracts. A Survey of 386 Cases. *Can. J. Ophthalmol.* 6, 178–182.

Patel, N., Anand, D., Monies, D., Maddirevula, S., Khan, A. O., Algoufi, T., et al. (2017). Novel Phenotypes and Loci Identified through Clinical Genomics Approaches to Pediatric Cataract. *Hum. Genet.* 136, 205–225. doi:10.1007/s00439-016-1747-6

Prokudin, I., Simons, C., Grigg, J. R., Storen, R., Kumar, V., Phua, Z. Y., et al. (2014). Exome Sequencing in Developmental Eye Disease Leads to Identification of Causal Variants in GJA8, CRYGC, PAX6 and CYP1B1. *Eur. J. Hum. Genet.* 22, 907–915. doi:10.1038/ejhg.2013.268

Rechsteiner, D., Issler, L., Koller, S., Lang, E., Bahr, L., Feil, S., et al. (2021). Genetic Analysis in a Swiss Cohort of Bilateral Congenital Cataract. *JAMA Ophthalmol.* 139, 691–700. doi:10.1001/jamaophthalmol.2021.0385

Reis, L. M., Tyler, R. C., Muheisen, S., Raggio, V., Salviati, L., Han, D. P., et al. (2013). Whole Exome Sequencing in Dominant Cataract Identifies a New Causative Factor, CRYBA2, and a Variety of Novel Alleles in Known Genes. *Hum. Genet.* 132, 761–770. doi:10.1007/s00439-013-1289-0

Ren, Z., Li, A., Shastry, B. S., Padma, T., Ayyagari, R., Scott, M. H., et al. (2000). A 5-base Insertion in the gammaC-Crystallin Gene Is Associated with Autosomal Dominant Variable Zonular Pulverulent Cataract. *Hum. Genet.* 106, 531–537. doi:10.1007/s004390000289

Richards, S., Aziz, N., Bale, S., Bick, D., Das, S., Gastier-Foster, J., et al. (2015). Standards and Guidelines for the Interpretation of Sequence Variants: a Joint Consensus Recommendation of the American College of Medical Genetics and Genomics and the Association for Molecular Pathology. *Genet. Med.* 17, 405–424. doi:10.1038/gim.2015.30

Santana, A., and Waiswo, M. (2011). The Genetic and Molecular Basis of Congenital Cataract. *Arq. Bras. Oftalmol.* 74, 136–142. doi:10.1590/s0004-27492011000200016

Santhiya, S. T., Shyam Manohar, M., Rawlley, D., Vijayalakshmi, P., Namperumalsamy, P., Gopinath, P. M., et al. (2002). Novel Mutations in the Gamma-Crystallin Genes Cause Autosomal Dominant Congenital Cataracts. *J. Med. Genet.* 39, 352–358. doi:10.1136/jmg.39.5.352

Shiels, A., Bennett, T. M., and Hejtmancik, J. F. (2010). Cat-Map: Putting Cataract on the Map. *Mol. Vis.* 16, 2007–2015.

Shiels, A., and Hejtmancik, J. F. (2015). Molecular Genetics of Cataract. *Prog. Mol. Biol. Transl. Sci.* 134, 203–218. doi:10.1016/bs.pmbts.2015.05.004

Slingsby, C., and Wistow, G. J. (2014). Functions of Crystallins in and Out of Lens: Roles in Elongated and Post-mitotic Cells. *Prog. Biophys. Mol. Biol.* 115, 52–67. doi:10.1016/j.pbiomolbio.2014.02.006

Stephan, D. A., Gillanders, E., Vanderveen, D., Freas-Lutz, D., Wistow, G., Baxevanis, A. D., et al. (1999). Progressive Juvenile-Onset Punctate Cataracts Caused by Mutation of the gammaD-Crystallin Gene. *Proc. Natl. Acad. Sci. U. S. A.* 96, 1008–1012. doi:10.1073/pnas.96.3.1008

Subbannayya, Y., Pinto, S. M., Mohanty, V., Dagamajalu, S., Prasad, T. S. K., and Murthy, K. R. (2020). What Makes Cornea Immunologically Unique and Privileged? Mechanistic Clues from a High-Resolution Proteomic Landscape of the Human Cornea. *OMICS* 24, 129–139. doi:10.1089/omi.2019.0190

Sun, H., Ma, Z., Li, Y., Liu, B., Li, Z., Ding, X., et al. (2005). Gamma-S Crystallin Gene (CRYGS) Mutation Causes Dominant Progressive Cortical Cataract in Humans. *J. Med. Genet.* 42, 706–710. doi:10.1136/jmg.2004.028274

Sun, Z., Zhou, Q., Li, H., Yang, L., Wu, S., and Sui, R. (2017). Mutations in Crystallin Genes Result in Congenital Cataract Associated with Other Ocular Abnormalities. *Mol. Vis.* 23, 977–986.

Taylan Sekeroglu, H., Karaosmanoglu, B., Taskiran, E. Z., Simsek Kiper, P. O., Alikasifoglu, M., Boduroglu, K., et al. (2020). Molecular Etiology of Isolated Congenital Cataract Using Next-Generation Sequencing: Single Center Exome Sequencing Data from Turkey. *Mol. Syndromol.* 11, 302–308. doi:10.1159/000510481

Yao, K., Jin, C., Zhu, N., Wang, W., Wu, R., Jiang, J., et al. (2008). A Nonsense Mutation in CRYGC Associated with Autosomal Dominant Congenital Nuclear Cataract in a Chinese Family. *Mol. Vis.* 14, 1272–1276.

Zhang, J., Sun, D., Wang, Y., Mu, W., Peng, Y., and Mi, D. (2019). Identification of a Novel CRYGC Mutation in a Pedigree Affected with Congenital Cataracts. *Zhonghua Yi Xue Yi Chuan Xue Za Zhi* 36, 697–700. doi:10.3760/cma.j.issn.1003-9406.2019.07.010

Zhang, L., Fu, S., Ou, Y., Zhao, T., Su, Y., and Liu, P. (2009). A Novel Nonsense Mutation in CRYGC Is Associated with Autosomal Dominant Congenital Nuclear Cataracts and Microcornea. *Mol. Vis.* 15, 276–282.

Zhong, Z., Wu, Z., Han, L., and Chen, J. (2017). Novel Mutations in CRYGC Are Associated with Congenital Cataracts in Chinese Families. *Sci. Rep.* 7, 189. doi:10.1038/s41598-017-00318-1

Zhuang, J., Cao, Z., Zhu, Y., Liu, L., Tong, Y., Chen, X., et al. (2019). Mutation Screening of Crystallin Genes in Chinese Families with Congenital Cataracts. *Mol. Vis.* 25, 427–437.

Conflict of Interest: The authors declare that the research was conducted in the absence of any commercial or financial relationships that could be construed as a potential conflict of interest.

Publisher's Note: All claims expressed in this article are solely those of the authors and do not necessarily represent those of their affiliated organizations, or those of the publisher, the editors and the reviewers. Any product that may be evaluated in this article, or claim that may be made by its manufacturer, is not guaranteed or endorsed by the publisher.

frontiers | Frontiers in Genetics

BRIEF RESEARCH REPORT
published: 01 June 2022
doi: 10.3389/fgene.2022.877174

Evaluation of ABCA1 and FNDC3B Gene Polymorphisms Associated With Pseudoexfoliation Glaucoma and Primary Angle-Closure Glaucoma in a Saudi Cohort

Altaf A. Kondkar[1,2,3], Tahira Sultan[1], Taif A. Azad[1], Essam A. Osman[1], Faisal A. Almobarak[1,2], Glenn P. Lobo[4] and Saleh A. Al-Obeidan[1,2]*

[1]Department of Ophthalmology, College of Medicine, King Saud University, Riyadh, Saudi Arabia, [2]Glaucoma Research Chair in Ophthalmology, College of Medicine, King Saud University, Riyadh, Saudi Arabia, [3]King Saud University Medical City, King Saud University, Riyadh, Saudi Arabia, [4]Department of Ophthalmology and Visual Neurosciences, University of Minnesota, Minneapolis, MN, United States

OPEN ACCESS

Edited by:
Zi-Bing Jin,
Capital Medical University, China

Reviewed by:
Karen Curtin,
The University of Utah, United States
Teera Poyomtip,
Ramkhamhaeng University, Thailand

***Correspondence:**
Altaf A. Kondkar
akondkar@gmail.com

Specialty section:
This article was submitted to Genetics of Common and Rare Diseases, a section of the journal Frontiers in Genetics

Received: *16 February 2022*
Accepted: *18 May 2022*
Published: *01 June 2022*

Citation:
Kondkar AA, Sultan T, Azad TA, Osman EA, Almobarak FA, Lobo GP and Al-Obeidan SA (2022) Evaluation of ABCA1 and FNDC3B Gene Polymorphisms Associated With Pseudoexfoliation Glaucoma and Primary Angle-Closure Glaucoma in a Saudi Cohort. Front. Genet. 13:877174. doi: 10.3389/fgene.2022.877174

Objective: It is plausible that common disease mechanisms exist in glaucoma pathophysiology. Accordingly, we investigated the genetic association of two previously reported primary open-angle glaucoma (POAG)-related gene polymorphisms, rs2472493 (A > G) in *ABCA1* and rs7636836 (C > T) in FNDC3B, in primary angle-closure glaucoma (PACG) and pseudoexfoliation glaucoma (PXG).

Methods: TaqMan genotyping was performed in a total of 442 subjects consisting of 246 healthy controls, 102 PACG patients, and 94 PXG patients. Statistical evaluations were performed to detect allelic and genotype association of the variants with the disease and clinical variables such as intraocular pressure (IOP) and cup/disc ratio.

Results: Overall, there was no allelic or genotype association of these variants in PACG and PXG. However, rs7636836[T] allele significantly increased the risk of PXG among men (p = 0.029, odds ratio [OR] = 2.69, 95% confidence interval = 1.11–6.51). Similarly, rs2472493 and rs7636836 genotypes also showed significant association with PXG among men in over-dominant model (p = 0.031, OR = 1.98, 95% CI = 1.06–3.71) and co-dominant model (p = 0.029, OR = 2.69, 95% CI = 1.11–6.51), respectively. However, none survived Bonferroni's correction. Besides, the synergic presence of rs2472493[G] and rs7636836[T] alleles (G-T) was found to significantly increase the risk of PACG (p = 0.026, OR = 2.85, 95% CI = 1.09–7.46). No significant genotype influence was observed on IOP and cup/disc ratio.

Conclusion: Our results suggest that the polymorphisms rs2472493 in ABCA1 and rs7636836 in FNDC3B genes may be associated with PXG among men, and a G-T allelic combination may confer an increased risk of PACG in the middle-eastern Saudi cohort. Further research in a larger population-based sample is needed to validate these findings.

Keywords: genetics, genotyping, glaucoma, intraocular pressure, ophthalmology, polymorphism, rs2472493, rs7636836

INTRODUCTION

Glaucoma is a complex multifactorial disease with high heritability and ethnic-specific predisposition, suggesting the involvement of genetic components in its pathogenesis (Chan et al., 2016). Among the various forms of glaucoma, primary angle-closure glaucoma (PACG) is a far more common type than primary open-angle glaucoma (POAG) in Asian populations, including Saudi Arabia (Al Obeidan et al., 2011; Chan et al., 2016) and involves anatomical blockage of the aqueous flow pathway (Weinreb et al., 2014). Likewise, pseudoexfoliation glaucoma (PXG) is the most severe type of open-angle glaucoma highly prevalent among the elderly, characterized by the abnormal deposition of pseudoexfoliative material (fibrillar extracellular matrix) in the anterior segment of the eye causing the aqueous blockage and associated with worse prognosis (Vazquez and Lee, 2014). Several disease-causing mutations and multiple susceptibility loci have been associated with different types of glaucoma in various ethnicities (Zukerman et al., 2021). However, the precise role of these genetic components and their underlying molecular mechanisms in glaucoma pathogenesis remains unclear.

Overlapping clinical manifestations among glaucoma types, such as high intraocular pressure (IOP), optic nerve damage, and retinal ganglion cell (RGC) apoptosis, suggest the plausibility of common disease pathways and genetic mechanisms in glaucoma pathogenesis. The previous genetic association studies of *MYOC* (Dai et al., 2008), *CYP1B1* (Chakrabarti et al., 2007), *LOXL1* (Shiga et al., 2018; Eliseeva et al., 2021), *ARHGEF12* (Aung et al., 2018), and *ACVR1* (Kondkar et al., 2020) that have been common to different types of glaucoma and therefore lend further support to this hypothesis. Besides, most of the studies investigating glaucoma genetics were conducted in Asian or Caucasian populations. Depending on the population being assessed, the same variants may or may not show an association. Therefore, replication studies must be performed to confirm the effects of these single nucleotide variants in other regions or with other ethnicities. The genetic basis of PACG and PXG in middle-eastern patients of Saudi origin is still largely unknown (Abu-Amero et al., 2010; Abu-Amero et al., 2013, 2015; Kondkar et al., 2021) and therefore warrants further genetic investigation. Accordingly, we hypothesized that genetic polymorphisms rs2472493 located upstream of the *ABCA1* gene and rs7636836 in *FNDC3B* were previously reported to be associated with POAG and elevated IOP (Hysi et al., 2014; Shiga et al., 2018), may also be associated with PACG and PXG in Saudi patients.

ABCA1 functions as a cholesterol efflux pump, and recent findings suggest its role in neuroinflammation, neurodegeneration, and RGC apoptosis (Howell et al., 2011; Awadalla et al., 2013). Whereas *FNDC3B* codes for an extracellular matrix protein involved in several signaling pathways including, transforming growth factor-beta (TGFβ) signaling (Prendes et al., 2013). Both genes are highly expressed in the human retina, optic nerve, trabecular meshwork, and RGC supporting its alleged role in glaucoma development and/or progression (Shiga et al., 2018). The genetic contribution of the variants at the *ABCA1* and *FNDC3B* locus among Saudi PACG and PXG patients is unknown. To date, there has been no study to address the relationship between the polymorphisms in *ABCA1* and *FNDC3B* in PACG and PXG in Saudi Arabs. Thus, in this exploratory study, we investigated whether single-nucleotide polymorphisms (SNPs) rs2472493 and rs7636836 upstream of *ABCA1* and in *FNDC3B* genes, respectively, were associated with PACG and PXG in a Saudi cohort.

MATERIALS AND METHODS

Study Design and Population

The retrospective case-control study was approved by the Institutional Review Board Ethics Committee at the College of Medicine of King Saud University (IRB protocol approval number # 08–657) and adhered to the Declaration of Helsinki principles with all the participants providing written informed consent. Patients of Saudi origin with a clinical diagnosis of PACG, PXG, and non-glaucoma controls were recruited at King Abdulaziz University Hospital, Riyadh, Saudi Arabia from April 2017 through December 2019.

PACG patients (n = 102) were diagnosed based on clinical evidence of anatomically closed-angle showing the occurrence of appositional or synechial closure of the anterior chamber angle (at least 270° of the angle is occluded); raised IOP (≥21 mmHg); the presence of optic disk damage with cup/disc ratio of at least 0.7 (at least in one eye); and loss of peripheral or advanced visual field (Abu-Amero et al., 2013). PXG patients (n = 94) showed the presence of flaky exfoliation material along the pupil edges or anterior lens capsule, glaucomatous optic neuropathy and associated visual field loss, and high IOP in either or both the eyes as described previously (Kondkar et al., 2018). Patients harboring secondary forms of glaucoma, history of optic neuropathies or visual impairment unrelated to glaucoma, steroid usage, ocular trauma, absence of sufficient fundus visualization for disk assessment, or refusal to enroll were excluded. A group of healthy Saudi Arab participants (n = 246) recruited from our ophthalmology screening clinics served as controls. These participants were: >40 years of age, with normal IOP (<21 mmHg), open angles on gonioscopy, healthy optic disc (cup/disc ratio <0.5), free from any form of glaucoma on examination, and no family history of glaucoma. Subjects refusing to participate in the study were excluded.

Genotyping of rs2472493 and rs7636836

Commercially available pre-designed TaqMan® assays, C__16235609_10 and C_189412462_10 purchased from Applied Biosystems (Catalog number: 4351379; Applied Biosystems Inc., Foster City, CA, United States) were used to genotype rs2472493 (A > G) and rs7636836 (C > T), respectively on ABI 7500 real-time PCR System (Applied Biosystems) according to the manufacturer instructions under recommended amplification conditions (Abu-Amero et al., 2013). Briefly, each assay utilizes two unlabeled PCR primers

and two allele-specific probes. Each probe is labeled with a different color reporter dye (VIC® for allele 1 and 6-carboxy-fluorescein (FAM) for allele 2) at the 5′ end. The allele-specific fluorogenic probes when hybridized to the DNA template are cleaved by the 5′ nuclease activity of the Taq polymerase resulting in fluorescence emission from the reporter dye. Each PCR reaction was performed as recommended by the supplier in a total volume of 25 µl and consisted of 1X TaqMan® Genotyping Master Mix (Applied Biosystems), 1X SNP Genotyping Assay Mix and 20 ng DNA or molecular grade water in no template control well. The amplification conditions consisted of incubation at 95°C for 10 min, followed by 40 cycles, denaturation at 92°C for 15 s and annealing/ extension at 60°C for 1 min. The VIC® and FAM fluorescence levels of the PCR products were measured at 60°C for 1 min. Analysis of fluorescence using the automated 2-color allele discrimination software on ABI 7500 showed clear discrimination of all genotypes on a two-dimensional graph.

Statistical Analysis

Hardy-Weinberg Equilibrium (HWE), gender distribution, allele and genotype associations were tested using Pearson's Chi-square analysis and Fisher's test where applicable. Normality testing of continuous variables was done using the Kolmogorov–Smirnov test. Accordingly, age differences and genotypes effects on glaucoma indices such as IOP, cup/disc ratio, and number of antiglaucoma medications were estimated using Mann-Whitney U test (2-groups comparison) and Kruskal–Wallis test (3-groups comparison). Binary logistic regression analysis was performed to test the effects of multiple factors (age, sex, genotypes) on glaucoma outcome. The analyses were performed using SPSS version 22 (IBM Inc., Chicago, Illinois, United States), Stat View software version 5.0 (SAS Institute, Cary, NC, United States), and SNPStats online software (https://www.snpstats.net/start.htm). The combined allelic (haplotype) effect was estimated using SHEsis (http://analysis.bio-x.cn/myAnalysis.php). Power analysis was done using Power Genetic Association (PGA) software (https://dceg.cancer.gov/tools/design/pga). A $p < 0.05$ (2-tailed) was considered significant. Bonferroni's correction p-value for multiple testing was considered where applicable.

RESULTS

Demographic Data Distribution

The demographic data of subjects included in the study is shown in **Supplementary Figure S1**. In comparison to the mean age of controls (59.5 years, ± 7.2), the mean age in PACG (60.6 years, ± 8.5) was not significantly different ($p = 0.225$), but the PXG cases (66.4 years, ± 9.7) were significantly older ($p < 0.001$). Besides, the frequency of gender distribution did not differ significantly in the PACG ($p = 0.105$) and PXG ($p = 0.078$) groups than in the controls.

Allele Frequency of rs2472493 in *ABCA1* and rs7636836 in *FNDC3B* Genes

Of the total number of 442 subjects genotyped for rs2472493 and rs7636836 polymorphisms in this study, there were seven samples with missing genotypes for rs2472493 that failed to amplify and none for rs7636836, giving an estimated call rate of 98% and 100%, respectively. The samples with missing genotypes were excluded from rs2472493 and combined genotype analysis. **Table 1** shows the minor allele frequency (MAF) distribution of rs2472493 and rs7636836 according to glaucoma types and gender in cases and controls. No significant deviation from HWE was observed ($p > 0.05$). Overall, the MAFs of both the polymorphisms showed no significant association with PACG and PXG. However, rs7636836 [T] variant in *FNDC3B* was significantly associated with increased risk of PXG among men (OR = 2.69, 95% CI = 1.11–6.51, $p = 0.029$). No such gender-specific association was observed for rs2472493 in *ABCA1*.

Genotype Analysis of rs2472493 (*ABCA1*) and rs7636836 (*FNDC3B*) in PACG

Genotype association analysis was performed in co-dominant, dominant, recessive, over-dominant, and log-additive genetic models using SNPStats software. Both rs2472493 and rs7636836 genotypes did not show any significant association with PACG (**Table 2**). Furthermore, genotype analysis of both the variants in PACG did not reveal any gender-specific association in any of the tested genetic models (**Supplementary Tables S1, S2**).

Genotype Analysis of rs2472493 (*ABCA1*) and rs7636836 (*FNDC3B*) in PXG

Overall, the polymorphisms rs2472493 and rs7636836 showed no significant association with PXG. However, a further gender stratification showed a significant moderate association of these polymorphisms with PXG among men (**Tables 3**, **4**). Rs2472493 in *ABCA1* showed a significantly increased risk of PXG in men in the over-dominant model (OR = 1.98, 95% CI = 1.06–3.71, $p = 0.031$) that did not remain significant after adjustment for age, sex, and Bonferroni correction (**Table 3**). Similarly, although no homozygous rs7636836 [T/T] genotypes were observed in the PXG group, the heterozygous rs7636836 [C/T] genotype in *FNDC3B* showed significant association with PXG in men (OR = 2.69, 95% CI = 1.11–6.51, $p = 0.029$) in the co-dominant model that was significant after adjustment for age and sex ($p = 0.026$) but did not survive Bonferroni correction (**Table 4**).

Combined Genotype and Allele Frequency Analysis in PACG and PXG

The combined genotype analysis of the *ABCA1* rs2472493 (A > G) and *FNDC3B* rs7636836 (C > T) polymorphisms did not show any significant effect on PACG susceptibility but did suggest that the presence of GG-CT genotype would increase the risk of

TABLE 1 | Minor allele frequency of rs2472493 in *ABCA1* and rs7636836 in *FNDC3B* genes according to glaucoma types and gender.

Type variant	Cases MAF	Controls MAF	Odds ratio (95%confidence interval)	*p*-value
PACG				
rs2472493[G]				
Total	0.44	0.39	1.17 (0.86–1.61)	0.320
Men	0.42	0.37	1.21 (0.77–1.90)	0.420
Women	0.45	0.42	1.11 (0.71–1.73)	0.660
rs7636836[T]				
Total	0.05	0.05	1.10 (0.54–2.24)	0.790
Men	0.03	0.04	0.79 (0.21–2.95)	0.720
Women	0.07	0.06	1.21 (0.52–2.85)	0.660
PXG				
rs2472493[G]				
Total	0.37	0.39	0.89 (0.63–1.28)	0.554
Men	0.38	0.37	1.05 (0.67–1.65)	0.823
Women	0.34	0.42	0.72 (0.40–1.29)	0.269
rs7636836[T]				
Total	0.07	0.05	1.42 (0.72–2.80)	0.320
Men	0.10	0.04	**2.69 (1.11–6.51)**	**0.029**
Women	0.02	0.06	0.31 (0.04–2.21)	0.150

abbreviations: MAF, minor allele frequency; PACG, primary angle-closure glaucoma; PXG, pseudoexfoliation glaucoma.
Significant odds ratio andp-value in bold.

TABLE 2 | Association of rs2472493 (*ABCA1*) and rs7636836 (*FNDC3B*) polymorphisms with the risk of primary angle-closure glaucoma compared to control under different genetic models.

SNP number	Model	Genotype	Control n (%)	PACG n (%)	Odds ratio (95% confidence interval)	*p*-value	AIC	BIC	*p*-value*
rs2472493	Co-dominant	A/A	97 (39.6)	35 (35.0)	1.00	0.610	420.4	431.9	0.720
		G/A	104 (42.5)	43 (43.0)	1.15 (0.68–1.94)				
		G/G	44 (18.0)	22 (22.0)	1.39 (0.73–2.63)				
	Dominant	A/A	97 (39.6)	35 (35.0)	1.00	0.420	418.8	426.4	0.590
		G/A-G/G	148 (60.4)	65 (65.0)	1.22 (0.75–1.98)				
	Recessive	A/A-G/A	201 (82.0)	78 (78.0)	1.00	0.390	418.7	426.3	0.450
		G/G	44 (18.0)	22 (22.0)	1.29 (0.73–2.29)				
	Over-dominant	A/A-G/G	141 (57.5)	57 (57.0)	1.00	0.930	419.4	427.1	0.930
		G/A	104 (42.5)	43 (43.0)	1.02 (0.64–1.64)				
	Log-additive	---	---	---	1.17 (0.86–1.61)	0.320	418.4	426.1	0.440
rs7636836	Co-dominant	C/C	224 (91.1)	91 (89.2)	1.00	0.370	425.1	436.6	0.370
		C/T	20 (8.1)	11 (10.8)	1.35 (0.62–2.94)				
		T/T	2 (0.8)	0 (0)	0.00 (0.00-NA)				
	Dominant	C/C	224 (91.1)	91 (89.2)	1.00	0.600	424.7	432.4	0.660
		C/T-T/T	22 (8.9)	11 (10.8)	1.23 (0.57–2.64)				
	Recessive	C/C-C/T	244 (99.2)	102 (100.0)	1.00	0.240	423.6	431.3	0.220
		T/T	2 (0.8)	0 (0)	0.00 (0.00-NA)				
	Over-dominant	C/C-T/T	226 (91.9)	91 (89.2)	1.00	0.440	424.4	432.1	0.480
		C/T	20 (8.1)	11 (10.8)	1.37 (0.63–2.96)				
	Log-additive	---	---	---	1.10 (0.54–2.24)	0.790	424.9	432	0.870

**Adjusted for age and sex.*
AIC, Akaike's information criterion; BIC, Bayesian information criterion; PACG, primary angle-closure glaucoma.

PACG by 2.5-fold (OR = 2.55, 95% CI = 0.49–13.30), albeit non-significantly ($p = 0.356$) (**Supplementary Table S3**). In addition, the analysis of synergic effects of *ABCA1* rs2472493 and *FNDC3B* rs7636836 alleles showed that the synergic presence of rs2472493 [G] and rs7636836[T] alleles (G-T) could lead to a significantly ($p = 0.026$) increased risk of PACG (OR = 2.85, 95% CI =

TABLE 3 | Genotype association analysis of polymorphism rs2472493 in *ABCA1* in pseudoexfoliation glaucoma.

Group	Genetic model	Genotype	Control n (%)	PXG n (%)	Odds ratio (95% confidence interval)	*p*-value	AIC	BIC	*p*-value[a]
Overall	Co-dominant	A/A	97 (39.6)	34 (37.8)	1.00	0.200	392.7	404.1	0.400
		G/A	104 (42.5)	46 (51.1)	1.26 (0.75–2.13)				
		G/G	44 (18.0)	10 (11.1)	0.65 (0.29–1.43)				
	Dominant	A/A	97 (39.6)	34 (37.8)	1.00	0.760	393.8	401.4	0.980
		G/A-G/G	148 (60.4)	56 (62.2)	1.08 (0.66–1.77)				
	Recessive	A/A-G/A	201 (82.0)	80 (88.9)	1.00	0.120	391.5	399.1	0.200
		G/G	44 (18.0)	10 (11.1)	0.57 (0.27–1.19)				
	Over-dominant	A/A-G/G	141 (57.5)	44 (48.9)	1.00	0.160	391.9	399.5	0.350
		G/A	104 (42.5)	46 (51.1)	1.42 (0.87–2.30)				
	Log-additive	---	---	---	0.90 (0.64–1.27)	0.560	393.5	401.2	0.530
Men	Co-dominant	A/A	56 (42.4)	19 (32.8)	1.00	0.079	234.7	244.5	0.150
		G/A	55 (41.7)	34 (58.6)	1.82 (0.93–3.57)				
		G/G	21 (15.9)	5 (8.6)	0.70 (0.23–2.12)				
	Dominant	A/A	56 (42.4)	19 (32.8)	1.00	0.210	236.2	242.7	0.460
		G/A-G/G	76 (57.6)	39 (67.2)	1.51 (0.79–2.89)				
	Recessive	A/A-G/A	111 (84.1)	53 (91.4)	1.00	0.160	235.8	242.3	0.140
		G/G	21 (15.9)	5 (8.6)	0.50 (0.18–1.40)				
	Over-dominant	A/A-G/G	77 (58.3)	24 (41.4)	1.00	**0.031**	233.1	239.6	0.086
		G/A	55 (41.7)	34 (58.6)	**1.98 (1.06–3.71)**				
	Log-additive	---	---	---	1.05 (0.67–1.65)	0.820	237.7	244.2	0.830
Women	Co-dominant	A/A	41 (36.3)	15 (46.9)	1.00	0.550	157.9	166.8	0.740
		G/A	49 (43.4)	12 (37.5)	0.67 (0.28–1.59)				
		G/G	23 (20.4)	5 (15.6)	0.59 (0.19–1.85)				
	Dominant	A/A	41 (36.3)	15 (46.9)	1.00	0.280	155.9	161.8	0.450
		G/A-G/G	72 (63.7)	17 (53.1)	0.65 (0.29–1.43)				
	Recessive	A/A-G/A	90 (79.7)	27 (84.4)	1.00	0.540	156.7	162.6	0.900
		G/G	23 (20.4)	5 (15.6)	0.72 (0.25–2.09)				
	Over-dominant	A/A-G/G	64 (56.6)	20 (62.5)	1.00	0.550	156.7	162.7	0.510
		G/A	49 (43.4)	12 (37.5)	0.78 (0.35–1.76)				
	Log-additive	---	---	---	0.75 (0.43–1.30)	0.290	156.0	161.9	0.560

p-value adjusted for age and sex in the overall group and by age in men and women groups.

***Best-fit model* p-*value*.**

abbreviations: AIC, Akaike's information criterion; BIC, Bayesian information criterion; OR (95% CI), Odds ratio (95% confidence interval); PXG, pseudoexfoliation glaucoma.

Significanct odds ratio and p-*value in bold.*

Bonnferoni corrected p-*value is 0.01.*

1.09–7.46) (**Supplementary Table S4**). The analysis, however, did not account for multiple testing corrections. In contrast, combined genotype and allele frequency analysis in PXG yielded no significant result (**Supplementary Tables S5, S6**).

Regression Analysis and Effect of Genotypes on Clinical Indices of Glaucoma

A binary logistic regression analysis was performed to detect the effect of age, sex, and polymorphisms rs2472493 in *ABCA1* and rs7636836 in *FNDC3B* on disease outcomes. None of these factors were found to have any significant effect on PACG and PXG outcomes. However, age remained a significant predictor of PXG (**Supplementary Table S7**). Furthermore, the genotype effect of rs2472493 (*ABCA1*) and rs7636836 (*FNDC3B*) polymorphisms on IOP, cup/disc ratio, and the number of antiglaucoma medications in the PACG and PXG patient groups were also examined. These phenotypes are clinical indicators related to disease severity. The analysis revealed no significant genotype effect on any of these clinical markers in both the PACG and PXG patient groups (**Supplementary Figure S2**).

DISCUSSION

Glaucoma is a complex polygenic disorder affected by multiple genetic and environmental factors. Previously, several genome-wide association studies have identified numerous genetic polymorphisms and susceptibility loci in different populations worldwide, few of which have been unique to specific ethnic groups (Zukerman et al., 2021). However, the genetic etiology of glaucoma in middle-eastern population is still lacking and therefore warrants further studies. Given the overlapping clinical manifestations and common genetic

TABLE 4 | Genotype association analysis of rs7636836 variant in *FNDC3B* in pseudoexfoliation glaucoma.

Group	Genetic model	Genotype	Control n (%)	PXG n (%)	Odds ratio (95% confidence interval)	*p*-value	AIC	BIC	*p*-value*
Overall	Co-dominant	C/C	224 (91.1)	81 (86.2)	1.00	0.170	403.3	414.8	0.280
		C/T	20 (8.1)	13 (13.8)	1.80 (0.85–3.78)				
		T/T	2 (0.8)	0 (0)	0.00 (0.00-NA)				
	Dominant	C/C	224 (91.1)	81 (86.2)	1.00	0.200	403.3	410.9	0.190
		C/T-T/T	22 (8.9)	13 (13.8)	1.63 (0.79–3.40)				
	Recessive	C/C-C/T	244 (99.2)	94 (100.0)	1.00	0.250	403.6	411.3	0.460
		T/T	2 (0.8)	0 (0)	0.00 (0.00-NA)				
	Over-dominant	C/C-T/T	226 (91.9)	81 (86.2)	1.00	0.120	402.6	410.2	0.150
		C/T	20 (8.1)	13 (13.8)	1.81 (0.86–3.81)				
	Log-additive	---	---	---	1.42 (0.72–2.80)	0.320	403.9	411.6	0.270
Men	--	C/C	121 (91.7)	49 (80.3)	1.00	**0.029**	240.0	246.6	**0.026**
		C/T	11 (8.3)	12 (19.7)	**2.69 (1.11–6.51)**				
		T/T	0	0	-				
Women	Co-dominant	C/C	103 (90.3)	32 (97.0)	1.00	0.330	160.4	169.3	0.500
		C/T	9 (7.9)	1 (3.0)	0.36 (0.04–2.93)				
		T/T	2 (1.8)	0 (0)	0.00 (0.00-NA)				
	Dominant	C/C	103 (90.3)	32 (97.0)	1.00	0.180	158.7	164.7	0.270
		C/T-T/T	11 (9.7)	1 (3.0)	0.29 (0.04–2.35)				
	Recessive	C/C-C/T	112 (98.2)	33 (100.0)	1.00	0.310	159.5	165.5	0.490
		T/T	2 (1.8)	0 (0)	0.00 (0.00-NA)				
	Over-dominant	C/C-T/T	105 (92.1)	32 (97.0)	1.00	0.290	159.4	165.4	0.350
		C/T	9 (7.9)	1 (3.0)	0.36 (0.04–2.99)				
	Log-additive	---	---	---	0.31 (0.04–2.21)	0.150	158.5	164.5	0.250

**p-value adjusted for age and sex in the overall group and by age in men and women groups.*

Note: Significant odds ratio and p-value in bold. Bonferroni corrected p-value is 0.01.

abbreviations: AIC, Akaike's information criterion; BIC, Bayesian information criterion; PXG, pseudoexfoliation glaucoma.

variants reported among glaucoma types, we investigated the association of two POAG-related gene polymorphisms, rs2472493 in *ABCA1* gene and rs7636836 near *FNDC3B*, in the PACG and PXG patient cohort of Saudi origin.

In our study, the MAF of rs2472493 in *ABCA1* was 0.44 and 0.37 in PACG and PXG, respectively, and were comparable to those in controls (0.39) and thus non-significant. The allele frequencies were similar to those reported in the Han Chinese and Uygur Chinese population of PACG (0.45) and PXG (0.40) patients, respectively (Luo et al., 2015). Likewise, the MAFs were comparable to the Hispanics (0.37), non-Hispanics (0.42), and African American (0.35) POAG subjects (Choquet et al., 2018), but lower than the East-Asians (0.56) (Choquet et al., 2018) and the European (0.51) POAG patients (Gharahkhani et al., 2014) highlighting slight ethnic and glaucoma type variability.

Previously, SNP rs2472493 in *ABCA1* was associated with POAG in the genome-wide meta-analysis of 18 population cohorts from the International Glaucoma Genetics Consortium (Hysi et al., 2014). Similar genome-wide findings were reported by Gharahkhani et al., in the Australian cohort (Gharahkhani et al., 2014) and by Chen et al., in POAG patients from Southern China (Chen et al., 2014). Thus, multiple population studies indicated that the ABCA1 gene might play a crucial role in POAG pathogenesis. In contrast, negative *ABCA1* gene associations have been reported in the Han Chinese cohort of 1,311 healthy controls and 1122 PACG patients (Luo et al., 2015), and in the 52 Jordanian Arab glaucoma patients (POAG and congenital) and 96 healthy individuals investigated for the *ABCA1* rs2472493 variant by Alkhatib et al. (2019). Although our study did not replicate the findings in the PXG and PACG patient cohort of Saudi origin, we observed a significant association of *ABCA1* rs2472493 polymorphism among men in the PXG cohort. However, there are no published reports of this variant being examined in PXG.

ABCA1 belongs to a large superfamily of ABC transmembrane transporters and is best known for its role in cholesterol efflux to lipid-free apolipoprotein AI and apolipoprotein E (Wang and Smith, 2014). ABCA1 is expressed in all the major tissues of the eye, including the trabecular meshwork, Schlemm's canal endothelial cells, RGCs, and optic nerve that are primarily involved in glaucoma (Chen et al., 2014). However, the exact mechanism(s) by which ABCA1 may be involved in glaucoma pathogenesis is still unclear. ABCA1 was demonstrated to inhibit ocular inflammation via activation of liver X-receptor in an experimental model of autoimmune uveitis (Yang et al., 2014). Using the glaucoma model, Li et al. demonstrated that ABCA1 was related to RGC death (Li et al., 2018). These studies suggest that ABCA1 may have a significant role in eye research. Likewise, using the Encyclopedia of DNA Elements (ENCODE) project data and Genevar database, Gharahkhani and colleagues, reported that the polymorphism

rs2472493 located upstream of *ABCA1* is an expression quantitative trait locus (eQTL) in lymphoblastoid cell lines that might alter the motif sequences for proteins such as FOXJ2 and SIX5 (Gharahkhani et al., 2014). Also, rs2472493 was found to be in high linkage disequilibrium with polymorphism rs2472494 near *ABCA1* that alters the regulatory motif for binding of *PAX6*, a gene involved in eye development. The authors thereby predicted a possible regulatory role for this polymorphism in gene expression in a pathway similar to that of rs2472494 variant near *ABCA1* gene (Gharahkhani et al., 2014). However, the exact mechanism(s) by which rs2472493 polymorphism in *ABCA1* might increase PXG risk in men is unknown. The effect of gender, gene-gene, and gene-environment interactions on *ABCA1* gene polymorphisms in lipid and lipoprotein metabolism have been well documented (Junyent et al., 2010; Coban et al., 2014; Shi et al., 2021). The *ABCA1* polymorphism might plausibly modulate the risk of PXG among men in a similar manner.

FNDC3B (also known as *FAD104*) is a known regulator of adipogenesis (Tominaga et al., 2004). *FNDC3B* codes for an extracellular matrix protein that has a vital role in cell adhesion and growth signaling pathways, including TGFβ, and Wnt/β-catenin signaling (Nishizuka et al., 2009; Goto et al., 2017; Li et al., 2020) all of which have been strongly implicated in glaucoma pathogenesis (Prendes et al., 2013; Zhong et al., 2013; Webber et al., 2018). Furthermore, *FNDC3B* is expressed in all the primary eye tissues relevant to glaucoma (Li et al., 2015; Shiga et al., 2018).

The variant rs7636836 in *FNDC3B* was one of the novel loci associated with POAG in a two-stage genome-wide study consisting of 7,378 Japanese POAG cases and 36,385 controls conducted by Shiga et al. (2018). However, further validation in Singapore Chinese, European, and Africans did not show any significant association (Shiga et al., 2018). In our study cohort, the MAF of rs7636836 in *FNDC3B* was 0.05 and 0.07 in PACG and PXG, respectively. The frequency distribution was similar to European (0.06) but lower than the Japanese (0.40) and Singaporean Chinese (0.21) POAG subjects reported by Shiga et al. (2018). Our data showed no significant allelic and genotype association between rs7636836 in *FNDC3B* and PACG/PXG. However, in men, a modest allelic and genotype association of rs7636836 in *FNDC3B* was observed in PXG. The potential mechanism(s) by which rs7636836 in *FNDC3B* would modulate the risk of PXG in men is unclear but could possibly be hormonal (androgen) related via Wnt signaling which can be stimulated by *FNDC3B* (Li et al., 2020). There is evidence for crosstalk between androgen receptor and Wnt/ß-catenin signaling pathway (Mumford et al., 2018). The androgen receptors are expressed in ocular tissues (Tachibana et al., 2000) and Wnt signaling is strongly implicated in the maintenance of glaucomatous trabecular meshwork (Dhamodaran et al., 2020). To the best of our knowledge, there are no published reports of studies evaluating this polymorphism in PACG and PXG patients.

Gene-gene and gene-environmental interactions have been suggested to play an essential role in the pathogenesis of complex human diseases and highlight the possible contribution of genetic background and environmental triggers in disease development and progression (Marchini et al., 2005; Pan, 2008; Brossard et al., 2015). Glaucoma is also a complex polygenic disease with no clear inheritance pattern, and similar mechanisms may exist to influence the disease outcomes (Zakharov et al., 2013). Interestingly, a combined allelic and genotype analysis of rs2472493 in *ABCA1* and rs7636836 in *FNDC3B* showed that G-T allele haplotype of *ABCA1* and *FNDC3B* was associated with a significantly increased risk of PACG. Although it is difficult to ascertain whether the risk observed in our study is attributable to a real haplotype effect or probably reflects a linkage with other variant(s) not included in this study, the possible role of rs2472493 in *ABCA1* and rs7636836 in *FNDC3B* in PACG cannot be completely ruled out and would need further research in a larger cohort.

Polymorphisms in *ABCA1* and *FNDC3B* have also been shown to influence IOP (Hysi et al., 2014). A recent study showed that ABCA1 regulated IOP by modulating caveolin-1, nitric oxide/endothelial nitric oxide synthase signaling pathway (Hu et al., 2020). However, the analysis of polymorphisms effect on clinical endophenotypes of PACG and PXG, such as IOP and cup/disc ratio in our cohort, showed no significant association.

Thus, our results show that rs2472493 in *ABCA1* and rs7636836 in *FNDC3B* may not have a major direct role in PACG and PXG in this ethnic group. However, the association of rs7636836 in *FNDC3B* and rs2472493 in *ABCA1* observed among PXG men; and that of G-T haplotype in PACG suggests that they may have a significant indirect role (possibly via epistatic interaction(s)) in PXG and PACG. But since the study was performed in a relatively small sample size and does not provide any mechanistic evidence, the results would require a cautious interpretation. Based on the observed allele frequencies, the study had an estimated power of >0.9 per allele for the *ABCA1* variant but was underpowered (0.6 per allele) for the *FNDC3B* variant to detect a relative risk of 2.0 with an alpha type I error of 0.05. Thus, the possibility of chance association cannot be ruled out and further emphasizes the need for replication in a large sample cohort potentially with age and gender-matched controls to confirm these findings.

In conclusion, our results suggest that the polymorphisms rs2472493 in ABCA1 and rs7636836 in FNDC3B genes may be associated with PXG among men, and a G-T allelic combination may confer an increased risk of PACG in the middle-eastern Saudi cohort. However, further investigations in larger population-based samples and different ethnicity are needed to draw definite conclusions and validate these findings. Moreover, considering the genetic heterogeneity of glaucoma *per se*, the plausible involvement of gene-gene and/or gene–environmental interactions must be important considerations for future research.

DATA AVAILABILITY STATEMENT

The original contributions presented in the study are included in the article/**Supplementary Material**, further inquiries can be directed to the corresponding author.

ETHICS STATEMENT

The studies involving human participants were reviewed and approved by The study involving human subjects was approved by the Institutional review board (IRB) and the research ethics committee of the College of Medicine, King Saud University (IRB

protocol# 08–657). The patients/participants provided their written informed consent to participate in this study.

AUTHOR CONTRIBUTIONS

AK: Conceptualization, Analysis, Investigation, Project administration, Writing—original draft, review and editing; TS, TA: Investigation, Methodology, Writing—review and editing; EO, FA: Data curation, Investigation, Writing—review and editing; GL: Data interpretation, Investigation, Writing—review and editing; SAA-O: Conceptualization, Data curation, Investigation, Project administration, Writing—review and editing. All authors read and approved the final manuscript.

FUNDING

This work was supported by King Saud University through the Vice Deanship of Scientific Research Chair and Glaucoma Research Chair in Ophthalmology. The funders had no role in study design, data collection and analysis, decision to publish, or manuscript preparation.

ACKNOWLEDGMENTS

The authors would like to thank the Vice Deanship of Scientific Research Chair, Glaucoma Research Chair in Ophthalmology at King Saud University, for their support. The authors would also like to thank Mr. Abdulrahman Al-Mosa for his clinical assistance in the study.

SUPPLEMENTARY MATERIAL

The Supplementary Material for this article can be found online at: https://www.frontiersin.org/articles/10.3389/fgene.2022.877174/full#supplementary-material

REFERENCES

Abu-Amero, K. K., Osman, E. A., Dewedar, A. S., Schmidt, S., Allingham, R. R., and Al-Obeidan, S. A. (2010). Analysis of LOXL1 Polymorphisms in a Saudi Arabian Population with Pseudoexfoliation Glaucoma. *Mol. Vis.* 16, 2805–2810. [pii].

Abu-Amero, K. K., Azad, T. A., Mousa, A., Osman, E. A., Sultan, T., and Al-Obeidan, S. A. (2013). A Catalase Promoter Variant Rs1001179 Is Associated with Visual Acuity but Not with Primary Angle Closure Glaucoma in Saudi Patients. *BMC Med. Genet.* 14, 84. doi:10.1186/1471-2350-14-84

Abu-Amero, K. K., Azad, T. A., Mousa, A., Osman, E. A., Sultan, T., and Al-Obeidan, S. A. (2015). Association of SOD2 Mutation (c.47T > C) with Various Primary Angle Closure Glaucoma Clinical Indices. *Ophthalmic Genet.* 36 (2), 180–183. doi:10.3109/13816810.2013.838276

Al Obeidan, S. A., Dewedar, A., Osman, E. A., and Mousa, A. (2011). The Profile of Glaucoma in a Tertiary Ophthalmic University Center in Riyadh, Saudi Arabia. *Saudi J. Ophthalmol.* 25 (4), 373–379. doi:10.1016/j.sjopt.2011.09.001

Alkhatib, R., Abudhaim, N., Al-Eitan, L., Abdo, N., Alqudah, A., and Aman, H. (2019). Genetic Analysis of ABCA1 Gene of Primary Glaucoma in Jordanian Arab Population. *Tacg* Vol 12, 181–189. doi:10.2147/TACG.S213818

Aung, T., Chan, A. S., and Khor, C.-C. (2018). Genetics of Exfoliation Syndrome. *J. Glaucoma* 27 (Suppl. 1), S12–S14. doi:10.1097/IJG.0000000000000928

Awadalla, M. S., Thapa, S. S., Hewitt, A. W., Burdon, K. P., and Craig, J. E. (2013). Association of Genetic Variants with Primary Angle Closure Glaucoma in Two Different Populations. *PLoS One* 8 (6), e67903. doi:10.1371/journal.pone.0067903

Brossard, M., Fang, S., Vaysse, A., Wei, Q., Chen, W. V., Mohamdi, H., et al. (2015). Integrated Pathway and Epistasis Analysis Reveals Interactive Effect of Genetic Variants atTERF1andAFAP1L2loci on Melanoma Risk. *Int. J. Cancer* 137 (8), 1901–1909. doi:10.1002/ijc.29570

Chakrabarti, S., Devi, K. R., Komatireddy, S., Kaur, K., Parikh, R. S., Mandal, A. K., et al. (2007). Glaucoma-AssociatedCYP1B1Mutations Share Similar Haplotype Backgrounds in POAG and PACG Phenotypes. *Invest. Ophthalmol. Vis. Sci.* 48 (12), 5439–5444. [pii]. doi:10.1167/iovs.07-0629

Chan, E. W. e., Li, X., Tham, Y.-C., Liao, J., Wong, T. Y., Aung, T., et al. (2016). Glaucoma in Asia: Regional Prevalence Variations and Future Projections. *Br. J. Ophthalmol.* 100 (1), 78–85. doi:10.1136/bjophthalmol-2014-306102

Chen, Y., Lin, Y., Vithana, E. N., Jia, L., Zuo, X., Wong, T. Y., et al. (2014). Common Variants Near ABCA1 and in PMM2 Are Associated with Primary Open-Angle Glaucoma. *Nat. Genet.* 46 (10), 1115–1119. doi:10.1038/ng.3078

Choquet, H., Paylakhi, S., Kneeland, S. C., Thai, K. K., Hoffmann, T. J., Yin, J., et al. (2018). A Multiethnic Genome-wide Association Study of Primary Open-Angle Glaucoma Identifies Novel Risk Loci. *Nat. Commun.* 9 (1), 2278. doi:10.1038/s41467-018-04555-4

Coban, N., Onat, A., Komurcu Bayrak, E., Gulec, C., Can, G., and Erginel Unaltuna, N. (2013). Gender Specific Association of ABCA1 Gene R219K Variant in Coronary Disease Risk through Interactions with Serum Triglyceride Elevation in Turkish Adults. *Anadolu Kardiyol. Derg.* 14 (1), 18–25. doi:10.5152/akd.2013.234

Dai, X., Nie, S., Ke, T., Liu, J., Wang, Q., and Liu, M. (2008). Two Variants in MYOC and CYP1B1 Genes in a Chinese Family with Primary Angle-Closure Glaucoma. *Zhonghua Yi Xue Yi Chuan Xue Za Zhi* 25 (5), 493–496. 940625107 [pii].

Dhamodaran, K., Baidouri, H., Sandoval, L., and Raghunathan, V. (2020). Wnt Activation after Inhibition Restores Trabecular Meshwork Cells toward a Normal Phenotype. *Invest. Ophthalmol. Vis. Sci.* 61 (6), 30. doi:10.1167/iovs.61.6.30

Eliseeva, N., Ponomarenko, I., Reshetnikov, E., Dvornyk, V., and Churnosov, M. (2021). LOXL1 Gene Polymorphism Candidates for Exfoliation Glaucoma Are Also Associated with a Risk for Primary Open-Angle Glaucoma in a Caucasian Population from Central Russia. *Mol. Vis.* 27, 262–269. [pii].

Gharahkhani, P., Burdon, K. P., Burdon, K. P., Fogarty, R., Sharma, S., Hewitt, A. W., et al. (2014). Common Variants Near ABCA1, AFAP1 and GMDS Confer Risk of Primary Open-Angle Glaucoma. *Nat. Genet.* 46 (10), 1120–1125. doi:10.1038/ng.3079

Goto, M., Osada, S., Imagawa, M., and Nishizuka, M. (2017). FAD104, a Regulator of Adipogenesis, Is a Novel Suppressor of TGF-β-Mediated EMT in Cervical Cancer Cells. *Sci. Rep.* 7 (1), 16365. doi:10.1038/s41598-017-16555-3

Howell, G. R., Macalinao, D. G., Sousa, G. L., Walden, M., Soto, I., Kneeland, S. C., et al. (2011). Molecular Clustering Identifies Complement and Endothelin Induction as Early Events in a Mouse Model of Glaucoma. *J. Clin. Invest.* 121 (4), 1429–1444. doi:10.1172/jci44646

Hu, C., Niu, L., Li, L., Song, M., Zhang, Y., Lei, Y., et al. (2020). ABCA1 Regulates IOP by Modulating Cav1/eNOS/NO Signaling Pathway. *Invest. Ophthalmol. Vis. Sci.* 61 (5), 33. doi:10.1167/iovs.61.5.33

Hysi, P. G., Cheng, C. Y., Springelkamp, H., Macgregor, S., Bailey, J. N. C., Wojciechowski, R., et al. (2014). Genome-wide Analysis of Multi-Ancestry Cohorts Identifies New Loci Influencing Intraocular Pressure and Susceptibility to Glaucoma. *Nat. Genet.* 46 (10), 1126–1130. doi:10.1038/ng.3087

Junyent, M., Tucker, K. L., Smith, C. E., Lane, J. M., Mattei, J., Lai, C. Q., et al. (2010). The Effects of ABCG5/G8 Polymorphisms on HDL-Cholesterol Concentrations Depend on ABCA1 Genetic Variants in the Boston Puerto Rican Health Study. *Nutr. Metabolism Cardiovasc. Dis.* 20 (8), 558–566. doi:10.1016/j.numecd.2009.05.005

Kondkar, A. A., Sultan, T., Alobaidan, A. S., Azad, T. A., Osman, E. A., Almobarak, F. A., et al. (2021). Association Analysis of Variants Rs35934224 in TXNRD2 and Rs6478746 in LMX1B in Primary Angle-Closure and Pseudoexfoliation Glaucoma. *Eur. J. Ophthalmol.* 11206721211042547, 112067212110425. doi:10.1177/11206721211042547

Kondkar, A. A., Sultan, T., Azad, T. A., Osman, E. A., Almobarak, F. A., and Al-Obeidan, S. A. (2020). Association Analysis of Polymorphisms Rs12997 in ACVR1 and Rs1043784 in BMP6 Genes Involved in Bone Morphogenic Protein Signaling Pathway in Primary Angle-Closure and Pseudoexfoliation Glaucoma Patients of Saudi Origin. *BMC Med. Genet.* 21 (1), 145. doi:10.1186/s12881-020-01076-0

Kondkar, A., Azad, T. A., Almobarak, F., Kalantan, H., Al-Obeidan, S., and Abu-Amero, K. (2018). Elevated Levels of Plasma Tumor Necrosis Factor Alpha in Patients with Pseudoexfoliation Glaucoma. *Opth* Vol 12, 153–159. doi:10.2147/OPTH.S155168

Li, L., Xu, L., Chen, W., Li, X., Xia, Q., Zheng, L., et al. (2018). Reduced Annexin A1 Secretion by ABCA1 Causes Retinal Inflammation and Ganglion Cell Apoptosis in a Murine Glaucoma Model. *Front. Cell. Neurosci.* 12, 347. doi:10.3389/fncel.2018.00347

Li, Y. Q., Chen, Y., Xu, Y. F., He, Q. M., Yang, X. J., Li, Y. Q., et al. (2020). FNDC3B 3′-UTR Shortening Escapes from microRNA-mediated Gene Repression and Promotes Nasopharyngeal Carcinoma Progression. *Cancer Sci.* 111 (6), 1991–2003. doi:10.1111/cas.14394

Li, Z., Allingham, R. R., Nakano, M., Jia, L., Chen, Y., Ikeda, Y., et al. (2015). A Common Variant Near TGFBR3 Is Associated with Primary Open Angle Glaucoma. *Hum. Mol. Genet.* 24 (13), 3880–3892. doi:10.1093/hmg/ddv128

Luo, H., Chen, Y., Ye, Z., Sun, X., Shi, Y., Luo, Q., et al. (2015). Evaluation of the Association between Common Genetic Variants Near theABCA1Gene and Primary Angle Closure Glaucoma in a Han Chinese Population. *Invest. Ophthalmol. Vis. Sci.* 56 (11), 6248–6254. doi:10.1167/iovs.15-16741

Marchini, J., Donnelly, P., and Cardon, L. R. (2005). Genome-wide Strategies for Detecting Multiple Loci that Influence Complex Diseases. *Nat. Genet.* 37 (4), 413–417. ng1537 [pii]. doi:10.1038/ng1537

Mumford, P. W., Romero, M. A., Mao, X., Mobley, C. B., Kephart, W. C., Haun, C. T., et al. (20181985). Cross Talk between Androgen and Wnt Signaling Potentially Contributes to Age-Related Skeletal Muscle Atrophy in Rats. *J. Appl. Physiology* 125 (2), 486–494. doi:10.1152/japplphysiol.00768.2017

Nishizuka, M., Kishimoto, K., Kato, A., Ikawa, M., Okabe, M., Sato, R., et al. (2009). Disruption of the Novel Gene Fad104 Causes Rapid Postnatal Death and Attenuation of Cell Proliferation, Adhesion, Spreading and Migration. *Exp. Cell Res.* 315 (5), 809–819. doi:10.1016/j.yexcr.2008.12.013

Pan, W. (2008). Network-based Model Weighting to Detect Multiple Loci Influencing Complex Diseases. *Hum. Genet.* 124 (3), 225–234. doi:10.1007/s00439-008-0545-1

Prendes, M. A., Harris, A., Wirostko, B. M., Gerber, A. L., and Siesky, B. (2013). The Role of Transforming Growth Factor β in Glaucoma and the Therapeutic Implications. *Br. J. Ophthalmol.* 97 (6), 680–686. doi:10.1136/bjophthalmol-2011-301132

Shi, Z., Tian, Y., Zhao, Z., Wu, Y., Hu, X., Li, J., et al. (2021). Association between the ABCA1 (R219K) Polymorphism and Lipid Profiles: a Meta-Analysis. *Sci. Rep.* 11 (1), 21718. doi:10.1038/s41598-021-00961-9

Shiga, Y., Akiyama, M., Nishiguchi, K. M., Sato, K., Shimozawa, N., Takahashi, A., et al. (2018). Genome-wide Association Study Identifies Seven Novel Susceptibility Loci for Primary Open-Angle Glaucoma. *Hum. Mol. Genet.* 27 (8), 1486–1496. doi:10.1093/hmg/ddy053

Tachibana, M., Kobayashi, Y., Kasukabe, T., Kawajiri, K., and Matsushima, Y. (2000). Expression of Androgen Receptor in Mouse Eye Tissues. *Invest. Ophthalmol. Vis. Sci.* 41 (1), 64–66.

Tominaga, K., Kondo, C., Johmura, Y., Nishizuka, M., and Imagawa, M. (2004). The Novel Gene Fad104, Containing a Fibronectin Type III Domain, Has a Significant Role in Adipogenesis. *FEBS Lett.* 577 (1-2), 49–54. doi:10.1016/j.febslet.2004.09.062

Vazquez, L. E., and Lee, R. K. (2014). Genomic and Proteomic Pathophysiology of Pseudoexfoliation Glaucoma. *Int. Ophthalmol. Clin.* 54 (4), 1–13. doi:10.1097/IIO.0000000000000047

Wang, S., and Smith, J. D. (2014). ABCA1 and Nascent HDL Biogenesis. *Biofactors* 40 (6), 547–554. doi:10.1002/biof.1187

Webber, H. C., Bermudez, J. Y., Millar, J. C., Mao, W., and Clark, A. F. (2018). The Role of Wnt/β-Catenin Signaling and K-Cadherin in the Regulation of Intraocular Pressure. *Invest. Ophthalmol. Vis. Sci.* 59 (3), 1454–1466. doi:10.1167/iovs.17-21964

Weinreb, R. N., Aung, T., and Medeiros, F. A. (2014). The Pathophysiology and Treatment of Glaucoma. *JAMA* 311 (18), 1901–1911. doi:10.1001/jama.2014.3192

Yang, H., Zheng, S., Qiu, Y., Yang, Y., Wang, C., Yang, P., et al. (2014). Activation of Liver X Receptor Alleviates Ocular Inflammation in Experimental Autoimmune Uveitis. *Invest. Ophthalmol. Vis. Sci.* 55 (4), 2795–2804. doi:10.1167/iovs.13-13323

Zakharov, S., Wong, T., Aung, T., Vithana, E., Khor, C., Salim, A., et al. (2013). Combined Genotype and Haplotype Tests for Region-Based Association Studies. *BMC Genomics* 14, 569. doi:10.1186/1471-2164-14-569

Zhong, Y., Wang, J., and Luo, X. (2013). Integrins in Trabecular Meshwork and Optic Nerve Head: Possible Association with the Pathogenesis of Glaucoma. *BioMed Res. Int.* 2013, 1–8. doi:10.1155/2013/202905

Zukerman, R., Harris, A., Verticchio Vercellin, A., Siesky, B., Pasquale, L. R., and Ciulla, T. A. (2021). Molecular Genetics of Glaucoma: Subtype and Ethnicity Considerations. *Genes* 12 (1), 55. doi:10.3390/genes12010055

Conflict of Interest: The authors declare that the research was conducted in the absence of any commercial or financial relationships that could be construed as a potential conflict of interest.

Publisher's Note: All claims expressed in this article are solely those of the authors and do not necessarily represent those of their affiliated organizations, or those of the publisher, the editors and the reviewers. Any product that may be evaluated in this article, or claim that may be made by its manufacturer, is not guaranteed or endorsed by the publisher.

frontiers | Frontiers in Genetics

ORIGINAL RESEARCH
published: 25 July 2022
doi: 10.3389/fgene.2022.845081

Compound Heterozygous Variants of the *CPAMD8* Gene Co-Segregating in Two Chinese Pedigrees With Pigment Dispersion Syndrome/Pigmentary Glaucoma

*Junkai Tan[1†], Liuzhi Zeng[2†], Yun Wang[3†], Guo Liu[4†], Longxiang Huang[5], Defu Chen[6], Xizhen Wang[3], Ning Fan[3], Yu He[2] and Xuyang Liu[1,7]**

[1]Xiamen Eye Center, Xiamen University, Xiamen, China, [2]Department of Ophthalmology, Chengdu First People's Hospital, Chengdu, China, [3]Shenzhen Eye Hospital, Shenzhen Eye Institute, Jinan University, Shenzhen, China, [4]Sichuan Provincial Key Laboratory for Human Disease Gene Study, Sichuan Provincial People's Hospital, University of Electronic Science and Technology of China, Chengdu, China, [5]Department of Ophthalmology, The First Affiliated Hospital of Fujian Medical University, Fuzhou, China, [6]School of Ophthalmology and Optometry, The Eye Hospital, Wenzhou Medical University, Wenzhou, China, [7]Department of Ophthalmology, Shenzhen People's Hospital, The 2nd Clinical Medical College, Jinan University, Shenzhen, China

The molecular mechanisms underlying the pathogenesis of pigment dispersion syndrome and pigmentary glaucoma remain unclear. In pedigree-based studies, familial aggregation and recurrences in relatives suggest a strong genetic basis for pigmentary glaucoma. In this study, we aimed to identify the genetic background of two Chinese pedigrees with pigmentary glaucoma. All members of these two pedigrees who enrolled in the study underwent a comprehensive ophthalmologic examination, and genomic DNA was extracted from peripheral venous blood samples. Whole-exome sequencing and candidate gene verifications were performed to identify the disease-causing variants; in addition, screening of the *CPAMD8* gene was performed on 38 patients of sporadic pigmentary glaucoma. Changes in the structure and function of abnormal proteins caused by gene variants were analyzed with a bioinformatics assessment. Pigmentary glaucoma was identified in a total of five patients from the two pedigrees, as were compound heterozygous variants of the *CPAMD8* gene. No signs of pigmentary glaucoma were found in carriers of monoallelic *CPAMD8* variant/variants. All four variants were inherited in an autosomal recessive mode. In addition to the 38 patients of sporadic pigmentary glaucoma, 13 variants of the *CPAMD8* gene were identified in 11 patients. This study reported a possible association between *CPAMD8* variants and pigment dispersion syndrome/pigmentary glaucoma.

Keywords: CPAMD8, pigmentary glaucoma, autosomal recessive inheritance, pedigree, compound heterozygous variant

OPEN ACCESS

Edited by:
Yang Sun,
Stanford University, United States

Reviewed by:
Bo Lei,
Henan Provincial People's Hospital, China
Jiamin Ouyang,
Sun Yat-sen University, China
Shiwani Sharma,
South Australian Health and Medical Research Institute (SAHMRI), Australia

****Correspondence:***
Xuyang Liu
xliu1213@126.com

[†]These authors have contributed equally to this work

Specialty section:
This article was submitted to Genetics of Common and Rare Diseases, a section of the journal Frontiers in Genetics

Received: *29 December 2021*
Accepted: *20 June 2022*
Published: *25 July 2022*

Citation:
Tan J, Zeng L, Wang Y, Liu G, Huang L, Chen D, Wang X, Fan N, He Y and Liu X (2022) Compound Heterozygous Variants of the CPAMD8 Gene Co-Segregating in Two Chinese Pedigrees With Pigment Dispersion Syndrome/Pigmentary Glaucoma. Front. Genet. 13:845081. doi: 10.3389/fgene.2022.845081

INTRODUCTION

Pigment dispersion syndrome (PDS) is a relatively rare ocular disorder that affects mostly males, especially in Caucasian countries (Niyadurupola and Broadway, 2008). PDS can lead to pigmentary glaucoma (PG), a type of open-angle glaucoma secondary to excessive deposition of pigment in the trabecular meshwork (TM). The deposited pigment blocks the conventional outflow pathway, leading to an increased resistance to aqueous humor outflow and elevated intraocular pressure (IOP). It is generally believed that the dispersed pigment originates from the shedding of the pigment epithelium located on the posterior surface of the iris (Scuderi et al., 2019). In a prospective study, the criteria for PDS were set as two of three signs: Krukenberg's spindle, iris transillumination defects, and/or TM pigmentation; in contrast, PG was diagnosed when two of three signs were seen in PDS eyes: IOP greater than 21 mmHg, glaucomatous optic nerve damage, and/or glaucomatous visual field (VF) loss (Tandon et al., 2019). However, iris transillumination defects were not common in East Asian populations probably because these defects cannot be detected in darkly pigmented irides of East Asian patients *via* slit-lamp examination (Qing et al., 2009). To date, the molecular mechanisms underlying the pathogenesis of PDS and PG remain unclear. In pedigree-based studies, familial aggregation and recurrences in relatives suggest a strong genetic basis for PG (Siddiqui et al., 2003). In addition, variants of the premelanosome (*PMEL*) gene were associated with heritable patients of PDS/PG (Lahola-Chomiak et al., 2019), and variants of the pigment dispersion–associated genes in animals, such as *Dct*, *Tyrp1*, and *Lyst*, mimicked some clinical features of PDS and PG (Chang et al., 1999; Anderson et al., 2008; Trantow et al., 2009); however, no studies have found a causal relationship between any variants within their human orthologs and PG. Therefore, it is likely that there are other genes involved in the pathogenesis of PDS/PG. Posterior bowing of the iris is frequently present in PDS/PG, causing iridozonular contact, zonular rubbing, and pigment dispersion, which results in excessive pigment deposition in the anterior chamber angle tissues, especially the TM, as aqueous humor and dispersed pigment follow the normal aqueous humor dynamics through the outflow pathway (Lyons and Amram, 2019). Giardina et al. identified the haplotypes of the *LOXL1* gene in a cohort of patients with PDS/PG and validated the pathogenic effects of the *LOXL1* variant in an animal model. They also speculated that *LOXL1* variant–induced defects of the iris stroma are the reason for iris concavity, a phenotype often present in PDS/PG patients (Giardina et al., 2014). However, another study showed that there was no correlation between *LOXL1* and PDS/PG (Rao et al., 2008). Hence, the specific pathogenic factor and mechanism of PDS/PG remain poorly understood. Nevertheless, these studies indicate that genetic factors could be associated with an increased risk of developing PDS/PG.

The human *CPAMD8* gene (complement 3- and pregnancy zone protein–like, alpha-2-macroglobulin domain–containing 8; OMIM 608841) encodes a protein involved in the immune system (Nagase et al., 1999; Li et al., 2004; Wiggs, 2020). Variants of the *CPAMD8* gene have been recently identified as causative factors for anterior segment dysgenesis (ASD) (Cheong et al., 2016; Bonet-Fernandez et al., 2020; Ma et al., 2020), morgagnian cataract (Hollmann et al., 2017), and different subtypes of glaucoma, including POAG, PACG, and congenital glaucoma (Bonet-Fernandez et al., 2020; Siggs et al., 2020; Wiggs, 2020; Li X. et al., 2021b), indicating that *CPAMD8* variants may lead to primary and secondary glaucoma; different variants of the *CPAMD8* gene may also determine the presentation and severity of ocular phenotypes.

In the current study, compound heterozygous *CPAMD8* variants were identified in two pedigrees with PG. Moreover, autosomal recessive inheritance was found in the study of PG pedigrees. Our study reported a possible association between the biallelic *CPAMD8* gene variants and PDS/PG.

METHODS

Human Subjects

Two Chinese pedigrees of PG and 38 sporadic PG patients were recruited at Shenzhen Eye Hospital and Chengdu First People's Hospital, respectively. Members of both pedigrees and sporadic PG patients were systematically interviewed about their medical history and clinically examined by experienced glaucoma specialists; in addition, peripheral blood was collected for DNA analysis. This study was approved by the Medical Ethics Committees of Shenzhen Eye Hospital, Chengdu First People's Hospital, and Xiamen Eye Center and was conducted according to the principles of the Declaration of Helsinki. Informed written consent was obtained from all participants prior to inclusion in the study.

Clinical Examination

All members enrolled in the study underwent a comprehensive ophthalmologic examination, which included best corrected visual acuity, IOP measurement, slit-lamp biomicroscopy, gonioscopy, and fundus examination. The ocular biometric parameters of each participant were measured *via* optical biometry (IOL Master 700, Carl Zeiss, Germany). Glaucomatous optic neuropathy (GON) was evaluated using slit-lamp examination with a concave preset lens (Hruby lens), fundus photography, and spectral domain optical coherence tomography (SD-OCT, Carl Zeiss). VF was examined using the Humphrey VF Analyzer (Carl Zeiss). The anterior chamber angle structure was recorded *via* ultrasound biomicroscopy (UBM, Tianjin Suowei Electronic Technology Co., Ltd., China) and gonioscopic photography.

The PDS/PG was diagnosed according to the criteria previously reported (Tandon et al., 2019) with minor modifications. In brief, for PDS, subjects should have two signs in at least one eye as follows: Krukenberg's spindle and heavily pigmented TM (Grade 3 or higher). For PG, subjects should have PDS plus at least two of the three signs in at least one eye as follows: IOP > 21 mmHg, GON (C/D ratio > 0.5), and glaucomatous VF defect. The degree of TM pigmentation was graded from 0 to 4 according to severity (0 = no pigment; 1 = light pigment; 2 = moderate pigment; 3 = heavy and non-confluent

pigment; and 4 = heavy and confluent pigment) (Tandon et al., 2019). The severity of Krukenberg's spindle was also graded from 0 to 4 (0 = none; 1 = few flecks; 2 = subtle spindle; 3 = dense spindle; 4 = diffuse pigment) (Tandon et al., 2019).

Whole-Exome Sequencing and Candidate Gene Validation

Genomic DNA of all individuals was extracted from peripheral venous blood samples using the Qiamp Blood DNA Mini Kit (QIAGEN GmbH, Hilden, Germany) according to the manufacturer's instructions. DNA integrity was evaluated *via* 1% agarose gel electrophoresis. Whole-exome sequencing (WES) was performed on three patients in pedigree 1 and the proband in pedigree 2 by Shanghai Genesky Biotechnologies, Inc., and Shanghai WeHealth BioMedical Technology, Co., Ltd, respectively, according to previously described methods (Bao et al., 2019). Exons and adjacent splicing regions (about 20 bp), as well as the full length of the mitochondrial genome, were captured and enriched by SeqCap EZ Exome Probes v3.0 (Roche, Switzerland) hybridization. After the quality control steps, the enriched genes were sequenced using an Illumina HiSeq X Ten platform (San Diego, CA).

The original WES data, excluding unqualified reads according to the quality control standard, were compared with the human reference genome sequence from the University of California Santa Cruz Genome Browser Database using the BWA software (hg19 version). The single-nucleotide variation and insertion and deletion (indel) variants were found using HaplotypeCaller of the genome analysis toolkit. The identified variants were classified *in silico* and filtered against the genome aggregation database (gnomAD, version 3.1, https://gnomad.broadinstitute.org/). Variants were filtered for minor allele frequency (MAF) ≤ 1% (0.01) in gnomAD. Professional databases and bioinformation prediction software, including SnapGene (version 4.3, www.snapgene.com), Ensembl (https://asia.ensembl.org/index.html), DUET (http://biosig.unimelb.edu.au/duet/stability), and VarSite (https://www.ebi.ac.uk/thornton-srv/databases/cgi-bin/VarSite/GetPage.pl?home=TRUE), were used for further annotation and screening of variants of interest, such as missense, synonymous, and noncanonical splicing variants, according to reference sequences NM_015692.5 and NP_056507.3. SnapGene was used to align the protein sequences among different species. The possible functional impact of an amino acid change was predicted using PolyPhen-2, SIFT, CADD, DUET, and VarSite. The first three prediction data (PolyPhen-2, SIFT, and CADD) were acquired from the Ensembl website for uniforming their versions used in the study. The XHMM and CLAMMS algorithms were employed to analyze the copy number variation of the probe coverage area.

The variant-filtering steps were summarized as follows: according to the autosomal recessive inheritance or compound heterozygous inheritance model, the exome sequencing data of patients from family 1 (II:1, II:4, and II:5) and family 2 (II:3) were screened. Homozygous variants and two or more heterozygous variants of the same gene were obtained after filtration. Genes fully or partially related to clinical phenotype were taken into consideration. Glaucoma-associated genes, including *MYOC*, *CYP1B1*, *FOXC1*, *LRP2*, *PITX2*, *PAX6*, *LTBP2*, *TEK*, *ANGPT1*, and *PMEL*, were given special attention. Information on candidate genes and variants from both families were obtained through literature and human gene mutation database (HGMD) search using the American College of Medical Genetics and Genomics (ACMG)/AMP (PMID) criteria (Richards et al., 2015).

Variant Analyses

Direct Sanger sequencing was used to determine the co-segregation of identified variants with the clinical phenotype in pedigrees. Candidate variants identified through the aforementioned variant-filtering steps were validated by Sanger sequencing in all members of the two pedigrees. The primer flanking regions of candidate variants of the *CPAMD8* gene (Gene ID 27151) were designed using Primer Premier 5 (**Table 1**) and synthesized by BGI (Guangzhou, China). Polymerase chain reaction (PCR) was performed using the MyCycler thermal cycler (Bio-Rad, Hercules, CA) in a 25-μL reaction system, which contained 0.1-μg genomic DNA, 40-μmol/L forward and reverse primers, 3-mmol/L magnesium chloride, and 2 × Taq Master Mix (SinoBio, Shanghai, China). The PCR conditions used were as follows: 5 min at 95°C for initial denaturation; 35 cycles of denaturation at 95°C for 30°s for melting; corresponding annealing temperature (TM value) in **Table 1** lasting for 30°s; 30°s at 72°C for extension; and a final additional extension step of 10 min at 72°C. Before sequencing, 1% agarose gel electrophoresis was used to purify the target PCR fragments using the QIAquick Gel Extraction Kit (QIAGEN, Shanghai, China). Sanger sequencing was performed on an ABI 377XL automated DNA sequencer (Applied Biosystems, Foster City, CA). Sequence data were compared in a pairwise manner with the related human genome database.

Screening of the CPAMP8 Gene in Sporadic Pigmentary Glaucoma Patients

The *CPAMP8* gene was screened in 38 sporadic PG patients *via* WES as described above. Variants were filtered with gnomAD (East Asian population); variants with MAF ≤ 0.01 were considered variants or functional SNPs (non-synonymous SNPs).

RESULTS

Clinical Features of Pigmentary Glaucoma Patients

Five patients from two pedigrees who carried biallelic *CPAMD8* compound heterozygous variants presented with typical clinical phenotypes of PDS/PG, including Krukenberg's spindle on the posterior surface of the cornea, heavily pigmented TM, elevated IOP, and GON. The clinical data of the patients in the two PG pedigrees with biallelic *CPAMD8* variants were summarized in **Table 2**.

A relatively mild phenotype was observed in patient II:4 from pedigree 1, including subtle Krukenberg's spindle and moderate

TABLE 1 | Primers used in polymerase chain reaction (PCR) for the amplification of the *CPAMD8* gene.

Variants	Primer sequence (forward/reverse)	Product size (bp)	TM value (°C)
c.520C>T, p.R174W	5′-ACAGTCACCCCCAAGTTACC-3′ 5′-GTGTTTTTCCTCCCTCCAGA-3′	266	56
c.1015G>A, p.V339M	5′-CAGAGGGTCCAAATCCACAG-3′ 5′-ATGCCCAAGAGAGAGGACTG-3′	385	55
c.1931A>G, p.Y644C	5′-TCCAATTCTGTTTCCAACCCA-3′ 5′-GGCTGGTCTCGAACTCCTTT-3′	510	60
c.3238G>A, p.G1080S	5′-CAGCTCTTGGGCTTCCTCAA-3′ 5′-CACAAAGCTGGTGTCACTGC-3′	520	59

pigmentation of the TM in both eyes, with elevated IOP, VF damage, and inferotemporal retinal nerve fiber layer (RNFL) defect in the left eye (**Table 2**). The patient's elder and younger brothers, the other two patients in pedigree 1 (II: 1 and II:5), presented with more significant glaucomatous manifestations, including increased IOP and GON. Diffuse Krukenberg's spindle and grade 4 TM pigmentation were observed in both eyes. An enlarged C/D ratio (0.8–0.9), VF defects, and thinning RNFL confirmed the diagnosis of GON. UBM photographs of patient II:1 and II:5 (pedigree 1) revealed that the iris was bowed backward bilaterally, creating a reverse pupillary block and leading to a possible contact between the posterior surface of the iris and the zonules or anterior lens capsule (**Figure 1** and **Table 2**).

The proband of pedigree 2 (II:3), a 46-year-old woman, underwent trabeculectomy in the right eye 2 years ago and presented with high myopia, poor corrected visual acuity, and controlled IOP with IOP-lowering medications in both eyes. Krukenberg's spindle, lens opacity, and heavily pigmented TM were seen in both eyes. Bilateral typical GON with C/D ratio close to 1.0 was also observed (**Figure 1** and **Table 2**).

The proband's sister (II:2) from pedigree 2 had undergone glaucoma surgeries three or four times and presented with poor visual acuity and elevated IOP in both eyes. Due to the uncontrolled IOP and corneal endothelial decompensation in the right eye, the KP, TM, and optic disc could not be observed in detail. Krukenberg's spindle, homogeneously and densely pigmented TM, and GON were detected in the left eye. UBM examination revealed a concave iris in both eyes of II:2 and II:3 in pedigree 2 (**Figure 1** and **Table 2**).

The IOP presented in **Table 2** were measured at the last follow-up visit of the patients, prior to which both II:1, II:5 in Family 1 and II:2, II:3 in Family 2 had undergone a single or multiple anti-glaucoma surgeries; five patients are currently treated with at least one anti-glaucoma drug. All the affected individuals, but not healthy individuals, in this study presented with elevated IOP before and during the treatments.

Elevated IOP, Krukenberg's spindle, homogeneously and densely pigmented TM, and GON were also seen in 38 sporadic PG patients (data not shown). As expected, iris transillumination was not observed in patients enrolled in this study.

Carriers of the monoallelic *CPAMD8* variant/variants were asymptomatic (**Supplementary Table S1**), except for the mother of two affected daughters in pedigree 2, who had a long history of inflammatory keratitis and presented with leucoma and normal IOP in both eyes. She denied a history of elevated IOP.

Variant Identification of *CPAMD8* in Two Pigmentary Glaucoma Pedigrees

Common genetic characteristics were found in both three-generation pedigrees as follows: no history of consanguineous marriage; all patients were first filial generation; parents and second filial generation were not diagnosed with either PDS or PG; and segregation was consistent with autosomal recessive inheritance. WES and Sanger sequencing were used to investigate the underlying genetic alterations in the two pedigrees as described below, using pedigree 2 as an example (**Figure 2A**). The original sequencing data was 11,820.95 MB, and the average sequencing depth of the target region was 142.71X, with a 98.15% coverage of average sequencing depth of up to ×30. No pathogenic or possible pathogenic variation of mitochondrial genome and no copy number variation fully or partially related to the clinical phenotype of the patients were detected. After performing the variant-filtering steps according to the autosomal recessive inheritance or compound heterozygous inheritance model, a total of 176 homozygous variants of 67 genes (**Supplementary Table S2**) or two or more heterozygous variants of the same genes were shared by all affected individuals (II:1, II:4, and II 5) of family 1; on the contrary, a total of 230 variants of 100 genes (**Supplementary Table S3**) using similar filtering strategy were identified in the proband from family 2 (II:3). Information of all candidate genes in both families was obtained through literature and HGMD search, in which only *CPAMD8* was previously reported in relation to glaucoma (Bonet-Fernandez et al., 2020; Siggs et al., 2020; Wiggs, 2020; Li X. et al., 2021b). Furthermore, Sanger sequencing verification of *CPAMD8* was carried out with all family members in both pedigrees. It was confirmed that compound heterozygous variants (c.520C>T, p.R174W and c.1015G>A, p.V339M in pedigree 1; c.1015G>A, p.V339M; c.1931A>G, p.Y644C and c.3238G>A, p.G1080S in pedigree 2) in *CPAMD8* were co-segregated in two pedigrees with PDS/PG patients (patient II:1, II:4, and II:5 from pedigree 1; patient II: 2 and II:3 from pedigree 2; **Figure 2A**). All variants in this study were rare, with one (p.G1080S) unavailable in gnomAD

TABLE 2 | Clinical data of patients in two pigmentary glaucoma (PG) pedigrees.

Pedigree	Patient	Diagnosis	Gender	Changes of nucleotide and amino acid	Age at last exam (years old)	BCVA		Last IOP (mmHg)		Krukenberg's spindle[a]		TM pigmentation[b]		C/D ratio		Visual field		RNFL (μm)	
						OD	OS	OD	OS	OD	OS	OD	OS	OD	OS	OD	OS	OD	OS
1	II:1	PG OU	M	c.520C>T, p.R174W/c.1015G>A, p.V339M	40	1.0	HM	15	19	4	4	4	4	0.8	0.9	NS	TI	58	57
	II:4	PDS OD; PG OS	F	c.520C>T, p.R174W/c.1015G>A, p.V339M	39	1.0	1.0	22	23	2	2	3	3–4	0.6	0.6	BSE	NS	101	89
2	II:5	PG OU	M	c.520C>T, p.R174W/c.1015G>A, p.V339M	37	1.0	0.3	20	19	4	4	4	4	0.8	0.8	NS	PS	76	57
	II:2	PG OU	F	c.1015G>A, p.V339M/c.1931A>G, p.Y644C/c.3238G>A, p.G1080S	48	NLP	0.3	36	15	NA	4	NA	4	NA	0.9	NA	TI	NA	48
	II:3	PG OU	F	c.1015G>A, p.V339M/c.1931A>G, p.Y644C/c.3238G>A, p.G1080S	46	0.3	0.6	14	14	3	3	4	4	0.9	0.8	TI	TI	45	54

Abbreviations: BCVA, best corrected visual acuity; BSE, blind spot enlargement; C/D, cup-to-disc; F, female; HM, hand move; IOP, intraocular pressure; M, male; N, normal; NA, not available; NLP, no light perception; NS, nasal step; OD, right eye; OS, left eye; OU, both eyes; PDS, pigment dispersion syndrome; PG, pigmentary glaucoma; PS, paracentral scotoma; RNFL, retinal nerve fiber layer; TI, temporal island; TM, trabecular meshwork.

[a]Grade of Krukenberg's spindle: 0 is defined as none; 1, few flecks; 2, subtle spindle; 3, dense spindle; 4, diffuse pigment (Tandon et al., 2019).

[b]Grade of TM, pigmentation: 0 is defined as no pigment; 1, light pigment, 2, moderate pigment; 3, heavy and non-confluent pigment; 4, heavy and confluent pigment (Tandon et al., 2019).

(East Asian), at a frequency consistent with that of rare recessive disease (**Table 3**).

Bioinformatics Analyses of the *CPAMD8* Variants in Two Pigmentary Glaucoma Pedigrees

In pedigree 1, compound heterozygous variants p.R174W (rs201333165) and p.V339M (rs369985652) in the *CPAMD8* gene were identified *via* WES. The genotype-phenotype co-segregation was verified *via* Sanger sequencing in the whole pedigree. Variant p.R174W of *CPAMD8* was inherited from the mother, whereas the other variant, p.V339M, was inherited from the father. The mode of inheritance was in accordance with compound heterozygous variation under a recessive inheritance pattern (**Figure 2**).

Two missense variants found in the *CPAMD8* gene of the subject were classified as "variants of uncertain significance" according to the ACMG guidelines. Three online predictive software, PolyPhen-2, SIFT, and DUET, classified these two variants as damaging, destabilizing, or deleterious (**Table 3**). The macroglobulin domain 2 (MG2) (**Figure 3A**) is a domain of α-2-macroglobulin (A2M) in eukaryotes (Janssen et al., 2005). A2Ms, among the core domains of *CPAMD8*, are plasma proteins that trap and inhibit a broad range of proteases and are major components of the eukaryotic innate immune system (Wong and Dessen, 2014). The arginine (Arg) residue at position 174 is highly conserved (**Figure 3B**; conservation = 0.9 from 37 aligned protein sequences from different organisms). The change from an Arg to a tryptophan side chain was highly unfavored in terms of conserved amino acid properties, which might result in a change in protein function.

In contrast to Arg at position 174, the valine residue at position 339 is relatively less conserved (**Figure 3B**; conservation = 0.7 from 43 aligned protein sequences from different organisms). This may not result in an obvious change in protein function.

In pedigree 2, three variants, p.V339M, p.Y644C, and p.G1080S, in the *CPAMD8* gene were identified *via* WES. Two variants, p.V339M and p.Y644C, were inherited from their father, whereas another variant, p.G1080S, was inherited from their mother. These variants were co-segregating with the clinical phenotype verified *via* Sanger sequencing and segregation analysis and were accordant with compound heterozygous variation under a recessive inheritance pattern (**Figure 2**).

Three missense variants found in the *CPAMD8* gene of the subject were classified as "variants of uncertain significance" according to the ACMG/AMP guidelines for variant classification. Variant p.V339M was presented in both pedigrees. Another two variants (p.Y644C and p.G1080S) were identified as highly conservative in different species (**Figure 3B**) and might result in instability of the CPAMD8 protein, as predicted by DUET (**Table 3**). The p.Y644C and p.G1080S variants were predicted to be damaging or deleterious by PolyPhen-2. SIFT predicted that the p.Y644C variant was deleterious and the p.G1080S variant was tolerable (**Table 3**). The heterozygous variant c.1931A>G of exon 17 in *CPAMD8*

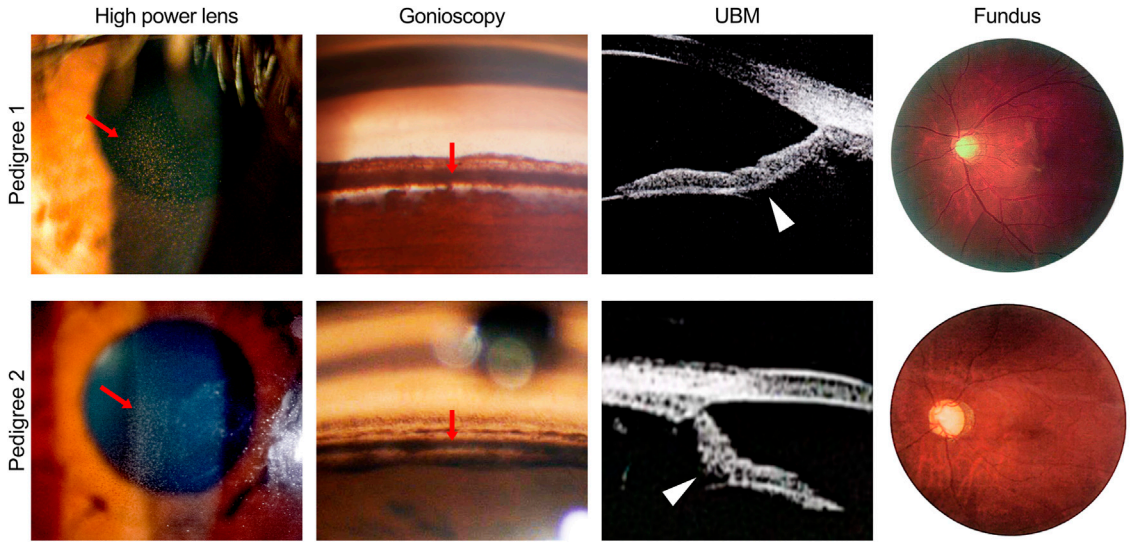

FIGURE 1 | Ocular phenotypes of patients in two pigmentary glaucoma (PG) pedigrees associated with *CPAMD8* variants. Clinical photography including slit-lamp biomicroscopy, gonioscopy, ultrasound biomicroscopy, and fundus photography. Representative signs of PG, such as Krukenberg's spindle, TM pigmentation, and reverse pupillary block, were indicated by red arrows and white arrowheads, respectively. In pedigree 1, representative images were acquired from the right eye of patient II:5. In pedigree 2, representative images were acquired from the left eye of patient II:2 (slit-lamp biomicroscopy and fundus photography) and the right eye of patient II:3 (gonioscopy and ultrasound biomicroscopy).

would result in the substitution of tyrosine (Tyr), a neutral amino acid at position 644, by hydrophobic cysteine. The Tyr residue at position 644 is very highly conserved (**Figure 3B**; conservation = 0.9 from 43 aligned protein sequences from different organisms), rendering it significant for protein function.

The heterozygous variant c.3238G>A of exon 25 in *CPAMD8* would result in the substitution of glycine (Gly) at position 1080 by serine, which is located at the end of the methyltransf-FA (farnesoic acid O-methyl transferase) domain (**Figure 3A**), a well-known key protein domain of the enzyme that catalyzes the formation of methyl farnesoate from farnesoic acid in the biosynthetic pathway of juvenile hormone (Li J. et al., 2021a). The Gly residue at position 1080 is fairly well conserved (**Figure 3B**; conservation = 0.8 from 47 aligned protein sequences), which means it is significant for protein function.

Screening of the *CPAMD8* Gene in Sporadic Pigmentary Glaucoma Patients

By screening the *CPAMD8* gene on 38 sporadic PG patients (**Table 4**), 13 variants (c.1015G>A, c.503T>C, c.5242C>G, c.1173_1174del, c.92+1G>T, c.3786+1G>A, c.2117G>A, c.215C>T, c.959C>T, c.979G>T, c.2009G>A c.5342C>G, and c.4685+1G>A) of the *CPAMD8* gene with MAF ≤0.01 were identified in 11 sporadic PG patients. Among them, one variant of *CPAMD8* (c.1015G>A, p.V339M) was identified in pedigree 1 and pedigree 2 as well as one sporadic patient (patient 1) of PG, which was not reported previously. In addition, one sporadic PG patient (patient 2) carried three heterozygous variants of *CPAMD8*.

DISCUSSION

In this study, compound heterozygous variants of the *CPAMD8* gene were identified in five patients from two unrelated Chinese PG pedigrees *via* filtering of WES data and Sanger sequencing verification. These compound heterozygous variants of the *CPAMD8* gene have not been previously reported in literatures. All variants appear to be damaging, destabilizing, or deleterious based on bioinformatics analysis. Through WES and filtering against several publicly accessible variation databases and eliminating all previously reported variants, other glaucoma-associated genes, including *MYOC*, *CYP1B1*, *FOXC1*, *LRP2*, *PITX2*, *PAX6*, *LTBP2*, *TEK*, *ANGPT1*, and *PMEL*, were excluded in these two pedigrees. Of the 13 variants of *CPAMD8* identified in 38 sporadic PG patients@ with MAF ≤ 0.01, compound heterozygous variants were likely present in two of them (**Table 4**), and their parents were asymptomatic. These results indicate that the *CPAMD8* gene variant is potentially associated with PDS/PG.

In previous studies, PDS was thought to be an autosomal dominant inherited disease (Scheie and Cameron, 1981; Mandelkorn et al., 1983; Tandon et al., 2019); meanwhile, there was only one autosomal recessive inheritance pattern for PG in a four-generation family reported (Stankovic., 1961; Lascaratos et al., 2013). Andersen et al. (Andersen et al., 1997) used microsatellite repeat markers distributed throughout the human genome to perform a genome screen of subjects from four pedigrees with PDS. They found that the responsible gene is located in a 10-centimorgan interval between markers D7S2462 and D7S2423 of chromosome 7. The two pedigrees in this study presented an autosomal recessive inheritance pattern. No PDS/PG phenotypes were found in the carriers of monoallelic *CPAMD8* variant/variants from these two pedigrees.

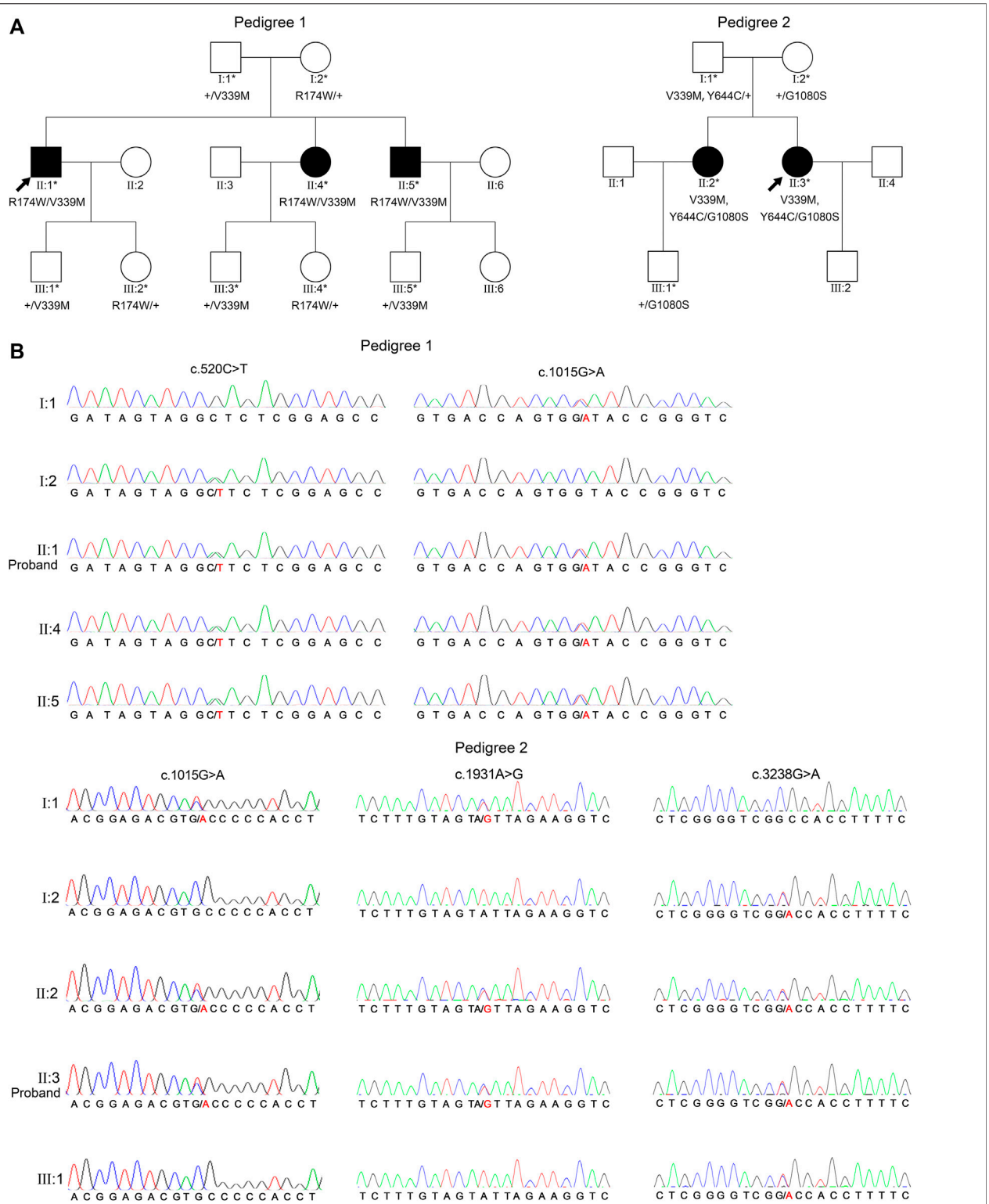

FIGURE 2 | Two PG pedigrees with *CPAMD8* variants and Sanger sequencing results of the *CPAMD8* gene. **(A)** The two PG pedigrees described from our research. Round symbols indicate female individuals; square symbols indicate male individuals; black symbols indicate PG patients; arrow marks indicate the proband; asterisks represent subjects involved in genetic research. The plus signs denote reference allele. **(B)** Sanger sequencing verification and segregation analysis of biallelic *CPAMD8* variants in two PG pedigrees. Variants are denoted in red font. Two different compound heterozygous variants of *CPAMD8* were identified in two PG pedigrees. Abbreviations: PG, pigmentary glaucoma.

TABLE 3 | Summary of PG pedigrees with *CPAMD8* Variants.

Pedigree	Position	Name	Exon	Changes of nucleotide and amino acid	Status	Variant type	PolyPhen-2	CADD	SIFT	DUET-protein stability	gnomAD_EA	ACMG/AMP variant classification
1	chr19: 17119354	*CPAMD8*	7	c.520C>T, p.R174W	CH	Missense	0.999, D	23, B	0.01, D	-0.216 kcal/mol, D	0.00019	VUS[a]
	chr19: 17108001	*CPAMD8*	11	c.1015G>A, p.V339M	CH	Missense	0.999, D	23, B	0.02, D	-0.822 kcal/mol, D	0.00347	VUS[b]
2	chr19: 17108001	*CPAMD8*	11	c.1015G>A, p.V339M	CH	Missense	0.999, D	23, B	0.02, D	-0.822 kcal/mol, D	0.00347	VUS[b]
	chr19: 17086046	*CPAMD8*	17	c.1931A>G, p.Y644C	CH	Missense	0.921, D	22, B	0.01, D	-1.977 kcal/mol, D	0.00019	VUS[a]
	chr19: 17038951	*CPAMD8*	25	c.3238G>A, p.G1080S	CH	Missense	0.883, D	23, B	0.17, T	-1.91 kcal/mol, D	NA	VUS[a]

Abbreviations: CH; compound heterozygous; D, damaging, deleterious, or destabilizing; EA, East Asian; NA, not available; T, tolerated; VUS, variants of uncertain significance.
[a]*Evidence of pathogenicity (PM2 + PP1 + PP3 + PP4).*
[b]*Evidence of pathogenicity (PP1 + PP3 + PP4).*

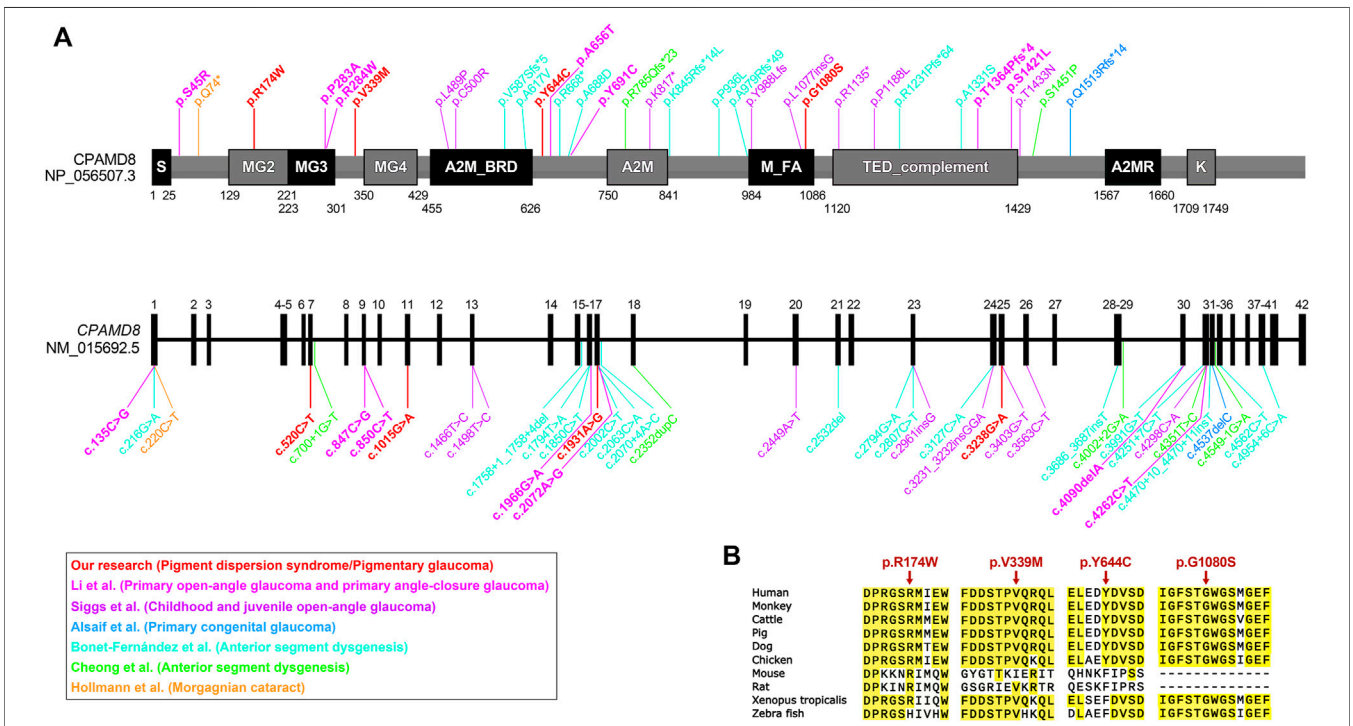

FIGURE 3 | Bioinformatics analyses of *CPAMD8* variants in two PG pedigrees. **(A)** Schematic representations showing variant sites on the sequence of the *CPAMD8* gene and CPAMD8 protein identified in our study and other studies of the association between *CPAMD8* gene and inherited ocular disorders (Cheong et al., 2016; Hollmann et al., 2017; Alsaif et al., 2019; Bonet-Fernandez et al., 2020; Siggs et al., 2020; Li X. et al., 2021b). Each study was plotted in a distinct color. Domains were indicated according to the Pfam database (https://pfam.xfam.org/). Abbreviations: S, signal peptide; A2M, α-2-macroglobulin domain; A2M_BRD, α-2-macroglobulin bait region domain; A2MR, α-macroglobulin receptor binding domain; MG, macroglobulin domain of α-2-macroglobulin; M_FA, farnesoic acid O-methyl transferase domain; TED, α-macroglobulin thioester domain; K, kazal-2 serine protease inhibitor domain. **(B)** Sequence alignments of the CPAMD8 protein among different species. Four missense variants were highly conserved in various species. The positions of the variant amino acids are indicated by red arrows.

For pedigree 1, we have followed up the pedigree for 10 years and never found other pedigree members presenting with any phenotype of PDS/PG or glaucoma. In pedigree 2, patient I:1 with monoallelic *CPAMD8* variants (c.1015G>A, p.V339M; c.1931A>G, p.Y644C) had no previous history of ocular abnormalities, and examinations on his eyes were unremarkable. Therefore, our data meet the necessary criteria indicating that *CPAMD8* is involved in the inheritance of PG in a rare autosomal recessive pattern.

It was recently suggested that *CPAMD8* variants may be involved in the development of ASD (Cheong et al., 2016; Bonet-Fernandez

TABLE 4 | Summary of sporadic PG patients with *CPAMD8* variants.

Patient number	Position	Name	Exon	Changes of nucleotide and amino acid	Variant type	PolyPhen-2	CADD	SIFT	DUET-protein stability	gnomAD_EA
1	chr19:17108001	*CPAMD8*	11	c.1015G>A, p.V339M	Missense	0.999, D	23.0, B	0.02, D	-0.822 kcal/mol, D	0.00347
	chr19:17120114	*CPAMD8*	6	c.503T>C, p.L168P	Missense	0.966, D	22.6, D	0.310, T	-1.036 kcal/mol, D	NA
2	chr19:17007300	*CPAMD8*	40	c.5242C>G, p.L1748V	Missense	0.103, B	16.99, B	0.189, T	-1.648 kcal/mol, D	NA
	chr19: 17104318_17104319	*CPAMD8*	12	c.1173_1174del, p.D391Efs*6	Frameshift	NA	NA	NA	NA	0.0001926
	chr19:17137360	*CPAMD8*	1	c.92+1G>T	Splicing	NA	33.0, D	NA	NA	NA
3	chr19:17025466	*CPAMD8*	28	c.3786+1G>A	Splicing	NA	33.0, D	NA	NA	NA
4	chr19:17081797	*CPAMD8*	18	c.2117G>A:p.R706Q	Missense	0.909, D	24, B	0.01, D	-0.239 kcal/mol, D	NA
5	chr19:17132869	*CPAMD8*	2	c.215C>T, p.P72L	Missense	0.01, B	11, B	0.05, D	-0.684 kcal/mol, D	0.01079
6	chr19:17108057	*CPAMD8*	11	c.959C>T, p.A320V	Missense	0.496, D	14, B	0.03, D	-0.192 kcal/mol, D	0.003277
7	chr19:17108037	*CPAMD8*	11	c.979G>T:p.G327W	Missense	1.000, D	25.10, D	0.001,D	-1.52 kcal/mol, D	NA
8	chr19:17085968	*CPAMD8*	17	c.2009G>A, p.R670Q	Missense	0.954, D	14, B	0.1, B	-0.22 kcal/mol, D	NA
9	chr19: 17007071	*CPAMD8*	41	c.5342C>G, p.P1781R	Missense	0, B	3, B	0.15, T	NA	0.00987
10	chr19:17108057	*CPAMD8*	11	c.959C>T, p.A320V	Missense	0.496, D	14, B	0.03, D	-0.192 kcal/mol, D	0.003277
11	chr19:17013458	*CPAMD8*	35	c.4685+1G>A	Splicing	NA	34.0, D	NA	NA	NA

Abbreviations: 1,000g2015aug_all, frequency of variation in 1,000 Genomes Project database (all population); 1,000g2015aug_eas; frequency of variation in 1,000 Genomes Project database (East Asian population); NA, not available; the variants from patient 1 (c.503T>C, p.L168P), 2 (c.5242C>G, p.L1748V and c.92+1G>T), 3, 4, 7, 8, and 11 were not available in the Ensembl website, and their prediction data including PolyPhen-2, SIFT, and CADD were acquired from their own websites or VarSite website; PolyPhen-2, (http://genetics.bwh.harvard.edu/pph2/); CADD, (https://cadd.gs.washington.edu/); SIFT, (http://provean.jcvi.org/); VarSite, (https://www.ebi.ac.uk/thornton-srv/databases/cgi-bin/VarSite/GetPage.pl?home=TRUE).

et al., 2020; Ma et al., 2020), morgagnian cataract (Hollmann et al., 2017), and different subtypes of glaucoma, including POAG, PACG, and congenital glaucoma (Bonet-Fernandez et al., 2020; Siggs et al., 2020; Li X. et al., 2021b). However, neither ASD nor morgagnian cataract was present in our study of PG patients with *CPAMD8* missense variants, although these ocular disorders share similar background of changed *CPAMD8*. Li et al. performed a cohort study of the association between *CPAMD8* variants and POAG/PACG and showed that biallelic truncation variants were more frequently associated with ASD, which usually presented with more severe phenotype, including iridocorneal adhesion and iris and ciliary body hypoplasia, whereas biallelic missense variants were more common in POAG/PACG (Li X. et al., 2021b), suggesting that the functional damages of CPAMD8 protein could be different for different variants/alterations in the *CPAMD8* gene. The type of variants/alterations may determine the presentation and severity of the ocular phenotypes. In agreement with the previous report, all alterations identified in our study of PDS/PG with milder phenotypes than ASD were missense variants. We also found patient II:4 (female) of pedigree 1 who had later-onset and milder PG phenotypes (PDS in the right eye and PG in the left eye) than her elder and younger affected brothers, indicating that the clinical phenotypes of genetic disorders were possibly influenced by other factors, such as gender, epigenetic changes, and environmental exposure (Yan et al., 2010; Sarkar et al., 2014; Choi et al., 2020).

Variants of pigment dispersion–associated genes in animals, such as *Dct*, *Tyrp1*, and *Lyst*, mimicked some clinical features of PDS and PG (Chang et al., 1999; Anderson et al., 2008; Trantow et al., 2009); however, no studies have found a causal relationship between any variants within their human orthologs and PG. It is likely that there are non-pigment–related genes involved in the pathogenesis of PDS/PG. Iris concavity is often present in PDS/PG patients and leads to iridozonular chafing and pigment release (Lyons and Amram, 2019). Potential mechanisms for iridozonular chafing remain unclear. In a cohort study of PDS/PG patients, the *LOXL1* variant was identified and further validated to be pathogenic in an animal model. It was speculated that this variant was responsible for iris stromal defects in PDS/PG patients (Giardina et al., 2014). This study provided a possible interpretation for close contact of iris epithelium and zonule, that stromal defects appear to be present in abnormal iris. However, another study showed that there was no correlation between *LOXL1* and PDS/PG (Rao et al., 2008). An animal study examined the eyes of old DBA/2J mice (2.5–18 months), characterized its ocular pigment abnormalities, and speculated that the loss of pigment cells in the anterior chamber was at least in part caused by iris stromal atrophy with aging (Schraermeyer et al., 2009). This finding indicates that normal iris stroma may be necessary for the stability of pigment epithelium. In the anterior segment of the eye, *CPAMD8* has been demonstrated to be expressed in neural crest–derived tissues, including the cornea, iris, ciliary body, and lens (Wiggs 2020). Siggs et al. found iris stromal hypoplasia in childhood and juvenile POAG patients with biallelic *CPAMD8* variants (Siggs et al., 2020), which implied a possible role of *CPAMD8* in iris stromal defects. Furthermore, *CPAMD8* belongs to the α-2-

macroglobulin/complement 3 protein family, whose members are involved in innate and acquired immune responses (Wiggs 2020). Wong et al. found that in the iris of patients with POAG or PCAG, the expression of IL-2 and IFN-γ (Th1 cytokine) increased, IL-6 (Th2 cytokine) decreased, and TGF-β (Th3 cytokine) increased. They also suggested the presence of an immune imbalance in glaucomatous eyes (Wong et al., 2015). In sum, whether *CPAMD8* is involved in the immunological abnormalities of iris stroma in some subtypes of glaucoma is unknown. In the current study, we confirmed that *CPAMD8* variants co-segregated with PDS/PG in two pedigrees. Further studies are needed to clarify whether *CPAMD8* plays a role in the pathogenesis of iris stromal abnormalities (such as immunological abnormalities), iris epithelial cell loss, and pigment dispersion. In addition, the CPAMD8 protein was mainly detected in the nonpigmented epithelial cells of iris tissues (Siggs et al., 2020; Li X. et al., 2021b), which also implied that the effect of *CPAMD8* variants on the loss of iris pigment epithelium may be indirect.

It is worth mentioning that iris transillumination defects, which are a feature of PDS and PG, were not observed in any patients in the two pedigrees or in sporadic PG patients, even though they presented with other typical clinical phenotypes of PDS/PG, including Krukenberg's spindle and heavily and homogenously pigmented TM. One of the reasons is probably the fact that iris transillumination defects cannot be detected in darkly pigmented irides of East Asian patients *via* traditional slit-lamp examination (Qing et al., 2009). However, infrared imaging techniques may help demonstrate iris transillumination defects in these patients who show other clinical signs of PDS (Roberts and Wernick, 2007).

In conclusion, our study identified compound heterozygous variants of the *CPAMD8* gene in these two Chinese pedigrees with PG inherited in an autosomal recessive manner. This study reported a possible association between the biallelic *CPAMD8* variants and PDS/PG. Because the *CPAMD8* ortholog is conspicuously absent in rodent genomes (Siggs et al., 2020), animal studies of the pathogenesis of PDS/PG with *CPAMD8* variants require special considerations.

DATA AVAILABILITY STATEMENT

The data analyzed in this study is subject to the following licenses/restrictions: The datasets for this article are not publicly available due to concerns regarding participant/patient anonymity. Requests to access these datasets should be directed to XL, xliu1213@126.com.

ETHICS STATEMENT

The studies involving human participants were reviewed and approved by the Medical Ethics Committees of Shenzhen Eye Hospital (Number: 20180717-10) and Chengdu First People's Hospital (Number: 2020-KT-011). The patients/participants provided their written informed consent to participate in this study. Written informed consent was obtained from the individual(s) for the publication of any potentially identifiable images or data included in this article.

AUTHOR CONTRIBUTIONS

XL, JT, LZ, YW, and GL designed and performed most of the studies, analyzed the data, and wrote the manuscript; NF, LH, XW, YH, and D-FC helped conduct this study and write the manuscript. XL coordinated the study, conceived and designed the experimental plan, and finalized the manuscript. All authors reviewed the manuscript.

FUNDING

This study was supported by grants from the National Natural Science Foundation of China (NSFC grants 82070963, 81770924, and 81900829), the Science and Technology Project in Medical and Health of Xiamen (Grants Nos. 3502Z20194066 and 3502Z20214ZD1214), and the Science and Technology Innovation Committee of Shenzhen (Grant No. JCYJ20210324125614039).

ACKNOWLEDGMENTS

The authors thank Zhilan Yuan, Yuanbo Liang, Liang Liang, Feng Wang, and Sujie Fan for their help and suggestions.

SUPPLEMENTARY MATERIAL

The Supplementary Material for this article can be found online at: https://www.frontiersin.org/articles/10.3389/fgene.2022.845081/full#supplementary-material

REFERENCES

Alsaif, H. S., Khan, A. O., Patel, N., Alkuraya, H., Hashem, M., Abdulwahab, F., et al. (2019). Congenital Glaucoma and CYP1B1: an Old Story Revisited. *Hum. Genet.* 138 (8-9), 1043–1049. doi:10.1007/s00439-018-1878-z

Andersen, J. S., Pralea, A. M., DelBono, E. A., Haines, J. L., Gorin, M. B., Schuman, J. S., et al. (1997). A Gene Responsible for the Pigment Dispersion Syndrome Maps to Chromosome 7q35-Q36. *Arch. Ophthalmol.* 115 (3), 384–388. doi:10.1001/archopht.1997.01100150386012

Anderson, M. G., Hawes, N. L., Trantow, C. M., Chang, B., and John, S. W. M. (2008). Iris Phenotypes and Pigment Dispersion Caused by Genes Influencing Pigmentation. *Pigment. Cell Melanoma Res.* 21 (5), 565–578. doi:10.1111/j.1755-148x.2008.00482.x

Bao, Y., Yang, J., Chen, L., Chen, M., Zhao, P., Qiu, S., et al. (2019). A Novel Mutation in the NDP Gene Is Associated with Familial Exudative Vitreoretinopathy in a Southern Chinese Family. *Genet. Test. Mol. Biomarkers* 23 (12), 850–856. doi:10.1089/gtmb.2019.0099

Bonet-Fernández, J.-M., Aroca-Aguilar, J.-D., Corton, M., Ramírez, A.-I., Alexandre-Moreno, S., García-Antón, M.-T., et al. (2020). *CPAMD8* Loss-Of-Function Underlies Non-dominant Congenital Glaucoma with Variable Anterior Segment Dysgenesis and Abnormal Extracellular Matrix. *Hum. Genet.* 139 (10), 1209–1231. doi:10.1007/s00439-020-02164-0

Chang, B., Smith, R. S., Hawes, N. L., Anderson, M. G., Zabaleta, A., Savinova, O., et al. (1999). Interacting Loci Cause Severe Iris Atrophy and Glaucoma in DBA/2J Mice. *Nat. Genet.* 21 (4), 405–409. doi:10.1038/7741

Cheong, S.-S., Hentschel, L., Davidson, A. E., Gerrelli, D., Davie, R., Rizzo, R., et al. (2016). Mutations in *CPAMD8* Cause a Unique Form of Autosomal-Recessive Anterior Segment Dysgenesis. *Am. J. Hum. Genet.* 99 (6), 1338–1352. doi:10.1016/j.ajhg.2016.09.022

Choi, H. R., Choi, S. H., Choi, S. M., Kim, J. K., Lee, C. R., Kang, S.-W., et al. (2020). Benefit of Diverse Surgical Approach on Short-Term Outcomes of MEN1-Related Hyperparathyroidism. *Sci. Rep.* 10, 10634. doi:10.1038/s41598-020-67424-5

Giardina, E., Oddone, F., Lepre, T., Centofanti, M., Peconi, C., Tanga, L., et al. (2014). Common Sequence Variants in the LOXL1gene in Pigment Dispersion Syndrome and Pigmentary Glaucoma. *BMC Ophthalmol.* 14, 52. doi:10.1186/1471-2415-14-52

Hollmann, A. K., Dammann, I., Wemheuer, W. M., Wemheuer, W. E., Chilla, A., Tipold, A., et al. (2017). Morgagnian Cataract Resulting from a Naturally Occurring Nonsense Mutation Elucidates a Role of *CPAMD8* in Mammalian Lens Development. *PLoS One* 12 (7), e0180665. doi:10.1371/journal.pone.0180665

Janssen, B. J. C., Huizinga, E. G., Raaijmakers, H. C. A., Roos, A., Daha, M. R., Nilsson-Ekdahl, K., et al. (2005). Structures of Complement Component C3 Provide Insights into the Function and Evolution of Immunity. *Nature* 437, 505–511. doi:10.1038/nature04005

Lahola-Chomiak, A. A., Footz, T., Nguyen-Phuoc, K., Neil, G. J., Fan, B., Allen, K. F., et al. (2019). Non-Synonymous Variants in Premelanosome Protein (*PMEL*) Cause Ocular Pigment Dispersion and Pigmentary Glaucoma. *Hum. Mol. Genet.* 28 (8), 1298–1311. doi:10.1093/hmg/ddy429

Lascaratos, G., Shah, A., and Garway-Heath, D. F. (2013). The Genetics of Pigment Dispersion Syndrome and Pigmentary Glaucoma. *Surv. Ophthalmol.* 58 (2), 164–175. doi:10.1016/j.survophthal.2012.08.002

Li, J., Wang, W., Zhao, Q., Fan, S., Li, Y., Yuan, P., et al. (2021a). A Haemocyte-Expressed Methyltransf_FA Domain Containing Protein (MFCP) Exhibiting Microbe Binding Activity in Oyster *Crassostrea gigas*. *Dev. Comp. Immunol.* 122, 104137. doi:10.1016/j.dci.2021.104137

Li, X., Sun, W., Xiao, X., Fang, L., Li, S., Liu, X., et al. (2021b). Biallelic Variants in *CPAMD8* Are Associated with Primary Open-Angle Glaucoma and Primary Angle-Closure Glaucoma. *Br. J. Ophthalmol.* Published Online First: 21 June 2021. doi:10.1136/bjophthalmol-2020-318668

Li, Z.-F., Wu, X.-h., and Engvall, E. (2004). Identification and Characterization of CPAMD8, a Novel Member of the Complement 3/α 2 -macroglobulin Family with a C-Terminal Kazal Domain. *Genomics* 83 (6), 1083–1093. doi:10.1016/j.ygeno.2003.12.005

Lyons, L., and Amram, A. (2019). Iris Transillumination Defects in Pigment Dispersion Syndrome. *N. Engl. J. Med.* 381 (20), 1950. doi:10.1056/nejmicm1903842

Ma, A., Yousoof, S., Grigg, J. R., Flaherty, M., Minoche, A. E., Cowley, M. J., et al. (2020). Revealing Hidden Genetic Diagnoses in the Ocular Anterior Segment Disorders. *Genet. Med.* 22 (10), 1623–1632. doi:10.1038/s41436-020-0854-x

Mandelkorn, R. M., Hoffman, M. E., Olander, K. W., Zimmerman, T., and Harsha, D. (1983). Inheritance and the Pigmentary Dispersion Syndrome. *Ann. Ophthalmol.* 15 (6), 577–582.

Nagase, T., Ishikawa, K., Kikuno, R., Hirosawa, M., Nomura, N., and Ohara, O. (1999). Prediction of the Coding Sequences of Unidentified Human Genes.XV. The Complete Sequences of 100 New cDNA Clones from Brain Which Code for Large Proteins *In Vitro*. *DNA Res.* 6 (5), 337–345. doi:10.1093/dnares/6.5.337

Niyadurupola, N., and Broadway, D. C. (2008). Pigment dispersion syndrome and pigmentary glaucoma - a major review. *Clin. Exp. Ophthalmol.* 36 (9), 868–882. doi:10.1111/j.1442-9071.2009.01920.x

Qing, G., Wang, N., Tang, X., Zhang, S., and Chen, H. (2009). Clinical characteristics of pigment dispersion syndrome in Chinese patients. *Eye* 23 (8), 1641–1646. doi:10.1038/eye.2008.328

Rao, K. N., Ritch, R., Dorairaj, S. K., Kaur, I., Liebmann, J. M., Thomas, R., et al. (2008). Exfoliation syndrome and exfoliation glaucoma-associated *LOXL1* variations are Not involved in pigment dispersion syndrome and pigmentary glaucoma. *Mol. Vis.* 14, 1254–1262.

Richards, S., Aziz, N., Bale, S., Bick, D., Das, S., Gastier-Foster, J., et al. (2015). Standards and guidelines for the interpretation of sequence variants: a joint consensus recommendation of the American College of Medical Genetics and Genomics and the Association for Molecular Pathology. *Genet. Med.* 17 (5), 405–424. doi:10.1038/gim.2015.30

Roberts, D. K., and Wernick, M. N. (2007). Infrared imaging technique may help demonstrate iris transillumination defects in blacks who show other pigment dispersion syndrome clinical signs. *J. Glaucoma* 16 (5), 440–447. doi:10.1097/ijg.0b013e3181405e72

Sarkar, K., Sadhukhan, S., Han, S.-S., and Vyas, Y. M. (2014). Disruption of hSWI/SNF complexes in T cells by WAS mutations distinguishes X-linked thrombocytopenia from Wiskott-Aldrich syndrome. *Blood* 124 (23), 3409–3419. doi:10.1182/blood-2014-07-587642

Scheie, H. G., and Cameron, J. D. (1981). Pigment dispersion syndrome: a clinical study. *Br. J. Ophthalmol.* 65 (4), 264–269. doi:10.1136/bjo.65.4.264

Schraermeyer, M., Schnichels, S., Julien, S., Heiduschka, P., Bartz-Schmidt, K.-U., and Schraermeyer, U. (2009). Ultrastructural analysis of the pigment dispersion syndrome in DBA/2J mice. *Graefes Arch. Clin. Exp. Ophthalmol.* 247, 1493–1504. doi:10.1007/s00417-009-1146-y

Scuderi, G., Contestabile, M. T., Scuderi, L., Librando, A., Fenicia, V., and Rahimi, S. (2019). Pigment dispersion syndrome and pigmentary glaucoma: a review and update. *Int. Ophthalmol.* 39 (7), 1651–1662. doi:10.1007/s10792-018-0938-7

Siddiqui, Y., Ten Hulzen, R. D., Cameron, J. D., Hodge, D. O., and Johnson, D. H. (2003). What is the risk of developing pigmentary glaucoma from pigment dispersion syndrome? *Am. J. Ophthalmol.* 135 (6), 592794–592799. doi:10.1016/s0002-9394(02)02289-4

Siggs, O. M., Souzeau, E., Taranath, D. A., Dubowsky, A., Chappell, A., Zhou, T., et al. (2020). Biallelic *CPAMD8* variants are a frequent cause of childhood and juvenile open-angle glaucoma. *Ophthalmology* 127 (6), 758–766. doi:10.1016/j.ophtha.2019.12.024

Stankovic, J. (1961). Ein Beitrag zur Kenntnis der Vererbung des Pigmentglaucom. *Klin. Monatsbl Augenheilkd* 139, 165–175.

Tandon, A., Zhang, Z., Fingert, J. H., Kwon, Y. H., Wang, K., and Alward, W. L. M. (2019). The heritability of pigment dispersion syndrome and pigmentary glaucoma. *Am. J. Ophthalmol.* 202, 55–61. doi:10.1016/j.ajo.2019.02.017

Trantow, C. M., Mao, M., Petersen, G. E., Alward, E. M., Alward, W. L. M., Fingert, J. H., et al. (2009). LystMutation in Mice Recapitulates Iris Defects of Human Exfoliation Syndrome. *Invest. Ophthalmol. Vis. Sci.* 50 (3), 1205–1214. doi:10.1167/iovs.08-2791

Wiggs, J. L. (2020). *CPAMD8*, a new gene for anterior segment dysgenesis and childhood glaucoma. *Ophthalmology* 127 (6), 767–768. doi:10.1016/j.ophtha.2020.02.035

Wong, M., Huang, P., Li, W., Li, Y., Zhang, S. S., and Zhang, C. (2015). T-helper1/T-helper2 cytokine imbalance in the iris of patients with glaucoma. *PLoS One* 10 (3), e0122184. doi:10.1371/journal.pone.0122184

Wong, S. G., and Dessen, A. (2014). Structure of a bacterial α2-macroglobulin reveals mimicry of eukaryotic innate immunity. *Nat. Commun.* 5, 4917. doi:10.1038/ncomms5917

Yan, J., Deng, H. X., Siddique, N., Fecto, F., Chen, W., Yang, Y., et al. (2010). Frameshift and novel mutations in FUS in familial amyotrophic lateral sclerosis and ALS/dementia. *Neurology* 75 (9), 807–814. doi:10.1212/wnl.0b013e3181f07e0c

Conflict of Interest: The authors declare that the research was conducted in the absence of any commercial or financial relationships that could be construed as a potential conflict of interest.

Publisher's Note: All claims expressed in this article are solely those of the authors and do not necessarily represent those of their affiliated organizations, or those of the publisher, the editors, and the reviewers. Any product that may be evaluated in this article, or claim that may be made by its manufacturer, is not guaranteed or endorsed by the publisher.

frontiers | Frontiers in Genetics

TYPE Original Research
PUBLISHED 23 September 2022
DOI 10.3389/fgene.2022.993157

OPEN ACCESS

EDITED BY
Emiliano Giardina,
University of Rome Tor Vergata, Italy

REVIEWED BY
Benedetto Falsini,
Università Cattolica del Sacro Cuore, Italy
Valerio Caputo,
University of Rome Tor Vergata, Italy

*CORRESPONDENCE
Zheng-Gao Xie,
zgxie87@163.com

†These authors share first authorship

SPECIALTY SECTION
This article was submitted to Genetics of Common and Rare Diseases, a section of the journal Frontiers in Genetics

RECEIVED 13 July 2022
ACCEPTED 22 August 2022
PUBLISHED 23 September 2022

CITATION
Wang X-F, Chen F-F, Zhou X, Cheng X-X and Xie Z-G (2022), A novel mutation in RS1 and clinical manifestations in a Chinese twin family with congenital retinoschisis.
Front. Genet. 13:993157.
doi: 10.3389/fgene.2022.993157

A novel mutation in RS1 and clinical manifestations in a Chinese twin family with congenital retinoschisis

Xiao-Fang Wang[1†], Fei-Fei Chen[1†], Xin Zhou[2†], Xin-Xuan Cheng[1] and Zheng-Gao Xie[1*]

[1]Department of Ophthalmology, Nanjing Drum Tower Hospital, The Affiliated Hospital of Nanjing University Medical School, Nanjing, China, [2]Department of Ophthalmology, The First People's Hospital of Kunshan Affiliated with Jiangsu University, Suzhou, China

Purpose: We aim to analyze the clinical and genetic features in a Chinese family with congenital retinoschisis by whole-exome sequencing and comprehensive clinical examination.

Methods: Six members were recruited from a Chinese family. Three of them were diagnosed as congenital retinoschisis, including two twin siblings. All subjects received a full eye examination. Whole-exome sequencing (WES) and Sanger sequencing were performed on two twin probands and all participants, respectively.

Results: A novel splice site mutation RS1.c.53-1G>A was identified in a Chinese congenital retinoschisis family. The mean onset age was 16.7 ± 2.4 years old. The average BCVA in patients was 0.37 ± 0.05. A typical spoke-wheel pattern was observed in all affected eyes. OCT examination results showed fovea schisis and schisis cavities were located in the inner nuclear layer in 100% eyes (6/6). ERG b/a ratio was decreased markedly, but was still more than 1 in the four eyes that were available.

Conclusion: The present study discovered a new pathogenic splice cite variant of RS1 in congenital retinoschisis, which expands the mutational spectrum. In contrast to previous research, the phenotype of patients with the same mutation within one family was highly similar. Early molecular testing is crucial for early diagnosis, clinical management, and genetic counseling of patients with congenital retinoschisis.

KEYWORDS

congenital retinoschisis, gene mutation, RS1, sequencing, genotype–phenotype

Introduction

Congenital retinoschisis is one of the most common early onset genetic retinal diseases with an estimated incidence ranging 1/5000 to 1/25,000 (Molday et al., 2012). This disease commonly occurs in male patients and typically manifests as bilateral varying degrees of decreased visual acuity during their juvenile period, foveal schisis with or without a peripheral schisis in the affected patients, and decreased of b/a ratio in electroretinogram (ERG) responses (a significant decrease of the b-wave amplitude relative to a-wave amplitude changes) (Alexander et al., 2001; Khan et al., 2001; Kjellstrom et al., 2010). The progression of congenital retinoschisis varies considerably, even in the same family. Frequently reported complications including macular holes (MH), retinal detachment (RD), vitreous hemorrhage (VH), and neovascular glaucoma may lead to adverse consequences during disease progression (Ip et al., 1999; Pimenides et al., 2005; Kim et al., 2006).

Although Hass et al. described retina split cases as early as 1898, the term "retinoschisis" was first formulated by Jager et al. in 1953 (Rao et al., 2018). Previous reports suggest that congenital retinoschisis cases is most frequently observed in males and can show as an X-linked inherited pattern (Gieser and Falls, 1961bib_Gieser_and_Falls_1961bib_Gieser_and_Falls_1961bib_Gieser_and_Falls_1961). To date, only the RS1 gene (Xp22.13. OMIM#300839) has been identified to be related to X-linked congenital retinoschisis. Over 250 mutations have been reported in Human Gene Mutation Database (HGMD: https://portal.biobase-international.com) (Kondo et al., 2019). The RS1 gene consists of six exons and five introns, spanning 32.43 kb of genomic DNA. This mRNA translates into a 224 amino acid protein, which is termed retinoschisin and contains a 23 amino acid N-terminus cleavable signal sequence (exon1-2), 39 amino acid RS domain(exon3), 157 amino acid highly conserved discoidin (DS) domain(exon4-6), and 5 amino acid C-terminal segment (end of exon6). Retinoschisin is mainly expressed in the photoreceptors and bipolar cells, and is thought to be involved in cell adhesion and signaling (Gehrig et al., 1999; Molday, 2007).

A highly heterogeneous clinical phenotype is common, even within the same family, in the presence of the same RS1 variant (Molday et al., 2012). However, early accurate diagnosis of congenital retinoschisis remains challenging. Genetic testing could help improve the effective, timely, and accurate diagnosis of congenital retinoschisis and guide appropriate intervention in the early stage. To increase our understanding of this disease, this study aims to report and analyze the molecular genetics and clinical features of X-linked congenital retinoschisis in Chinese twins family patients. These results could strongly support genetic counseling and target gene therapy for this disease.

Methods

Patients and research ethics

This research followed the Helsinki declaration and was approved by the ethics committee of Nanjing Drum Tower hospital. Informed consent is taken from all the participants in the study.

Six members were recruited from the same family at the Nanjing Drum Tower hospital. Three of them were diagnosed as congenital retinoschisis based on medical history and ophthalmological examinations, including optical coherence tomography (OCT), electroretinogram (ERG), and fundus photography by ophthalmologist of the Ophthalmological Department in Nanjing Drum Tower hospital. Among them, two patients are same-sex twins. Peripheral blood was obtained from the affected and unaffected members.

Clinical data

Participants were assessed by medical family histories and detailed ophthalmic examinations, including best-corrected visual acuity (BCVA), slit-lamp examination, intraocular pressure (Goldmann tonometry), dilated fundoscopy, fundus photography (Topcon TRC50LX; Topcon, Tokyo, Japan), OCT (Heidelberg Engineering, Heidelberg, Germany), and full-field electroretinography (Roland Consult, Germany, based on the standards of the International Society for Clinical Electrophysiology of Vision (ISCEV)).

DNA extraction and sequencing

DNA was extracted from peripheral blood in accordance with standard procedures. DNA libraries were prepared using KAPA Hyper Exome Kits (Roche, Switzerland) and were sequenced on a MGISEQ-2000 platform (BGI, Inc., Shenzhen, China) according to the manufacturer's protocols. The targeted sequencing covered more than 99% of the target regions. The average sequencing depth was 180X, with over 99% of on target bases containing a depth reaching up to 20X. Sequenced reads were aligned to reference genome (UCSC, hg19) using BWA. SNV and Indel calls, as well as genotypes detection were conducted using the GATK tool. ExomeDepth was used to detect copy number variants (CNVs). Sequencing was completed by HuaDa Genomic Co. Ltd. (Shenzhen, Guangdong, China).

TABLE 1 Clinical data of patients with congenital retinoschisis.

Subject	Sex	Onset age (years)	BCVA	XLRS type	Schisis localization	ERG(b/a)		Complications	Mutation	State
						Scotopic3.0	Photopic3.0			
III:5	M	15	0.4/0.4	Foveal	INL	1.35/1.06	2.15/1.17	N	RS1. c.53-1G>A	Hemizygous
III:6	M	15	0.4/0.4	Foveal	INL	1.06/1.21	1.93/1.96	N	RS1. c.53-1G>A	Hemizygous
III:4	F	N	1.0/1.0	N	N	NA	NA	N	RS1. c.53-1G>A	Heterozygous
II:3	M	40	0.3/0.3	Foveal	INL	NA	NA	N	RS1. c.53-1G>A	Hemizygous
II:5	M	N	1.0/1.0	N	N	NA	NA	N	N	N
II:6	F	N	1.0/1.0	N	N	NA	NA	N	RS1. c.53-1G>A	Heterozygous

Note: N, no; NA, not available; INL, inner nuclear layer.

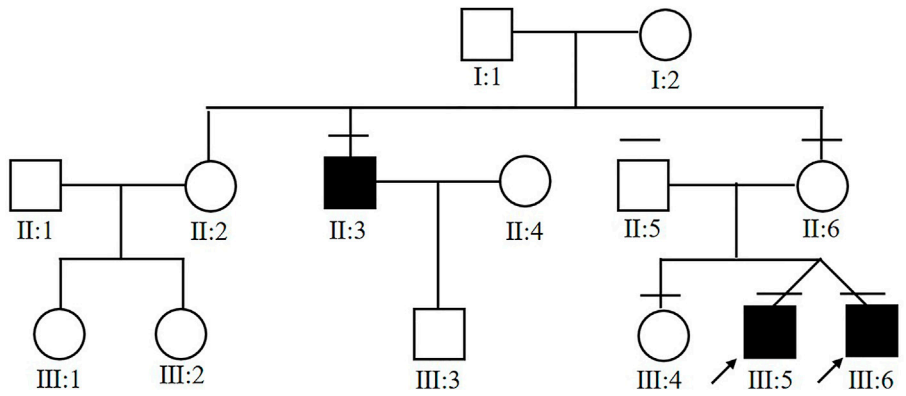

FIGURE 1
Pedigree chart of the affected family. Arrow indicates proband. Black filled symbols indicate patients.

Mutation analysis

The pathogenicity of candidate variants identified in the probands were predicted by various bioinformatics tools: Mutation Taster, Splice AI, dbscSNV_RF, dbscSNV_ ADA, FATHMM, CADD, GERP++, SiPhy, PhyloP Vertebrates, PhyloP Placetal Mammals. We used SpliceTool (https://rddc.tsinghua-gd.org/search-middle?to=SplitToolModel) and varSEAK (https://varseak.bio/) to perform the splice functional analysis. Allele frequency was assessed by the 1000G, ExAC, ESP6500, GnomAD, GWAS, Clinvar database. The Sanger sequencing was performed on DNA samples from probands for genotype confirmation and from family members for family co-segregation analysis. The reference genomic sequence version of RS1 was NM_000330.3.

Results

Clinical data

Demographic data

Six members from the same family were included in this study (Figure 1). All of the three affected subjects (III:5, III:6, II:3) were males with a median onset age 16.7 ± 2.4. Two of the patients (III:5 and III:6) were twins. Decreased vision in both eyes was the only first symptom in III:5, III:6, and II:3. No complications were observed in patients with congenital retinoschisis after careful examination by an ophthalmologist. The mean BCVA in both eyes was 0.37 ± 0.05. Interestingly, the twin patients had the same corrected vision. No abnormal manifestation was found in Anterior segment examination

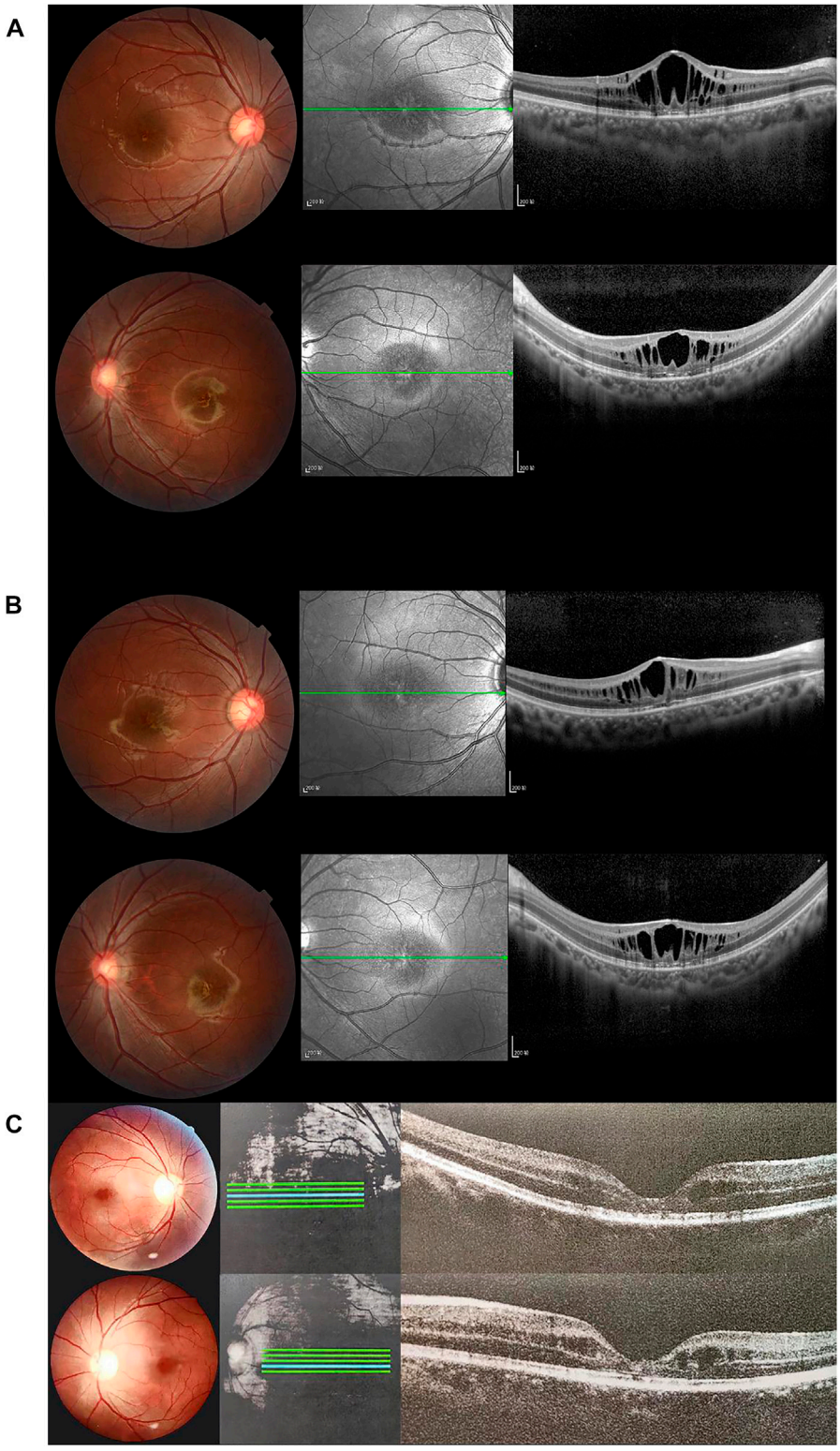

FIGURE 2
Fundus photographs and optical coherence tomography (OCT) images of patients and healthy subjects. Right eye (above), left eye (below). **(A)** Fundus photographs and OCT findings of fovea schisis of **III**:5. **(B)** Fundus photographs and OCT findings of fovea schisis of III:6. **(C)** Fundus photographs and OCT findings of fovea schisis of II:3. **(D)** Fundus photographs and OCT findings of normal fundus of II:6. **(E)** Fundus photographs and OCT findings of normal fundus of II:5. **(F)** Fundus photographs and OCT findings of normal fundus of III:4.

10.3389/fgene.2022.993157

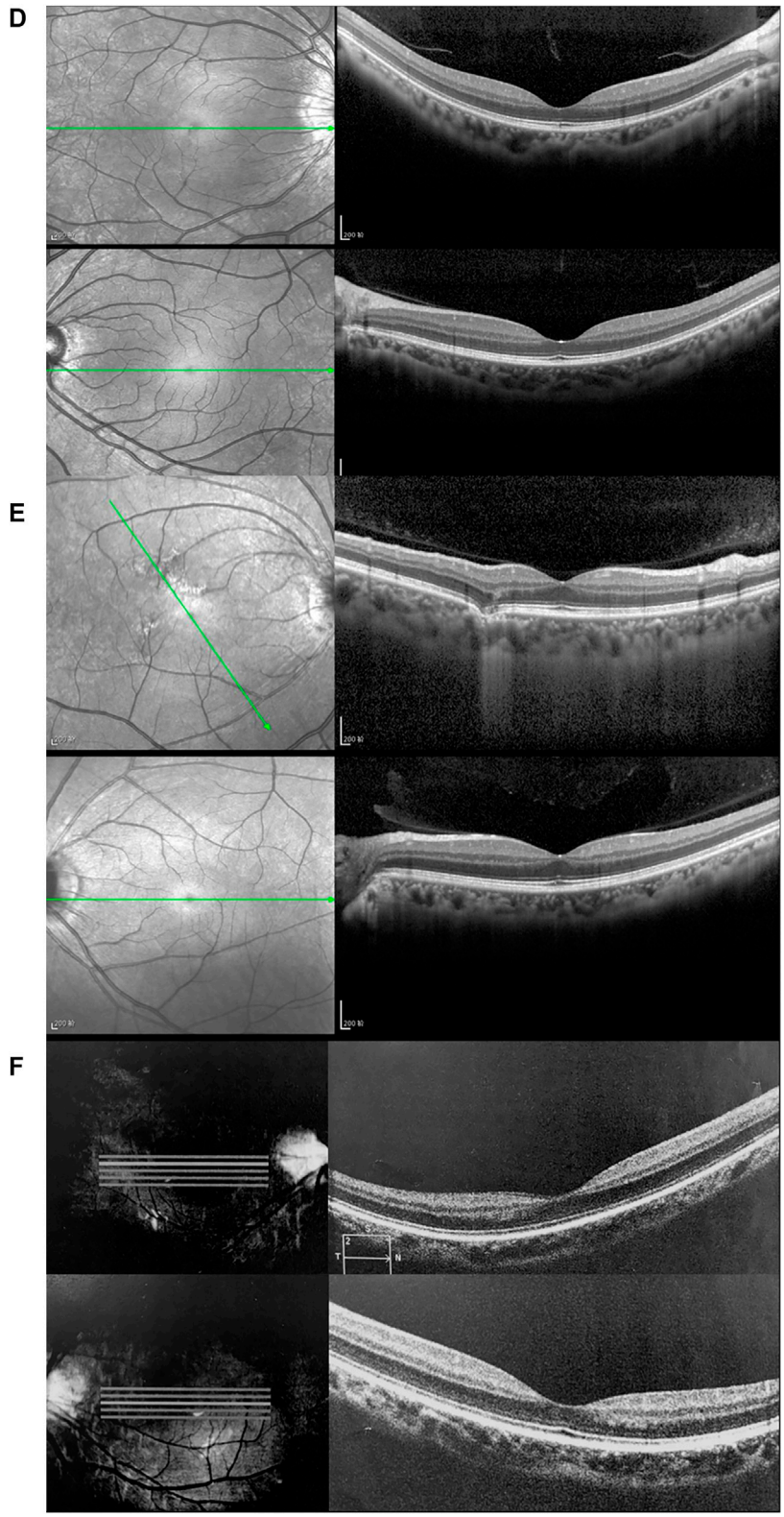

FIGURE 2

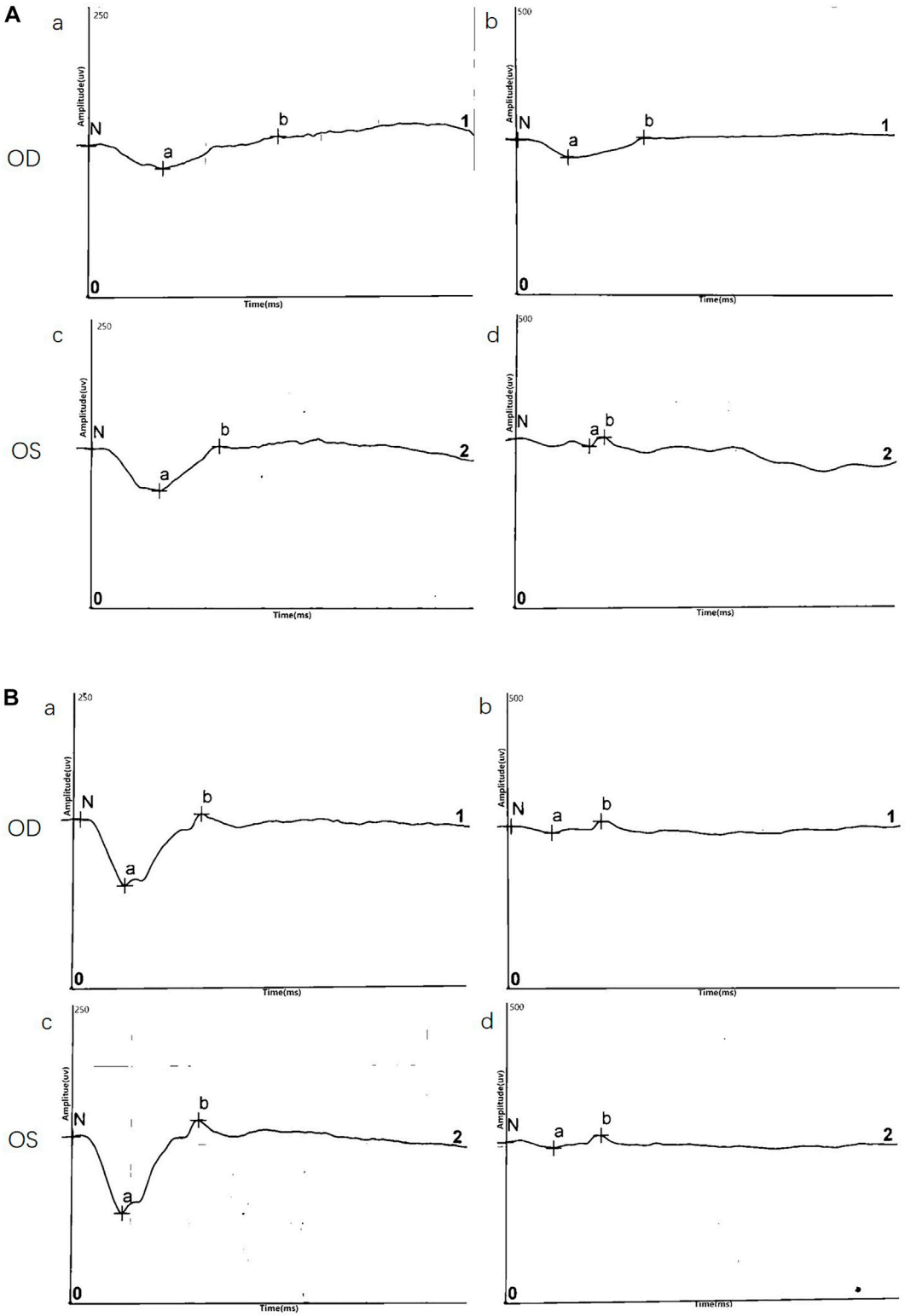

FIGURE 3
Representative electroretinography (ERG) responses. **(A)** ERG results of III:5**(B)** ERG results of III:6. Left side: dark-adapted ERG (DA 3.0 ERG); Right side: light-adapted ERG (LA 3.0 ERG).

TABLE 2 ERG responses for probands III:5 and III:6.

	a wave (OD/OS)		b wave (OD/OS)		b/a ratio	
	III:5	III:6	III:5	III:6	III:5	III:6
DA 3.0	213/243	76.4/136	225/293	103/145	1.06/1.21	1.35/1.06
DA 10.0	293/314	108/176	273/315	132/200	0.93/1.00	1.22/1.14
LA 3.0	38.7/39.5	35.2/48.8	74.6/77.6	75.8/57.4	1.93/1.96	2.15/1.18

and the IOP in all patients. All of the information is collected in Table 1.

Fundus photograph

Normal fundus findings were seen in six eyes of three healthy people. Fundus images showed a typical spoke-wheel pattern in fovea region of both eyes in all patients (Figure 2). Besides, fundoscopy revealed bilateral changes in fovea region.

OCT

OCT data was available for 12 eyes of three patients and three healthy members. OCT images of unaffected subjects revealed normal structures. Meanwhile, fovea schisis was observed in all eyes of the three patients. The average macular thickness was 388.7 ± 143.0 (μm, range). Schisis cavities were predominantly localized in the INL (6/6, 100%). We also found all the affected eyes had disruption of the EZ integrity. The details are summarized in Figure 2 and Table 1.

ERG

ERG data was obtained for two twins probands (four eyes) and demonstrated a reduction in b/a ratio with a b-wave that decreased disproportionately than the a-wave. Surprisingly, except data of DA10.0 ERG on one eye, no electronegative ERG waveform was recorded in the affected eyes. Although almost all eyes (4/4, 100%) showed a reduced b-wave on DA ERGs and LA ERGs, they had a normal or nearly normal a-wave. ERG results are shown in Figure 3 and Table 2.

Genetic characteristics

In the twin probands, we detected a novel pathogenic splice site mutation c.53-1G>A in RS1 gene. Sanger sequencing and co-segregated analysis were performed to validate this mutation in the family. III:5, III:6, and II:3 harbored a hemizygous mutation, while III:4 and II:6 were healthy heterozygous carriers (Table 1; Figure 4). The pathogenicity of the c.53-1G>A mutation was evaluated by various tools. The mutant alleles frequency was absent in all databases, including 1000G, ExAC, ESP6500, GnomAD, ClinVar, and GWAS. This mutation was predicted to be disease-causing by bioinformatic tools: Mutation Taster, SpliceAI, dbscSNV_RF, and dbscSNV_ADA. Additionally, c.53-1G>A was confirmed to be highly conserved among organisms (Table 3). The prediction results of SpliceTool and varSEAK show that this mutation changed the mRNA splicing pattern, leading to abnormal transcription and translation of RS1 protein (Figure 4).

Discussion

This study described the molecular, clinical, and imaging features of three male patients, including two twins probands from the same family. All patients manifested reduced visual acuity in both eyes at an early age. A typical spoke-wheel appearance and fovea schisis were observed in Fundus images and OCT images of the affected eyes, respectively. The b/a wave ratio on the ERG was dramatically decreased in all patients harboring hemizygous mutation c.53-1G>A from this family. This is the first time that the characteristics of twin brothers in have been compared the presence of the same mutation within the same pedigree.

Our fundus results were slightly different from previous studies. Peripheral and fovea schisis was present in 77.27% in Li et al.'s study. Gao et al. and Hahn et al. mentioned that foveal schisis were present in 92.86 and 70.4%, respectively. In addition, inner nuclear layer schisis was detected in 46.43%, and spoke-wheel pattern was only seen in 50.7% patients. Here, all of the fundus images of patients showed a typical spoke-wheel pattern. Foveal schisis and inner nuclear layer schisis were observed in all of the affected eyes. This inconsistency may be caused by the small sample size and the common root of the same pedigree (Huang et al., 2020; Gao et al., 2021; Hahn et al., 2022).

Several reports found that almost all patients showed a normal or nearly normal a-wave, which is consistent with a preservation of photoreceptor function (Bowles et al., 2011). Similarly, our findings reconfirmed that the dysfunction region lies beyond the photoreceptors. Most patients demonstrated a typical electronegative ERG waveform. However, the b/a ratio remained more than 1 in 100% of eyes in our study, which indicates that maybe synaptic function of retina was not totally disrupted and corresponds to the results in previous publications (Bowles et al., 2011; Vincent et al., 2013; Ores et al., 2018).

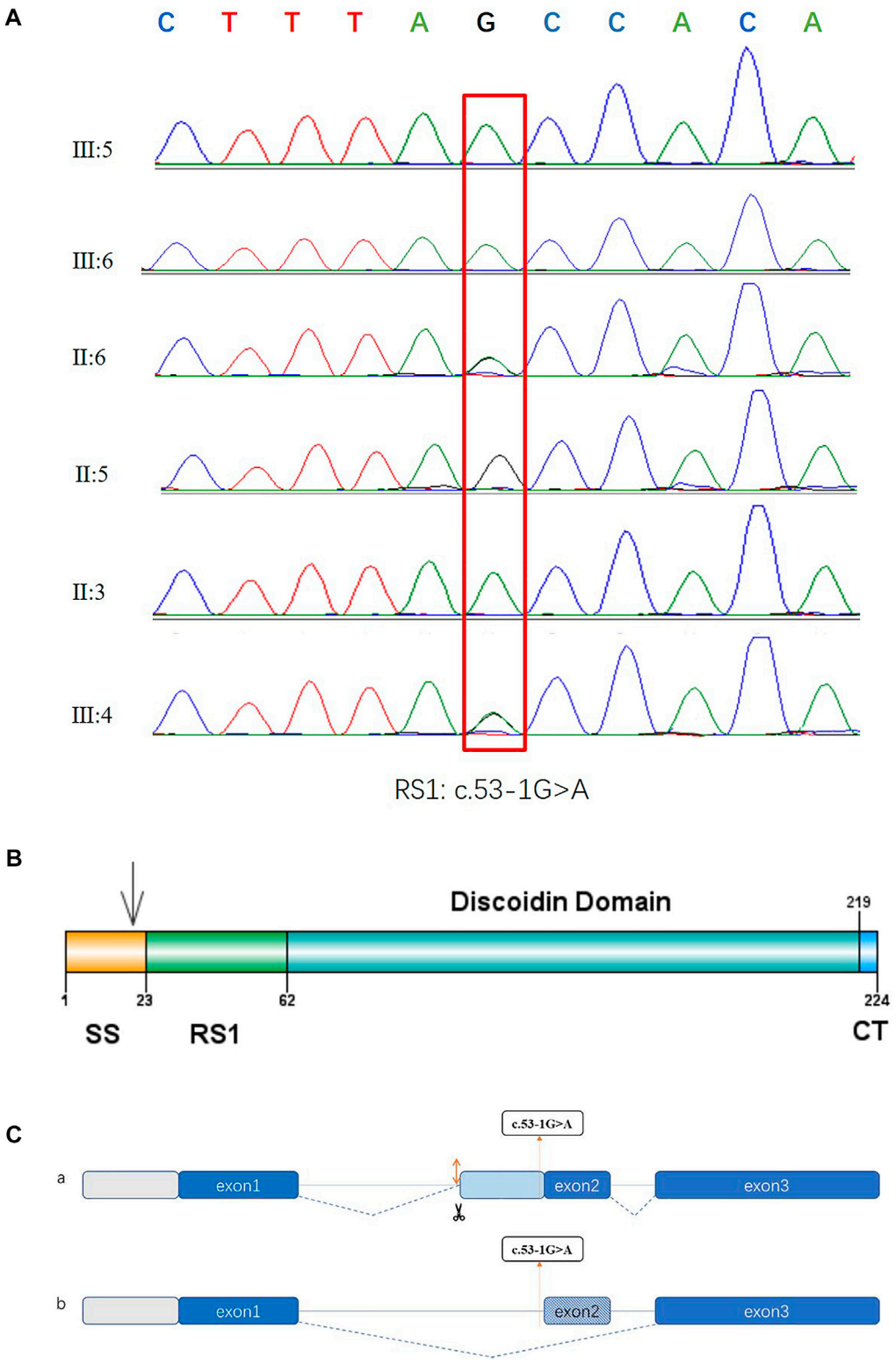

FIGURE 4
Sequencing diagrams of the RS1 mutation, domain diagram of the RS1 protein and prediction results of splice pattern of the identified mutation in this study. **(A)** Red box indicates the mutation site. **(B)** The RS1 protein comprises three domains. SS: N-terminal sequence or signal sequence. RS1: RS1 domain. DS: Discoidin domain. CT: C-terminal segment. **(C)** Two predictive splice patterns. **(a)** Insertion of 29 bp into intron 1 causes alternative splicing acceptor, leading to a frameshift and the premature termination of translation. **(b)** 26 bp deletion at splice region causes exon skipping, resulting in a frameshift and the premature termination of translation.

TABLE 3 Overviews of the pathogenicity evaluation of the RS1mutation.

Mutation	Type	Exon	Domain	AA change	Allele frequency						Prediction									
					1000G	ExAC	ESP6500	GnoraAD	GWAS	ClinVar	Mutation taster	SpliceAI	dbscSNV RF	dbscSNV ADA	FATHNIM	CADD	GERP++	SiPhy	PhyloP vertebrates	PhyloP placental mammals
c.53-1G>A	splice I	Intron 1	SS	-	0	0	0	0	0	0	D	D	D	D	C	C	C	C	C	C

Note: D, disease causing; C, conserved.

X-linked congenital retinoschisis showed a high genetic and phenotypic heterogeneity. Several studies have illustrated that patients with the same variants, even within the same family, have distinct phenotypes. However, no clear association between genotype and phenotype has yet been established (Xiao et al., 2016; Huang et al., 2020). Our findings were inconsistent with previous research. Clinical appearance and fundus changes were greatly similar in the twin siblings (III:5 and III:6), which might be explained by their highly similar genetic modifiers, environmental factors, or transcript profiles. However, further experiments are required to determine whether some genotype–phenotype correlation exists among patients.

This study also found a new pathogenic splice site mutation c.53-1G>A in intron 1 in a pedigree with congenital retinoschisis. Previous studies have reported that splice site mutation could cause exon skipping, intron retention, creation of an intronic pseudo-exon, or activation of cryptic splice site. Here, the prediction results suggested that this splice mutation may create an alternative splice acceptor or result in exon skipping, leading to a frameshift and premature termination. This novel mutation was indicated to be clustered in signal sequence, and aberrant spliced mRNA eventually produced abnormal protein synthesis and localization (Figure 4) (Wang et al., 2006; Vijayasarathy et al., 2010; Molday et al., 2012). The mechanisms of the involvement of RS1 protein in congenital retinoschisis remain uncertain. It is widely accepted that the RS1 protein (retinoschisin) is specifically expressed in bipolar cells, photoreceptors, and amacrine cells, and serves as a cell adhesin protein to stabilize the retina structure (Grayson et al., 2000; Molday et al., 2001). Another hypothesis contends that retinoschisin seems to be involved in regulating fluid balance both inside and outside the retinal cells (Renner et al., 2006; Molday et al., 2012). Thus, mutations causing congenital retinoschisis may impair the intercellular adhesion and change the tissue structure. According to previous reports, about 251 mutations have been identified. Mutations localized in the DS domain accounted for the largest proportion and missense type was the most common mutation (Hu et al., 2017; Chen et al., 2020). Female carriers seldom present with abnormal retinal function. Heterozygotes, II:6 and III:4 in our study were phenotypically normal. This result is in line with previous research. In some female patients with heterozygous mutation, ERG abnormalities may result from skewed X-inactivation (McAnany et al., 2016).

Several surgical and non-surgical treatment options have been used. Carbonic anhydrase inhibitors (CAIs) and vitrectomy have been reported to be useful adjuncts for gene therapy. Recent studies in the X-linked congenital retinoschisis mouse model also identified restoration of retinal structure and function after RS1 gene therapy. Clinical trials for RS1 gene therapy are underway in United States, but the effect of treatment remains to be explored (Cukras et al., 2018; Vijayasarathy et al., 2021). We detected a new disease-causing mutation in RS1 gene

and compared the clinical features of patients, which expands the mutation spectrum and furthers our understanding of the disease. This could support diagnosis and treatment of X-linked congenital retinoschisis.

In conclusion, although our sample size was small, we did find a novel pathogenic variant c.53-1G>A in RS1 gene, which broadens the mutant spectrum. This study also analyzed the clinical characteristics of a twin brother and raised new insights to clinical heterogeneity of X-linked congenital retinoschisis. The present study may not only help to guide genetic counseling, accurate diagnosis, and early intervention of this disease but it also provides promising perspectives for future gene therapy of congenital retinoschisis patients.

Data availability statement

The datasets for this article are not publicly available due to concerns regarding participant/patient anonymity. Requests to access the datasets should be directed to the corresponding author.

Ethics statement

The studies involving human participants were reviewed and approved by Ethics Committee of Nanjing Drum Tower hospital. Written informed consent to participate in this study was provided by the participants' legal guardian/next of kin. Written informed consent was obtained from the individual(s), and minor(s)' legal guardian/next of kin, for the publication of any potentially identifiable images or data included in this article.

Author contributions

Z-GX conceived, supervised the study, and provided funding supports. XZ evaluated clinical characteristics for the enrolled patients. X-FW, F-F C, and X-XC carried out the experiments. X-FW performed the data analysis and wrote the manuscript. Z-GX revised the manuscript. All authors contributed to the article and approved the submitted version.

Acknowledgments

We thank all of the subjects for their participation in this study.

Conflict of interest

The authors declare that the research was conducted in the absence of any commercial or financial relationships that could be construed as a potential conflict of interest.

Publisher's note

All claims expressed in this article are solely those of the authors and do not necessarily represent those of their affiliated organizations, or those of the publisher, the editors, and the reviewers. Any product that may be evaluated in this article, or claim that may be made by its manufacturer, is not guaranteed or endorsed by the publisher.

References

Alexander, K., Barnes, C., and Fishman, G. (2001). High-frequency attenuation of the cone ERG and ON-response deficits in X-linked retinoschisis. *Invest.. Ophthalmol. Vis. Sci.* 42 (9), 2094–2101.

Bowles, K., Cukras, C., Turriff, A., Sergeev, Y., Vitale, S., Bush, R. A., et al. (2011). X-Linked retinoschisis: RS1 mutation severity and age affect the ERG phenotype in a cohort of 68 affected male subjects. *Invest.. Ophthalmol. Vis. Sci.* 52 (12), 9250–9256. doi:10.1167/iovs.11-8115

Chen, C., Xie, Y., Sun, T., Tian, L., Xu, K., Zhang, X., et al. (2020). Clinical findings and RS1 genotype in 90 Chinese families with X-linked retinoschisis.. *Mol. Vis.* 26, 291–298.

Cukras, C., Wiley, H. E., Jeffrey, B. G., Sen, H. N., Turriff, A., Zeng, Y., et al. (2018). Retinal AAV8-RS1 gene therapy for X-linked retinoschisis: Initial findings from a phase I/IIa trial by intravitreal delivery. *Mol. Ther.* 26 (9), 2282–2294. doi:10.1016/j.ymthe.2018.05.025

Gao, F. J., Dong, J. H., Wang, D. D., Chen, F., Hu, F. Y., Chang, Q., et al. (2021). Comprehensive analysis of genetic and clinical characteristics of 30 patients with X-linked juvenile retinoschisis in China. *Acta Ophthalmol.* 99 (4), e470–e479. doi:10.1111/aos.14642

Gehrig, A., White, K., Lorenz, B., Andrassi, M., Clemens, S., and Weber, B. (1999). Assessment of RS1 in X-linked juvenile retinoschisis and sporadic senile retinoschisis. *Clin. Genet.* 55 (6), 461–465. doi:10.1034/j.1399-0004.1999.550611.x

Gieser, E. P., and Falls, H. F. (1961). Hereditary retinoschisis. *Am. J. Ophthalmol.* 51 (6), 1193–1200. doi:10.1016/0002-9394(61)92457-6

Grayson, C., Reid, S., Ellis, J., Rutherford, A., Sowden, J., Yates, J., et al. (2000). Retinoschisin, the X-linked retinoschisis protein, is a secreted photoreceptor protein, and is expressed and released by Weri-Rb1 cells. *Hum. Mol. Genet.* 9 (12), 1873–1879. doi:10.1093/hmg/9.12.1873

Hahn, L. C., van Schooneveld, M. J., Wesseling, N. L., Florijn, R. J., Ten Brink, J. B., Lissenberg-Witte, B. I., et al. (2022). X-linked retinoschisis: Novel clinical observations and genetic spectrum in 340 patients. *Ophthalmology* 129 (2), 191–202. doi:10.1016/j.ophtha.2021.09.021

Hu, Q. R., Huang, L. Z., Chen, X. L., Xia, H. K., Li, T. Q., and Li, X. X. (2017). Genetic analysis and clinical features of X-linked retinoschisis in Chinese patients. *Sci. Rep.* 7, 44060. doi:10.1038/srep44060

Huang, L., Sun, L., Wang, Z., Chen, C., Wang, P., Sun, W., et al. (2020). Clinical manifestation and genetic analysis in Chinese early onset X-linked retinoschisis. *Mol. Genet. Genomic Med.* 8 (10), e1421. doi:10.1002/mgg3.1421

Ip, M., Garza-Karren, C., Duker, J. S., Reichel, E., Swartz, J. C., Amirikia, A., et al. (1999). Differentiation of degenerative retinoschisis from retinal detachment using optical coherence tomography. *Ophthalmology* 106 (3), 600–605. doi:10.1016/s0161-6420(99)90123-9

Khan, N., Jamison, J., Kemp, J., and Sieving, P. (2001). Analysis of photoreceptor function and inner retinal activity in juvenile X-linked retinoschisis. *Vis. Res.* 41 (28), 3931–3942. doi:10.1016/s0042-6989(01)00188-2

Kim, L. S., Seiple, W., Fishman, G. A., and Szlyk, J. P. (2006). Multifocal ERG findings in carriers of X-linked retinoschisis. *Doc. Ophthalmol.* 114 (1), 21–26. doi:10.1007/s10633-006-9034-9

Kjellstrom, S., Vijayasarathy, C., Ponjavic, V., Sieving, P. A., and Andreasson, S. (2010). Long-term 12 year follow-up of X-linked congenital retinoschisis. *Ophthalmic Genet.* 31 (3), 114–125. doi:10.3109/13816810.2010.482555

Kondo, H., Oku, K., Katagiri, S., Hayashi, T., Nakano, T., Iwata, A., et al. (2019). Novel mutations in the RS1 gene in Japanese patients with X-linked congenital retinoschisis. *Hum. Genome Var.* 6, 3. doi:10.1038/s41439-018-0034-6

McAnany, J. J., Park, J. C., Collison, F. T., Fishman, G. A., and Stone, E. M. (2016). Abnormal 8-Hz flicker electroretinograms in carriers of X-linked retinoschisis. *Doc. Ophthalmol.* 133 (1), 61–70. doi:10.1007/s10633-016-9551-0

Molday, L., Hicks, D., Sauer, C., Weber, B., and Molday, R. (2001). Expression of X-linked retinoschisis protein RS1 in photoreceptor and bipolar cells. *Invest.. Ophthalmol. Vis. Sci.* 42 (3), 816–825.

Molday, R. S. (2007). Focus on molecules: Retinoschisin (RS1). *Exp. Eye Res.* 84 (2), 227–228. doi:10.1016/j.exer.2005.12.013

Molday, R. S., Kellner, U., and Weber, B. H. F. (2012). X-linked juvenile retinoschisis: Clinical diagnosis, genetic analysis, and molecular mechanisms. *Prog. Retin. Eye Res.* 31 (3), 195–212. doi:10.1016/j.preteyeres.2011.12.002

Ores, R., Mohand-Said, S., Dhaenens, C. M., Antonio, A., Zeitz, C., Augstburger, E., et al. (2018). Phenotypic characteristics of a French cohort of patients with X-linked retinoschisis. *Ophthalmology* 125 (10), 1587–1596. doi:10.1016/j.ophtha.2018.03.057

Pimenides, D., George, N. D., Yates, J. R., Bradshaw, K., Roberts, S. A., Moore, A. T., et al. (2005). X-Linked retinoschisis: Clinical phenotype and RS1 genotype in 86 UK patients. *J. Med. Genet.* 42 (6), e35. doi:10.1136/jmg.2004.029769

Rao, P., Dedania, V. S., and Drenser, K. A. (2018). Congenital X-linked retinoschisis: An updated clinical review. *Asia. Pac. J. Ophthalmol.* 7 (3), 169–175. doi:10.22608/APO.201803

Renner, A. B., Kellner, U., Cropp, E., and Foerster, M. H. (2006). Dysfunction of transmission in the inner retina: Incidence and clinical causes of negative electroretinogram. *Graefes Arch. Clin. Exp. Ophthalmol.* 244 (11), 1467–1473. doi:10.1007/s00417-006-0319-1

Vijayasarathy, C., Sui, R., Zeng, Y., Yang, G., Xu, F., Caruso, R. C., et al. (2010). Molecular mechanisms leading to null-protein product from retinoschisin (RS1) signal-sequence mutants in X-linked retinoschisis (XLRS) disease. *Hum. Mutat.* 31 (11), 1251–1260. doi:10.1002/humu.21350

Vijayasarathy, C., Zeng, Y., Brooks, M. J., Fariss, R. N., and Sieving, P. A. (2021). Genetic rescue of X-linked retinoschisis mouse (Rs1(-/y)) retina induces quiescence of the retinal microglial inflammatory state following AAV8-RS1 gene transfer and identifies gene networks underlying retinal recovery. *Hum. Gene Ther.* 32 (13-14), 667–681. doi:10.1089/hum.2020.213

Vincent, A., Robson, A. G., Neveu, M. M., Wright, G. A., Moore, A. T., Webster, A. R., et al. (2013). A phenotype-genotype correlation study of X-linked retinoschisis. *Ophthalmology* 120 (7), 1454–1464. doi:10.1016/j.ophtha.2012.12.008

Wang, T., Zhou, A., Waters, C. T., O'Connor, E., Read, R. J., and Trump, D. (2006). Molecular pathology of X linked retinoschisis: Mutations interfere with retinoschisin secretion and oligomerisation. *Br. J. Ophthalmol.* 90 (1), 81–86. doi:10.1136/bjo.2005.078048

Xiao, Y., Liu, X., Tang, L., Wang, X., Coursey, T. G., Guo, X., et al. (2016). X-linked retinoschisis: Phenotypic variability in a Chinese family. *Sci. Rep.* 6, 20118. doi:10.1038/srep20118

frontiers | Frontiers in Genetics

TYPE Original Research
PUBLISHED 04 October 2022
DOI 10.3389/fgene.2022.1019208

OPEN ACCESS

EDITED BY
Jeremy Guggenheim,
Cardiff University, United Kingdom

REVIEWED BY
Qingnan Liang,
Baylor College of Medicine,
United States
Xian-Jie Yang,
University of California, Los Angeles,
United States

*CORRESPONDENCE
Yihua Zhu,
zhuyihua209@163.com
Juhua Yang,
julian_yang@fjmu.edu.cn

SPECIALTY SECTION
This article was submitted to Genetics of Common and Rare Diseases, a section of the journal Frontiers in Genetics

RECEIVED 14 August 2022
ACCEPTED 16 September 2022
PUBLISHED 04 October 2022

CITATION
Zhou B, Lin X, Li Z, Yao Y, Yang J and Zhu Y (2022), Structure–function–pathogenicity analysis of C-terminal myocilin missense variants based on experiments and 3D models. *Front. Genet.* 13:1019208. doi: 10.3389/fgene.2022.1019208

Structure–function–pathogenicity analysis of C-terminal myocilin missense variants based on experiments and 3D models

Biting Zhou[1], Xiaojia Lin[1], Zhong Li[2], Yihua Yao[1], Juhua Yang[2]* and Yihua Zhu[1]*

[1]Department of Ophthalmology, The First Affiliated Hospital of Fujian Medical University, Fuzhou, China, [2]Department of Bioengineering and Biopharmaceutics, School of Pharmacy, Fujian Medical University, Fuzhou, China

MYOC is a common pathogenic gene for primary open-angle glaucoma and encodes the protein named myocilin. Multiple MYOC variations have been found, with different clinical significance. However, the pathogenesis of glaucoma induced by MYOC mutations has not been fully clarified. Here, we analyze the molecular and cellular biological differences caused by multiple variant myocilins, including protein secretion characteristics, structural changes, subcellular localization, cellular autophagic activity and oxidative stress. Denaturing and nondenaturing electrophoresis showed myocilin to be a secreted protein with the tendency to self-oligomerize. The full-length myocilin and its C-terminal cleavage fragment are secreted. Secretion analysis of 23 variant myocilins indicated that secretion defects are closely related to the pathogenicity of MYOC variants. Structural analysis showed that the alteration of steric clash is associated with the secretion characteristics and pathogenicity of myocilin variants. Immunocytochemistry results demonstrated that mutated myocilins are retained in the endoplasmic reticulum and disrupt autophagy. MTT assay, MitoTracker staining, and DCFH-DA staining showed increased oxidative injury in cells expressing MYOC mutants. Taken together, MYOC mutations are able to induce cell dysfunction via secretion defects and intracellular accumulation resulting from steric clash alterations.

KEYWORDS

MYOC, primary open-angle glaucoma, structure, function, pathogenicity

Introduction

Primary open-angle glaucoma (POAG) is the most common type of glaucoma, with an overall global prevalence of 2.4% (Zhang et al., 2021). The prevalence of POAG varies among different countries, races, sexes and ages. The highest prevalence is in the African population, at 4.5% (Kapetanakis et al., 2016). The prevalence of POAG in Europe and

Asia is 2.1 and 1.9% (Kapetanakis et al., 2016), respectively. Due to the large-scale population and the rapid expansion of population aging in Asia, it is estimated that the prevalence of POAG in Asia will increase to 49% by 2050 (Kapetanakis et al., 2016). People with POAG experience high intraocular pressure (IOP) and progressive optic nerve degeneration (Lei et al., 2019), rendering POAG a main cause of blindness and a severe public health problem. High IOP, as a result of damage to the trabecular meshwork (TM) and increased outflow resistance, is a major but the only controllable risk factor for POAG.

It has been reported that the risk of POAG among first-degree family members of POAG patients is significantly higher than that among first-degree family members of non-POAG patients, indicating that POAG has genetic susceptibility (Gong et al., 2007). MYOC is a major pathogenic gene of POAG, with a mutation frequency of 10%–30% (Huang et al., 2018). MYOC mutations are responsible for 2%–4% of POAG cases and 8%–36% of juvenile open-angle glaucoma (JOAG) cases (Wiggs et al., 1998; Fingert et al., 1999; Souzeau et al., 2013). To date, more than 270 MYOC variants have been found, including POAG-causing mutations, neutral polymorphisms and variations with uncertain clinical significance (Hewitt et al., 2008).

MYOC encodes myocilin, a secreted and glycosylated protein that is expressed in ocular and nonocular organs such as the heart and skeletal muscle. Nevertheless, mutation of MYOC only leads to glaucoma lesions in eyes. MYOC consists of three exons, and the olfactomedin (OLF) in the C-terminal of myocilin is estimated to houses over 90% of reported POAG-causing mutations (Scelsi et al., 2021). The exact function of myocilin remains unclear. It was reported that myocilin may be involved in interaction between cells and the extracellular matrix (ECM) (Kasetti et al., 2016; Joe et al., 2017), neurite outgrowth (Jurynec et al., 2003), cell migration (Kwon and Tomarev, 2011), mitochondrial injury of TM cells (Sakai et al., 2007), oligodendrocyte differentiation and myelination of the optic nerve (Kwon et al., 2014) and programmed cell death during retinal development (Koch et al., 2014). Previous studies have shown that MYOC knock-in or knockout mice exhibit no POAG phenotype, supporting a gain-of-function disease model (Kim et al., 2001; Gould et al., 2004; Scelsi et al., 2021). Furthermore, different MYOC mutants have been reported to have variable effects on cellular biological functions. However, functional studies reported thus far are not all-inclusive; namely, the secretion property, cellular stress responses, ECM production, cell proliferation and adhesion of mutant myocilins have not been studied together (Gobeil et al., 2006; Jia et al., 2009; Stothert et al., 2014; Yan et al., 2020), thus creating a gap in the understanding of the precise molecular mechanism that leads to POAG for each mutation. This wide functional heterogeneity of MYOC missense mutations calls for a structure–function correlation approach.

Therefore, the purpose of this study was to decipher the factors that determine the pathogenicity of MYOC variations in TM. To accomplish this, we examined molecular and cellular biological differences mediated by multiple MYOC variants, including protein secretion characteristics, structural changes, subcellular localization, cellular autophagy activity and oxidative stress.

Materials and methods

Myocilin constructs

cDNAs encoding wild-type myocilin (MYOC, NM_000261.1) and mutated myocilins were cloned into the *EcoRI-NheI* sites of the pcDNA3.1 mammalian expression vector. The primer sequences used to generate these myocilin cDNAs are shown in Supplementary Table S1. A total of 23 MYOC mutant plasmids were constructed. All constructs used in this study were verified by direct DNA sequencing.

Cell culture and transfection

Details of the cells used in this study are shown in the table below.

HEK 293T and COS-7 cell lines were maintained in Dulbecco's modified Eagle's medium (DMEM) supplemented with 10% fetal bovine serum (FBS), 100 U/ml penicillin and 100 μg/ml streptomycin. iHTMCs were cultured in DMEM/F-12 medium supplemented with 15% FBS, 100 U/ml penicillin and 100 μg/ml streptomycin. All cultures were maintained at 37°C in a humidified atmosphere of 95% air and 5% CO_2. Cells were transfected with plasmids containing wild-type (WT) or mutant MYOC cDNA by transfection reagents (Lipofectamine 2000, Invitrogen, CA, United States, Cat# 11668-019 or X-tremeGene™ 360 Transfection Reagent, Roche, Mannheim, Germany, Cat# 8724105001) following the manufacturer's instructions. To ensure the stability and consistency of the transfection efficiency of various plasmids, cells were simultaneously transfected with a cDNA construct encoding GFP and the transfection rate was measured *via* calculating the ratio of GFP-positive cells under a fluorescence microscope.

Cellular fractions preparation

After 48 h of transfection with OPTI-MEM (no FBS), the culture medium was harvested and centrifuged at 5,000 × g for 5 min at 4°C to remove dead cells, followed by 16,000 × g for 10 min at 4°C for further removal of cellular debris. The collected culture medium was concentrated using Amicon Ultra15 Centrifugal Filters (10K, Millipore, MA, United States, Cat# UFC801008) by centrifugation at 4,500 × g for 30 min at 4°C. Adhered cells were washed twice with ice-cold PBS, followed

Name	Source
Human embryonic kidney 293T (HEK 293T) cells	GENE (Shanghai, China)
COS-7 cells	Beyotime (Shanghai, China)
Immortalized human trabecular meshwork cells (iHTMCs)	Meisen CTCC (Zhejiang, China)

by resuspension in RIPA cell lysis buffer (Beyotime, Cat# P0013B) containing the proteinase inhibitor PMSF (1:100, Beyotime, Cat# ST505) and the phosphatase inhibitor PhosSTOP (Roche, Mannheim, Germany, REF 04906845001). After incubation on ice for 30 min and centrifugation, the supernatants (soluble cell fraction) were carefully separated from the pellets (insoluble cell fraction). For denaturing SDS–PAGE, aliquots of culture medium and cell fractions were treated with 4× protein loading buffer containing β-mercaptoethanol and SDS and boiled for 10 min. For nondenaturing PAGE, samples were treated with 4× protein loading buffer without β-mercaptoethanol, SDS and boiling. Samples were normalized for protein content using the Bradford assay using bovine serum albumin as a control.

Western blotting and antibodies

For western blotting analysis, aliquots of culture medium and intracellular fractions of cultured cell lines (both soluble and insoluble) were fractionated by 10%–12% SDS–PAGE. For non-denaturing PAGE, samples were loaded onto 4%–12% polyacrylamide gradient gels (GeneScript, Nanjing, China, Cat# M00654) without SDS. The proteins were transferred onto a PVDF membrane and blocked for 1 h at room temperature with 5% milk. The membrane was incubated with primary antibodies against different domains of myocilin: anti-myocilin from Millipore (1:2,000, CA, United States, Cat# MABN866) corresponding to the N-terminal fragment (aa 33-214) of human myocilin and MYOC rabbit polyclonal antibody derived from Abclonal (1:2,000, Wuhan, China, Cat# A1589) corresponding to the C-terminal fragment (aa 245-504). After overnight incubation at 4°C, the membrane was incubated with the corresponding horseradish peroxidase (HRP)-conjugated goat anti-mouse (1:5,000, Affinity Biosciences, Cat# S0002) or rabbit (1:5,000; Affinity Biosciences, Cat# S0001) secondary antibody at room temperature for 2 h. Enhanced chemiluminescence was used to visualize protein bands.

Immunocytochemistry assay

Cells were grown on confocal plates, fixed and permeabilized with methanol for 15 min at −20°C, followed by three washes with PBS. The cells were incubated for 1 h in blocking buffer (5% normal donkey serum and 0.3% Triton X-100 in PBS), followed by incubation with an anti-MYOC primary (1:400, Millipore), anti-Grp94 primary (1:200, Affinity Biosciences, Cat# AF5287), or anti-LC3 primary (1:200, Cell Signaling Technology, Cat# 4108) antibody overnight at 4°C. After gentle washing, the respective fluorescent secondary antibody purchased from Abcam (donkey anti-mouse IgG H&L, Alexa Fluor 594, Cat#ab150108, 1:1,000; donkey anti-rabbit IgG H&L, Alexa Fluor 488, Cat#ab150073, 1:1,000) was added, and the cells were incubated at 37°C for 2 h in the dark. Nuclei were stained with 0.01 mg/ml Hoechst 33342. At least six fields of view were photographed for each group of cells using a laser-scanning confocal microscope (Leica, Nussloch, Germany) and a digital camera using LAS AF software.

Cell viability assay

Cell viability was detected using 3-(4,5-dimethylthiazol-2-yl)-2,5-diphenyltetrazolium bromide (MTT; Yeasen, Shanghai, China, Cat# 40201ES80). Cells were seeded in 96-well plates. After appropriate treatment, the cells were incubated in culture medium with 0.5 mg/ml MTT for 4 h. The formed dark blue crystals were dissolved with DMSO, and absorbance was measured at 570 nm using a microplate reader.

Measurement of reactive oxygen species and mitochondrial membrane potential

Cellular oxidative injury was evaluated by detecting reactive oxygen species (ROS) generation and mitochondrial membrane potential (MMP). The generation of ROS was measured by the DCFH-DA probe (Beyotime, Cat#S0033S), and MMP was detected by the Mito-Tracker Red CMXRos probe (Beyotime, Cat#C1049) according to the manufacturers' instruction and previous studies (Jurado-Campos et al., 2021; Gu et al., 2022). Briefly, cells were cultured and treated in 24-well plates, and incubated with corresponding probes at 37°C in the dark for 30 min. After washing with PBS, the samples were examined under a fluorescence microscope.

Structural analysis

Swiss-PdbViewer software v4.1.0 was employed for structural analyses. The crystal structure of human myocilin-OLF (PDB: 4 WXQ) was selected as a template. Mutations were induced in the template one at a time using the mutate tool of the Swiss-PdbViewer software, and analyses were performed based on the "best" rotamer of the new amino acid. We examined the 1) solvent accessibility of

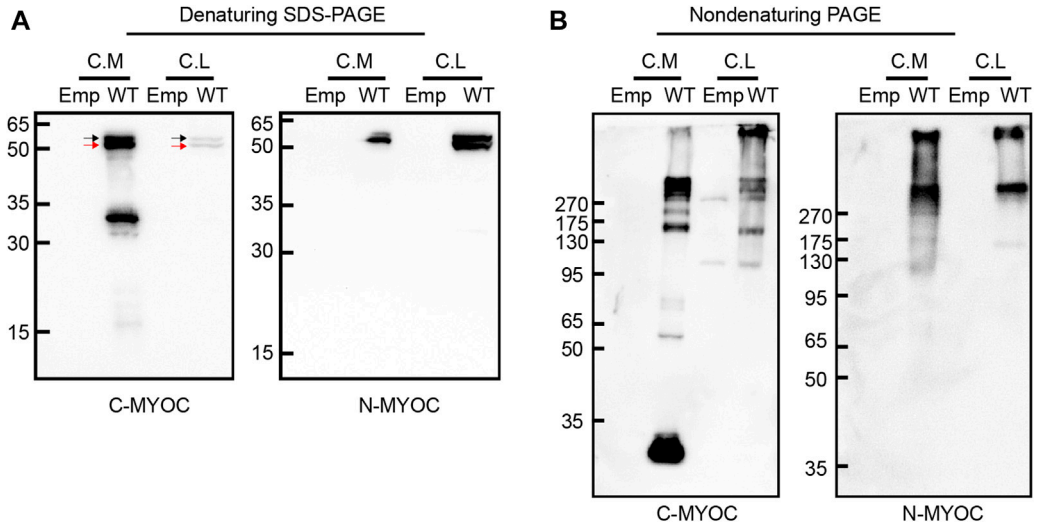

FIGURE 1
Molecular characterization of intracellular and extracellular myocilin. **(A,B)** A cDNA construct encoding the empty vector (Emp) or wild-type (WT) myocilin was transfected into HEK 293T cells. Forty-eight hours after transfection, myocilin was analyzed in the culture medium (C. M) and cell lysates (C. L) by denaturing SDS–PAGE **(A)** and nondenaturing PAGE **(B)**. Myocilin detection was carried out by western blotting using an anti-C-terminal (C-MYOC) or anti-N-terminal (N-MYOC) MYOC antibody. Black arrow: glycosylated myocilin band. Red arrow: nonglycosylated myocilin band. C. M, culture medium; C. S, RIPA-soluble cell fraction; C. I, RIPA-insoluble cell fraction.

the residues, 2) gain/loss of H-bonds, 3) induction of steric clash, 4) change in surface electrostatic potential (SEP) and 5) alteration of the molecular surface.

Statistical analysis

All experiments were performed at least 3 times. Data are presented as the mean ± SD. GraphPad Prism eight was used to determine statistical significance. Data were analyzed using one-way ANOVA with Tukey's post-hoc test for comparisons between more than two groups. $p < 0.05$ was considered statistically significant.

Results

Molecular characteristics of myocilin

We overexpressed WT myocilin in HEK 293T cells and detected the molecular characteristics of intracellular and extracellular myocilin via denaturing SDS–PAGE and nondenaturing PAGE. As shown in Figure 1A, myocilin was present in the cell medium under denaturing conditions, with two bands near 50–65 kDa that were recognized by two different myocilin antibodies. The upper band was concluded to be glycosylated myocilin (black arrow) and the lower band to be nonglycosylated myocilin (red arrow) (Caballero and Borrás, 2001). There was also a band near 30–35 kDa, which was detected only when using a C-terminal antibody; it was concluded to be the C-terminal cleavage portion of myocilin. In addition, intracellular myocilin presented as a doublet band slightly larger than 50 kDa. Nondenaturing PAGE was used to observe the native status of proteins, which keep higher-order structure without treatment of SDS, DTT and boiling. Under nondenaturing conditions (Figure 1B), except for a band smaller than 35 kDa in cell medium, bands indicating multiple oligomeric states with molecular weights of over 130 kDa were observed for both intracellular and extracellular myocilin, supporting a tendency of myocilin to self-oligomerize.

Secretion profile of myocilin variants

Myocilin contains three exons, and the N- and C-termini are the two major regions of homology. To investigate the effect of variations in different domains on myocilin secretion, we constructed 23 MYOC plasmids with variations covering all three exons (Figure 2A). The variants were chosen based on the structural and functional characteristics of myocilin (Supplementary Table S2), and all variants tested have been reported in previous human populations or pedigree screens

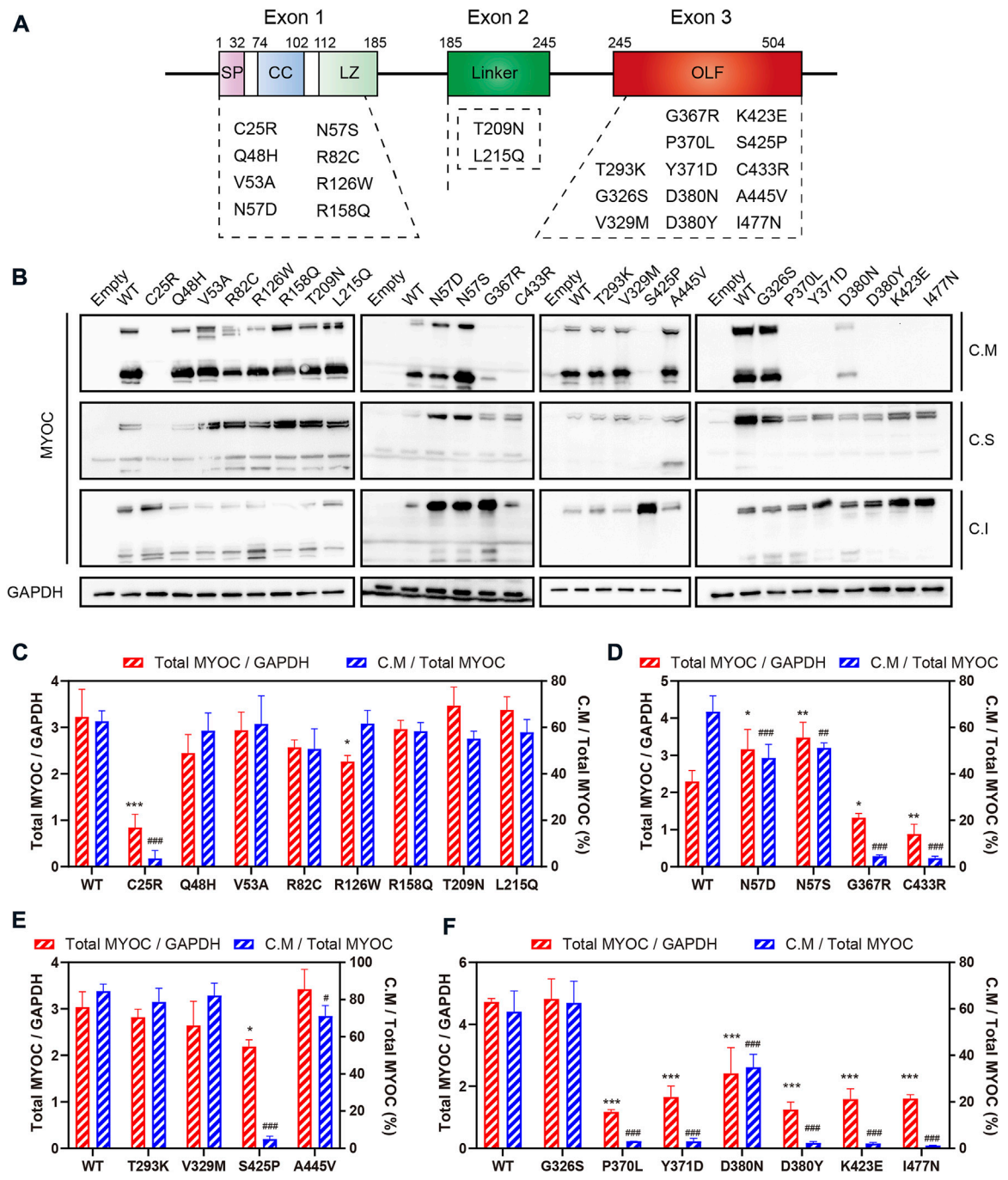

FIGURE 2
Secretion analysis of myocilin variants. **(A)** Structure of myocilin. MYOC gene has three exons, encoding myocilin that consists of signal peptide (SP), coiled-coil domain (CC), leucine zipper (LZ), linker and olfactomedin (OLF) domain. The variants listed in the dotted box are the variants studied in this study. **(B)** Western blot analysis of intracellular and extracellular myocilin in HEK 293T cells expressing different MYOC variants. Forty-eight hours after transfection, myocilin was detected in the culture medium (C. M) and in RIPA-soluble and -insoluble cell fractions (C. S and C. I) by denaturing SDS–PAGE. An MYOC antibody that recognizes the C-terminus of myocilin was used to detect expression of myocilin. **(C–F)** Densitometric analysis of immunoblotting bands. C.M = full myocilin detected in C.M + short C-terminal products detected in C.M. Total MYOC = C.M + C.S + C.I. N = 3.

10.3389/fgene.2022.1019208

TABLE 1 Localization, pathogenicity and secretion characteristics of 23 MYOC variants.

Number	Mutation	Location	Domain	Glaucoma causing	Secretion
1	C25R	Exon 1	SP	Uncertain pathogenicity	-
2	Q48H	Exon 1	CC	Neutral polymorphism	+
3	V53A	Exon 1	CC	Neutral polymorphism	+
4	N57D	Exon 1	CC	Neutral polymorphism	+
5	N57S	Exon 1	CC	Neutral polymorphism	+
6	R82C	Exon 1	CC	Neutral polymorphism	+
7	R126W	Exon 1	LZ	Neutral polymorphism	+
8	R158Q	Exon 1	LZ	Neutral polymorphism	+
9	T209N	Exon 2	Linker	Uncertain pathogenicity	+
10	L215Q	Exon 2	Linker	Glaucoma-causing mutation	+
11	T293K	Exon 3	OLF	Neutral polymorphism	+
12	G326S	Exon 3	OLF	Glaucoma-causing mutation	+
13	V329M	Exon 3	OLF	Neutral polymorphism	+
14	G367R	Exon 3	OLF	Glaucoma-causing mutation	-
15	P370L	Exon 3	OLF	Glaucoma-causing mutation	-
16	Y371D	Exon 3	OLF	Glaucoma-causing mutation	-
17	D380N	Exon 3	OLF	Uncertain pathogenicity	+
18	D380Y	Exon 3	OLF	Glaucoma-causing mutation	-
19	K423E	Exon 3	OLF	Glaucoma-causing mutation	-
20	S425P	Exon 3	OLF	Glaucoma-causing mutation	-
21	C433R	Exon 3	OLF	Glaucoma-causing mutation	-
22	A445V	Exon 3	OLF	Neutral polymorphism	+
23	I477N	Exon 3	OLF	Glaucoma-causing mutation	-

Note: SP, signal peptide; CC, coiled-coil domain; LZ, leucine zipper; OLF, olfactomedin domain. +: secretion, -: nonsecretion. The clinical significance of MYOC, variants refers to the study of Hewitt et al. (2008).

for MYOC (Table 1). Among the 23 variants, ten have been described as glaucoma-causing mutations, ten are neutral polymorphisms, and three are considered uncertain.

The plasmids constructed were transfected into HEK 293T cells, and proteins in the cell medium, soluble cell fraction and insoluble cell fraction were extracted and analyzed by denaturing SDS–PAGE using an antibody against the C-terminal region of myocilin. As shown in Figure 2B, among the N-terminal (exon 1 and exon 2) variants, only the C25R variant was absent from the culture medium, indicating that this variant was not secreted into the medium. In addition, five of the thirteen variants occurring in the C-terminus (exon 3) were secreted into the culture medium. Of the 14 secreted variants, ten featured neutral polymorphisms and two disease-causing mutations; the other two were defined as uncertain. Notably, 100% of the neutral-polymorphism proteins (10/10) were secreted, whereas 80% of the proteins encoded by disease-causing variants (8/10) were retained inside the cells (Table 1), suggesting that secretion is an important parameter that determines the pathogenicity of MYOC variations.

To further explore the effect of MYOC variations on the expression and secretion of myocilin, densitometric analysis was performed to quantify the level of myocilin in different cellular fractions (Figures 2C–F). We found that MYOC mutations located in C-terminus resulted in significantly decreased expression of total myocilin, which is mainly existed in insoluble cellular fraction (Figures 2D–F and Supplementary Figure S1). Interestingly, although D380N variation reduced the expression and secretion of myocilin, myocilin was still detectable in the culture medium (Figure 2F). Among the variations in N-terminus, C25R variation decreased the level of total myocilin dramatically and the protein was mainly existed in the insoluble fraction, which may be responsible for its nonsecretion (Figure 2C). Notably, variations in glycosylated site (N57) increased the level of total myocilin and decreased the percentage of C.M-myocilin (Figure 2D).

Structural analysis of myocilin missense variations

From the perspective of protein structure, we assessed the structural alterations induced by the 13 variations in the OLF domain because most variations of nonsecreted myocilin and most pathogenic mutations occur in this region. The 3D model

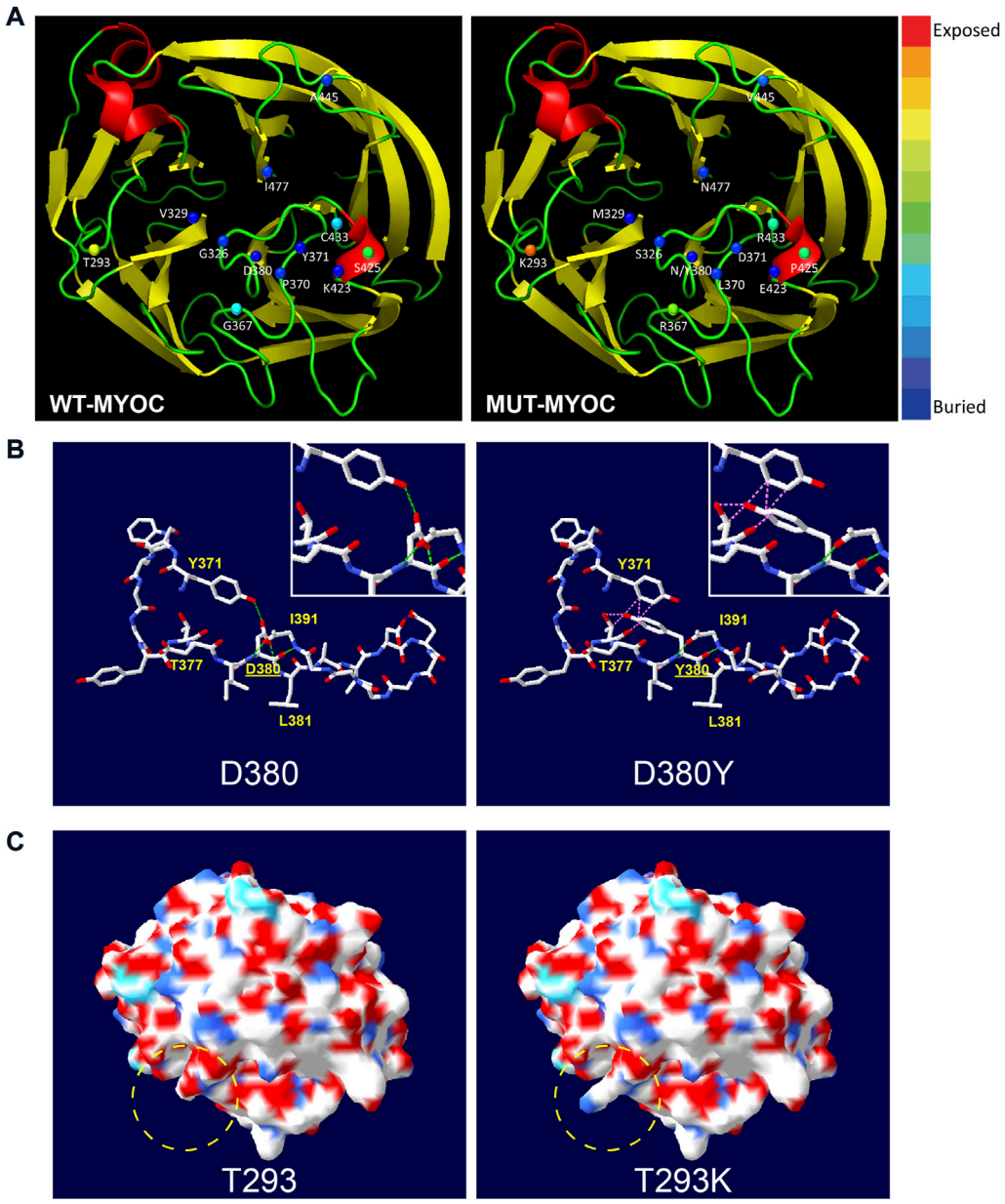

FIGURE 3
Structural alteration of myocilin-OLF induced by C-terminal MYOC variations using Swiss PdB Viewer. **(A)** Solvent accessibility analysis of WT-myocilin (left panel) and mutated-myocilin (right panel). A cartoon view of the myocilin-C-terminus homology (PDB: 4WXQ) model is shown. Twelve residues involved in 13 missense changes are represented as spheres colored according to solvent accessibility (using Swiss PdB Viewer, by which blue through red correspond to buried-through-exposed residues; see color bar). **(B)** Alteration of H-bonds and steric clashes induced by MYOC/p.D380Y mutation. H-bonds are drawn as green dotted lines, and clashes appear as pink dotted lines. **(C)** Changes in molecular surface including electrostatic potential (SEP) and structure of MYOC/p.T293K mutation. The molecular surface is colored according to SEP using Swiss PdB Viewer, with red–white-blue corresponding to acidic-neutral-basic potential. The yellow dotted circle represents the region of significant alteration of SEP and surface structure. See also Supplementary Figures S2,S3.

of OLF structure of myocilin (PDB: 4WXQ) was applied for structural analysis. As illustrated in Figure 3A, 6 of the 13 variations involve structurally exposed residues, including three POAG mutations, 2 neutral polymorphisms and one uncertain variation. S425P is a relatively buried residue, and another 6 variations did not change solvent accessibility. Next, we analyzed alterations in H-bonds and the induction of steric clash caused by MYOC variations. Figures 3B,C shows the common structural alterations in two MYOC mutants. As shown in Figure 3B, D380Y mutant results in loss of H-bond with L381 and Y371 and

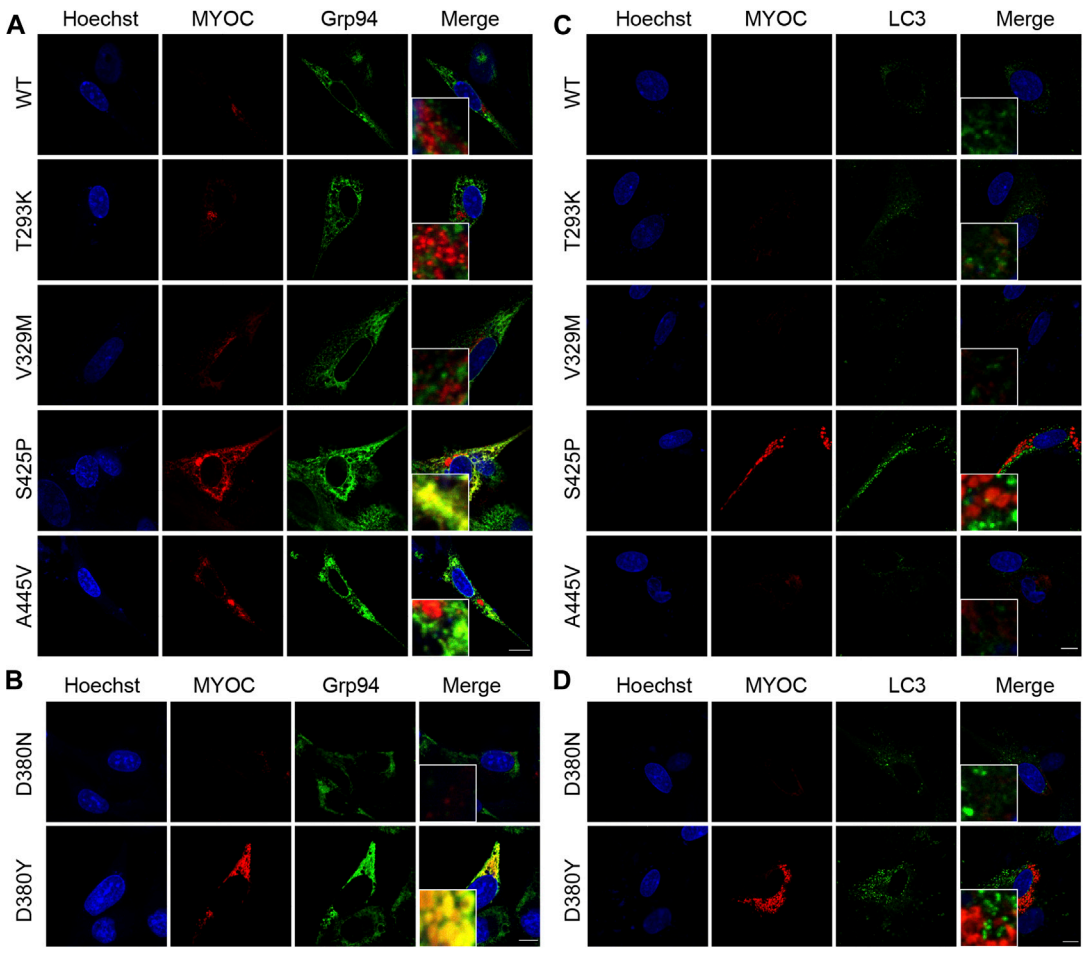

FIGURE 4
Nonsecreted MYOC mutants induce ER stress and impair autophagy. **(A,B)** Confocal double immunofluorescence for myocilin (red) and Grp94 (green) in iHTMCs transiently expressing WT or mutated MYOC. Nonsecreted mutations, including S425P and D380Y, show considerable colocalization of myocilin with Grp94. Scale bar: 25 μm. **(C,D)** iHTMCs expressing WT or mutant myocilins were immunolabeled with LC3 (green) and MYOC (red). S425P and D380Y mutants present increased intracellular myocilin and LC3, with no colocalization of these two proteins. Scale bar: 25 μm.

causes induction of steric clash with Y371 and T377. While Figure 3C shows that T293K mutant alters SEP from acidic to basic, and leads to the change of molecular surface. Structural alterations of other C-terminal variants are shown in Supplementary Figures S2,S3. Of the 13 variations, 9 alter the H-bonding pattern of the molecule (causing gain and/or loss of H-bonds with other residues), and three induce a change in steric clash. Furthermore, molecular surface analysis of characteristics including the SEP and surface structure revealed that alterations in both occur with the T293K, G367R, P370L, C433R and A445V mutations but that no SEP or surface structure alterations occur for G326S, V329M, Y371D, D380N, D380Y, K423E and I477N. Interestingly, S425P does not alter surface structure but does reduce acidic potential.

Correlation analysis of structure-secretion-pathogenicity in myocilin variants

To research correlation among the structure, secretion and pathogenicity of myocilin variations, we analyzed another 20 C-terminal variations with secretion phenotypes determined by previous studies (Fan et al., 2006; Gobeil et al., 2006; Hogewind et al., 2007). The structural alterations and secretion status of a total of 33 C-terminal variations are summarized in Supplementary Table S3. An interesting relationship between secretion and alteration of steric clash was found. Among 10 variant myocilins with changes in steric clash, 100% present secretion defects; 90% are defined as mutation and

10% as uncertain. In addition, among 10 secreted myocilin variants, 100% show no change in steric clash, 20% are identified as mutation, 60% are considered nonpathogenic variations, and 20% are uncertain variations. Therefore, structural alteration (steric clash) may play important roles in influencing the secretion characteristics of myocilin variants, which determine the pathogenicity of myocilin variants.

MYOC mutation induces retention of myocilin in the ER and impairs autophagic activity

It was described in Donegan's work that T293K, V329M, S425P and A445V variants were predicted with different clinical signification from original assignment. Therefore, we investigated the colocalization of myocilin and the ER marker Grp94 by confocal double immunofluorescence in iHTMCs expressing these variants, together with D380N and D380Y variants, which present opposite secretion property in the same site. As depicted in Figure 4A, few myocilin puncta were observed in cells transfected with WT or the T293K, V329M, or A445V-MYOC plasmid. In addition, no colocalization of myocilin and Grp94 was found in these cells. Conversely, iHTMCs expressing S425P-myocilin presented clustered myocilin puncta that prominently colocalized with Grp94. Furthermore, iHTMCs transfected with plasmids containing the D380N or D380Y MYOC variation shared the same location but exhibited opposite secretion phenotypes. We observed considerable codistribution of MYOC and Grp94 in cells expressing D380Y-myocilin compared with cells expressing D380N-myocilin (Figure 4B), suggesting that MYOC mutation induces retention of myocilin in the ER, which is likely to trigger ER stress.

The autophagy activity in cells expressing pathogenic or nonpathogenic myocilin variants was further explored to study the effect of MYOC mutation on cellular pathophysiology. As shown in Figure 4C, expression of LC3, an autophagic marker, was higher in iHTMCs expressing the S425P mutant than in iHTMCs expressing the WT protein or other variants. However, little or no colocalization of LC3 with myocilin was found at high magnification. Similarly, the D380Y mutation resulted in more MYOC and LC3 puncta than the D380N variation, but no colocalizing puncta was found (Figure 4D). Therefore, MYOC mutations may impair autophagy activity.

MYOC mutations promote cellular oxidative stress

To evaluate whether pathogenic MYOC mutations cause cellular oxidative stress, we transfected COS-7 cells with two secreted variants (one pathogenic variation L215Q and one neutral polymorphism V329M) and two nonsecreted mutants (G367R and P370L that were reported to cause severe POAG phenotypes), and H_2O_2 sensitivity, ROS generation and mitochondrial function were analyzed. Under physiological conditions, there were no significant differences in cell viability between cells transfected with WT MYOC and those transfected with MYOC variants (Figure 5A). Next, we demonstrated that treatment of control COS-7 cells with H_2O_2 did not decrease cell viability at a concentration of H_2O_2 below 100 μM (Figure 5B). When cells expressing WT MYOC were treated with 100 μM H_2O_2, no significant decrease in cell viability was observed. However, similar treatment of cells expressing G367R- or P370L-mutated myocilin significantly reduced cell viability, indicating higher sensitivity to H_2O_2 for mutant-expressing cells than WT protein-expressing cells (Figure 5C). ROS are the major product of oxidative stress and are mainly derived from mitochondria. Our assessment of ROS generation with the probe DCFH-DA and of mitochondrial function by MitoTracker staining suggested that nonsecreted MYOC mutants induce ROS accumulation and mitochondrial injury (Figures 5D–G). Conversely, cells expressing L215Q or V329M variant showed no significant difference in cell viability (under H_2O_2 treatment), ROS generation and mitochondrial function, compared to that in WT group.

Discussion

In ocular tissues, myocilin has been identified in the TM, sclera, aqueous humor, ciliary body, choroid, cornea, iris, lamina cribosa, vitreous, retina and optic nerve (Resch and Fautsch, 2009). Myocilin is mainly existed in TM cells and only causes glaucoma when mutated. Furthermore, HEK 293T, COS-1, COS-7 and ARPE-19 (from human retinal pigment epithelium) cell lines that were used alone or in combination according to previous researches to explore the general and the ocular characteristics and function of myocilin (Sanchez-Sanchez et al., 2007; Shepard et al., 2007; Aroca-Aguilar et al., 2008). It should be noted that in the TM cells (both immortalized and primary) and the cell lines mentioned above, endogenous myocilin is unable to be detected. Therefore, we performed intracellular and extracellular molecular characterization of myocilin and explored possible correlations between structural alterations and functional consequences using HEK 293T, COS-7 and iHTM cells expressing exogenous myocilin. iHTMCs were used to explore the ER localization of variant myocilins in cells, and their colocalization with autophagy marker LC3. Since the transfection efficiency of iHTMCs is not sufficient for the analysis of protein secretion and cellular oxidative stress, we selected HEK 293T and COS-7 cells that are easily transfected for our study. Compared with HEK 293T cells, COS-7 cells are more adherent and show advantages in staining experiments. Therefore, COS-7 cells were used in the study of oxidative stress.

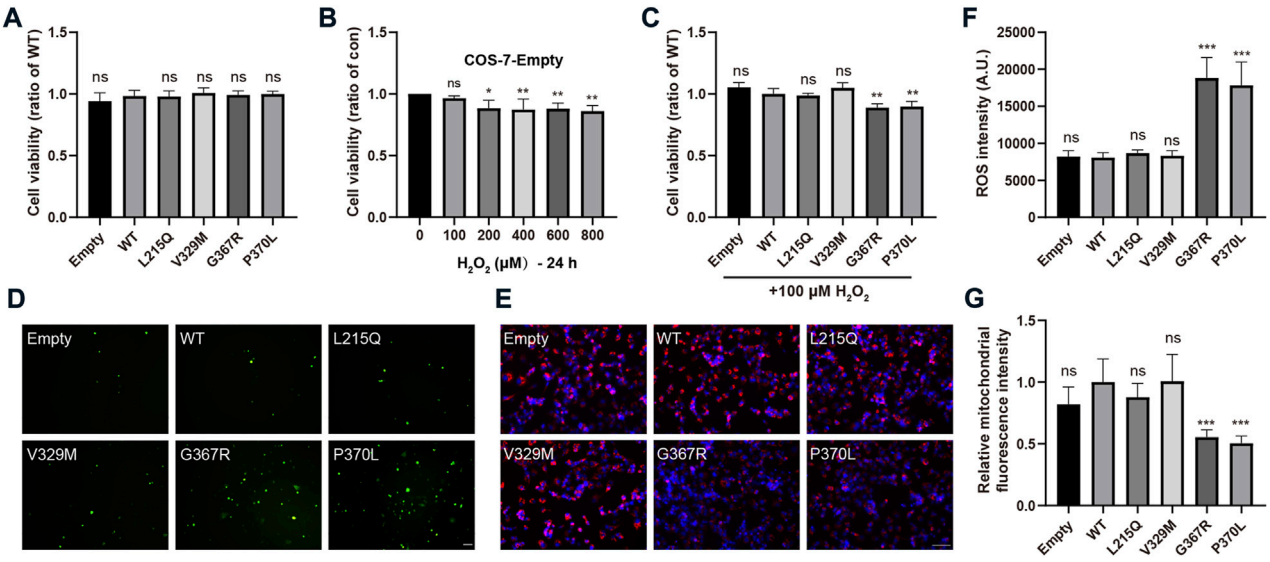

FIGURE 5
MYOC mutations induce cellular oxidative injury. **(A–C)** COS-7 cell viability was measured by MTT assays. **(A)** Expression of WT- or mut-myocilin had no effect on the viability of COS-7 cells. **(B)** Twenty-four hours of incubation with H_2O_2 at 100 μM did not inhibit the growth of COS-7 cells transduced with empty vector. **(C)** COS-7 cells transfected with different vectors were exposed to 100 μM H_2O_2 for 24 h. MYOC mutations increased the toxicity of H_2O_2 to COS-7 cells. **(D,F)** Increased ROS generation measured by DCFH-DA staining in COS-7 cells expressing G367R- or P370L-mutated myocilin. Scale bar: 100 μm. **(E,G)** Mitochondrial staining by MitoTracker showed that transfection of G367R- or P370L-mutated myocilin in COS-7 cells induced a decline in MMP. Scale bar: 100 μm. N ≥ 3. *$p < 0.05$, **$p < 0.01$, ***$p < 0.001$, ns: no significance.

Sanchez-Sanchez et al. (2007) characterized intracellular proteolytic cleavage of myocilin and identified calpain II as a myocilin-processing protease. The processed C-terminal domain is reportedly secreted into cell culture medium or the human aqueous humor, whereas the N-terminal fragment remains inside the cell (Aroca-Aguilar et al., 2008; Wang et al., 2019). However, Kwon et al. (2009) reported that the N-terminal fragment is also secreted into the medium. In accordance with previous studies, we detected full-length myocilin as well as cleaved C-terminal products both inside and outside cells. Nevertheless, the processed N-terminal fragments may have been mostly retained inside the cell and were probably part of the insoluble cell fraction, as they were not detected in the cell medium or soluble cell fraction. It was reported that the perfusion of the C-terminal fragment of myocilin did not influence outflow resistance of aqueous humor (Goldwich et al., 2003). However, the exact role of C-terminal fragment of myocilin in TM or other tissues remains to be clarified. Myocilin can dimerize or multimerize with itself through its leucine zipper or coiled-coil domain. Under nondenaturing conditions, the culture medium and cell lysates of cells overexpressing myocilin for 48 h demonstrated a regular size pattern of myocilin aggregates consisting of various bands larger than 130 kDa, suggesting that myocilin is prone to self-oligomerization. This oligomerization has been reported to be maintained by disulfide bonds (Martin et al., 2021). According to Aroca-Aguilar et al. (2008), coexpression of WT and mutated myocilin resulted in the same pattern of aggregates, which does not support obstruction of aqueous humor outflow due to an increase in the molecular size of myocilin aggregates. Regardless, the secreted products that result from proteolytic cleavage and self-aggregation may regulate interaction of myocilin with ECM proteins such as fibronectin, collagen VI, decorin and laminin (Ueda and Yue, 2003). Overall, changes in the ECM composition will increase the resistance of aqueous humor outflow and result in high IOP.

Secretion status of myocilin could be defined by immunoblotting or luciferase assay (Nakahara and Hulleman, 2022). Our data agreed very well with previous studies showing intracellular sequestration of the G367R, P370L, K423E, C433R, I477N myocilin mutants and secretion of the N57S, Q48H, R82C, R126W, R158Q, T293K, A445V variants (Shepard et al., 2003; Gobeil et al., 2006). Secretion property of eleven variants were first tested in this study. These were the V53A, N57D, T209N, L215Q, G326S, V329M, D380N which were secreted, and the C25R, Y371D, D380Y, S425P which were not released outside the cells. Interestingly, N-terminal variants of myocilin were secreted in addition to the C25R variant; in contrast, 69.7%

(23/33) of C-terminal variations, located in the OLF domain of myocilin, resulted in secretion defects. In terms of pathogenicity, 100% of MYOC neutral polymorphisms induced normal secretion of myocilin, but 87% (20/23) of MYOC mutation-encoded myocilin caused secretion defects. Together with quantification data, we propose that the secretion defect of C25R variant is due to the dysfunction of signal peptide, causing the variant protein cannot enter ER for processing and be degraded at early stage. In line with the work of Kasetti *et al*, we found that MYOC mutations in C-terminus increased the level of insoluble myocilin (Kasetti et al., 2021). Therefore, the nonsecretion of C-terminal mutants may be caused by the decreased solubility of myocilin resulting from protein misfolding.

The crystal structure of myocilin has been illustrated by previous studies (Hill et al., 2017; Martin et al., 2021). The OLF domain is highly conserved and participates in protein–protein interactions, which are associated with various human diseases, including inflammatory bowel disease, cancer, and glaucoma (Hill et al., 2015). Mutations in the OLF domain of myocilin promote the formation of amyloid fibrils, which are difficult to be degraded (Orwig et al., 2012; Hill et al., 2014). Donegan et al. (2015) identified three regions of myocilin-OLF that are sensitive to amyloid aggregation: Loop B-10/C-11 and cation-Π; a hydrophobic β-sheet; and Ca^{2+} site environs. In our study, mutations in Loop B-10/C-11 and cation-Π (G367R, P370L, and K423E) and the hydrophobic β-sheet (C433R and I477N) resulted in cellular myocilin accumulation. Notably, two mutations in D380 (D380N and D380Y), which are located in the Ca^{2+} site environs, showed different results. D380N mutation led to extracellular and intracellular myocilin, whereas intracellular myocilin was only detected with the D380Y variant. This may be due to the different changes in protein structure caused by these mutations. Conformational alterations, such as H-bonds and steric clashes, may influence the folding of proteins, which can further change their function or characteristics (Rose, 2021). Correlation analysis of structure-secretion-pathogenicity of variant myocilins revealed a possible role for steric clash in affecting the secretion and pathogenicity of myocilin variants. This hypothesis may explain the difference in secretion characteristics between D380N and D380Y variants, as well as G326S and G326R variants. Certainly, more research is needed to elucidate the mechanism by which the OLF domain affects the function of myocilin.

Myocilin is mainly expressed in TM cell, and excessively accumulated in ER when MYOC is mutated or overexpressed, which may trigger or disrupt protein clearance mechanisms including ER-associated degradation (ERAD) and autophagy (Kasetti et al., 2021; Tanji et al., 2021). However, previous studies only reported the difference between WT-MYOC and mutated-MYOC (Y437H, G364V, Q368X, *etc*), ignoring the alteration induced by MYOC neutral polymorphisms. In this study, two nonsecreted variants (S425P, D380Y) and four secreted variants (T293K, V329M, A445V, D380N) that have not yet been studied were chosen for further research. We found that compared to the MYOC neutral polymorphism, myocilin encoded by MYOC mutations accumulates in the ER and induces autophagy impairment. A study by Bosley et al identified a spectrum of mitochondrial dysfunction in POAG patients that is associated with cellular oxidative stress and suggests that mitochondrial abnormalities may be a risk factor for POAG (Abu-Amero et al., 2006). In addition, it is reported that mutant myocilin sensitizes cells to oxidative stress and anti-oxidative stress enzyme deficiency promoted the occurrence and degree of POAG phenotype in mouse model that carrying MYOC mutation (Joe and Tomarev, 2010; Joe et al., 2015). Consistently, we demonstrated that MYOC mutations (G367R, P370L) inhibited mitochondrial function and increased cell sensitivity to oxidative stress. Combined with previous findings, the pathogenicity of MYOC variations is associated with myocilin secretion defects, altered steric clash, ER localization, decreased autophagic activity and increased oxidative stress. The secretion disorder of myocilin may be an important determinant in the pathogenic mechanism of MYOC mutations.

According to the work of Donegan et al., the pathogenicity of four variants (T293K, V329M, S425P, A445V) were evaluated differently than original assignments based on location in myocilin-OLF structure (Donegan et al., 2015). However, based on the latest database, the clinical significance of three of these four variants (T293K, S425P, A445V) is consistent with Donegan's prediction (Hewitt et al., 2008). Our study revealed that V329M variant, a controversial variant, exhibited no secretion defect and ER localization, as well as autophagic disruption and oxidative injury in cells. L215Q, G326S, and T377M-MYOC variations are defined as POAG-causing mutations. However, the L215Q mutation has only been reported in one case thus far, and the G326S mutation lacks specific functional analysis and clear genetic evidence, rendering the clinical significance of these two variations unclear (Hewitt et al., 2008). Moreover, no abnormal molecular or cellular biology was observed in cells expressing L215Q and G326S in this study. Consequently, we propose that V329M, L215Q and G326S variants are non-pathogenic. The secretion property of T377M-myocilin was examined by dot blot assay in a previous study, showing a weak gray band, indicating significantly reduced secretion of T377M-myocilin or a false positive band caused by other interfering factors (Gobeil et al., 2006). Therefore, we speculate that a secretion defect of MYOC variants is a prerequisite for the POAG phenotype, which is associated with altered steric clash of myocilin variants. MYOC mutations induce autophagy dysfunction through ER retention.

In summary, we found an interesting correlation between steric clash alterations and the secretion property of MYOC

missense mutants. Nonsecreted myocilin is retained in the ER, inducing a series of stress responses, including impaired autophagic degradation and increased oxidative injury. Considering that the *in silico* approach has inherent limitations of not considering the global changes that can only be studied in solution, our findings need to be validated by further comprehensive experimental analysis. Nevertheless, the *in silico* approach can help to elucidate the molecular pathogenesis of POAG and pave the way for similar analyses for other diseases involving the OLF domain.

Data availability statement

The original contributions presented in the study are included in the article/Supplementary Material, further inquiries can be directed to the corresponding authors.

Author contributions

YZ, JY, and BZ conceived the projects; BZ and YZ designed experiments; BZ, YY, XL, and ZL performed experiments; XL and ZL prepared the tables and figures; BZ, XL, ZL, and YY wrote the manuscript; YZ, and JY reviewed the manuscript. All authors contributed to editing and approving the final manuscript.

Funding

The work was partially supported by grants from the National Natural Science Foundation of China (No. 81970789) and Natural Science Foundation of Fujian Province (No. 2020J05251).

Acknowledgments

The authors would like to thank Ling Lin and Zhihong Huang from the Public Technology Service Center (Fujian Medical University, Fuzhou, Fujian, China) for their technical assistance.

Conflict of interest

The authors declare that the research was conducted in the absence of any commercial or financial relationships that could be construed as a potential conflict of interest.

Publisher's note

All claims expressed in this article are solely those of the authors and do not necessarily represent those of their affiliated organizations, or those of the publisher, the editors and the reviewers. Any product that may be evaluated in this article, or claim that may be made by its manufacturer, is not guaranteed or endorsed by the publisher.

Supplementary material

The Supplementary Material for this article can be found online at: https://www.frontiersin.org/articles/10.3389/fgene.2022.1019208/full#supplementary-material

SUPPLEMENTARY FIGURE S1
Expression of myocilin in different cell fractions. Myocilin detected in different cell fractions was quantified by ImageJ. The nonsecreted variants mainly existed in the insoluble fraction.

SUPPLEMENTARY FIGURE S2
Alteration of H-bonds and steric clashes induced by MYOC mutations. H-bonds are drawn as green dotted lines, and clashes appear as pink dotted lines. The yellow arrow indicated the altered H-bond or steric clash.

SUPPLEMENTARY FIGURE S3
Changes in molecular surface including electrostatic potential (SEP) and structure of MYOC mutations. The molecular surface is colored according to SEP using Swiss PdB Viewer, with red–white–blue corresponding to acidic-neutral-basic potential. The yellow dotted circle represents the region of significant alteration of SEP and surface structure.

SUPPLEMENTARY TABLE S1
Primer sequences for myocilin cDNAs.

SUPPLEMENTARY TABLE S2
Reasons for selection of MYOC variants.

SUPPLEMENTARY TABLE S3
Structure-secretion-pathogenicity analysis of C-terminal myocilin variants.

References

Abu-Amero, K. K., Morales, J., and Bosley, T. M. (2006). Mitochondrial abnormalities in patients with primary open-angle glaucoma. *Invest. Ophthalmol. Vis. Sci.* 47 (6), 2533–2541. doi:10.1167/iovs.05-1639

Aroca-Aguilar, J. D., Sánchez-Sánchez, F., Martínez-Redondo, F., Coca-Prados, M., and Escribano, J. (2008). Heterozygous expression of myocilin glaucoma mutants increases secretion of the mutant forms and reduces extracellular processed myocilin. *Mol. Vis.* 14, 2097–2108. doi:10.1016/j.visres.2008.09.022

Caballero, M., and Borrás, T. (2001). Inefficient processing of an olfactomedin-deficient myocilin mutant: Potential physiological relevance to glaucoma. *Biochem. Biophys. Res. Commun.* 282 (3), 662–670. doi:10.1006/bbrc.2001.4624

Donegan, R. K., Hill, S. E., Freeman, D. M., Nguyen, E., Orwig, S. D., Turnage, K. C., et al. (2015). Structural basis for misfolding in myocilin-associated glaucoma. *Hum. Mol. Genet.* 24 (8), 2111–2124. doi:10.1093/hmg/ddu730

Fan, B. J., Leung, D. Y., Wang, D. Y., Gobeil, S., Raymond, V., Tam, P. O., et al. (2006). Novel myocilin mutation in a Chinese family with juvenile-onset open-angle glaucoma. *Arch. Ophthalmol.* 124 (1), 102–106. doi:10.1001/archopht.124.1.102

Fingert, J. H., Héon, E., Liebmann, J. M., Yamamoto, T., Craig, J. E., Rait, J., et al. (1999). Analysis of myocilin mutations in 1703 glaucoma patients from five different populations. *Hum. Mol. Genet.* 8 (5), 899–905. doi:10.1093/hmg/8.5.899

Gobeil, S., Letartre, L., and Raymond, V. (2006). Functional analysis of the glaucoma-causing TIGR/myocilin protein: Integrity of amino-terminal coiled-coil regions and olfactomedin homology domain is essential for extracellular adhesion and secretion. *Exp. Eye Res.* 82 (6), 1017–1029. doi:10.1016/j.exer.2005.11.002

Goldwich, A., Ethier, C. R., Chan, D. W., and Tamm, E. R. (2003). Perfusion with the olfactomedin domain of myocilin does not affect outflow facility. *Invest. Ophthalmol. Vis. Sci.* 44 (5), 1953–1961. doi:10.1167/iovs.02-0863

Gong, G., Kosoko-Lasaki, S., Haynatzki, G., Lynch, H. T., Lynch, J. A., and Wilson, M. R. (2007). Inherited, familial and sporadic primary open-angle glaucoma. *J. Natl. Med. Assoc.* 99 (5), 559–563. doi:10.3122/jabfm.2007.03.070066

Gould, D. B., Miceli-Libby, L., Savinova, O. V., Torrado, M., Tomarev, S. I., Smith, R. S., et al. (2004). Genetically increasing Myoc expression supports a necessary pathologic role of abnormal proteins in glaucoma. *Mol. Cell. Biol.* 24 (20), 9019–9025. doi:10.1128/mcb.24.20.9019-9025.2004

Gu, M. J., Hyon, J. Y., Lee, H. W., Han, E. H., Kim, Y., Cha, Y. S., et al. (2022). Glycolaldehyde, an advanced glycation end products precursor, induces apoptosis via ROS-mediated mitochondrial dysfunction in renal mesangial cells. *Antioxidants (Basel)* 11 (5), 934. doi:10.3390/antiox11050934

Hewitt, A. W., Mackey, D. A., and Craig, J. E. (2008). Myocilin allele-specific glaucoma phenotype database. *Hum. Mutat.* 29 (2), 207–211. doi:10.1002/humu.20634

Hill, S. E., Donegan, R. K., and Lieberman, R. L. (2014). The glaucoma-associated olfactomedin domain of myocilin forms polymorphic fibrils that are constrained by partial unfolding and peptide sequence. *J. Mol. Biol.* 426 (4), 921–935. doi:10.1016/j.jmb.2013.12.002

Hill, S. E., Donegan, R. K., Nguyen, E., Desai, T. M., and Lieberman, R. L. (2015). Molecular details of olfactomedin domains provide pathway to structure-function studies. *PLoS One* 10 (6), e0130888. doi:10.1371/journal.pone.0130888

Hill, S. E., Nguyen, E., Donegan, R. K., Patterson-Orazem, A. C., Hazel, A., Gumbart, J. C., et al. (2017). Structure and misfolding of the flexible tripartite coiled-coil domain of glaucoma-associated myocilin. *Structure* 25 (11), 1697–1707. e1695. doi:10.1016/j.str.2017.09.008

Hogewind, B. F., Gaplovska-Kysela, K., Theelen, T., Cremers, F. P., Yam, G. H., Hoyng, C. B., et al. (2007). Identification and functional characterization of a novel MYOC mutation in two primary open angle glaucoma families from The Netherlands. *Mol. Vis.* 13, 1793–1801. doi:10.1016/j.jmb.2007.06.084

Huang, C., Xie, L., Wu, Z., Cao, Y., Zheng, Y., Pang, C. P., et al. (2018). Detection of mutations in MYOC, OPTN, NTF4, WDR36 and CYP1B1 in Chinese juvenile onset open-angle glaucoma using exome sequencing. *Sci. Rep.* 8 (1), 4498. doi:10.1038/s41598-018-22337-2

Jia, L. Y., Gong, B., Pang, C. P., Huang, Y., Lam, D. S., Wang, N., et al. (2009). Correction of the disease phenotype of myocilin-causing glaucoma by a natural osmolyte. *Invest. Ophthalmol. Vis. Sci.* 50 (8), 3743–3749. doi:10.1167/iovs.08-3151

Joe, M. K., Lieberman, R. L., Nakaya, N., and Tomarev, S. I. (2017). Myocilin regulates metalloprotease 2 activity through interaction with TIMP3. *Invest. Ophthalmol. Vis. Sci.* 58 (12), 5308–5318. doi:10.1167/iovs.16-20336

Joe, M. K., Nakaya, N., Abu-Asab, M., and Tomarev, S. I. (2015). Mutated myocilin and heterozygous Sod2 deficiency act synergistically in a mouse model of open-angle glaucoma. *Hum. Mol. Genet.* 24 (12), 3322–3334. doi:10.1093/hmg/ddv082

Joe, M. K., and Tomarev, S. I. (2010). Expression of myocilin mutants sensitizes cells to oxidative stress-induced apoptosis: Implication for glaucoma pathogenesis. *Am. J. Pathol.* 176 (6), 2880–2890. doi:10.2353/ajpath.2010.090853

Jurado-Campos, A., Soria-Meneses, P. J., Sánchez-Rubio, F., Niza, E., Bravo, I., Alonso-Moreno, C., et al. (2021). Vitamin E delivery systems increase resistance to oxidative stress in red deer sperm cells: Hydrogel and nanoemulsion carriers. *Antioxidants (Basel)* 10 (11), 1780. doi:10.3390/antiox10111780

Jurynec, M. J., Riley, C. P., Gupta, D. K., Nguyen, T. D., McKeon, R. J., and Buck, C. R. (2003). TIGR is upregulated in the chronic glial scar in response to central nervous system injury and inhibits neurite outgrowth. *Mol. Cell. Neurosci.* 23 (1), 69–80. doi:10.1016/s1044-7431(03)00019-8

Kapetanakis, V. V., Chan, M. P., Foster, P. J., Cook, D. G., Owen, C. G., and Rudnicka, A. R. (2016). Global variations and time trends in the prevalence of primary open angle glaucoma (POAG): A systematic review and meta-analysis. *Br. J. Ophthalmol.* 100 (1), 86–93. doi:10.1136/bjophthalmol-2015-307223

Kasetti, R. B., Maddineni, P., Kiehlbauch, C., Patil, S., Searby, C. C., Levine, B., et al. (2021). Autophagy stimulation reduces ocular hypertension in a murine glaucoma model via autophagic degradation of mutant myocilin. *JCI Insight* 6 (5), e143359. doi:10.1172/jci.insight.143359

Kasetti, R. B., Phan, T. N., Millar, J. C., and Zode, G. S. (2016). Expression of mutant myocilin induces abnormal intracellular accumulation of selected extracellular matrix proteins in the trabecular meshwork. *Invest. Ophthalmol. Vis. Sci.* 57 (14), 6058–6069. doi:10.1167/iovs.16-19610

Kim, B. S., Savinova, O. V., Reedy, M. V., Martin, J., Lun, Y., Gan, L., et al. (2001). Targeted disruption of the myocilin gene (myoc) suggests that human glaucoma-causing mutations are gain of function. *Mol. Cell. Biol.* 21 (22), 7707–7713. doi:10.1128/MCB.21.22.7707-7713.2001

Koch, M. A., Rosenhammer, B., Koschade, S. E., Braunger, B. M., Volz, C., Jägle, H., et al. (2014). Myocilin modulates programmed cell death during retinal development. *Exp. Eye Res.* 125, 41–52. doi:10.1016/j.exer.2014.04.016

Kwon, H. S., Lee, H. S., Ji, Y., Rubin, J. S., and Tomarev, S. I. (2009). Myocilin is a modulator of Wnt signaling. *Mol. Cell. Biol.* 29 (8), 2139–2154. doi:10.1128/MCB.01274-08

Kwon, H. S., Nakaya, N., Abu-Asab, M., Kim, H. S., and Tomarev, S. I. (2014). Myocilin is involved in NgR1/Lingo-1-mediated oligodendrocyte differentiation and myelination of the optic nerve. *J. Neurosci.* 34 (16), 5539–5551. doi:10.1523/jneurosci.4731-13.2014

Kwon, H. S., and Tomarev, S. I. (2011). Myocilin, a glaucoma-associated protein, promotes cell migration through activation of integrin-focal adhesion kinase-serine/threonine kinase signaling pathway. *J. Cell. Physiol.* 226 (12), 3392–3402. doi:10.1002/jcp.22701

Lei, L., Li, S., Liu, X., and Zhang, C. (2019). The clinical feature of myocilin Y437H mutation in a Chinese family with primary open-angle glaucoma. *Br. J. Ophthalmol.* 103 (10), 1524–1529. doi:10.1136/bjophthalmol-2018-313069

Martin, M. D., Huard, D. J. E., Guerrero-Ferreira, R. C., Desai, I. M., Barlow, B. M., and Lieberman, R. L. (2021). Molecular architecture and modifications of full-length myocilin. *Exp. Eye Res.* 211, 108729. doi:10.1016/j.exer.2021.108729

Nakahara, E., and Hulleman, J. D. (2022). A simple secretion assay for assessing new and existing myocilin variants. *Curr. Eye Res.* 47 (6), 918–922. doi:10.1080/02713683.2022.2047205

Orwig, S. D., Perry, C. W., Kim, L. Y., Turnage, K. C., Zhang, R., Vollrath, D., et al. (2012). Amyloid fibril formation by the glaucoma-associated olfactomedin domain of myocilin. *J. Mol. Biol.* 421 (2-3), 242–255. doi:10.1016/j.jmb.2011.12.016

Resch, Z. T., and Fautsch, M. P. (2009). Glaucoma-associated myocilin: A better understanding but much more to learn. *Exp. Eye Res.* 88 (4), 704–712. doi:10.1016/j.exer.2008.08.011

Rose, G. D. (2021). Protein folding - seeing is deceiving. *Protein Sci.* 30 (8), 1606–1616. doi:10.1002/pro.4096

Sakai, H., Shen, X., Koga, T., Park, B. C., Noskina, Y., Tibudan, M., et al. (2007). Mitochondrial association of myocilin, product of a glaucoma gene, in human trabecular meshwork cells. *J. Cell. Physiol.* 213 (3), 775–784. doi:10.1002/jcp.21147

Sanchez-Sanchez, F., Martinez-Redondo, F., Aroca-Aguilar, J. D., Coca-Prados, M., and Escribano, J. (2007). Characterization of the intracellular proteolytic cleavage of myocilin and identification of calpain II as a myocilin-processing protease. *J. Biol. Chem.* 282 (38), 27810–27824. doi:10.1074/jbc.M609608200

Scelsi, H. F., Barlow, B. M., Saccuzzo, E. G., and Lieberman, R. L. (2021). Common and rare myocilin variants: Predicting glaucoma pathogenicity based on genetics, clinical, and laboratory misfolding data. *Hum. Mutat.* 42 (8), 903–946. doi:10.1002/humu.24238

Schedin-Weiss, S., Winblad, B., and Tjernberg, L. O. (2014). The role of protein glycosylation in Alzheimer disease. *Febs J.* 281 (1), 46–62. doi:10.1111/febs.12590

Schwarz, F., and Aebi, M. (2011). Mechanisms and principles of N-linked protein glycosylation. *Curr. Opin. Struct. Biol.* 21 (5), 576–582. doi:10.1016/j.sbi.2011.08.005

Shepard, A. R., Jacobson, N., Millar, J. C., Pang, I. H., Steely, H. T., Searby, C. C., et al. (2007). Glaucoma-causing myocilin mutants require the Peroxisomal targeting signal-1 receptor (PTS1R) to elevate intraocular pressure. *Hum. Mol. Genet.* 16 (6), 609–617. doi:10.1093/hmg/ddm001

Shepard, A. R., Jacobson, N., Sui, R., Steely, H. T., Lotery, A. J., Stone, E. M., et al. (2003). Characterization of rabbit myocilin: Implications for human myocilin glycosylation and signal peptide usage. *BMC Genet.* 4, 5. doi:10.1186/1471-2156-4-5

Souzeau, E., Burdon, K. P., Dubowsky, A., Grist, S., Usher, B., Fitzgerald, J. T., et al. (2013). Higher prevalence of myocilin mutations in advanced glaucoma in comparison with less advanced disease in an Australasian disease registry. *Ophthalmology* 120 (6), 1135–1143. doi:10.1016/j.ophtha.2012.11.029

Stothert, A. R., Suntharalingam, A., Huard, D. J., Fontaine, S. N., Crowley, V. M., Mishra, S., et al. (2014). Exploiting the interaction between Grp94 and aggregated myocilin to treat glaucoma. *Hum. Mol. Genet.* 23 (24), 6470–6480. doi:10.1093/hmg/ddu367

Tanji, T., Cohen, E., Shen, D., Zhang, C., Yu, F., Coleman, A. L., et al. (2021). Age at glaucoma diagnosis in germline myocilin mutation patients: Associations with

polymorphisms in protein stabilities. *Genes (Basel)* 12 (11), 1802. doi:10.3390/genes12111802

Ueda, J., and Yue, B. Y. (2003). Distribution of myocilin and extracellular matrix components in the corneoscleral meshwork of human eyes. *Invest. Ophthalmol. Vis. Sci.* 44 (11), 4772–4779. doi:10.1167/iovs.02-1002

Wang, H., Li, M., Zhang, Z., Xue, H., Chen, X., and Ji, Y. (2019). Physiological function of myocilin and its role in the pathogenesis of glaucoma in the trabecular meshwork (Review). *Int. J. Mol. Med.* 43 (2), 671–681. doi:10.3892/ijmm.2018.3992

Wiggs, J. L., Allingham, R. R., Vollrath, D., Jones, K. H., De La Paz, M., Kern, J., et al. (1998). Prevalence of mutations in TIGR/Myocilin in patients with adult and juvenile primary open-angle glaucoma. *Am. J. Hum. Genet.* 63 (5), 1549–1552. doi:10.1086/302098

Yan, X., Wu, S., Liu, Q., Li, Y., Zhu, W., and Zhang, J. (2020). Accumulation of Asn450Tyr mutant myocilin in ER promotes apoptosis of human trabecular meshwork cells. *Mol. Vis.* 26, 563–573.

Zhang, N., Wang, J., Li, Y., and Jiang, B. (2021). Prevalence of primary open angle glaucoma in the last 20 years: A meta-analysis and systematic review. *Sci. Rep.* 11 (1), 13762. doi:10.1038/s41598-021-92971-w

frontiers | Frontiers in Genetics

TYPE Brief Research Report
PUBLISHED 04 January 2023
DOI 10.3389/fgene.2022.1089784

OPEN ACCESS

EDITED BY
Jeremy Guggenheim,
Cardiff University, United Kingdom

REVIEWED BY
Leah Owen,
The University of Utah, United States
Fuxin Zhao,
Wenzhou Medical University, China

*CORRESPONDENCE
Marzena Gajecka,
gamar@man.poznan.pl

SPECIALTY SECTION
This article was submitted to Genetics of Common and Rare Diseases, a section of the journal Frontiers in Genetics

RECEIVED 04 November 2022
ACCEPTED 08 December 2022
PUBLISHED 04 January 2023

CITATION
Swierkowska J, Vishweswaraiah S, Mrugacz M, Radhakrishna U and Gajecka M (2023), Differential methylation of microRNA encoding genes may contribute to high myopia. *Front. Genet.* 13:1089784. doi: 10.3389/fgene.2022.1089784

Differential methylation of microRNA encoding genes may contribute to high myopia

Joanna Swierkowska[1], Sangeetha Vishweswaraiah[2], Malgorzata Mrugacz[3], Uppala Radhakrishna[2] and Marzena Gajecka[1,4]*

[1]Institute of Human Genetics, Polish Academy of Sciences, Poznan, Poland, [2]Department of Obstetrics and Gynecology, Oakland University William Beaumont School of Medicine, Royal Oak, MI, United States, [3]Department of Ophthalmology and Eye Rehabilitation, Medical University of Bialystok, Bialystok, Poland, [4]Chair and Department of Genetics and Pharmaceutical Microbiology, Poznan University of Medical Sciences, Poznan, Poland

Introduction: High myopia (HM), an eye disorder with a refractive error ≤–6.0 diopters, has multifactorial etiology with environmental and genetic factors involved. Recent studies confirm the impact of alterations in DNA methylation and microRNAs (miRNAs) on myopia. Here, we studied the combined aspects evaluating to the role of methylation of miRNA encoding genes in HM.

Materials and Methods: From the genome-wide DNA methylation data of 18 Polish children with HM and 18 matched controls, we retrieved differentially methylated CG dinucleotides localized in miRNA encoding genes. Putative target genes of the highest-ranked miRNAs were obtained from the miRDB and included in overrepresentation analyses in the ConsensusPathDB. Expression of target genes was assessed using the RNA sequencing data of retinal ARPE-19 cell line.

Results: We identified differential methylation of CG dinucleotides in promoter regions of *MIR3621*, *MIR34C*, *MIR423* (increased methylation level), and *MIR1178*, *MIRLET7A2*, *MIR885*, *MIR548I3*, *MIR6854*, *MIR675*, *MIRLET7C*, *MIR99A* (decreased methylation level) genes. Several targets of these miRNAs, e.g. *GNAS*, *TRAM1*, *CTNNB1*, *EIF4B*, *TENM3* and *RUNX* were previously associated with myopia/HM/refractive error in Europeans in genome-wide association studies. Overrepresentation analyses of miRNAs' targets revealed enrichment in pathways/processes related to eye structure/function, such as axon guidance, transcription, focal adhesion, and signaling pathways of TGF-β, insulin, MAPK and EGF-EGFR.

Conclusion: Differential methylation of indicated miRNA encoding genes might influence their expression and contribute to HM pathogenesis *via* disrupted regulation of transcription of miRNAs' target genes. Methylation of genes encoding miRNAs may be a new direction in research on both the mechanisms determining HM and non-invasive indicators in diagnostics.

KEYWORDS

DNA methylation, epigenetic changes, childhood myopia, early-onset high myopia, microRNA target genes, miRNA encoding genes

1 Introduction

High myopia (HM) is an eye disorder with a refractive error ≤−6.0 diopters (D) (Young et al., 2007; Flitcroft et al., 2019). It is a complex trait with a multifactorial etiology, including genetic and environmental factors such as near work (Pärssinen et al., 2014), artificial light exposure (Czepita et al., 2004), lack of activity outdoor (Pärssinen et al., 2014; Xiong et al., 2017; Lingham et al., 2021), a higher level of education (Verhoeven et al., 2013) and urbanization (Czepita et al., 2008; Ip et al., 2008; Uzma et al., 2009) or diet with high sugar intake (Galvis et al., 2017). Genetic contribution to refractive error and HM could be monogenic caused by rare mutations but is more often polygenic since a number of genomic regions, candidate genes, and sequence variants involved in HM pathogenesis have been identified (Inamori et al., 2007; Han et al., 2009; Metlapally et al., 2010; Wakazono et al., 2016; Xiao et al., 2016; Wang et al., 2017; Napolitano et al., 2018; Cai et al., 2019; Tideman et al., 2021). Thus far, 27 myopia *loci* have been documented in Online Mendelian Inheritance in Man and we have identified three novel HM *loci* at 7p22.1-7p21.1, 7p12.3-7p11.2, and 12p12.3-12p12.1 in Polish patients (Rydzanicz et al., 2011). Recently, we also recognized two variants in *FLRT3* and *SLC35E2B* genes segregating with the HM phenotype (Swierkowska et al., 2021).

MicroRNAs (miRNAs) constitute an important and highly conserved class of small non-coding RNAs, about 22 nucleotides in length, which play important roles in regulating gene expression (Jiang et al., 2017). MicroRNAs have been reported to be involved in eye development and their abnormal expression or activity were linked to common retinal disorders such as age-related macular degeneration, diabetic retinopathy or retinitis pigmentosa (Xu, 2009; Andreeva and Cooper, 2014; Raghunath and Perumal, 2015; Li et al., 2019; Zuzic et al., 2019). The role of miRNAs, including miR-328 and miR-29a, were also suggested in myopia (Chen et al., 2012; Metlapally et al., 2016; Tkatchenko et al., 2016; Jiang et al., 2017; Mei et al., 2017; Zhang et al., 2017; Kunceviciene et al., 2019, 2021; Tanaka et al., 2019; Xiao et al., 2021; Liu et al., 2022).

Recently, based on the DNA methylation data, we have studied genes overlapping CG dinucleotides that were differentially methylated in Polish children with HM when compared to controls (Vishweswaraiah et al., 2019; Swierkowska et al., 2022). To date, the methylation of miRNA encoding genes has not been studied in myopia or HM and no study was performed in children with HM on the role of miRNA encoding genes. Therefore here, to complement our previously published findings on DNA methylation in Polish children with HM, we assessed the role of methylation in miRNA encoding genes.

2 Materials and methods

2.1 Patients

A total of 18 Polish Caucasian children with HM and 18 children without HM evaluated as the control group were ascertained at the Department of Paediatric Ophthalmology at Medical University of Bialystok. The participants underwent extensive ophthalmological examinations, including cycloplegic autorefraction, and ocular biometry measurements. The guidelines of the International Myopia Institute, that defines HM as a spherical equivalent refractive error of an eye ≤−6.0 D when ocular accommodation is relaxed (Flitcroft et al., 2019), were followed. Ophthalmic characteristics of HM children and control individuals were described elsewhere (Vishweswaraiah et al., 2019; Swierkowska et al., 2022). The study protocol was approved by the Institutional Review Boards at Poznan University of Medical Sciences in Poland. The written informed consent in accordance with the Declaration of Helsinki was obtained from parents of each child.

2.2 Assessment of CG dinucleotides in the miRNA encoding genes

DNA methylation analyses was previously performed on genomic DNA extracted from peripheral blood samples using Infinium MethylationEPIC BeadChip arrays (Illumina, Inc., San Diego, CA, United States) covering over 850,000 methylation sites (Vishweswaraiah et al., 2019). The detailed methodology was described elsewhere (Vishweswaraiah et al., 2019). Differentially methylated CG dinucleotides located in miRNA encoding genes (including promoter region) and meeting the following criteria: 1) at least 5% difference in methylation level between HM cases and controls, 2) FDR-corrected p-value < 0.05, and 3) no overlap of CG dinucleotides with single nucleotide polymorphisms (SNPs) to avoid potential confounding factors, were retrieved from the previously obtained DNA methylation data. Mean methylation values were calculated for the group of children with HM and the group of children without HM. To avoid any gender-specific methylation bias, CG dinucleotides located on chromosomes X and Y were excluded from the analysis (Kiwerska et al., 2022). Detailed workflow of the study was presented in Figure 1.

Then, to confirm the possibility of altered expression of miRNA encoding genes due to the differential methylation of the promoter region, we applied additional selection criteria. Differential methylation difference of 10% and localization of CG dinucleotides in 5′UTR, exon 1, 0–200 bases upstream of the

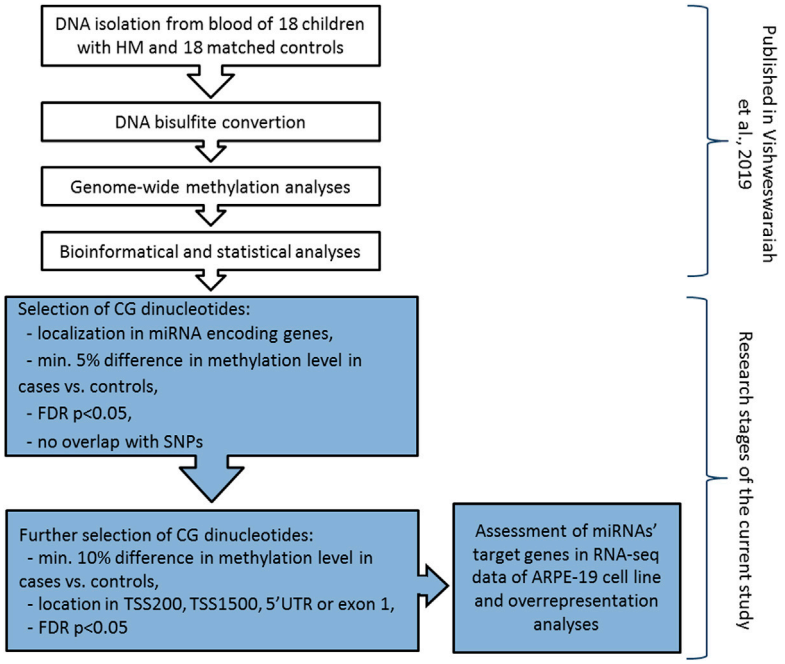

FIGURE 1
Detailed workflow of miRNA encoding genes methylation analyses in children with HM and matched controls. The research steps marked in white have been already published (Vishweswaraiah et al., 2019). Grey colour indicates the steps performed in the current study. TSS200 means 0–200 bases upstream of the transcriptional start site, TSS1500 means 200–1500 bases upstream of the transcriptional start site, UTR stands for untranslated region, FDR is false discovery rate, and SNP is single nucleotide polymorphism.

transcriptional start site (TSS200), or 200–1500 bases upstream of the transcriptional start site (TSS1500) were chosen (Figure 1). Again, the significance of the FDR-corrected *p*-value of < 0.05 was considered. Selected CG dinucleotides localized in the promoter regions of genes encoding miRNAs and those miRNAs were considered as the highest-ranked.

Expression of the highest-ranked miRNA encoding genes and their associations with eye structure and function were assessed in miRBase (http://www.mirbase.org/index.shtml), GeneCards (https://www.genecards.org/), National Center for Biotechnology Information—Gene (NCBI, https://www.ncbi.nlm.nih.gov/), GWAS Catalog (https://www.ebi.ac.uk/gwas/), Mouse Genome Informatics (MGI, http://www.informatics.jax.org/), and available literature data.

2.3 Analyses of RNA sequencing data of miRNAs' putative target genes

Predicted target genes (target score in a range of 50–100) of the highest-ranked miRNAs were obtained from miRDB (http://mirdb.org/) database. The prediction is more reliable with the higher target score. Thus, the expression data of miRNAs' target genes with target score of ≥90 in the miRDB, was retrieved from available online raw data of RNA sequencing (RNA-seq, GEO: GSE88848) (Samuel et al., 2017) performed on ARPE-19 cell line derived from human retinal pigment epithelium (Figure 1). Transcripts per million (TPM) reads measured at 4 days culture and 4 months culture were available. However, the results of 4 days culture were considered, as the morphology of the ARPE-19 cell line and gene expression may change during the increasing number of passages in the cell culture.

The extensive list of target genes was limited to 5% of the genes with the highest and 5% of the genes with the lowest expression level (>5 TPM) in the ARPE-19 cell line, and assessed in the Human Protein Atlas (proteinatlas.org), GWAS Catalog, GeneCards (https://www.genecards.org/), NCBI, UniProt (https://www.uniprot.org/), MGI databases, and available literature data.

2.4 Target genes and pathway overrepresentation analyses

All putative target genes (target score ≥50) of the highest-ranked miRNAs obtained from miRDB were included in the overrepresentation analyses in the Consensus PathDB (http://cpdb.molgen.mpg.de/CPDB) (Figure 1). Following settings were considered: *p*-value cutoff = 0.01 and an overlap of at least five genes from our uploaded gene list, with the Consensus PathDB

TABLE 1 The highest-ranked CG dinucleotides in promoter regions of miRNA encoding genes, with at least 10% difference between HM cases and controls in methylation level.

TargetID	Chromosomal localization	MiRNA encoding gene	Myopia *locus*	*p*-value	FDR *p*-value	Methylation level in HM cases ± SD (%) [range]	Methylation level in controls ± SD (%) [range]	Difference in methylation level (%)	Localization in a gene
Increased methylation level									
cg18576861	9q34.3	*MIR3621*		2.29×10^{-42}	1.98×10^{-36}	34.09 ± 21.44 [8.9–93.7]	17.27 ± 2.78 [11.5–22.0]	16.82	TSS1500
cg17369088	17q11.2	*MIR423*		5.51×10^{-41}	4.76×10^{-35}	21.09 ± 14.95 [2.1–61.4]	8.18 ± 4.29 [0.6–16.0]	12.91	TSS200
cg08827001	11q23.1	*MIR34C*		3.91×10^{-42}	3.39×10^{-36}	34.16 ± 21.27 [5.1–86.1]	21.94 ± 13.11 [0–45.0]	12.23	TSS200
Decreased methylation level									
cg21913981	12q24.23	*MIR1178*	Nearby the MYP3 (12q21-q23)	5.15×10^{-30}	4.45×10^{-24}	64.65 ± 20.06 [7.5–84.8]	82.02 ± 1.67 [79.5–85.6]	−17.38	TSS200
cg18590130	11q24.1	*MIRLET7A2*		2.79×10^{-30}	2.41×10^{-24}	69.71 ± 17.62 [21.3–87.3]	85.71 ± 3.31 [81.1–93.1]	−16.00	TSS1500
cg05365685	3p25.3	*MIR885*		2.90×10^{-23}	2.51×10^{-17}	72.92 ± 16.6 [19.6–87.0]	86.06 ± 1.55 [84.0–89.9]	−13.14	TSS200
cg10443315	8p23.1	*MIR548I3*	MYP10 (8p23)	2.94×10^{-19}	2.54×10^{-13}	69.17 ± 13.19 [31.4–84.7]	82.06 ± 4.35 [71.6–89.1]	−12.89	TSS1500
cg21281732	9q22.33	*MIR6854*		2.90×10^{-27}	2.51×10^{-21}	78.26 ± 19.21 [10.6–92.3]	90.43 ± 1.97 [86.0–93.2]	−12.17	TSS1500
cg13210239	11p15.5	*MIR675*		8.46×10^{-11}	7.31×10^{-5}	61.51 ± 14.08 [15.8–76.3]	72.56 ± 2.88 [68.7–80.0]	−11.05	TSS1500
cg25353401	21q21.1	*MIRLET7C; MIR99A*		1.57×10^{-13}	1.36×10^{-7}	69.54 ± 10.85 [15.8–76.3]	80.46 ± 4.99 [70.7–91.2]	−10.93	TSS1500; TSS1500

10.3389/fgene.2022.1089784

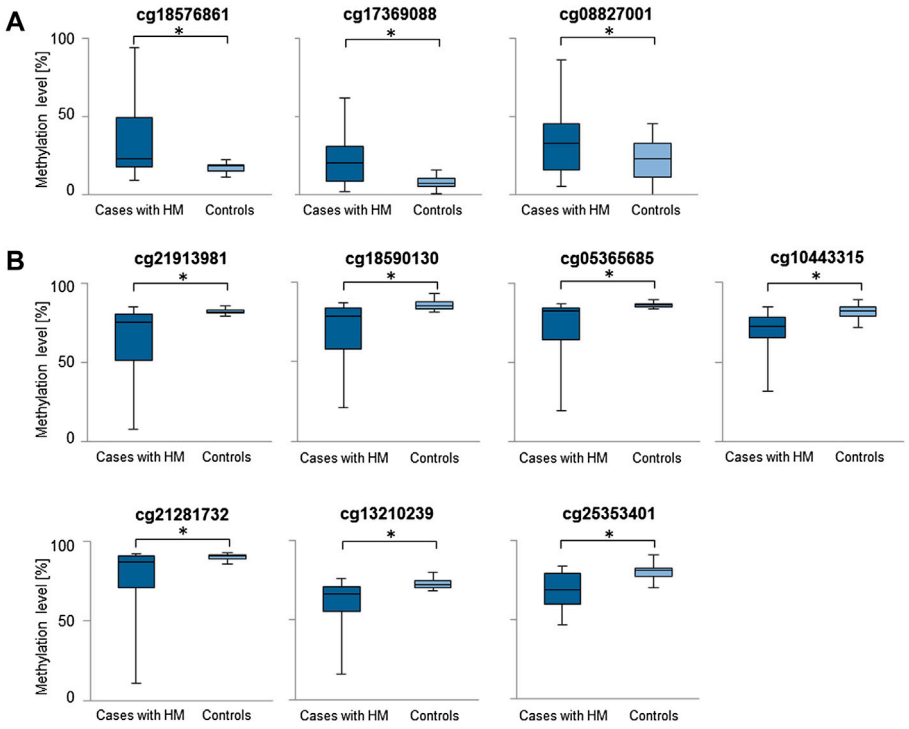

FIGURE 2
Comparisons of methylation levels of the highest-ranked CG dinucleotides between cases with HM and controls. Presented are CG dinucleotides with at least 10% methylation difference between HM cases and controls and location in miRNA encoding genes promoter regions. Standard deviation is included and asterisk (*) stands for the statistically significant difference in methylation level (FDR-corrected p-value < 0.05). **(A)** CG dinucleotides with increased methylation level in HM cases *versus* controls. **(B)** CG dinucleotides with decreased methylation level in HM cases *versus* controls.

gene set. Pathways with q-value, p-value adjusted for FDR, less than 0.01 were considered.

2.5 Statistical analyses

To confirm that the number of the highest-ranked CG dinucleotides was higher than expected by chance, the permutation test of the case-control status of samples and the Student's t-test were applied. p-value < 0.05 was considered.

3 Results

3.1 Characteristics of the study participants

Children with sporadic HM presented with a refractive error in a range of −6.0 to −15.0 D in at least one eye (mean value of −8.25 D), and axial length ranging from 26.22 to 27.85 mm (mean value of 26.22 mm). Children in the control group had no signs of HM with refractive error ranging from −0.5 D to + 0.5 D (mean −0.25 D), and an axial length between 22.42 mm and 24.11 mm (mean 22.55 mm). All the children were Caucasians, between the ages of 3 and 12 years (mean age of 9.61 years in children with HM and 10.33 years in children without HM). The ratio of boys to girls was comparable between groups. In the HM group 61% and 39% of children and in the control group 56% and 44% were boys or girls, respectively. Detailed characteristics of the patients and controls are presented elsewhere (Vishweswaraiah et al., 2019; Swierkowska et al., 2022).

3.2 Identification of differentially methylated CG dinucleotides in miRNA encoding genes

Considering the increased methylation level, CG dinucleotides within miRNA encoding genes found with a difference in methylation level in a range of 5.24–16.82% in HM cases vs. controls are listed in Supplementary Table S1. Similarly, considering the decreased methylation level, CG dinucleotides with a difference in methylation level in a range of 5.00–17.38% are provided in Supplementary Table S2. For

further analyses we selected differentially methylated CG dinucleotides with at least 10% difference in methylation level, localized in promoter regions of miRNA encoding genes as the highest-ranked CG dinucleotides (Table 1, Figure 2). All the selected CG dinucleotides were found with the FDR-corrected p-value < 0.0001 and passed the statistical analyses (p-value < 0.05). The highest difference in methylation level between HM cases vs. controls was observed for the cg18576861 in TSS1500 of *MIR3621* (increase of 16.82%) and cg21913981 in TSS200 of *MIR1178* (decrease of 17.38%).

3.3 Target genes of the highest-ranked miRNAs are expressed in retinal cells

According to the MGI, several the highest-ranked miRNA encoding genes summarized in Table 1, such as *MIR423*, *MIRLET7A2*, *MIRLET7C*, *MIR99A*, have been reported with low expression in a murine eye (GXD: E-GEOD-63810, GXD: E-GEOD-33141, GXD: E-MTAB-6133), but none of them were found to be expressed in ARPE-19 cell line.

For the highest-ranked miRNA encoding genes, we obtained predicted target genes from the miRDB database. Target genes of the highest-ranked miRNAs encoding genes with increased and decreased methylation level are presented in Supplementary Tables S3, S4, respectively.

To narrow the list of miRNAs' target genes that are probably related to HM, target genes with a target score ≥90 in miRDB were also assessed for expression level in the RNA-seq data (Supplementary Tables S5, S6). Target genes with the highest and the lowest expression level, the role in the function or structure of the eye or localization in myopia *loci* were characterized and summarized in Supplementary Table S7.

3.4 Pathways and molecular processes related to myopia/eye disorders

The analyses revealed enrichment in biological pathways related to eye structure and function (Supplementary Tables S8, S9). In our results the most common significant pathways/processes that could be related to myopia were axon guidance, transcription, TGF-β signaling pathway, insulin signaling, focal adhesion, MAPK signaling pathway, and EGF-EGFR signaling pathway.

4 Discussion

To compliment the already performed analyses on differentially methylated genes in HM in Polish children (Vishweswaraiah et al., 2019; Swierkowska et al., 2022), we focused here on CG dinucleotides located in miRNA encoding genes. We report significant increase in methylation level of CG dinucleotides located in the promoter regions of *MIR3621*, *MIR34C*, *MIR423*, and significant decrease in the promoter regions of *MIR1178*, *MIRLET7A2*, *MIR885*, *MIR548I3*, *MIR6854*, *MIR675*, *MIRLET7C*, and *MIR99A* genes.

From the indicated miRNA encoding genes, two encoded miRNAs were previously reported in myopia studies. The first one, miR-885, was identified in exosomes in aqueous humor of myopic patients undergoing cataract surgery (Chen et al., 2019). Second one, let-7a, had confirmed significant differential expression in mice sclera of myopic form-deprived eyes when compared to control eyes, supporting the involvement of miRNAs in eye growth regulation (Metlapally et al., 2016). The expression of the let-7a-5p was also significantly downregulated in lens epithelium samples of patients with senile cataract, and a significant difference in expression between nuclear and anterior subcapsular cataracts has been found for the let-7a-5p (Kim et al., 2021). This miRNA was also significantly downregulated in rat glaucomatous retina when compared with controls (Jayaram et al., 2015). Moreover, functional analyses indicated that let-7a could be crucial for RPE differentiation and maintenance of the epithelial phenotype of the cells (Shahriari et al., 2020). Furthermore, upregulation of let-7a-5p represses TGF-β2-induced proliferation, migration, invasion and epithelial-mesenchymal transition in human lens epithelial cells (Liu and Jiang, 2020).

The second indicated miRNA let-7, let-7c-3p, was downregulated in anterior lens capsules of age-related cataract patients aged over 65 years relative to the patients under the age of 65 years (Li et al., 2020). Also, let-7c-3p inhibited autophagy by targeting ATG3 in human lens epithelial cells (Li et al., 2020). Furthermore, increased expression of let-7c was detected in fetal sclera when compared to sclera of the adults (Metlapally et al., 2013), and was only expressed in plasma of patients with age-related macular degeneration and not in plasma of controls (Ertekin et al., 2014). Both let-7a-5p and let-7c-5p were significantly upregulated in aqueous humor samples of normal-tension glaucoma patients when compared to the control group (Seong et al., 2021).

Previously, another miRNA, miR-34c, was found to affect the growth of trigeminal sensory neurons and the repair of diabetic corneal nerve endings in diabetic corneal neuropathy (Hu et al., 2019). Functional experiments demonstrated that miR-34c could reverse the oncogenic function of lncRNA DANCR (differentiation antagonizing non-protein coding RNA) in retinoblastoma tumorigenesis (Wang et al., 2018), and that miR-34c acts as tumor suppressor in uveal melanoma cell proliferation and migration through the down regulation of multiple targets (Dong and Lou, 2012).

A study has shown that miR-423-5p is highly expressed in the vitreous of eyes with proliferative diabetic retinopathy (Hirota et al., 2015), and in aqueous humor of patients with intraocular tuberculosis (Chadalawada et al., 2022).

Moreover, miR-675 regulates the expression of the *CRYAA* gene, that its dysfunction causes cataract as it contributes to the transparency and refractive index of the lens, by targeting the binding site within the 3′UTR (Liu et al., 2018). LncRNA H19, a precursor of miR-675, is significantly up-regulated in the nuclear age-related cataract lenses, and its reduction inhibits miR-675 expression (Liu et al., 2018). Therefore, in general literature supports our results about the possible involvement of miR-885, miR-34c, miR-423, let-7a-2, miR-675, and miR-let7c in HM in children.

Several putative target genes of the highest-ranked miRNAs were previously associated with eye diseases in genome-wide association studies (GWAS). Also, a *GNAS* gene was associated with HM (Tideman et al., 2021), *TRAM1*, *CTNNB1*, *TENM3* and *RUNX* with myopia and/or refractive error (Han et al., 2020; Hysi et al., 2020; Xue et al., 2022), and *EIF4B* with low myopia/hyperopia (Tideman et al., 2021) in Europeans. Moreover, genes *CBX3*, *NAP1L1*, *EIF4B*, *PLS3*, *MRFAP1*, *GPATCH8*, *TENM3*, *BAZ2A*, *AMMECR1*, *JAZF1*, *PIM3*, *DNA2*, *GTPBP1*, *ITGB3*, *DDI2* are localized in myopia/HM *loci*. Furthermore, mutations in *DCBLD2*, *GNAS*, *CTNNB1*, *BZW1*, *ACTN4*, *LIMCH1*, *FKBP1B, VAV2, ENKD1, ITGB3* cause abnormal murine eye phenotype (MGI:1920629, MGI:95777, MGI:88276, MGI:1914132, MGI:1890773, MGI:1924819, MGI:1336205, MGI:102718, MGI:2142593, MGI:96612). Abnormal transcription of the listed target genes might have a crucial role in HM pathogenesis.

Overrepresentation analyses of miRNAs' targets revealed enrichment in biological pathways/processes related to eye structure and function, such as axon guidance, transcription, focal adhesion, insulin signaling, and signaling pathways of TGF-β, MAPK, and EGF-EGFR. Similarly, Mei et al. also revealed significant enrichment of target genes of differentially expressed miRNAs in murine eyes with form-deprivation myopia in such processes as regulation of transcription, axon guidance, and TGF-β signaling pathway (Mei et al., 2017). Flitcroft et al. (2018) as well identified several biological processes already implicated in refractive error development, including focal adhesion, axon guidance, and extracellular matrix remodeling (Flitcroft et al., 2018). As for the insulin signaling, intravitreally injected insulin promoted axial eye growth in chicks (Penha et al., 2012), and Liu et al. (2015) showed significant association of SNPs in the *INS-IGF2* region, and the *INSR* (insulin receptor) gene with HM (Liu et al., 2015). Summarizing, indicated molecular pathways/processes could be related to HM in the studied children.

The study limitation is the assessment of DNA methylation in blood samples instead of eye tissue. Retinal samples could not be obtained from the ascertained children. However, other studies were also performed on patients' blood instead of eye tissue, making all results comparable (Hsi et al., 2019). Still, our previously published results in aspects of methylation and the current data were obtained and compiled for the same patients and controls, which effectively brings it all together. Further analyses of a larger cohort, including assessments of children's lifestyle and other environmental factors data, are needed. Moreover, we did not examine whether the children's mothers were exposed to pollution, heavy metals, smoking, or nutritional habits during pregnancy, as these are well-known factors affecting methylation in children (Alvarado-Cruz et al., 2018). Furthermore, the ARPE-19 cell line is not fully representative of primary tissue data and epigenetic modifications and expression may be altered within ARPE-19 cultured cells from the primary human state. However, functional studies are necessary to be performed to confirm or deny the findings of this computational study and *in silico* obtained results.

To conclude, differential methylation of CG dinucleotides in promoters of the miRNA encoding genes, *MIR3621*, *MIR34C*, *MIR423*, *MIR1178*, *MIRLET7A2*, *MIR885*, *MIR548I3*, *MIR6854*, *MIR675*, *MIRLET7C*, *MIR99A*, might influence their expression. Therefore, these findings may contribute to HM pathogenesis *via* the disrupted regulation of transcription of miRNAs' target genes and biological pathways crucial for eye development and function. Further studies of methylation may shed light on the molecular mechanisms underlying both genetic and environmental phenotypic effects. Moreover, the identified features concerning specific CG dinucleotides in miRNA encoding genes could be promising for developing non-invasive biomarkers of HM, detectable in blood.

Data availability statement

The original contributions presented in the study are included in the article/Supplementary Material, further inquiries can be directed to the corresponding author.

Ethics statement

The studies involving human participants were reviewed and approved by Institutional Review Boards at Poznan University of Medical Sciences in Poland. Written informed consent to participate in this study was provided by the participant's legal guardian/next of kin.

Author contributions

JS; analyzed the data, provided funding, performed literature review, and wrote the paper, SV; generated the methylation data and participated in the data analysis, MM; performed medical examination of patients and controls, collected study biological material, UR; generated the methylation data and revised the paper, MG; provided mentorship, reviewed and edited the paper. All authors accepted the final version of the manuscript.

Funding

Supported by National Science Centre in Poland in part, grant no. 2019/35/N/NZ5/03150 (to JS).

Acknowledgments

We would like to thank Adam Ustaszewski for his assistance with the statistical analyses.

Conflict of interest

The authors declare that the research was conducted in the absence of any commercial or financial relationships that could be construed as a potential conflict of interest.

Publisher's note

All claims expressed in this article are solely those of the authors and do not necessarily represent those of their affiliated organizations, or those of the publisher, the editors and the reviewers. Any product that may be evaluated in this article, or claim that may be made by its manufacturer, is not guaranteed or endorsed by the publisher.

Supplementary material

The Supplementary Material for this article can be found online at: https://www.frontiersin.org/articles/10.3389/fgene.2022.1089784/full#supplementary-material

References

Alvarado-Cruz, I., Alegría-Torres, J. A., Montes-Castro, N., Jiménez-Garza, O., and Quintanilla-Vega, B. (2018). Environmental epigenetic changes, as risk factors for the development of diseases in children: A systematic review. *Ann. Glob. Health* 84, 212–224. doi:10.29024/aogh.909

Andreeva, K., and Cooper, N. G. F. (2014). MicroRNAs in the neural retina. *Int. J. Genomics* 2014, 165897. doi:10.1155/2014/165897

Cai, X.-B., Shen, S.-R., Chen, D.-F., Zhang, Q., and Jin, Z.-B. (2019). An overview of myopia genetics. *Exp. Eye Res.* 188, 107778. doi:10.1016/j.exer.2019.107778

Chadalawada, S., Kathirvel, K., Lalitha, P., Rathinam, S. R., and Devarajan, B. (2022). Dysregulated expression of microRNAs in aqueous humor from intraocular tuberculosis patients. *Mol. Biol. Rep.* 49, 97–107. doi:10.1007/s11033-021-06846-4

Chen, C.-F., Hua, K., Woung, L.-C., Lin, C.-H., Chen, C.-T., Hsu, C.-H., et al. (2019). Expression profiling of exosomal miRNAs derived from the aqueous humor of myopia patients. *Tohoku J. Exp. Med.* 249, 213–221. doi:10.1620/tjem.249.213

Chen, K.-C., Hsi, E., Hu, C.-Y., Chou, W.-W., Liang, C.-L., and Juo, S.-H. H. (2012). MicroRNA-328 may influence myopia development by mediating the *PAX6* gene. *Invest. Ophthalmol. Vis. Sci.* 53, 2732–2739. doi:10.1167/iovs.11-9272

Czepita, D., Gosławski, W., Mojsa, A., and Muszyńska-Lachota, I. (2004). Role of light emitted by incandescent or fluorescent lamps in the development of myopia and astigmatism. *Med. Sci. Monit.* 10, CR168–171.

Czepita, D., Mojsa, A., and Zejmo, M. (2008). Prevalence of myopia and hyperopia among urban and rural schoolchildren in Poland. *Ann. Acad. Med. Stetin.* 54, 17–21.

Dong, F., and Lou, D. (2012). MicroRNA-34b/c suppresses uveal melanoma cell proliferation and migration through multiple targets. *Mol. Vis.* 18, 537–546.

Ertekin, S., Yıldırım, O., Dinç, E., Ayaz, L., Fidancı, S. B., and Tamer, L. (2014). Evaluation of circulating miRNAs in wet age-related macular degeneration. *Mol. Vis.* 20, 1057–1066.

Flitcroft, D. I., He, M., Jonas, J. B., Jong, M., Naidoo, K., Ohno-Matsui, K., et al. (2019). Imi - defining and classifying myopia: A proposed set of standards for clinical and epidemiologic studies. *Invest. Ophthalmol. Vis. Sci.* 60, M20–M30. doi:10.1167/iovs.18-25957

Flitcroft, D. I., Loughman, J., Wildsoet, C. F., Williams, C., and Guggenheim, J. A. (2018). Novel myopia genes and pathways identified from syndromic forms of myopia. *Invest. Ophthalmol. Vis. Sci.* 59, 338–348. doi:10.1167/iovs.17-22173

Galvis, V., Tello, A., Camacho, P. A., Parra, M. M., and Merayo-Lloves, J. (2017). Bio-environmental factors associated with myopia: An updated review. *Arch. Soc. Espanola Oftalmol.* 92, 307–325. doi:10.1016/j.oftal.2016.11.016

Han, W., Leung, K. H., Fung, W. Y., Mak, J. Y. Y., Li, Y. M., Yap, M. K. H., et al. (2009). Association of *PAX6* polymorphisms with high myopia in Han Chinese nuclear families. *Invest. Ophthalmol. Vis. Sci.* 50, 47–56. doi:10.1167/iovs.07-0813

Han, X., Ong, J.-S., An, J., Craig, J. E., Gharahkhani, P., Hewitt, A. W., et al. (2020). Association of myopia and intraocular pressure with retinal detachment in European descent participants of the UK biobank cohort: A mendelian randomization study. *JAMA Ophthalmol.* 138, 671–678. doi:10.1001/jamaophthalmol.2020.1231

Hirota, K., Keino, H., Inoue, M., Ishida, H., and Hirakata, A. (2015). Comparisons of microRNA expression profiles in vitreous humor between eyes with macular hole and eyes with proliferative diabetic retinopathy. *Graefes Arch. Clin. Exp. Ophthalmol.* 253, 335–342. doi:10.1007/s00417-014-2692-5

Hsi, E., Wang, Y.-S., Huang, C.-W., Yu, M.-L., Juo, S.-H. H., and Liang, C.-L. (2019). Genome-wide DNA hypermethylation and homocysteine increase a risk for myopia. *Int. J. Ophthalmol.* 12, 38–45. doi:10.18240/ijo.2019.01.06

Hu, J., Hu, X., and Kan, T. (2019). MiR-34c participates in diabetic corneal neuropathy via regulation of autophagy. *Invest. Ophthalmol. Vis. Sci.* 60, 16–25. doi:10.1167/iovs.18-24968

Hysi, P. G., Choquet, H., Khawaja, A. P., Wojciechowski, R., Tedja, M. S., Yin, J., et al. (2020). Meta-analysis of 542, 934 subjects of European ancestry identifies new genes and mechanisms predisposing to refractive error and myopia. *Nat. Genet.* 52, 401–407. doi:10.1038/s41588-020-0599-0

Inamori, Y., Ota, M., Inoko, H., Okada, E., Nishizaki, R., Shiota, T., et al. (2007). The *COL1A1* gene and high myopia susceptibility in Japanese. *Hum. Genet.* 122, 151–157. doi:10.1007/s00439-007-0388-1

Ip, J. M., Rose, K. A., Morgan, I. G., Burlutsky, G., and Mitchell, P. (2008). Myopia and the urban environment: Findings in a sample of 12-year-old Australian school children. *Invest. Ophthalmol. Vis. Sci.* 49, 3858–3863. doi:10.1167/iovs.07-1451

Jayaram, H., Cepurna, W. O., Johnson, E. C., and Morrison, J. C. (2015). MicroRNA expression in the glaucomatous retina. *Invest. Ophthalmol. Vis. Sci.* 56, 7971–7982. doi:10.1167/iovs.15-18088

Jiang, B., Huo, Y., Gu, Y., and Wang, J. (2017). The role of microRNAs in myopia. *Graefes Arch. Clin. Exp. Ophthalmol.* 255, 7–13. doi:10.1007/s00417-016-3532-6

Kim, Y. J., Lee, W. J., Ko, B.-W., Lim, H. W., Yeon, Y., Ahn, S. J., et al. (2021). Investigation of MicroRNA expression in anterior lens capsules of senile cataract patients and MicroRNA differences according to the cataract type. *Transl. Vis. Sci. Technol.* 10, 14. doi:10.1167/tvst.10.2.14

Kiwerska, K., Kowal-Wisniewska, E., Ustaszewski, A., Bartkowiak, E., Jarmuz-Szymczak, M., Wierzbicka, M., et al. (2022). Global DNA methylation profiling reveals differentially methylated CpGs between salivary gland pleomorphic adenomas with distinct clinical course. *Int. J. Mol. Sci.* 23, 5962. doi:10.3390/ijms23115962

Kunceviciene, E., Budiene, B., Smalinskiene, A., Vilkeviciute, A., and Liutkeviciene, R. (2021). Association of hsa-mir-328-3p expression in whole blood with optical density of retinal pigment epithelial cells. *Vivo* 35, 827–831. doi:10.21873/invivo.12323

Kunceviciene, E., Liutkeviciene, R., Budiene, B., Sriubiene, M., and Smalinskiene, A. (2019). Independent association of whole blood miR-328 expression and polymorphism at 3'UTR of the *PAX6* gene with myopia. *Gene* 687, 151–155. doi:10.1016/j.gene.2018.11.030

Li, T., Huang, Y., Zhou, W., and Yan, Q. (2020). Let-7c-3p regulates autophagy under oxidative stress by targeting *ATG3* in lens epithelial cells. *Biomed. Res. Int.* 2020, 6069390. doi:10.1155/2020/6069390

Li, Z., Dong, Y., He, C., Pan, X., Liu, D., Yang, J., et al. (2019). RNA-seq revealed novel non-proliferative retinopathy specific circulating MiRNAs in T2DM patients. *Front. Genet.* 10, 531. doi:10.3389/fgene.2019.00531

Lingham, G., Yazar, S., Lucas, R. M., Milne, E., Hewitt, A. W., Hammond, C. J., et al. (2021). Time spent outdoors in childhood is associated with reduced risk of myopia as an adult. *Sci. Rep.* 11, 6337. doi:10.1038/s41598-021-85825-y

Liu, H., and Jiang, B. (2020). Let-7a-5p represses proliferation, migration, invasion and epithelial-mesenchymal transition by targeting *Smad2* in TGF-β2-induced human lens epithelial cells. *J. Biosci.* 45, 59. doi:10.1007/s12038-020-0001-5

Liu, S., Chen, H., Ma, W., Zhong, Y., Liang, Y., Gu, L., et al. (2022). Non-coding RNAs and related molecules associated with form-deprivation myopia in mice. *J. Cell. Mol. Med.* 26, 186–194. doi:10.1111/jcmm.17071

Liu, X., Liu, C., Shan, K., Zhang, S., Lu, Y., Yan, B., et al. (2018). Long non-coding RNA *H19* regulates human lens epithelial cells function. *Cell. Physiol. biochem.* 50, 246–260. doi:10.1159/000494003

Liu, X., Wang, P., Qu, C., Zheng, H., Gong, B., Ma, S., et al. (2015). Genetic association study between INSULIN pathway related genes and high myopia in a Han Chinese population. *Mol. Biol. Rep.* 42, 303–310. doi:10.1007/s11033-014-3773-6

Mei, F., Wang, J., Chen, Z., and Yuan, Z. (2017). Potentially important MicroRNAs in form-deprivation myopia revealed by bioinformatics analysis of MicroRNA profiling. *Ophthalmic Res.* 57, 186–193. doi:10.1159/000452421

Metlapally, R., Gonzalez, P., Hawthorne, F. A., Tran-Viet, K.-N., Wildsoet, C. F., and Young, T. L. (2013). Scleral micro-RNA signatures in adult and fetal eyes. *PloS One* 8, e78984. doi:10.1371/journal.pone.0078984

Metlapally, R., Ki, C.-S., Li, Y.-J., Tran-Viet, K.-N., Abbott, D., Malecaze, F., et al. (2010). Genetic association of insulin-like growth factor-1 polymorphisms with high-grade myopia in an international family cohort. *Invest. Ophthalmol. Vis. Sci.* 51, 4476–4479. doi:10.1167/iovs.09-4912

Metlapally, R., Park, H. N., Chakraborty, R., Wang, K. K., Tan, C. C., Light, J. G., et al. (2016). Genome-wide scleral micro- and messenger-RNA regulation during myopia development in the Mouse. *Invest. Ophthalmol. Vis. Sci.* 57, 6089–6097. doi:10.1167/iovs.16-19563

Napolitano, F., Di Iorio, V., Testa, F., Tirozzi, A., Reccia, M. G., Lombardi, L., et al. (2018). Autosomal-dominant myopia associated to a novel *P4HA2* missense variant and defective collagen hydroxylation. *Clin. Genet.* 93, 982–991. doi:10.1111/cge.13217

Pärssinen, O., Kauppinen, M., and Viljanen, A. (2014). The progression of myopia from its onset at age 8-12 to adulthood and the influence of heredity and external factors on myopic progression. A 23-year follow-up study. *Acta Ophthalmol.* 92, 730–739. doi:10.1111/aos.12387

Penha, A. M., Burkhardt, E., Schaeffel, F., and Feldkaemper, M. P. (2012). Effects of intravitreal insulin and insulin signaling cascade inhibitors on emmetropization in the chick. *Mol. Vis.* 18, 2608–2622.

Raghunath, A., and Perumal, E. (2015). Micro-RNAs and their roles in eye disorders. *Ophthalmic Res.* 53, 169–186. doi:10.1159/000371853

Rydzanicz, M., Nath, S. K., Sun, C., Podfigurna-Musielak, M., Frajdenberg, A., Mrugacz, M., et al. (2011). Identification of novel suggestive *loci* for high-grade myopia in Polish families. *Mol. Vis.* 17, 2028–2039.

Samuel, W., Jaworski, C., Postnikova, O. A., Kutty, R. K., Duncan, T., Tan, L. X., et al. (2017). Appropriately differentiated *ARPE-19* cells regain phenotype and gene expression profiles similar to those of native RPE cells. *Mol. Vis.* 23, 60–89.

Seong, H., Cho, H.-K., Kee, C., Song, D. H., Cho, M.-C., and Kang, S. S. (2021). Profiles of microRNA in aqueous humor of normal tension glaucoma patients using RNA sequencing. *Sci. Rep.* 11, 19024. doi:10.1038/s41598-021-98278-0

Shahriari, F., Satarian, L., Moradi, S., Zarchi, A. S., Günther, S., Kamal, A., et al. (2020). MicroRNA profiling reveals important functions of miR-125b and let-7a during human retinal pigment epithelial cell differentiation. *Exp. Eye Res.* 190, 107883. doi:10.1016/j.exer.2019.107883

Swierkowska, J., Karolak, J. A., Gambin, T., Rydzanicz, M., Frajdenberg, A., Mrugacz, M., et al. (2021). Variants in *FLRT3* and *SLC35E2B* identified using exome sequencing in seven high myopia families from Central Europe. *Adv. Med. Sci.* 66, 192–198. doi:10.1016/j.advms.2021.02.005

Swierkowska, J., Karolak, J. A., Vishweswaraiah, S., Mrugacz, M., Radhakrishna, U., and Gajecka, M. (2022). Decreased levels of DNA methylation in the *PCDHA* gene cluster as a risk factor for early-onset high myopia in young children. *Invest. Ophthalmol. Vis. Sci.* 63, 31. doi:10.1167/iovs.63.9.31

Tanaka, Y., Kurihara, T., Hagiwara, Y., Ikeda, S.-I., Mori, K., Jiang, X., et al. (2019). Ocular-component-specific miRNA expression in a murine model of lens-induced myopia. *Int. J. Mol. Sci.* 20, 3629. doi:10.3390/ijms20153629

Tideman, J. W. L., Pärssinen, O., Haarman, A. E. G., Khawaja, A. P., Wedenoja, J., Williams, K. M., et al. (2021). Evaluation of shared genetic susceptibility to high and low myopia and hyperopia. *JAMA Ophthalmol.* 139, 601–609. doi:10.1001/jamaophthalmol.2021.0497

Tkatchenko, A. V., Luo, X., Tkatchenko, T. V., Vaz, C., Tanavde, V. M., Maurer-Stroh, S., et al. (2016). Large-scale microRNA expression profiling identifies putative retinal miRNA-mRNA signaling pathways underlying form-deprivation myopia in mice. *PloS One* 11, e0162541. doi:10.1371/journal.pone.0162541

Uzma, N., Kumar, B. S., Khaja Mohinuddin Salar, B. M., Zafar, M. A., and Reddy, V. D. (2009). A comparative clinical survey of the prevalence of refractive errors and eye diseases in urban and rural school children. *Can. J. Ophthalmol.* 44, 328–333. doi:10.3129/i09-030

Verhoeven, V. J. M., Buitendijk, G. H. S., Rivadeneira, F., Uitterlinden, A. G., Vingerling, J. R., Hofman, A., et al. (2013). Education influences the role of genetics in myopia. *Eur. J. Epidemiol.* 28, 973–980. doi:10.1007/s10654-013-9856-1

Vishweswaraiah, S., Swierkowska, J., Ratnamala, U., Mishra, N. K., Guda, C., Chettiar, S. S., et al. (2019). Epigenetically dysregulated genes and pathways implicated in the pathogenesis of non-syndromic high myopia. *Sci. Rep.* 9, 4145. doi:10.1038/s41598-019-40299-x

Wakazono, T., Miyake, M., Yamashiro, K., Yoshikawa, M., and Yoshimura, N. (2016). Association between *SCO2* mutation and extreme myopia in Japanese patients. *Jpn. J. Ophthalmol.* 60, 319–325. doi:10.1007/s10384-016-0442-4

Wang, G.-F., Ji, Q.-S., Qi, B., Yu, G.-C., Liu, L., and Zhong, J.-X. (2017). The association of lumican polymorphisms and high myopia in a Southern Chinese population. *Int. J. Ophthalmol.* 10, 1516–1520. doi:10.18240/ijo.2017.10.06

Wang, J.-X., Yang, Y., and Li, K. (2018). Long noncoding RNA *DANCR* aggravates retinoblastoma through miR-34c and miR-613 by targeting MMP-9. *J. Cell. Physiol.* 233, 6986–6995. doi:10.1002/jcp.26621

Xiao, H., Lin, S., Jiang, D., Lin, Y., Liu, L., Zhang, Q., et al. (2021). Association of extracellular signal-regulated kinase genes with myopia: A longitudinal study of Chinese children. *Front. Genet.* 12, 654869. doi:10.3389/fgene.2021.654869

Xiao, X., Li, S., Jia, X., Guo, X., and Zhang, Q. (2016). X-linked heterozygous mutations in *ARR3* cause female-limited early onset high myopia. *Mol. Vis.* 22, 1257–1266.

Xiong, S., Sankaridurg, P., Naduvilath, T., Zang, J., Zou, H., Zhu, J., et al. (2017). Time spent in outdoor activities in relation to myopia prevention and control: A meta-analysis and systematic review. *Acta Ophthalmol.* 95, 551–566. doi:10.1111/aos.13403

Xu, S. (2009). microRNA expression in the eyes and their significance in relation to functions. *Prog. Retin. Eye Res.* 28, 87–116. doi:10.1016/j.preteyeres.2008.11.003

Xue, Z., Yuan, J., Chen, F., Yao, Y., Xing, S., Yu, X., et al. (2022). Genome-wide association meta-analysis of 88, 250 individuals highlights pleiotropic mechanisms of five ocular diseases in UK Biobank. *EBioMedicine* 82, 104161. doi:10.1016/j.ebiom.2022.104161

Young, T. L., Metlapally, R., and Shay, A. E. (2007). Complex trait genetics of refractive error. *Arch. Ophthalmol.* 125, 38–48. doi:10.1001/archopht.125.1.38

Zhang, Y., Hu, D.-N., Zhu, Y., Sun, H., Gu, P., Zhu, D., et al. (2017). Regulation of matrix metalloproteinase-2 secretion from scleral fibroblasts and retinal pigment epithelial cells by miR-29a. *Biomed. Res. Int.* 2017, 2647879. doi:10.1155/2017/2647879

Zuzic, M., Rojo Arias, J. E., Wohl, S. G., and Busskamp, V. (2019). Retinal miRNA functions in health and disease. *Genes* 10, E377. doi:10.3390/genes10050377

frontiers | Frontiers in Genetics

TYPE Original Research
PUBLISHED 06 March 2023
DOI 10.3389/fgene.2023.1135698

OPEN ACCESS

EDITED BY
Denis Plotnikov,
Kazan State Medical University, Russia

REVIEWED BY
Nirmala Dushyanthi Sirisena,
University of Colombo, Sri Lanka
Barbara Whitman,
Saint Louis University, United States

*CORRESPONDENCE
Jie Lei,
306533368@qq.com
WeiYing Jiang,
jiangwy@mail.sysu.edu.cn
HongYi Li,
lihongyi@mail.sysu.edu.cn

SPECIALTY SECTION
This article was submitted to Genetics of Common and Rare Diseases, a section of the journal Frontiers in Genetics

RECEIVED 12 January 2023
ACCEPTED 15 February 2023
PUBLISHED 06 March 2023

CITATION
Chen X, Fang Z, Pang T, Li D, Lei J, Jiang W and Li H (2023), Identification of novel variations of oculocutaneous albinism type 2 with Prader–Willi syndrome/Angelman syndrome in two Chinese families.
Front. Genet. 14:1135698.
doi: 10.3389/fgene.2023.1135698

Identification of novel variations of oculocutaneous albinism type 2 with Prader–Willi syndrome/Angelman syndrome in two Chinese families

XiaoFei Chen[1,2], ZiShui Fang[2,3], Ting Pang[2], DongZhi Li[4], Jie Lei[2,5]*, WeiYing Jiang[2]* and HongYi Li[2]*

[1]Maternity and Child Care Center of Dezhou, DeZhou, China, [2]Department of Medical Genetics, Zhongshan School of Medicine, Guangzhou, China, [3]Beijing Key Laboratory of Urogenital Diseases (Male) Molecular Diagnosis and Treatment Center, National Urological Cancer Center, Department of Urology, Peking University First Hospital, Institution of Urology, Peking University, Beijing, China, [4]Prenatal Diagnosis Center, Guangzhou Women and Children's Medical Center, Guangzhou, China, [5]Shenzhen Nanshan Maternity and Child Healthcare Hospital, Shenzhen, China

Objective: Oculocutaneous albinism (OCA) is an autosomal recessive disorder caused by a variety of genomic variations. Our aim is to identify the molecular basis of OCA in two families and lay the foundation for prenatal diagnosis.

Methods: Four types of OCA-causing mutations in the TYR, *p*, TYRP1, or SLC45A2 genes were screened. Linkage analysis was performed because the mutations found in the *p* gene violated the laws of classical Mendelian heredity. Primer-walking sequencing combined with microsatellite and single-nucleotide polymorphism analysis was used to ascertain deletion ranges. Bioinformatics methods were used to assess the pathogenicity of the new mutations.

Results: Proband 1 was diagnosed as OCA2 with Prader–Willi syndrome (PWS) due to a novel atypical paternal deletion (chromosome 15: 22330347–26089649) and a pathogenic mutation, c.1327G>A (Val443Ile), in the *p* gene of the maternal chromosome. The prenatal diagnosis results for family 1 indicated the fetus was a heterozygous carrier (c.1327G>A in the *p* gene) with a normal phenotype. Proband 2 was diagnosed as OCA2 with Angelman syndrome (AS) due to a typical maternal deletion of chromosome 15q11-q13 and a novel mutation, c.1514T>C (Phe505Ser), in the *p* gene of the paternal chromosome. This novel mutation c.1514T>C (Phe505Ser) in the *p* gene was predicted as a pathogenic mutation.

Conclusion: Our study has shown clear genotype–phenotype correlations in patients affected by distinct deletions of the PWS or AS region and missense mutations in the *p* gene. Our results have enriched the mutation spectrum of albinism diseases and provided insights for more accurate diagnosis and genetic counseling.

KEYWORDS

Prader–Willi syndrome, Angelman syndrome, oculocutaneous albinism type 2, mutation, prenatal diagnosis

Introduction

Oculocutaneous albinism (OCA), which is characterized by impaired eye development plus variable hair, skin, and ocular hypopigmentation, is a genetically inherited autosomal recessive condition, with a prevalence as high as 1/2000 and a carrier ratio of 1/70 worldwide (Gargiulo et al., 2011). Individuals with OCA are susceptible to the harmful effects of solar ultraviolet radiation, including extreme Sun sensitivity, photophobia, and skin cancer (Wright et al., 2015). Four known genes, *TYR* (OCA1), *p* (OCA2), TYRP1 (OCA3), and SLC45A2 (OCA4) have been isolated in association with OCA. Mutations in these genes affected the correct sorting and trafficking of their respective proteins, which ultimately hampers the maturation of melanosomes and melanin production (Bailus and Segal, 2014; Costin et al., 2003; Kamaraj et al., 2016). Recently, two new genes SLC24A5 and C10orf11 have been identified. The gene SLC24A5 (OCA5), is involved in the maturation of melanosomes, whereas gene C10orf11 (OCA6) is involved in melanocyte differentiation (Grønskov et al., 2013; Wei et al., 2013).

Of note, among these different forms of OCA, OCA2 is sometimes associated with Prader–Willi syndrome (PWS) or Angelman syndrome (AS) because the *p* gene is localized in the distal part of the PWS/AS region (Fridman et al., 2003). PWS is a neurogenetic disorder, characterized by obesity, short stature, muscular weakness, intellectual deficiencies, and deviant social behavior (Cassidy et al., 2012; JiangLev-Lehman et al., 1999). Approximately 70% of cases occur when part of the father's chromosome 15 is deleted. In another 25% of cases, the person has two copies of chromosome 15 from their mother and none from their father. AS is a monogenic neurological disorder characterized by ataxia, intellectual disability, speech impairment, sleep disorders, and seizures. AS occurs due to lack of function in a part of the chromosome 15 inherited from a person's mother. Most of the time, it is due to a deletion or mutation of the *UBE3A* gene on that chromosome (Bailus and Segal, 2014). PWS and AS were the first recognized human genomic imprinting disorders. Both syndromes are caused by several different genetic alterations in the chromosome region 15q11.2-q13. However, deletion-related PWS and AS cases do not represent a genetically homogeneous group, as they are composed of two main groups: Class I, with breakpoints at BP1 (proximal) and BP3 (distal), and Class II, with breakpoints at BP2 (proximal) and BP3 (distal) (Faundes et al., 2014). The *p* gene is not imprinted, and both alleles are expressed. PWS and AS patients with typical deletions are thus hemizygous for the *p* gene. It is also well-established that PWS and AS deletion patients usually show hypopigmentation of the skin and hair and *p* causes this hypopigmentation as well (Clayton-Smith, 1993; Spritz et al., 1997), although the mechanism has not yet been established.

Here, we reported two OCA2 patients with PWS/AS. The former was OCA2 with PWS due to a novel, atypical deletion of approximately 3.8 Mb in the paternally inherited chromosome 15 and a pathogenic mutation, c.1327G>A (Val443Ile), in the *p* gene of the maternal chromosome. The latter was OCA2 with AS due to a typical deletion in the maternally inherited chromosome 15q11-q13 and a novel mutation, c.1514T>C (Phe505Ser), in the *p* gene of the paternal chromosome. The present study provided valuable information for better evaluation of patients with albinism and more efficient patient identification.

Subjects and methods

Patients

Patient 1 (Proband 1) is a 13-month-old girl born at term after a normal pregnancy. She had normal birth weight, length, and head circumference but had light yellow hair, gray eyes, and milky skin with hypotonia (Figure 1). Her mother (23 years old) and father (27 years old) had normal phenotypes.

Patient 2 (Proband 2) is a 50-day-old male newborn with an albinism phenotype; no other obviously abnormal phenotypes were found (Figure 2). His parents and older brother had normal phenotypes.

FIGURE 1
DNA sequencing results of family 1. Proband 1 carried homozygous mutation c.1327G>A in the *p* gene; her father was wild-type (c.1327G); her mother carried heterozygous mutation c.1327G > A/G; the fetus carried heterozygous mutation c.1327G>A/G.

FIGURE 2
DNA sequencing results of family 2. Proband 2 carried homozygous mutation c.1514T>C in the *p* gene; his father carried heterozygous mutation c.1514T>C/T; his mother was wild-type (c.1514T); his older brother was wild-type (c.1514T).

Mutation screening of OCA genes

After obtaining written informed consent from all participating individuals, peripheral blood samples and an amniotic fluid sample were collected from the two families. Genomic DNA was extracted using a DNA extraction kit (TIANamp Blood Genomic DNA Purification Kit; Tiangen Biotech, Beijing, China). The coding region and the exon–intron boundaries of *TYR*, *p*, *TYRP1*, and *SLC45A2* were amplified by PCR. Mutation screening was performed in the two families using direct DNA sequencing.

Haplotype analysis

Linkage analysis was performed because the mutations found in the *p* gene violated the laws of classical Mendelian heredity, which suggested that it was likely to be associated with PWS or AS. The fine mapping sequences were obtained from the Human Genome Database (GDB). Haplotype analysis was performed with six microsatellite markers (STRs): D15S646, D15S817, D15S1513, D15S822, D15S659, and D15SFES (as shown in Table 1). To further determine the extent of the deletion, we designed primers 1–7 in the D15S817–D15S1513 direction, the primers A–H in the D15S1513–D15S817 direction, and primers D1–D7 in the D15S659–D15S822 direction on 15q11-q13. The information of these primers is shown in Table 2. Subsequently, primer-walking sequencing combined with SNP linkage analysis was performed to determine the deletion ranges. Prenatal genetic testing was carried out by DNA sequencing and haplotype analysis. Physical sketch maps of the *p* gene, STRs, and primers (1–7, A–D, D1–D7) as well as the typical breakpoints (BP1, BP2, and BP3) on the chromosome region 15q11.2-q13 are shown in Figure 3.

Pathogenicity evaluation of the novel mutation

The mutation sites were acquired from the Human Gene Mutation Database (http://www.hamd.cf.ac.uk/), Hermansky–Pudlak Syndrome database (http://liwewilab.genetics.ac.cn/HPSD/), Albinism Database (http://albinismdb.med.umn.edu/) and SNP database (http://www.ncbi. nlm.nih.gov/SNP/), as well as the Ensembl website (http://asia. ensembl.org/index.html) to exclude the possibility of common polymorphisms. In addition, the pathogenicity of mutation sites was also analyzed using web-based computational pathogenicity prediction tools including Align GVGD (http://agvgd.iarc.fr/agvgdinput.php), SIFT (http://sift.jcvi.org/), and PolyPhen-2 (http://genetics.bwh.harvard.edu/pph2/).

Results

Mutation screening results

The mother of proband 1 was heterozygous for c.1327G>A (Val443Ile) in exon 13 of the *p* gene, and the father of proband 1 was wild-type (c.1327G) at this site. However, for proband 1, only one pathogenic homozygous mutation, c.1327G>A (Val443Ile), was detected in exon 13 of the *p* gene, violating the laws of classical Mendelian heredity. In prenatal diagnosis, the fetus was a carrier of the heterozygous mutation c.1327G>A in the *p* gene. The sequencing results are shown in Figure 4.

In the second family, the father of proband 2 was heterozygous for c.1514T>C (Phe505Ser) in exon 15 of the *p* gene, while the mother and older brother of proband 2 were wild-type (c.1514T) at this site. Interestingly, in proband 2, only one novel homozygous mutation, c.1514T>C (Phe505Ser), was detected in exon 15 of the *p* gene (as shown in Figure 5).

Linkage analysis results

Because of these "violations" of the laws of Mendelian heredity, theoretically speaking, three possibilities exist: first, *de novo* mutations occurring during the development of the fertilized zygote; second, uniparental disomy (UPD) of chromosome 15; and third, a deletion mutation in paternal chromosome 15. According to a linkage analysis of family 1, paternal deletions were present at D15S1513 and D15S822, but normal alleles were found at D15S646, D15S817, D15S659, and

TABLE 1 Primers for the STRs.

Primer	Location	STR	Sequence 5′-3′
D15S646	15q11.2	TAT	F: 5′AGGACAGGAGAAAGGAATTAGGAT3′ R: 5′GCTAGATGACGGGTTAGTGGGT3′
D15S817	15q11.2	GATA	F: 5′GAACCGTTCATACTACCAAAG 3′ R: 5′TACTGAGGGTTTAACCAAGG 3′
D15S1513	15q12	GATA	F: 5′ACATCCTCCACGTACGAATAATA 3′ R: 5′CAGGATATGTTTTTTGGGGAT 3′
D15S822	15q11.2	TCTA	F: 5′GTGTGAAGTGACAGAAGAGAGCA 3′ R: 5′TCCTATTGAGAGTCCATTGAGATT 3′
D15S659	15q11.2	TATC	F: 5′TGGTAGTCTGGACACCTATTGC 3′ R: 5′AGGCAGTAATGGTTAGTGGAGAA 3′
FES	15q25.1	TAAA	F: 5′CCCCATCTCTACTGAAAAAGCAA 3′ R: 5′GGGTCACTCTGGGGATTTGG3′

TABLE 2 Primers for the SNPs.

Primer	Location	Sequence 5′-3′
1	chr15: 22273981-22276481	F: 5′TATCGCTTTTCTTTTACTGAC 3′
		R: 5′TCCTTCCCTCAACTACTCC 3′
2	chr15: 22297213-22297826	F: 5′CATCACCCCTCTGGTTGTCAT 3′
		R: 5′TCCAGACCCAGGGACTATCAT 3′
3	chr15: 22312426-22313016	F: 5′ACTTACTATAAGCGACTACCATT 3′
		R: 5′TTTCTAGTGTGATATTTGGAGAC 3′
4	chr15: 22313906-22314256	F: 5′ACTCCTTAACATATTGGGGTGA 3′
		R: 5′CCTGGGAGTCCAGAGAGAGA 3′
5	chr15: 22322315-22323034	F: 5′CAAATACGGAATGTGAGGTCCTG 3′
		R: 5′CACAAGACAAATGCACAATCAACT 3′
6	chr15: 22326235-22326805	F: 5′TTCAAATTCCTAGCCTCAAGCAG 3′
		R: 5′AGCTGTGCCCTCTGACTACATTG 3′
7	chr15: 22329848-22330347	F: 5′AAGGGTATGGTTCTGTGTGTAAG 3′
		R: 5′AGTTTCAAGTTTATCATAAAACCA 3′
A	chr15: 22790005-22790715	F: 5′CTGTTGGGTGCCTGGATAGA 3′
		R: 5′ATGGTTATGAAAATGAGGTGCT 3′
B	chr15: 22518350-22519347	F: 5′CACAGCGAAAGAAACTATCAAT 3′
		R: 5′AGGTCAATAAAGAAATCAATGG 3′
C	chr15: 22458684-22459484	F:5′GAGCTCATATGCAGAAACTAA 3′
		R:5′TAATACTGGAAAATGACACAAA 3′
D	chr15: 22438713-22439295	F: 5′CTTTGAAGAAAATCCCAGAGA 3′
		R: 5′CTATGTCTTGAAAAATTGCCA 3′
E	chr15: 22435496-22436048	F: 5′GAACAGCAAATGTTCCTGCC 3′
		R: 5′GGTCACTCCCACCCTAATAATG 3′
F	chr15: 22429425-22429940	F: 5′GCTCATTCCCTGTTTACTGTG 3′
		R: 5′ATTTTTTGCTTCCAGACCTAT 3′
G	chr15: 22330366-22330837	F: 5′AATTGTACCTTGCCACTTTG 3′
		R: 5′CAGTCATACCTAATCTCTTTCC 3′
D1	chr15: 43844144-43844774	F: 5′TCACTGGATGTGAGCTGTCC 3′
		R: 5′GCAAGTAGGCAAAAAGAAGAG 3′
D2	chr15: 39698389-39698897	F: 5′GTACTCCCTTCCTGCTCCCT 3′
		R: 5′AAGTGTAGCCACAAGAGACCA 3′
D3	chr15: 32986240-32986885	F: 5′ATTTCATTGTTTTCAGTCTTT 3′
		R: 5′TCTTCCAGTTTCTCTACTTTTA 3′
D4	chr15: 28835913-28836416	F: 5′GCGATCTCAGCTCACTACAAC 3′
		R: 5′AACCTTGGTAAACTGAGGCAA 3′
D5	chr15: 27117598-27118068	F: 5′CCAGGACTCTGTAAGCTCTAG 3′
		R: 5′TTCACCTAATGCTTCAGTACTA 3′

(Continued on following page)

TABLE 2 (*Continued*) Primers for the SNPs.

Primer	Location	Sequence 5′-3′
D6	chr15: 26153681-26154397	F: 5′GGATAGATCCTTGGAGATGGGA 3′
		R: 5′CAGCAGTCCTGAAATTGCATGA 3′
D7	chr15: 26089649-26090302	F: 5′CCATAAGGAAAATATTAAAACCA 3′
		R: 5′CAGCATCTGCTTTTATGAATAAC 3′
P13	chr15: 25601391-25947825	F: 5′TCTCGGCCCCCCTAGGACAT 3′
		R: 5′CTCAACCGCCCCCACCTTTT 3′

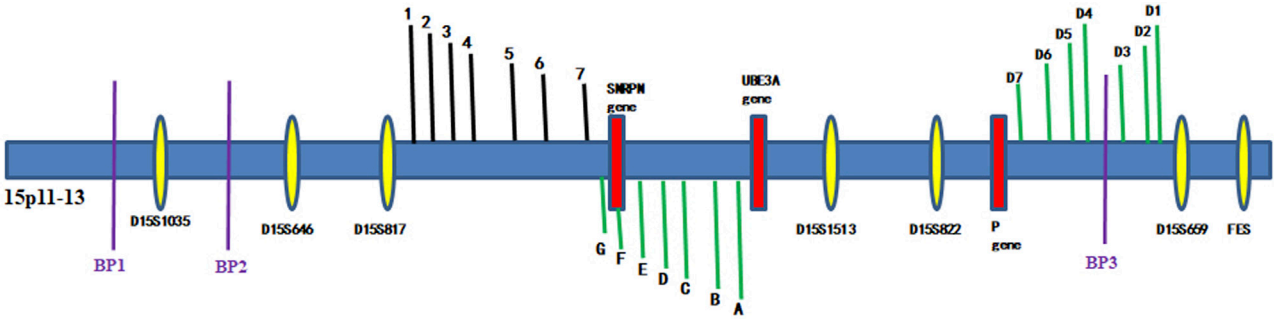

FIGURE 3
Haplotype schematic map of the members of family 1. The arrow indicates proband 1. She was affected by OCA2 with PWS due to an atypical deletion (chr15: 22330347–26089649, approximately 3.8 Mb) on paternal chromosome 15 and a point mutation c.1327G>A (Val443Ile) in the *p* gene of maternal chromosome 15.

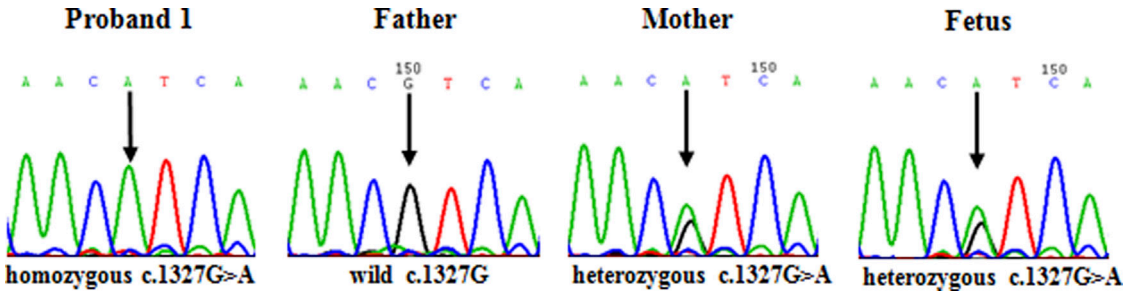

FIGURE 4
Haplotype schematic map of the core members of family 2. The arrow indicates proband 2. He was diagnosed as OCA2 with AS due to a typical maternal deletion on maternal chromosome 15q11-13 and a novel pathogenic point mutation c.1514T>C (Phe505Ser) in the *p* gene of paternal chromosome 15.

D15SFES in proband 1. The results of the linkage analysis are shown in Figure 6. Because D15S646, D15S817, D15S1513, and D15S822 are located between breakpoint 2 and breakpoint 3 of the PWS/AS chromosomal region and D15S659 and D15SFES are outside the region, these results suggested that a microdeletion was present on chromosome 15, smaller than that of the internationally reported Class II. Primer-walking sequencing combined with SNP linkage analysis revealed that proband 1 had a microdeletion (chr15: 22330347-26089649, approximately 3.8 Mb) between primers G and D7, which was in line with the distal breakpoint BP3 but significantly below the upstream proximal breakpoint BP2. Therefore, this variation represents a novel deletion found in PWS. In prenatal diagnosis of family 1, linkage analysis confirmed that the fetal chromosome was normal in the PWS region, as shown in Figure 6.

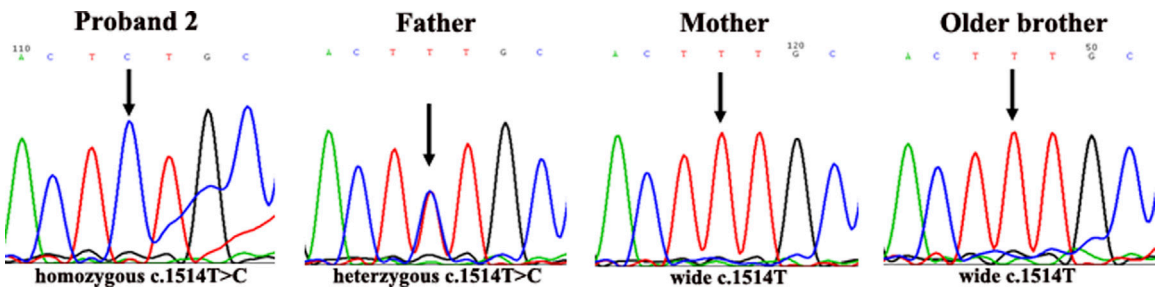

FIGURE 5
Conservation comparison results of *p*.505F in ten species. This site is highly conserved among ten species.

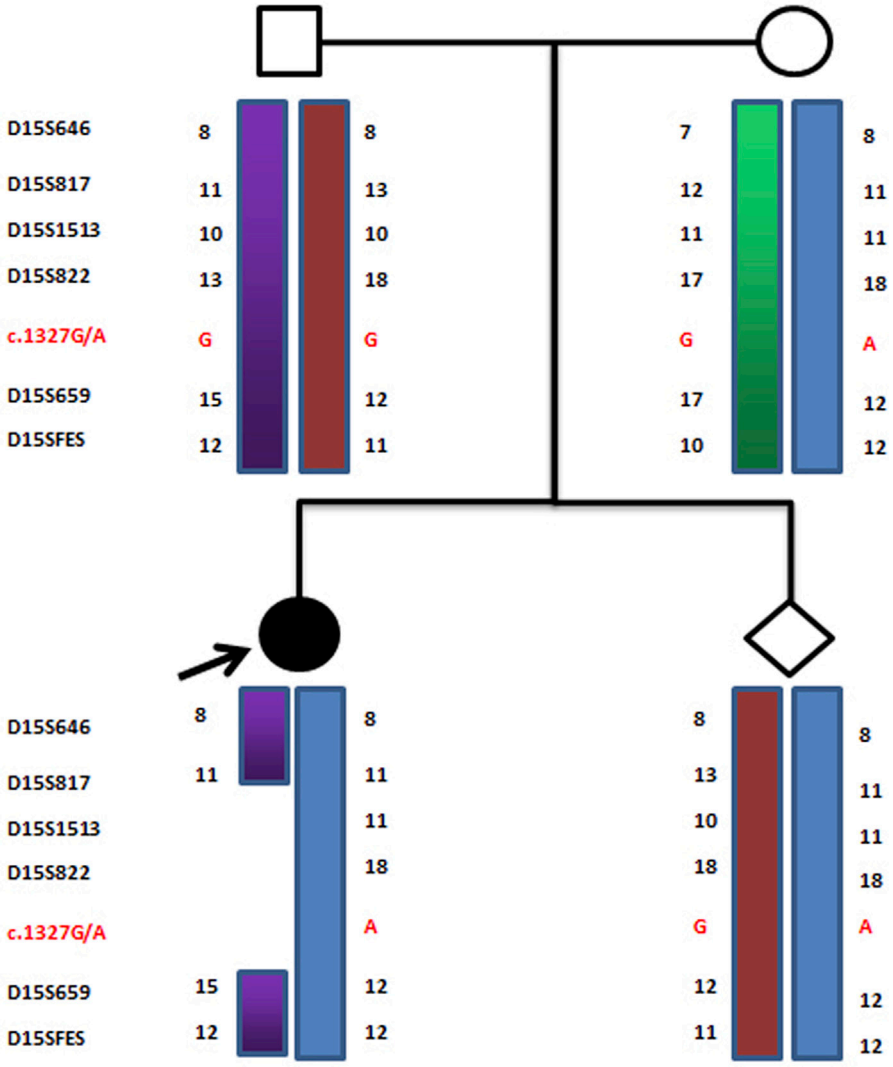

FIGURE 6
Photograph of proband 1 at 13 months. She was diagnosed as OCA2 with PWS.

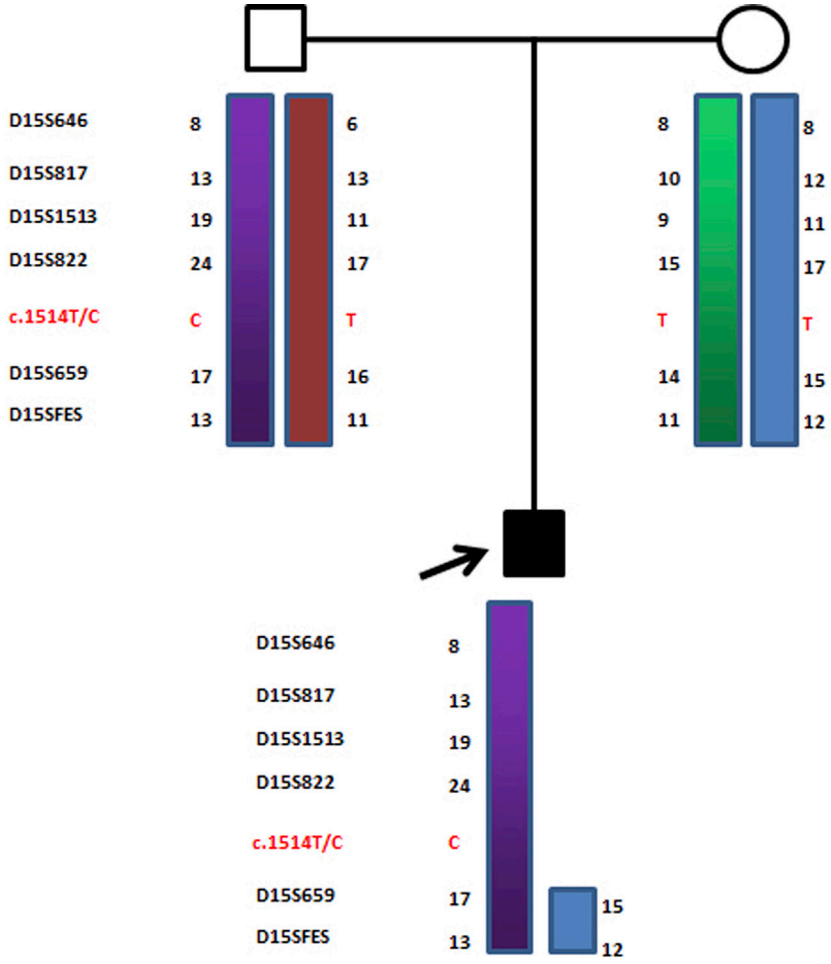

FIGURE 7
Photograph of proband 2 at 50 days. He was diagnosed as OCA2 with AS.

Similarly, in proband 2, D15S659 and D15SFES were inherited from both parents, but D15S646, D15S817, D15S1513, and D15S822 showed maternal deletion (as shown in Figure 7). STR linkage analysis combined with DNA sequencing revealed that proband 2 suffered from OCA2 with AS.

Pathogenicity evaluation of the novel mutation

After a careful assessment using the Human Gene Mutation Database, Hermansky–Pudlak syndrome Database, Albinism Database and SNP database, as well as the Ensembl website to exclude the possibility of a common polymorphism, a previously potential unreported mutation c.1514T>C (Phe505Ser) on the *p* gene was considered. This site is highly conserved among ten species, i.e., human, mouse, monkey, chimpanzee, pig, cattle, chicken, sheep, rat, and zebrafish, as shown in Figure 8. Web-based computational pathogenicity prediction tools including Align GVGD, SIFT, and PolyPhen-2 indicated that this novel missense mutation is pathogenic.

Follow-up

Proband 1 showed microcephaly and partial myelinization at 6 months using magnetic resonance imaging (MRI). In addition, her occipitofrontal head circumference (OFC) was at the third percentile at 1 year, and she had hypotonia, unusual hand movements, and developmental delays. Then, she exhibited over-eating, almond-shaped eyes, low ears, narrow eyes, fat, and smaller hands and feet. In addition, her hair became fawn-colored, and she exhibited language barriers and hypoplasia of sexual organs with increasing age. The newborn in family 1 had a normal phenotype at birth.

Proband 2 exhibited developmental retardation, dyskinesia, and language barriers during growth and development, which corresponded to the symptoms of AS. In addition, when proband 2 developed a fever (body temperature exceeding 38.5°C), febrile seizure occurred.

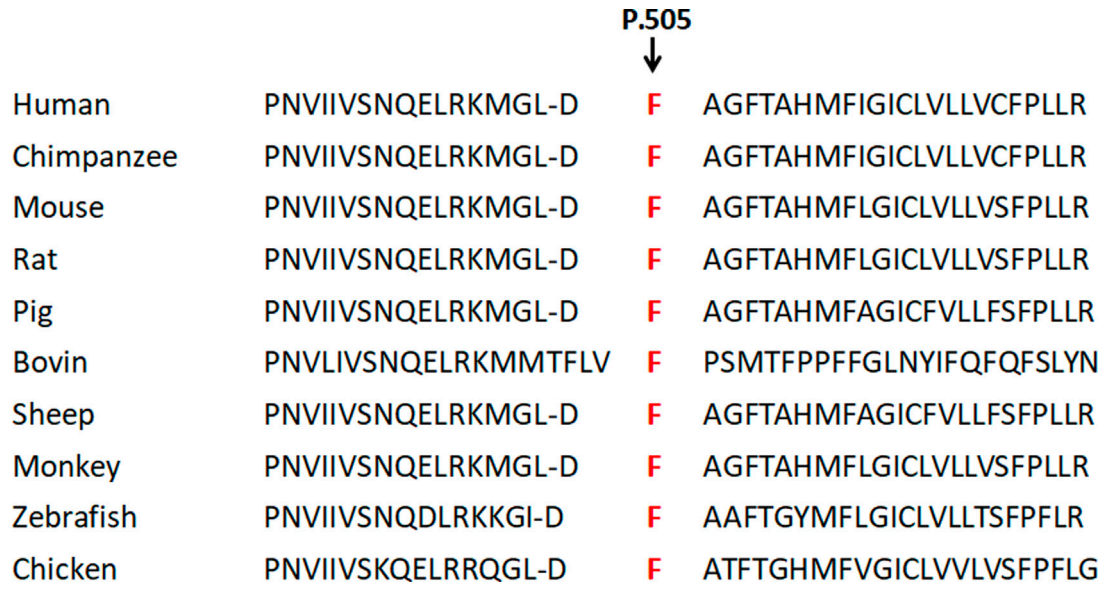

FIGURE 8
Physical sketch map of the *p* gene, STRs, and primers (1–7, A–D, D1–D7) as well as the breakpoints on the chromosome region 15q11.2-q13. (BP1, breakpoint 1; BP2, breakpoint 2; BP3, breakpoint 3).

Discussion

Generally, the clinical recognition of OCA is relatively easy because of the cutaneous hypopigmentation associated with the presence of nystagmus, foveal hypoplasia with little retinal melanin pigment, and reduced visual acuity. However, determining the specific type of OCA still requires diagnostic techniques based on molecular biology. Furthermore, OCA is sometimes associated with PWS/AS because of their similar genomic regions: the *p* gene corresponding to OCA2 is located on chromosome 15q11-q12, within the PWS/AS chromosome region.

In this study, we performed a comprehensive mutational analysis. Finally, the causes of the probands' conditions were identified. Proband 1 was affected with OCA2 and PWS with an atypical deletion (approximately 3.8 Mb) on paternal chromosome 15 and the pathogenic mutation c.1327G>A (Val443Ile) in the *p* gene of the maternal chromosome. The atypical deletion mutation was smaller than the classical deletion mutation. In addition, we performed prenatal genetic diagnosis for family 1 and found that the fetus was a heterozygous carrier (c.1327G>A/G) with a normal phenotype. Proband 2 was diagnosed as OCA2 with AS due to a typical maternal deletion on chromosome 15 and a novel mutation, c.1514T>C (Phe505Ser), in the *p* gene of the paternal chromosome.

A previous study has shown that the prevalence of OCA2 resulting from the 2.7-kb deletion in exon 7 of the *p* gene is 1 in 1,800 in individuals of African origin (Durham-Pierre et al., 1994). However, the incidence of OCA caused by deletions in chromosome 15 and point mutations in the *p* gene remains unknown in the Chinese population. The current study showed that there existed deletion mutations in the OCA gene that failed to be detected through direct sequencing. Molecular classification of PWS/AS is important because it indicates a risk of recurrence in the siblings of PWS/AS patients. Thus, a precise determination of molecular class in PWS and AS patients is essential for accurate genetic counseling of parents seeking a future pregnancy (Fridman et al., 2003; Cassidy et al., 2012). The recognition of OCA with PWS/AS is as important as early treatment to improve the prognosis of this dismal disease, enhance survival and quality of life, and provide a basis for prenatal diagnosis.

In our study, a new deletion mutation of PWS was found through primer-walking sequencing and SNP analysis of 15q11-13. The discovery of this novel variation enriched the known genetic heterogeneity of PWS in China. As various degrees of hypopigmentation are associated with PWS and AS patients, the study of the *p* gene in a hemizygous state could contribute to the understanding of its effect on human pigmentation during development and potentially disclose the presence of modifier pigmentation gene (s) in the PWS/AS region (Fridman et al., 2003; Spritz et al., 1997).

Conclusion

In this study, we reported on two OCA families. One was affected by OCA2 with PWS due to an atypical deletion (chr15: 22330347–26089649, approximately 3.8 Mb) on paternal chromosome 15 and a point mutation c.1327G>A (Val443Ile) in the *p* gene of maternal chromosome 15, and we performed prenatal diagnosis for family 1, which indicated that the fetus was a heterozygous carrier (c.1327G>A/G in the *p* gene) with a normal phenotype. Another family was diagnosed as OCA2 with AS due to a typical maternal deletion on maternal chromosome 15q11-13 and a novel pathogenic point mutation c.1514T>C (Phe505Ser) in the *p* gene of paternal chromosome 15. These findings increased the spectrum of clinical conditions associated with *p* gene mutations. Our study

indicates the necessity of further investigation for concurrent PWS/AS in patients with developmental delays and albinism.

Data availability statement

The datasets presented in this study can be found in online repositories. The names of the repository/repositories and accession number (s) can be found in the article/Supplementary Material.

Ethics statement

The studies involving human participants were reviewed and approved by the Ethics Committee of Sun Yat-sen University (20120101). Written informed consent to participate in this study was provided by the participants' legal guardian/next of kin. Written informed consent was obtained from the individual (s), and minor (s)' legal guardian/next of kin, for the publication of any potentially identifiable images or data included in this article.

Author contributions

HL and WJ designed the study. XC, JL, and ZF collected the probands and implemented PCR. TP and DL performed SNP analysis and bioinformatics analysis.

Funding

This study was supported by the National Natural Science Foundation of China grant no. 30672003.

Acknowledgments

We thank the probands and their families for taking part in our study.

Conflict of interest

The authors declare that the research was conducted in the absence of any commercial or financial relationships that could be construed as a potential conflict of interest.

Publisher's note

References

Bailus, B. J., and Segal, D. J. (2014). The prospect of molecular therapy for Angelman syndrome and other monogenic neurologic disorders. *Bailus Segal BMC Neurosci.* 15, 76. doi:10.1186/1471-2202-15-76

Cassidy, S. B., Schwartz, S., Miller, J. L., and Driscoll, D. J. (2012). Prader-Willi syndrome. *Genet. Med.* 14, 10–26. doi:10.1038/gim.0b013e31822bead0

Clayton-Smith, J. (1993). Clinical research on angelman syndrome in the United Kingdom: Observations on 82 affected individuals. *Am. J. Med. Genet.* 46, 12–15. doi:10.1002/ajmg.1320460105

Costin, G. E., Valencia, J. C., Vieira, W. D., Lamoreux, M. L., and Hearing, V. J. (2003). Tyrosinase processing and intracellular trafficking is disrupted in mouse primary melanocytes carrying the underwhite (uw) mutation. A model for Oculocutaneous albinism (OCA) type 4. *J. Cell Sci.* 116, 3203–3212. doi:10.1242/jcs.00598

Driscoll, D. J., JenniferMiller, L., Schwartz, S., and Cassidy, S. B. (2023). *Prader-Willi syndrome*. Initial Posting: October 6, 1998; Last Revision: December 14, 2017.

Durham-Pierre, D., Gardner, J. M., Nakatsu, Y., King, R. A., Francke, U., Ching, A., et al. (1994). African origin of an intragenic deletion of the human P gene in tyrosinase positive oculocutaneous albinism. *Nat. Genet.* 7, 176–179. doi:10.1038/ng0694-176

Faundes, V., Maria, L. S., María, L. S., Aliaga, S., Curotto, B., Pugin, A., et al. (2014). Molecular classes in 209 patients with prader-willi or angelman syndromes: Lessons for genetic counseling. *Am. J. Med. Genet. PART A* 167A, 261–263. doi:10.1002/ajmg.a.36801

Fridman, C., Hosomi, N., Varela, M. C., Souza, A. H., Fukai, K., and Koiffmann, C. P. (2003). Angelman syndrome associated with oculocutaneous albinism due to an intragenic deletion of the P gene. *Am. J. Med. Genet.* 119, 180–183. doi:10.1002/ajmg.a.20105

Gargiulo, A., Testa, F., Rossi, S., Di Iorio, V., Fecarotta, S., de Berardinis, T., et al. (2011). Molecular and clinical characterization of albinism in a large cohort of Italian patients. *Invest. Ophthalmol. Vis. Sci.* 14, 1281–1289. doi:10.1167/iovs.10-6091

Grønskov, K., Dooley, C. M., Østergaard, E., Kelsh, R. N., Hansen, L., Levesque, M. P., et al. (2013). Mutations in c10orf11, a melanocyte-differentiation gene, cause autosomal-recessive albinism. *Am. J. Hum. Genet.* 92, 415–421. doi:10.1016/j.ajhg.2013.01.006

Jiang, Y., Lev-Lehman, E., Bressler, J., Tsai, T. F., and Beaudet, A. L. (1999). Genetics of angelman syndrome. *Am. J. Hum. Genet.* 65, 1–6. doi:10.1086/302473

Kamaraj, B., and Purohit, R. (2016). Mutational analysis on membrane associated transporter protein (matp) and their structural consequences in oculocutaeous albinism type 4 (OCA4)- A molecular dynamics approach. *J. Cell. Biochem.* 117, 2608–2619. doi:10.1002/jcb.25555

Spritz, R. A., Bailin, T., Nicholls, R. D., Lee, S. T., Park, S. K., Mascari, M. J., et al. (1997). Hypopigmentation in the Prader-Willi syndrome correlates with P gene deletion but not with haplotype of the hemizygous P allele. *Am. J. Med. Genet.* 71, 57–62. doi:10.1002/(sici)1096-8628(19970711)71:1<57:aid-ajmg11>3.0.co;2-u

Wei, A. H., Zang, D. J., Zhang, Z., Liu, X. Z., He, X., Yang, L., et al. (2013). Exome sequencing identifies SLC24A5 as a candidate gene for nonsyndromic oculocutaneous albinism. *J. Invest. Dermatol* 133, 1834–1840. doi:10.1038/jid.2013.49

Wright, C. Y., Norval, M., and Hertle, R. W. (2015). Oculocutaneous albinism in sub-saharan africa: Adverse sun-associated health effects and photoprotection. *Photochem Photobiol.* 91, 27–32. doi:10.1111/php.12359

frontiers | Frontiers in Genetics

TYPE Original Research
PUBLISHED 20 March 2023
DOI 10.3389/fgene.2023.1139161

OPEN ACCESS

EDITED BY
Jeremy Guggenheim,
Cardiff University, United Kingdom

REVIEWED BY
Diego Maria Michele Fornasari,
University of Milan, Italy
Afagh Alavi,
University of Social Welfare and Rehabilitation Sciences, Iran

*CORRESPONDENCE
Liqiang Wang,
liqiangw301@163.com
Jifeng Yu,
jeffernyu@126.com

†These authors have contributed equally to this work

SPECIALTY SECTION
This article was submitted to Genetics of Common and Rare Diseases, a section of the journal Frontiers in Genetics

RECEIVED 06 January 2023
ACCEPTED 27 February 2023
PUBLISHED 20 March 2023

CITATION
Yu H, Wu J, Cong J, Chen M, Huang Y, Yu J and Wang L (2023), Congenital insensitivity to pain associated with *PRDM12* mutation: Two case reports and a literature review.
Front. Genet. 14:1139161.
doi: 10.3389/fgene.2023.1139161

Congenital insensitivity to pain associated with *PRDM12* mutation: Two case reports and a literature review

Hanrui Yu[1,2†], Jie Wu[3†], Jinju Cong[4†], Mingxiong Chen[5], Yifei Huang[2], Jifeng Yu[6*] and Liqiang Wang[2*]

[1]Medical School of Chinese PLA, Beijing, China, [2]Department of Ophthalmology, The Third Medical Center, Chinese PLA General Hospital, Beijing, China, [3]Department of Ophthalmology, Hainan Hospital of Chinese PLA General Hospital, Sanya, China, [4]Aier Eye Hospital, Qianjiang, Hubei Province, China, [5]School of Medicine, Nankai University, Tianjin, China, [6]Department of Ophthalmology, Beijing Children Hospital, Capital Medical University, National Center for Children's Health, Beijing, China

Background: *PRDM12* is a newly discovered gene responsible for congenital insensitivity to pain (CIP). Its clinical manifestations are various and not widely known.

Methods: The clinical data of two infants diagnosed with CIP associated with *PRDM12* mutation were collected. A literature review was performed, and the clinical characteristics of 20 cases diagnosed with a mutation of *PRDM12* were summarized and analyzed.

Results: Two patients had pain insensitivity, tongue and lip defects, and corneal ulcers. The genomic analysis results showed that variants of *PRDM12* were detected in the two families. The case 1 patient carried heterozygous variations of c.682+1G > A and c.502C > T (p.R168C), which were inherited from her father and mother, respectively. We enrolled 22 patients diagnosed with CIP through a literature review together with our cases. There were 16 male (72.7%) and 6 female (27.3%) patients. The age of onset ranged from 6 months to 57 years. The prevalence of clinic manifestation was 14 cases with insensitivity to pain (63.6%), 19 cases with self-mutilation behaviors (86.4%), 11 cases with tongue and lip defects (50%), 5 cases with mid-facial lesions (22.7%), 6 cases with distal phalanx injury (27.3%), 11 cases of recurrent infection (50%), 3 cases (13.6%) with anhidrosis, and 5 cases (22.7%) with global developmental delay. The prevalence of ocular symptoms was 11 cases (50%) with reduced tear secretion, 6 cases (27.3%) with decreased corneal sensitivity, 7 cases (31.8%) with disappeared corneal reflexes, 5.5 cases (25%, 0.5 indicated a single eye) with corneal opacity, 5 cases (22.7%) with corneal ulceration, and 1 case (4.5%) with a corneal scar.

Conclusion: The syndrome caused by *PRDM12* mutation is a clinically distinct and diagnosable disease that requires joint multidisciplinary management to control the development of the disease and minimize the occurrence of complications.

KEYWORDS

Prdm12, insensitivity to pain, corneal disease, self-mutilation behavior, HSAN, hereditary and sensory autonomic neuropathy

Introduction

Pain is a protective perception response to most harmful stimuli. Insensitivity to pain leads to an unguarded body, vulnerable to damage. Congenital insensitivity to pain (CIP) is a group of rare genetic pain loss disorders defined by its congenital onset. Hereditary sensory and autonomic neuropathy (HSAN) is also a genetic pain loss disorder that tends to develop gradually over time. Occasionally CIP and HSAN can overlap as the difference is not clear (Lischka et al., 2022). HSAN has been classified into types I–VIII according to the main mutation genes: *SPTLC1*, *SPTLC2*, *ALT1*, *WNK1*, *SCN9A*, *NTRK1*, *NGFβ*, *SCN11A*, and *PRDM12* (Rotthier et al., 2012; Schwartzlow and Kazamel, 2019). Types VI, VII, and VIII of HSAN correspond to types I, II, and III of CIP (Schwartzlow and Kazamel, 2019).

PRDM12 is a newly identified causative gene for CIP. Members of the PRDM protein family have a PR domain and differing numbers of Zn-finger repeats. PRDM proteins regulate gene expression by either directly altering the chromatin structure through intrinsic methyltransferase activity or indirectly by attracting chromatin remodeling complexes (Di Zazzo et al., 2013). The human *PRDM12* gene is localized on chromosome 9 at 9q33-q34, according to the Entrez Gene [Gene ID: 59335]. It has been proved that *PRDM12* plays an important role in human pain perception (Nahorski et al., 2015; Drissi et al., 2020). The nerve growth factor (NGF)/tyrosine receptor kinase A (TrkA) signaling pathway is required for the survival and specification of nociceptors and plays a major role in pain processing. *PRDM12* regulates the expression of NGF receptor TrkA to guide the development of nociceptive sensory neurons (Desiderio et al., 2019).

Mutations in *PRDM12* are currently believed to cause HSAN-VIII and midface toddler excoriation syndrome (MiTES). HSAN is a rare hereditary neuropathy classified into types I–VIII (Rotthier et al., 2012; Schwartzlow and Kazamel, 2019). The mutation of the *PRDM12* gene leads to the autosomal recessive HSAN-VIII type, also known as CIP3. The clinical symptoms vary, including growth delays, anhidrosis, self-mutilation behaviors, and self-injury-induced oral and corneal ulcers. Some injuries could be cured with treatment, while others could lead to lifelong tissue defects if left untreated. For instance, the patient reported by Gaur et al. (2018) suffered from frequent self-mutilation behaviors due to insensitivity to pain. He was only 1 year old when he had severe corneal scarring, a lip defect, and distal phalangeal injury caused by self-mutilation behaviors. Likewise, Moss et al. (2018) also reported a disease associated with *PRDM12* mutations called MiTES. Unlike CIP3, MiTES is a relatively singular clinical presence with mostly scarring in the midface rather than a widespread insensitivity to pain (Moss et al., 2018). Thus, the two syndromes caused by *PRDM12* easily cause appearance damage to patients, which seriously affects the quality of life.

Because the clinical manifestations caused by *PRDM12* mutation are various, a lack of gene analysis as a routine clinical examination makes it difficult to diagnose this disease. Therefore, syndromes caused by a *PRDM12* mutation are prone to be missed. Without early detection and early diagnosis, early treatment and early prevention are impossible. At the same time, due to the diversity of clinical manifestations of such diseases, including corneal ulcers, oral ulcers and infection, multidisciplinary collaborative management is needed, which increases the difficulty of treatment.

Our study hopes to summarize the clinical symptoms and treatment plans of two patients with *PRDM12* mutations admitted to our hospital and 20 patients with *PRDM12* mutations reported in the literature, analyze the impact of related symptoms on patients, formulate corresponding clinical management measures, and systematically elaborate the comprehensive prevention and treatment plan for patients with a *PRDM12* mutation. It provides new ideas and comprehensive knowledge for the diagnosis and treatment of this disease.

Materials and methodology

Two patients with *PRDM12* mutations confirmed in Beijing Children's Hospital affiliated with Capital Medical University were included in this study. All the children's guardians were informed and signed written informed consent. The terms "PRDM12," "Hereditary sensory and autonomic neuropathy-VIII," "Congenital insensitivity to pain 3," and "Midface toddler excoriation syndrome" were searched in the National Library of Medicine of the United States (PubMed) from the time of establishment to October 2022. Inclusion criteria were the discovery of associated pathogenic genes.

Genetic testing

Genomic DNA was extracted from the peripheral blood of patients to construct a genomic library, and then the exon and adjacent intron regions (50bp) of all human genes were captured by probe hybridization and enriched. The enriched target gene fragments were sequenced by a next-generation high throughput sequencer (Illumina). NextGene V2.3.4 software was used to compare the sequencing data with the human genome hg19 reference sequence provided by the UCSC database, and the coverage of target regions and sequencing quality were evaluated.

Results

Case 1

An 11-month female infant presented with recurrent corneal and oral ulcers that had persisted for 6 months. The infant developed corneal ulcers the size of rice grains in both eyes and oral ulcers successively at the age of 5 months. The local hospital treated her for "traumatic ulcers," but she showed no significant improvement. The sizes of corneal and oral ulcers increased gradually.

The patient's family had visited several major hospitals for the corneal ulcers. Traditional treatments such as tobramycin, levofloxacin, calf blood deproteinized extract eye gel, ganciclovir eye gel, and interferon eye drops were applied successively with no obvious improvement. The corneal ulcer gradually got worse, as did her oral ulcers. For the oral ulcer, symptomatic treatments were applied with no obvious improvement. The oral bacterial culture results found *Staphylococcus aureus* and *Streptococcus salivarius*,

10.3389/fgene.2023.1139161

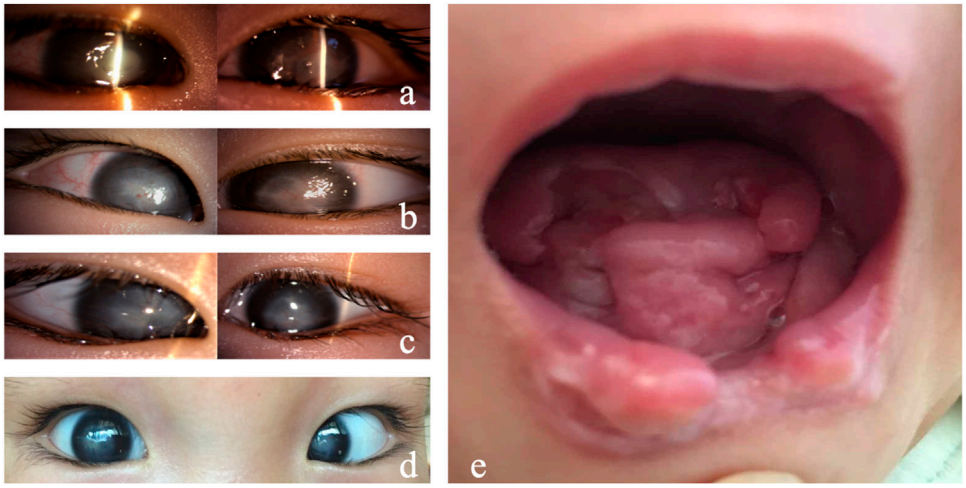

FIGURE 1
Clinical manifestations of Case 1. **(A)** Both eyes showed conjunctival hyperemia, corneal ulceration, deep stromal infiltration, borderline ambiguity, and opacity. **(B)** On day 7, the corneal ulcers in both eyes gradually healed, and the conjunctival congestion was reduced. **(C)** On day 14, the corneal ulcers healed in both eyes. **(D)** On day 40, conjunctival hyperemia (–) occurred in both eyes, the corneal epithelium was intact, and corneal leukoplakia formed. **(E)** Tongue and lip defects and oral ulcers.

which were susceptible to benzoxicillin. The systemic use of linezolid and ertapenem to control the recurrent infection received little response.

When the patient was admitted to our hospital, the ophthalmic examination found conjunctival congestion and corneal ulcers in both eyes. The corneal ulcers infiltrated the deep stromal layer with an unclear borderline (Figure 1A). The chronic oral ulcer had caused profound defects of tongue and lip (Figure 1E). The medical history showed that the patient had no perspiration after birth, insensitivity to pain, developmental delay, and no obvious joint deformity. Based on the systemic clinical manifestations, we considered that the child had HSAN, so we conducted genetic testing on the child. The report showed a mutation of *PRDM12*. The patient carried pathogenic compound heterozygous variations of c.682+1G > A and c.502C > T (p.Arg168Cys), which were inherited from her father and mother, respectively. The ACMG criteria showed c.682+1G > A is pathogenic, and c.502C > T (p.Arg168Cys) is of uncertain significance. Her parents were not consanguineous in marriage. The diagnosis was confirmed as PRDM12 mutation-related CIP.

As for the treatment, considering the infant with unknown etiology, weak general conditions, fever, and no sweat, surgery is not optimal as the anesthesia is risky. In addition, the penetrating keratoplasty requires intense care after surgery, which could be difficult as she perceives no pain. A strong eye rubbing or a delayed blink could lead to graft damage. After a comprehensive systemic status assessment, we used natamycin eye drops and gatifloxacin eye gel for both eyes and continued anti-infection symptomatic treatment for the whole body. The corneal ulcer improved significantly 2 days later. The oral secretion culture results showed *Candida guilliermondii* infection. After 7 days of ocular antifungal treatment, the corneal ulcer was limited, and conjunctival congestion was relieved. Systemic antifungal treatment with fluconazole injection was added. The patient's condition gradually stabilized, and the fever was controlled (Figure 1B). After 2 weeks, systemic medication was gradually stopped, and the corneal and oral ulcers gradually healed (Figure 1C). Thereafter, the systemic medical treatment was symptomatic, and the eyes were regularly moisturized with preservative-free, artificial tears (0.3% sodium hyaluronate) eye drops. The cornea remained stable 4 weeks after discharge (Figure 1D).

FIGURE 2
Clinical manifestations of Case 2. **(A,B)** Conjunctival hyperemia, corneal ulcer; **(C)** tongue and lip defects and oral ulcers.

TABLE 1 Review of cases with *PRDM12*-related pain insensitivity.

Authors, years	Number of cases	Sex	Age at presentation	Clinical manifestations	Therapy	Outcome
Chen et al. (2015)	21	Male: 13 Female: 8	30–40 years	Insensitivity to pain and temperature, self-mutilation behavior, mutilation of tongue and lips, mutilation of distal phalanges, loss of corneal reflexes, corneal scarring, recurrent infections, normal intellect	-	-
Zhang et al. (2016)	5	Male: 4 Female: 1	23–57 years	Insensitivity to pain, self-mutilation behavior, mutilation of tongue and lips, mutilation of distal phalanges, loss of corneal reflexes, decreased tear secretion, corneal abrasions, recurrent infections, normal intellect	-	Two individuals had no useful vision in one eye, and in one, multiple corneal grafts had failed
Saini et al. (2017)	1	Male	2 years	Insensitivity to pain and temperature, self-mutilation behavior, mutilation of tongue and lips, reduced blink, global development delay, normal sweating, and tear overflow	-	-
Elhennawy et al. (2017)	1	Male	8 months	Insensitivity to pain and temperature, self-mutilation behavior, loss of corneal reflexes, recurrent infections, reduced sweat, and tear production. Oral manifestations: premature loss of teeth associated with dental traumata and self-mutilation, severe soft tissue injuries, dental caries and submucosal abscesses, hypomineralization of primary teeth, and mandibular osteomyelitis	Anti-infection treatment	-
Moss et al. (2018)	5	Male: 4 Female: 1	1–4 years	Self-mutilation behavior, global developmental delay, skin excoriations on nose, forehead, medial aspect of eyes, and chin (MiTES)	-	-
Gaur et al. (2018)	1	Male	1 year	Insensitivity to pain, self-mutilation behavior, mutilation of tongue and lips, mutilation of distal phalanges, loss of corneal sensation, corneal scarring, normal intellect	Corneal transplant	-
Navya et al. (2019)	1	Male	1 year	Insensitivity to pain, self-mutilation behavior, mutilation of tongue and lips, mutilation of distal phalanges, recurrent infections, global development delay	Systemic anti-infection treatment, limit biting	Healing of lesions in the thumb and oral mucosa
Kaur et al. (2020)	1	Male	1 year	Insensitivity to pain and temperature, self-mutilation behavior, mutilation of tongue and lips, corneal opacification, decreased lacrimation	Permanent left blepharoplasty, right corneal transplantation	-
Suthar et al. (2022)	2	Male: 1 Female: 1	6 months	Insensitivity to pain and temperature, self-mutilation behavior, persistent rhinitis, mutilation of tongue and lips, corneal ulcer, global development delay	-	-
Kusumesh et al. (2022)	1	Female	2 years	Insensitivity to pain and temperature, self-mutilation behavior, mutilation of distal phalanges, corneal opacification, loss of sweating and tears, abnormal tooth development	-	-
Elsana et al. (2022)	3	Male: 2 Female: 1	3–11 years	reduced tear production, loss of corneal reflexes, disappearance of corneal blink reflex, corneal opacification, corneal ulcer, corneal scarring	Lateral tarsorrhaphy, corneal transplant	-
Index children	2	Female: 2	1–2 years	Insensitivity to pain, self-mutilation behavior, mutilation of tongue and lips, loss of corneal reflexes, corneal opacification, corneal ulcer, decreased lacrimation, recurrent infections, global developmental delay	Systemic anti-infection treatment	Case 1 can now live normally without affecting vision

10.3389/fgene.2023.1139161

TABLE 2 Clinical features of patients diagnosed with *PRDM12* mutations.

Authors, years	Number of cases	Sex	Age at presentation	Clinical manifestation													
				Insensitivity to pain	Self-mutilation behavior	Mutilation of tongue and lips	Mid-facial lesion	Mutilation of distal phalanges	No sweating	Recurrent infections	Ocular manifestations						Global developmental delay
											Reduced tear production	Global developmental delay	Disappeared corneal reflexes	Corneal opacity	Corneal ulcer	Corneal scarring	
Zhang et al. (2016)	5	Male: 4 Female: 1	23–57 years	5	5	3	-	3	1	5	5	-	5	-	-	-	-
Saini et al. (2017)	1	Male	2 years	1	1	1	-	-	-	-	-	1	-	-	-	-	1
Elhennawy et al. (2017)	1	Male	8 months	1	1	1	-	-	1	1	-	-	1	-	-	-	-
Moss et al. (2018)	4	Male: 4	1–4 years	-	4	-	4	-	-	-	-	-	-	-	-	-	-
Gaur et al. (2018)	1	Male	1 year	1	1	1	-	1	-	-	-	1	-	-	-	1	-
Navya et al. (2019)	1	Male	1 year	1	1	1	-	1	-	1	-	-	-	-	-	-	-
Kaur et al. (2020)	1	Male	1 year	1	1	1	-	-	-	1	1	1		1	-	-	-
Suthar et al. (2022)	2	Male: 1 Female: 1	6 months	1	1	1	-	-	-	-	-	-	-	-	1	-	2
Kusumesh et al. (2022)	1	Female	2 years	1	1	-	1	1	-	1	1	-	1	1	-	-	-
Elsana et al. (2022)	3	Male: 2 Female: 1	3–11 years	-	-	-	-	-	-	-	3	2	-	2.5	3	-	-
Index children	2	Female: 2	1–2 years	2	2	2	-	-	2	2	1	1	-	1	1	-	2

10.3389/fgene.2023.1139161

TABLE 3 Mutation sites identified in a patient with a *PRDM12* gene mutation.

Authors, years	Number of cases	Sex	Age at presentation	Mutation sites in the *PRDM12* gene
Zhang et al. (2016)	5	Male:4 Female: 1	23–57 years	-
Saini et al. (2017)	1	Male	2 years	homozygous mutation c.224–2A > G in the *PRDM12* gene
Elhennawy et al. (2017)	1	Male	8 months	homozygous mutation c.516G>C (p. Glu172Asp) in the *PRDM12* gene
Moss et al. (2018)	4	Male: 4	1–4 years	heterozygous for a partial gene deletion of *PRDM12* involving at least exon 5; heterozygous expansion of the *PRDM12* polyalanine tract to 18/17 alanine residues
Gaur et al. (2018)	1	Male	1 year	homozygous mutation
Navya et al. (2019)	1	Male	1 year	mutation in exon 5 of *PRDM12* gene
Kaur et al. (2020)	1	Male	1 year	a heterozygous, missense variation in exon 2 of *PRDM12* gene (chr9:g.133542114G>C) that results in the amino acid substitution of arginine for glycine at codon 115 (p.Gly115Arg) and another heterozygous, missense variation in exon 3 of *PRDM12* gene (chr9:g.133543652C>A; Depth: 63) that results in the amino acid substitution of lysine for asparagine at codon 174 (p.Asn174Lys)
Suthar et al. (2022)	2	Male: 1 Female: 1	6 months	Female: a homozygous missense variant (c.451G>A; p.Asp151Asn)
Kusumesh et al. (2022)	1	Female	2 years	homozygous mutation in the *PRDM12* gene on chromosome 9q34
Elsana et al. (2022)	3	Male: 2 Female: 1	3–11 years	homozygous for the *PRDM12* variant: Chr9:133543585 (GRCh37/hg19); c.455C>A (p.Ala152Asp)
Index children	2	Female: 2	1–2 years	heterozygous variations of c.682+1G > A and c.502C > T (p.Arg168Cys)

10.3389/fgene.2023.1139161

Case 2

A 15-month female infant presented with corneal opacity in both eyes for 5 months. She came to the hospital with a body temperature of 38.5 °C. The ophthalmic examination showed that the corneal reflex disappeared, tear secretion decreased, conjunctival congestion was present in both eyes, and both eyes showed corneal opacity (Figure 2A,B). Her tongue and lip were defective (Figure 2C). A purulent mossy attachment was noted around the oral cavity, on the oral mucosa and on the tongue surface. She was born at full term. The parents recalled little blinking after her birth. Eight months after birth, the infant manifested continuously sucking and biting the lower lip with no obvious incentives. Large mucosal ulcers were also noticed in the oral cavity. Oral anti-infection treatment and behavioral interventions such as sticking the lower lip with medical tape or usage of a pacifier to correct the habit of biting the lower lip were not effective. At the age of 10 months, her right eye was noticed to be cloudy, and her motor and intellectual development were delayed. Their parents were not consanguineous in marriage. There was no history of genetic family disease. Confirmation of the PRDM12 mutation in the patient was made through telephone follow-up with her family members. The type of mutation is not available, and co-segregation analysis has not been performed in this family. The diagnosis was confirmed as PRDM12 mutation-related CIP.

Literature review

A total of 11 articles that had reported the *PRDM12* mutation-related disease were retrieved, including 20 cases with detailed case reports. Together with our cases, 22 cases were included. The demographic characteristics and ocular, oral, facial, and skeletal manifestations of the patients were summarized and analyzed. We summarized the clinical manifestations of all patients with *PRDM12* mutations reported so far in Table 1 and summarized the patients with detailed disease descriptions in Table 2. All variations of *PRDM12* are summarized in Table 3.

Among the 22 patients, there were 16 males (72.7%) and 6 females (27.3%). The age of onset ranged from 6 months to 57 years. The prevalence of clinic manifestation was 14 cases with insensitivity to pain (63.6%), 19 cases with self-mutilation behaviors (86.4%), 11 cases with tongue and lip defects (50%), 5 cases with a mid-facial lesion (22.7%), 6 cases with distal phalanx injury (27.3%), 11 cases of recurrent infection (50%), 3 cases (13.6%) with anhidrosis, and 5 cases (22.7%) with global developmental delay. The prevalence of ocular symptoms was 11 cases (50%) with reduced tear secretion, 6 cases (27.3%) with decreased corneal sensitivity, 7 cases (31.8%) with disappeared corneal reflexes, 5.5 cases (25%, 0.5 indicated a single eye) with corneal opacity, 5 cases (22.7%) with corneal ulceration, and 1 case (4.5%) with a corneal scar.

Discussion

CIP3 is a rare inherited pain loss disorder with various clinical manifestations. As the symptoms varied, including insensitivity to pain, self-mutilation behaviors, recurrent infections, and self-injury-induced oral and corneal ulcers, doctors tend to only notice a single symptom and overlook the overall presentation, resulting in misdiagnosis and missed diagnosis.

Genetic analysis, as the only means of genetic disorder diagnosis, can accurately locate the mutated gene, identify the type of disease, and give clues in the prenatal examination. Studies have shown that the number of newborns diagnosed with HSAN-III has decreased significantly over the past decade with the help of prenatal testing (Couzin-Frankel, 2010). Fetuses with *PRDM12* mutations may also be identified prenatally by such means. A comprehensive understanding of the *PRDM12* mutation-related disease could be helpful for early diagnosis and treatment (Imhof et al., 2020). No association was found among the *PRDM12* mutation sites in the 22 reported patients. However, the mutation may affect the structure of the protein and affect the distribution of pain perception. The aim of this study is to systematically review *PRDM12* mutation-related CIP based on our two patients and the 20 cases reported in the literature. The overall findings of our study demonstrated that CIP due to *PRDM12* mutations usually resulted in pain insensitivity, facial and limb defects, and recurrent infections, which significantly damaged children's growth.

Insensitivity to pain and other pain-related features

Pain insensitivity is one of the most distinctive features of all diseases caused by *PRDM12* mutations. The insensitivity to pain caused by *PRDM12* mutation leads to the defect of the nociceptors during embryonic development (Chen et al., 2015; Landy et al., 2021; Rienzo et al., 2021). With the inability to feel pain, patients often unconsciously show some self-mutilation behaviors. Self-inflicted injuries are more vulnerable to infection and decreased immunity. Recurring infections are the outcome. This causes great difficulties for parents in looking after their children. Self-mutilation behaviors cause defects in various body parts at an early age, which can have lifelong effects on life and appearance. Treatment was limited to plastic surgery, such as functional alginate dressings (Jones et al., 2006), autologous skin grafts (Hu et al., 2015), and cell-based wound healing therapy (Rodrigues et al., 2019). Another difficulty in treating CIP3 is recurrent infection. Because the patient cannot perceive the injury, the healing process may be accompanied by new wounds.

Ophthalmological complications

Patients with *PRDM12* mutations present with reduced tear secretion, corneal abrasions, and loss of corneal reflexes, resulting in keratitis and corneal scarring (Chen et al., 2015; Zhang et al., 2016). We found that almost every patient had some degree of corneal injury, indicating that the corneal symptoms deserve attention.

There is no clear report in the literature on why patients with *PRDM12* mutations have different degrees of eye damage, and we expect to explore this next. Because HSAN autosomal recessive patients often develop the disease at an early age, before irreversible damage is caused, eye symptoms tend to give us a better warning (Schwartzlow and Kazamel, 2019). For example, patients with dry

eye signs on the ocular surface, corneal opacity or decreased corneal sensitivity, if further aggravated, such as corneal opacity or increased secretions, should seek medical attention in time to minimize the damage.

As shown in Table 1, when selecting the treatment plan, except for the two patients reported by us, conservative treatment was adopted, and most of the patients with detailed reports of their disease were controlled through corneal transplantation and other operations. In Case 1, penetrating keratoplasty was considered to repair corneal ulcers during a visit to another hospital. Yagev et al. (1999) reported that a child with binocular corneal ulcers caused by painless syndrome was treated with penetrating keratoplasty under good overall condition, but the postoperative effect was poor. Corneal transplantation is a relatively complicated ophthalmic operation that imposes high requirements on patients' general condition and postoperative nursing (Tan et al., 2012). CIP patients tend to have poor systemic status due to recurrent infections. Moreover, uncontrolled eye rubbing and eye damage will inevitably occur after surgery, resulting in artificial transplant failure. Therefore, after carefully considering the circumstances and full communication with the parents, we adopted conservative treatment. The patient's vision recovered well, and her daily life was not affected. For Case 1, controlling fever and infection in the early stage is the focus of treatment. When the physician could not find the cause, we started from the local symptoms of the eye and adopted antifungal treatment, which not only avoided the corneal perforation but also effectively controlled the systemic condition of the child.

Others

CIP3 can also lead to global developmental delays. Although the proportion is relatively low, it has a great impact on the growth of children. If the doctor suspects this disease when treating the patients, parents should be reminded to assess the intelligence of their child and avoid missed diagnoses.

MiTES, meanwhile, could be an early warning sign of *PRDM12*-CIP. MiTES patients often present with pathological itching in the mid-face, an inability to manage the damaged area due to pain insensitivity, and mid-facial lesions after persistent scratching (Moss et al., 2018). Although there is no other evidence of damage to *PRDM12*-CIP in the disease profile of MiTES patients, four of five had mutations in *PRDM12*. MiTES, therefore, should be considered if a child is observed unconsciously scratching the midface area. Medical attention is needed to avoid the possibility of MiTES' progression to *PRDM12*-CIP. Facial defects often cause the appearance of patients with terror, and their normal growth and integration into society cause great difficulties. Attention should also be paid to the mental health status of this group (McCarron et al., 2021).

Conclusion

Patients with a *PRDM12* gene mutation benefit from early detection and diagnosis. Early intervention can greatly control the progression of the disease so that the appearance and vision of the patients will not be affected to the greatest extent. Secondly, different treatment measures should be implemented according to age stages and the severity of the disease, and symptomatic treatment against infection should always be maintained. Finally, the patient's family should attend to the patient's psychological problems.

Data availability statement

The original contributions presented in the study are included in the article/Supplementary material; further inquiries can be directed to the corresponding authors.

Ethics statement

Ethical review and approval was not required for the study on human participants in accordance with the local legislation and institutional requirements. Written informed consent was obtained from the minor(s)' legal guardian/next of kin for the publication of any potentially identifiable images or data included in this article.

Author contributions

Data curation: HY; writing (original draft): HY, JW, and JC; writing (review and editing): all authors.

Funding

This work was supported by the Natural Science Foundation of China (82070921).

Acknowledgments

We thank the families for their help.

Conflict of interest

The authors declare that the research was conducted in the absence of any commercial or financial relationships that could be construed as a potential conflict of interest.

Publisher's note

References

Chen, Y. C., Auer-Grumbach, M., Matsukawa, S., Zitzelsberger, M., Themistocleous, A. C., Strom, T. M., et al. (2015). Transcriptional regulator PRDM12 is essential for human pain perception. *Nat. Genet.* 47, 803–808. doi:10.1038/ng.3308

Couzin-Frankel, J. (2010). Chasing a disease to the vanishing point. *Science* 328, 298–300. doi:10.1126/science.328.5976.298

Desiderio, S., Vermeiren, S., Van Campenhout, C., Kricha, S., Malki, E., Richts, S., et al. (2019). Prdm12 directs nociceptive sensory neuron development by regulating the expression of the NGF receptor TrkA. *Cell Rep.* 26, 3522–3536. doi:10.1016/j.celrep.2019.02.097

Di Zazzo, E., De Rosa, C., Abbondanza, C., and Moncharmont, B. (2013). PRDM proteins: Molecular mechanisms in signal transduction and transcriptional regulation. *Biology* 2, 107–141. doi:10.3390/biology2010107

Drissi, I., Woods, W. A., and Woods, C. G. (2020). Understanding the genetic basis of congenital insensitivity to pain. *Br. Med. Bull.* 133, 65–78. doi:10.1093/bmb/ldaa003

Elhennawy, K., Reda, S., Finke, C., Graul-Neumann, L., Jost-Brinkmann, P. G., and Bartzela, T. (2017). Oral manifestations, dental management, and a rare homozygous mutation of the PRDM12 gene in a boy with hereditary sensory and autonomic neuropathy type VIII: A case report and review of the literature. *J. Med. case Rep.* 11, 233. doi:10.1186/s13256-017-1387-z

Elsana, B., Imtirat, A., Yagev, R., Gradstein, L., Majdalani, P., Iny, O., et al. (2022). Ocular manifestations among patients with congenital insensitivity to pain due to variants in PRDM12 and SCN9A genes. *Am. J. Med. Genet. Part A* 188, 3463–3468. doi:10.1002/ajmg.a.62968

Gaur, N., Meel, R., Anjum, S., and Singh, P. (2018). Hereditary sensory and autonomic neuropathy in a male child: 'The other side of not feeling pain'. *BMJ case Rep.* 2018, bcr2018226873. doi:10.1136/bcr-2018-226873

Grover, R., and Sanders, R. (1998). Plastic surgery. *BMJ* 317, 397–400. doi:10.1136/bmj.317.7155.397

Hu, Z. C., Chen, D., Guo, D., Liang, Y. Y., Zhang, J., Zhu, J. Y., et al. (2015). Randomized clinical trial of autologous skin cell suspension combined with skin grafting for chronic wounds. *Br. J. Surg.* 102, e117–e123. doi:10.1002/bjs.9688

Imhof, S., Kokotović, T., and Nagy, V. (2020). PRDM12: New opportunity in pain research. *Trends Mol. Med.* 26 (10), 895–897. doi:10.1016/j.molmed.2020.07.007

Jones, V., Grey, J. E., and Harding, K. G. (2006). Wound dressings. *BMJ* 332, 777–780. doi:10.1136/bmj.332.7544.777

Kaur, J., Singanamalla, B., Suresh, R. G., and Saini, A. G. (2020). Insensitivity to pain, self-mutilation, and neuropathy associated with PRDM12. *Pediatr. Neurol.* 110, 95–96. doi:10.1016/j.pediatrneurol.2020.03.007

Kusumesh, R., Ambastha, A., Singh, V., and Singh, A. (2022). Hereditary sensory and autonomic neuropathy type VIII: Congenital insensitivity to pain with anhidrosis. *Indian dermatology online J.* 13, 257–258. doi:10.4103/idoj.idoj_427_21

Landy, M. A., Goyal, M., Casey, K. M., Liu, C., and Lai, H. C. (2021). Loss of Prdm12 during development, but not in mature nociceptors, causes defects in pain sensation. *Cell Rep.* 34, 108913. doi:10.1016/j.celrep.2021.108913

Lischka, A., Lassuthova, P., Çakar, A., Record, C. J., Van Lent, J., Baets, J., et al. (2022). Genetic pain loss disorders. *Nat. Rev. Dis. Prim.* 8 (1), 41. doi:10.1038/s41572-022-00365-7

McCarron, R. M., Shapiro, B., Rawles, J., and Luo, J. (2021). Depression. *Ann. Intern. Med.* 174, ITC65–ITC80. doi:10.7326/AITC202105180

Moss, C., Srinivas, S. M., Sarveswaran, N., Nahorski, M., Gowda, V. K., Browne, F. M., et al. (2018). Midface toddler excoriation syndrome (MiTES) can be caused by autosomal recessive biallelic mutations in a gene for congenital insensitivity to pain, PRDM12. *Br. J. dermatology* 179, 1135–1140. doi:10.1111/bjd.16893

Nahorski, M. S., Chen, Y. C., and Woods, C. G. (2015). New mendelian disorders of painlessness. *Trends Neurosci.* 38, 712–724. doi:10.1016/j.tins.2015.08.010

Navya, M. K., Pramod, G. V., Sujatha, G. P., and Ashok, L. (2019). Congenital insensitivity to pain in a 1-year-old boy. *J. Indian Soc. Pedod. Prev. Dent.* 37, 308–310. doi:10.4103/JISPPD.JISPPD_340_18

Rienzo, M., Di Zazzo, E., Casamassimi, A., Gazzerro, P., Perini, G., Bifulco, M., et al. (2021). PRDM12 in health and diseases. *Int. J. Mol. Sci.* 22, 12030. doi:10.3390/ijms222112030

Rodrigues, M., Kosaric, N., Bonham, C. A., and Gurtner, G. C. (2019). Wound healing: A cellular perspective. *Physiol. Rev.* 99, 665–706. doi:10.1152/physrev.00067.2017

Rotthier, A., Baets, J., Timmerman, V., and Janssens, K. (2012). Mechanisms of disease in hereditary sensory and autonomic neuropathies. *Nat. Rev. Neurol.* 8, 73–85. doi:10.1038/nrneurol.2011.227

Saini, A. G., Padmanabh, H., Sahu, J. K., Kurth, I., Voigt, M., and Singhi, P. (2017). Hereditary sensory polyneuropathy, pain insensitivity and global developmental delay due to novel mutation in PRDM12 gene. *Indian J. Pediatr.* 84, 332–333. doi:10.1007/s12098-016-2284-y

Schwartzlow, C., and Kazamel, M. (2019). Hereditary sensory and autonomic neuropathies: Adding more to the classification. *Curr. neurology Neurosci. Rep.* 19, 52. doi:10.1007/s11910-019-0974-3

Suthar, R., Sharawat, I. K., Eggermann, K., Padmanabha, H., Saini, A. G., Bharti, B., et al. (2022). Hereditary sensory and autonomic neuropathy: A case series of six children. *Neurol. India* 70, 231–237. doi:10.4103/0028-3886.338691

Tan, D. T., Dart, J. K., Holland, E. J., and Kinoshita, S. (2012). Corneal transplantation. *Lancet (London, Engl.)* 379 (9827), 1749–1761. doi:10.1016/S0140-6736(12)60437-1

Yagev, R., Levy, J., Shorer, Z., and Lifshitz, T. (1999). Congenital insensitivity to pain with anhidrosis: Ocular and systemic manifestations. *Am. J. Ophthalmol.* 127, 322–326. doi:10.1016/s0002-9394(98)00370-5

Zhang, S., Malik Sharif, S., Chen, Y. C., Valente, E. M., Ahmed, M., Sheridan, E., et al. (2016). Clinical features for diagnosis and management of patients with PRDM12 congenital insensitivity to pain. *J. Med. Genet.* 53, 533–535. doi:10.1136/jmedgenet-2015-103646

frontiers | Frontiers in Genetics

TYPE Review
PUBLISHED 12 April 2023
DOI 10.3389/fgene.2023.1130106

OPEN ACCESS

EDITED BY
Jordi Pérez-Tur,
Spanish National Research Council (CSIC), Spain

REVIEWED BY
Yeunjoo E. Song,
Case Western Reserve University, United States
Andrew DeWan,
Yale University, United States

*CORRESPONDENCE
Xiaoyi Raymond Gao,
raymond.gao@osumc.edu

RECEIVED 22 December 2022
ACCEPTED 05 April 2023
PUBLISHED 12 April 2023

CITATION
Gao XR, Chiariglione M, Choquet H and Arch AJ (2023), 10 Years of GWAS in intraocular pressure.
Front. Genet. 14:1130106.
doi: 10.3389/fgene.2023.1130106

10 Years of GWAS in intraocular pressure

Xiaoyi Raymond Gao[1,2,3]*, Marion Chiariglione[1], Hélène Choquet[4] and Alexander J. Arch[1]

[1]Department of Ophthalmology and Visual Sciences, The Ohio State University, Columbus, OH, United States, [2]Department of Biomedical Informatics, The Ohio State University, Columbus, OH, United States, [3]Division of Human Genetics, The Ohio State University, Columbus, OH, United States, [4]Division of Research, Kaiser Permanente Northern California, Oakland, CA, United States

Intraocular pressure (IOP) is the only modifiable risk factor for glaucoma, the leading cause of irreversible blindness worldwide. In this review, we summarize the findings of genome-wide association studies (GWASs) of IOP published in the past 10 years and prior to December 2022. Over 190 genetic loci and candidate genes associated with IOP have been uncovered through GWASs, although most of these studies were conducted in subjects of European and Asian ancestries. We also discuss how these common variants have been used to derive polygenic risk scores for predicting IOP and glaucoma, and to infer causal relationship with other traits and conditions through Mendelian randomization. Additionally, we summarize the findings from a recent large-scale exome-wide association study (ExWAS) that identified rare variants associated with IOP in 40 novel genes, six of which are drug targets for clinical treatment or are being evaluated in clinical trials. Finally, we discuss the need for future genetic studies of IOP to include individuals from understudied populations, including Latinos and Africans, in order to fully characterize the genetic architecture of IOP.

KEYWORDS

intraocular pressure, GWAS, ExWAS, polygenic risk score, Mendelian randomization, underrepresented population

Introduction

The first genome-wide association study (GWAS) of intraocular pressure (IOP) was published in 2012 (van Koolwijk et al., 2012). Since then, numerous common genetic variants associated with IOP have been discovered (Hysi et al., 2014; Springelkamp et al., 2014; Choquet et al., 2017; Springelkamp et al., 2017; Gao et al., 2018; Khawaja et al., 2018; MacGregor et al., 2018). Recently, a study using whole-exome sequencing data on large-scale biobanks has also led to significant new gene discoveries in the genetic architecture of IOP, demonstrating the important contribution of rare variants to this glaucoma endophenotype (Gao et al., 2022). On the tenth anniversary of the first IOP GWAS, it is time to reflect on the progress that has been made in this field and to consider the future direction of the genetics of IOP.

IOP is the amount of fluid pressure in the eye which is mainly determined by the balance between aqueous humor production and drainage (Civan and Macknight, 2004; Machiele et al., 2022). Elevated IOP is a major risk factor for primary open-angle glaucoma (POAG), the most common form of glaucoma that affects around 90% of glaucoma patients (Lang, 2007). Currently, IOP is the only modifiable risk factor for glaucoma, and lowering IOP helps to prevent the onset and delay the progression of POAG (Collaborative Normal-Tension Glaucoma Study Group, 1998; Heijl et al., 2002; Kass et al., 2002). IOP can be influenced by

many factors, such as time of the day (Qassim et al., 2020a), measurement techniques, such as the Goldmann applanation tonometer and the ocular response analyzer (Martinez-de-la-Casa et al., 2006), age and ethnic background (Klein et al., 1992; Wu and Leske, 1997; Baek et al., 2015), and genetics. Studies have found that the heritability of IOP ranges from 0.35 to 0.67, depending on the study design (Klein et al., 2004; Chang et al., 2005; van Koolwijk et al., 2007; Carbonaro et al., 2009; Zheng et al., 2009; Sanfilippo et al., 2010; Asefa et al., 2019). Identifying genetic factors that contribute to IOP aid in uncovering the biological mechanisms regulating this trait (Ojha et al., 2013; Xu et al., 2021), which provides new management avenues for IOP and POAG.

GWASs have identified over 190 genetic loci associated with IOP (Choquet et al., 2017; Gao et al., 2018; Khawaja et al., 2018; MacGregor et al., 2018), demonstrating the contribution of common genetic variants to this trait. Additionally, these studies have shown that there is a strong bivariate genetic correlation between IOP and POAG ranging from 0.49 to 0.71 (Aschard et al., 2017; MacGregor et al., 2018) and a significant polygenic overlap between these two traits (Hysi et al., 2014; Khawaja et al., 2018). While numerous loci have been associated with IOP, these common variants typically have small effect sizes, contrary to those seen in rare variants, which can have large effect sizes (Gao et al., 2018; Gao et al., 2022). The role of rare genetic variants in IOP was recently reported in a large-scale exome-wide association study (ExWAS) that identified 40 novel genes associated with IOP (Gao et al., 2022).

Over the last 10 years, GWASs and ExWAS have provided strong evidence that IOP is a polygenic trait and a powerful endophenotype for POAG. These studies have also revealed valuable biological insights, pleiotropic effects, and potential drug targets associated with IOP genetic loci. The results of these studies have been applied to the development of polygenic risk scores (PRSs), which could potentially be used to stratify and screen for POAG risk in a population using IOP information (Khawaja et al., 2018; MacGregor et al., 2018; Gao et al., 2019; Qassim et al., 2020b). Moreover, the results of these studies have been applied to the development of genetic instruments that may be used in Mendelian randomization (MR) studies to better understand the nature of the relationships between eye traits and conditions (Han et al., 2020; Hysi et al., 2020; Choquet et al., 2022). In this review, we summarize these findings and discuss the potential future of GWASs in the study of IOP.

GWAS and ExWAS

GWASs have revolutionized the field of complex diseases and traits genetics over the past 17 years (Visscher et al., 2017; Tam et al., 2019). They involve examining the association between diseases or traits and hundreds of thousands (Klein et al., 2005) to millions of densely spaced single nucleotide polymorphisms (SNPs) (Gao and Edwards, 2011). These studies do not require any prior biological knowledge and are therefore an agnostic method for identifying the genetic effects of complex human diseases and traits. They are based on the assumption that densely genotyped common variants (minor allele frequency [MAF] $\geq$ 1%) will have sufficient statistical power to detect associations. This approach has been successful in numerous cases for mapping small genomic regions to diseases and traits (Welter et al., 2014). Many of these regions would not have been considered good candidates for targeted genotyping based on biological knowledge or previous evidence of linkage. Most of the findings from GWASs are collected in the GWAS Catalog, a database of all published GWASs maintained by the National Human Genome Research Institute (NHGRI) and the European Bioinformatics Institute (EBMI-EBI) (MacArthur et al., 2017). A standardized significance threshold of a p-value less than 5×10^{-8} has been adopted by the genetics community as the genome-wide level of significance, which is based on the assumption of one million independent pieces of genetic information in the human genome (Risch and Merikangas, 1996; Pe'er et al., 2008).

Each individual GWAS can have a limited sample size, which affects its statistical power. Additionally, genetic association signals that are identified need to be independently replicated in order to be considered reliable. To overcome these limitations, researchers often use genome-wide association meta-analysis (Willer et al., 2010; McGuire et al., 2021), which combines the results of multiple GWAS studies, and genotype imputation (Li and Abecasis, 2006; Marchini et al., 2007), which can infer ungenotyped variants from known data. Together, these methods can provide a more comprehensive and robust analysis of the genetic basis of a particular trait or disease.

More recently, other genome-wide studies, including whole-exome and whole-genome sequencing studies have been conducted in parallel of GWASs to assess rare variants associations and their roles in the genetic causes of diseases/traits. ExWAS employs whole-exome sequencing data that focuses on specific parts of the genome that encodes proteins, called exons, and allows for changes within such regions to be identified and analyzed. To address the relatively low statistical power issues in rare-variant analysis, researchers have designed many collapsing or gene-based methods (Li and Leal, 2008; Madsen and Browning, 2009; Wu et al., 2010; Wu et al., 2011; Lee et al., 2012a; Lee et al., 2012b; Zhou et al., 2018; Zhou et al., 2020).

Study inclusion criteria

To identify previously published IOP GWAS and ExWAS papers, we queried two websites: GWAS Catalog and PubMed, using the keywords "intraocular pressure" and "exome intraocular pressure," respectively. We found 28 studies in the GWAS Catalog and three in PubMed. We then manually curated the search results to focus on studies with IOP as the main phenotype. Finally, we excluded studies that did not report novel significant IOP loci. As a result, Table 1 includes the 14 studies (GWAS and ExWAS) that were selected based on these two criteria: 1) IOP as the target phenotype of GWAS analyses; and 2) reported novel findings being genome-wide or exome-wide significant, either single variant ($p < 5.0 \times 10^{-8}$) or gene-based ($p < 2.5 \times 10^{-6}$), over the past 10 years. One study (Ozel et al., 2014) that reported borderline genome-wide significance ($p = 8 \times 10^{-8}$) was included in Table 1 as well. These criteria excluded two IOP studies (Chen et al., 2015; Chakraborty et al., 2021) that reported suggestively significant findings ($P \sim 5.0 \times 10^{-5}$ or $P \sim 5.0 \times 10^{-6}$).

TABLE 1 Genome-wide and exome-wide association studies of intraocular pressure in the last 10 years.

Study name	Year	Novel loci	Sample size	Population	Total association count	Replication sample size	Number of single-variants tested
GWAS							
van Koolwijk et al.	2012	2	11,972	European	2	7,482	2.5 Million
Blue Mountains Eye Study (BMES);Wellcome Trust Case Control Consortium 2 (WTCCC2)	2013	1	2,175	European	1	4,866	6.2 Million
Ozel et al.	2014	1	6,000	European	1	-	2.54 Million
Nag et al.	2014	1	2,774	European	1	22,789	1.87 Million
Hysi et al.	2014	4	35,296	European (*n* = 27,558)	8	99,844	-
				Asian (*n* = 7,738)			
Springelkamp et al.	2015	1	8,105	European	1	7,471	1000 Genomes phase 1 imputation[a]
Springelkamp et al.	2017	1	37,930	European (*n* = 29,578)	10	47,833	8 Million
				Asian (*n* = 8,352)			
Choquet et al.	2017	40	69,756	European (*n* = 56,819)	47	Springelkamp et al. (2017) summary statistics, 37,930	15 Million
				Latino (*n* = 5,748)			
				Asian (*n* = 5,119)			
				African (*n* = 2,070)			
Gao et al.	2018	145[b]/103[c]	115,486	European	191	Springelkamp et al. (2017) summary statistics, 37,930	11.9 Million
Khawaja et al.	2018	68	139,555	European	112	6,595 (EPIC-Norfolk)	9.1 Million
						29,578 (IGGC)	
MacGregor et al.	2018	85	103,914 (UKB) and 29,578 (IGGC)	European	106	-	40 Million
Huang et al.	2019	17	8,552	Chinese	21	2,981	1000 Genomes phase 1 imputation[a]
Simcoe et al.	2020	3	102,407	European	3	6,599 (EPIC-Norfolk)	590,896
						331,682 (UKB)	
ExWAS							
Gao et al.	2022	40	110,260	European (*n* = 98,674)	46	FinnGen summary statistics, 340,048	15 Million
				African (*n* = 3,286)			
				Asian (*n* = 3,755)			
				Others (*n* = 4,545)			

[a]Variants were imputed from the 1000 Genomes Project phase 1 reference panel, but the exact number of variants was not reported.
[b]Genetic loci identified using genotyped and imputed variants.
[c]Genetic loci identified using directly genotyped variants.
UKB: UK Biobank; IGGC: the International Glaucoma Genetics Consortium.

GWAS of IOP

van Koolwijk et al. (2012) reported the first GWAS on IOP in 2012. They used 11,972 participants from four cohorts in The Netherlands, conducted linear regression analysis in each cohort, and then performed meta-analyses. They further carried out replication using cohorts from UK, Australia, Canada, and The Wellcome Trust Case Control Consortium 2 (WTCCC2)/Blue Mountains Eye Study (BMES). Variants rs11656696 at *GAS7* and rs7555523 at *TMCO1* were significantly associated at the genome-wide level with IOP and were also associated with POAG. After 2012, multiple groups continued to rely on meta-analysis of GWASs as their primary method for identifying genetic loci related to IOP.

Researchers from The Blue Mountains Eye Study and The Wellcome Trust Case Control Consortium 2 (2013) identified rs59072263, a common variant between *GLCCI1* and *ICA1* at 7q21, which had a combined $p = 1.10 \times 10^{-8}$ in a meta-analysis of three cohorts: BMES ($n = 2{,}175$), EPIC-Norfold (n = 2,461), and TwinsUK ($n = 2033$). Ozel et al. (2014) performed a GWAS and a meta-analysis of IOP in participants of European ancestry from three cohorts, i.e., the NEI Glaucoma Human Genetics Collaboration (NEIGHBOR), GLAUcoma Genes and ENvironment (GLAUGEN) study, and a subset of the Age-related Macular Degeneration-Michigan, Mayo, Age-Related Eye Disease Studies (AREDS) and Pennsylvania study, totaling >6,000 individuals. Although no association with IOP reached genome-wide significance in any single cohort, the combination of results from all cohorts in a meta-analysis revealed a borderline genome-wide significant association at the *TMCO1* locus (rs7518099-G, $p = 8.0 \times 10^{-8}$). Nag et al. (2014) reported that rs2286885 within *FAM125B* was associated with IOP in the TwinsUK cohort (N = 2,774) and replicated the signal in 12 independent replication cohorts of European ancestry (combined $n = 22{,}789$). Hysi et al. (2014) carried out a large-scale meta-analysis of 18 cohorts from the International Glaucoma Genetics Consortium (IGGC, $n = 35{,}296$, 27,558 individuals of European ancestry and 7,738 individuals of Asian ancestry) and found four new IOP loci, rs6445055 in *FNDC3B*, rs2472493 near *ABCA1*, rs8176693 in *ABO*, and rs747782 on 11p11.2, among which loci, i.e., *ABCA1* (rs2472493), *FNDC3B* (rs6445055), and 11p11.2 (rs12419342), were also associated with POAG risk in four independent cohorts (all of European ancestry, 4,284 cases and 95,560 controls). In the meta-analysis of the Rotterdam Study I and II cohorts ($n = 8{,}105$ participants), Springelkamp et al. (2015) identified three SNPs in *ARHGEF12* that reached genome-wide significance. In a following larger meta-analysis of individuals of European and Asian descent ($n = 37{,}930$), Springelkamp et al. (2017) identified rs55796939 near *ADAMTS8* as a new locus for IOP. Using multiple longitudinal IOP measurements from electronic health records, Choquet et al. (2017) conducted a large multi-ethnic meta-analysis of IOP in the Kaiser Permanente GERA cohort, combining 69,756 individuals of European ($n = 56{,}819$), Hispanic/Latino ($n = 5{,}748$), East Asian ($n = 5{,}119$), and African ($n = 2{,}070$) ancestry, and reported 40 novel loci. Around 2017, large and multiethnic biobank datasets gradually became accessible to general researchers and, significantly boosted genetic discoveries related to IOP.

In 2018, with the advent of the biobank era, three groups reported genetic loci for IOP using the large UK Biobank prospective cohort dataset (Allen et al., 2014; Sudlow et al., 2015). Gao et al. (2018) described a GWAS of IOP using 115,486 European UKB participants and identified 103 and 145 novel loci using directly genotyped SNPs and an imputed genetic dataset, respectively. In addition to uncovering common variants, Gao et al. (2018) also reported low-frequency variant (MAF in the range of 0.005–0.01) associations with IOP, including rs28991009 in *ANGPTL7*. rs28991009 was subsequently studied in another report by Tanigawa et al. (2020). Khawaja et al. (2018) performed a meta-analysis of 139,555 European participants from UKB ($n = 103{,}382$), the International Glaucoma Genetics Consortium (IGGC) ($n = 29{,}578$) and EPIC-Norforlk ($n = 6{,}595$), and identified 68 novel genomic loci associated with IOP. MacGregor et al. (2018) identified 85 novel loci for IOP using a combined analysis of 133,492 participants from UKB ($n = 103{,}914$) and results from IGCC ($n = 29{,}578$). The large number of novel IOP loci identified by independent groups clearly demonstrated the power of the large-scale UKB dataset.

In the 2 years following 2018, two studies reported common-variant associations for IOP. Huang et al. (2019) reported 17 newly identified loci for IOP from a GWAS of 8,552 Chinese participants. In contrast to previous studies that explored autosomal SNPs, Simcoe et al. (2020) performed association analyses across the X chromosome using 102,407 participants from UKB and identified three loci, located within or near *MXRA5* (rs2107482), *GPM6B* (rs66819623), and *NDP*/*EFHC2* (rs12558081), associated with IOP.

Figure 1 shows the relationship between the number of novel IOP loci identified and the sample sizes used in 13 previously published GWASs and one ExWAS (described in more details in the next section) in the last 10 years. With larger sample sizes, typically more novel loci are identified. For instance, for a cohort size of about 12,000–35,000 European individuals, only one to four novel IOP loci were identified from GWASs. When the sample size increased to around 110,000 European individuals, more than 100 novel loci were identified, which represent a significant increase in the number of identified loci compared to studies with less than 40,000 individuals. However, for not well studied populations, such as East Asian, even less than 9,000 individuals generated 17 novel loci. This may indicate some genetic differences of IOP among different ethnic groups. For the three reports in 2018, i.e., Gao et al. (2018), Khawaja et al. (2018), MacGregor et al. (2018), different numbers of novel IOP loci were identified among different research groups, though there was a large overlap of the UKB sample used, possibly due to different analytic approaches, including MAF cutoff, phenotype definition, and number of principal components of genetic ancestry adjusted for.

ExWAS of IOP

ExWAS is similar to, but different from, a common-variant GWAS. It focuses on coding regions and a different set of genetic variants, specifically rare ones typically with MAF less than 0.01, which represent a new avenue for IOP genetics research. In a very recent study, Gao et al. (2022) reported the largest rare-variant study of IOP to date using whole-exome sequences of 110,260 UKB

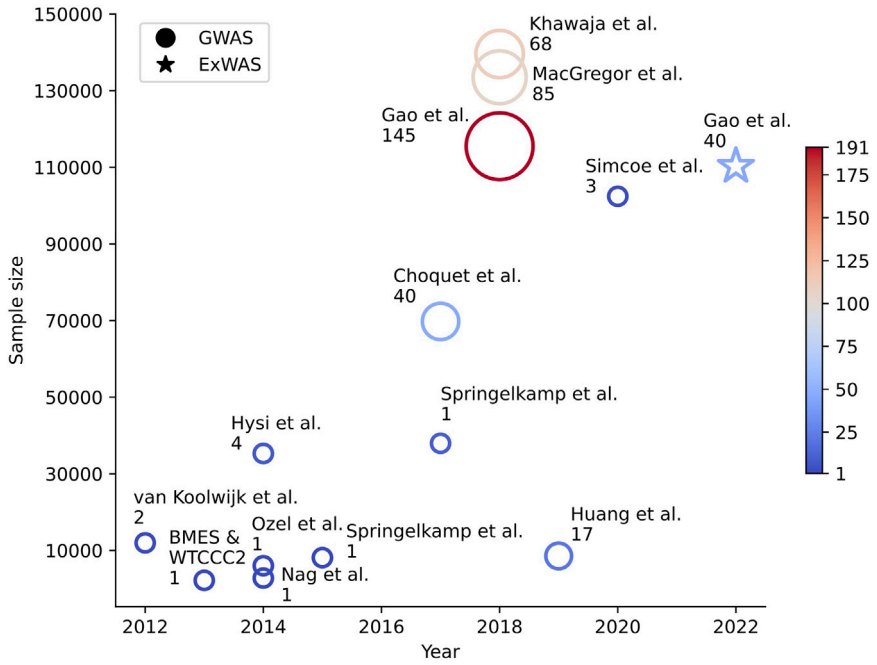

FIGURE 1
Number of novel intraocular pressure loci and study sample size in the last 10 years. Genetic association studies for IOP published in the past 10 years are represented by either (a) a circle for GWAS or (b) a star for ExWAS. The x-axis shows the year the study was published, and the y-axis shows the sample size of the study. The color and size of each plotted icon are proportional to the total number of loci and the number of novel loci discoveries that were reported in the corresponding study, respectively.

participants. In addition to confirming known IOP genes, Gao's group identified 40 novel genes harboring rare variants associated with IOP, including *BOD1L1*, *ACAD10*, *HLA-B*, *ADRB1*, *PTPRB*, *RPL26*, *RPL10A*, *EGLN2*, and *MTOR*. This study demonstrated the power of including and aggregating rare variants in gene discovery. About half of the identified IOP genes were also found to be associated with glaucoma phenotypes in UKB and the FinnGen cohort, a large biobank study focused on the population of Finland (Kurki et al., 2022). Most of the novel rare variants associated with IOP in Gao et al. (2022)'s study showed large effect sizes, which is consistent with the pattern that rare variants can show much larger effect sizes than common variants observed in many other studies (Gorlov et al., 2011; Zuk et al., 2014; Forgetta et al., 2020; Van Hout et al., 2020).

Biological insights

The above GWAS and ExWAS studies of IOP provided invaluable biological insights into both IOP and POAG. For example, van Koolwijk et al. (2012) found that *GAS7* and *TMCO1* are highly expressed in glaucoma-related ocular tissues, such as ciliary body, trabecular meshwork, lamina cribrosa, optic nerve, and retina. Hysi et al. (2014) found that *FNDC3B* and *ABCA1* also showed association with POAG and both genes were expressed in most ocular tissues. In Choquet et al. (2017), Choquet et al. (2018), functional studies support IOP-related influences of *FMNL2* and *LMX1B*, with certain *LMX1B* mutations causing high IOP and glaucoma resembling POAG in mice. In Gao et al. (2018), the top five Reactome pathways associated with IOP included the olfactory signaling pathway, defective *B3GALTL* causing Peters-plus syndrome, O-glycosylation of TSR domain-containing proteins, *ABC* transports in lipid homeostasis, and extracellular matrix organization. The loci reported by Khawaja et al. (2018) suggest that angiopoietin-receptor tyrosine kinase signaling, lipid metabolism, mitochondrial function, and developmental processes play a significant role in the risk of elevated IOP. Additionally, 14 of these associations were significantly associated with POAG after correction for multiple comparisons. MacGregor et al. (2018) studied the expression of genes at the newly identified IOP loci that were also associated with glaucoma in various human ocular tissues, including the corneal epithelium, corneal stroma, corneal endothelium, trabecular meshwork, ciliary body pigmented epithelium, neurosensory retina, optic nerve head, and optic nerve. They found that the expression of their newly associated genes was more enriched in the trabecular meshwork than other ocular tissues. MacGregor et al. further used FANTOM5 Cap Analysis of Gene Expression data and found evidence of correlation between enhancers with associated SNPs and the promoters of nine genes, including *PTPN1*, *BCLAF1*, and *GAS7*, in stromal and eye tissues. Nair et al. (2021) showed that mice deficient in GLIS1 developed chronically elevated IOP and GLIS1 impacts the expression of several other IOP and glaucoma-related genes, including *MYOC* and *CYP1B1*.

Numerous IOP genes also showed apparent pleiotropic nature (Choquet et al., 2017; Gao et al., 2018). Pleiotropy is the phenomenon in which a single gene or genetic variant has multiple effects on different traits (Stearns, 2010; Solovieff et al.,

2013). Pleiotropy is important because it helps explain how a single genetic change can have multiple effects on an organism. It also helps to explain why certain traits and conditions may be inherited together, even if they seem unrelated. In addition to glaucoma risk, Choquet et al. (2017) reported that several their own IOP loci are also associated with cup area, central corneal thickness, and Axenfeld-Rieger syndrome. Gao et al. (2018) studied the pleiotropic effects of 671 variants (from directly genotyped variants found in 149 unique loci) using the GWAS catalog. Many neurological disorders associated with eye diseases were directly linked to the included SNPs, such as primary open-angle, primary angle closure, and high-pressure glaucoma, as well as age-related macular degeneration. In addition, ocular parameters such as central corneal thickness, axial length, optic cup area, and iris characteristics were mapped. The SNPs were also matched to digestive and immune disorders, cancer, and cardiovascular and hematological measurements, including blood pressure, body mass index, and type 2 diabetes. Pleiotropy undoubtedly plays an important role in furthering our understanding of human biology and disease (Gao and Huang, 2019), including IOP and glaucoma. Studying the pleiotropic nature of human traits can provide new insights into disease prevention and treatment (Gao, 2020), e.g., drugs that have been approved for the treatment of one disease could be repurposed for the management of IOP based on information about pleiotropy. This may lead to the discovery of novel uses for existing drugs.

Drug targets

One of the goals of GWAS/ExWAS is to facilitate drug target discoveries, which has been the endeavor of many pharmaceutical companies. Drug candidates that have genetics support are twice as likely to be successful as those without genetics support (Nelson et al., 2015). Focused analyses of *CAV1*/*CAV2* revealed their association with IOP and replicated the previously reported associations with POAG in both effect size and direction (Ozel et al., 2014). Knockout mice exhibit elevated IOP and decreased outflow facility, demonstrating the direct role for *CAV1* in IOP homeostasis (Elliott et al., 2014). The extracellular matrix (ECM) was also shown to be associated with IOP (Choquet et al., 2017; Gao et al., 2018; MacGregor et al., 2018). ECM plays an important role in regulating the outflow of aqueous humor and may be a promising target for new therapies, such as those targeting the rho kinase, nitric oxide, adenosine A_1, prostaglandin EP_4, and potassium channel pathways involved in the conventional outflow of aqueous humor (Prasanna et al., 2016). Manipulating the ECM in the aqueous outflow pathway impacts IOP in genetic knockouts (Vranka et al., 2015). Furthermore, *ANGPTL7* was shown to modulate the trabecular meshwork's ECM and the response of this tissue to steroids (Comes et al., 2011) and may serve as a good candidate for glaucoma therapy (Borrás, 2017). Six genes, namely, *ADRB1*, *PTPRB*, *RPL26*, *RPL10A*, *EGLN2*, and *MTOR*, out of Gao et al. (2022)'s gene-based investigation have existing therapeutic molecular targets. The most notable one, *ADRB1*, is the target of cardiovascular and glaucoma drugs, including the broad class of glaucoma drugs targeting the beta-adrenergic receptor antagonists, or beta-blockers, known to lower IOP. The other five genes are targets in many clinical trials involving razuprotafib (targeting *PTPRB*), ataluren, ELX-02, MT-3724 (targeting *RPL26* and *RPL10A*), roxadustat, daprodustat, vadadustat (targeting *EGLN2*), and perhexiline (targeting *MTOR*), providing candidates for drug repurposing for possible glaucoma treatment.

Applications of GWAS/ExWAS results

In addition to the biological insights that we can gain from all these GWAS and ExWAS studies, there are two other major categories of applications, i.e., PRS and MR, utilizing the summary statistics from GWAS/ExWAS studies to make powerful predictions, e.g., to stratify individuals into high and low risk groups, and to infer possible causal effects.

Polygenic risk scores

Similarly to the three IOP GWASs reported in 2018, studies by Khawaja et al. (2018), MacGregor et al. (2018), and Gao and Fan (2018) also explored the use of IOP PRS or SNPs to predict glaucoma. Both Khawaja et al. (2018), and MacGregor et al. (2018) used $p < 5 \times 10^{-8}$ to select IOP SNPs for predicting glaucoma. Khawaja et al. used a regression-based model instead of PRS and got an area under the receiver operating characteristic curve (AUC) of 0.74. MacGregor et al. used an allele-score approach by combining the IOP and vertical cup disc ratio (VCDR) allele scores for their glaucoma prediction. Individuals in the top 5%, 10%, and 20% of their allele scores were at significantly increased risk of POAG compared to those in the bottom 5%, 10%, and 20% (OR = 7.8, 5.6, and 4.2, respectively). Gao and Fan (2018) tested a grid of *p*-value cutoffs for selecting SNPs, such as 0.01, 0.001, 10^{-4}, 5×10^{-5}, and 5×10^{-8}. They found that 5×10^{-5} gave better prediction accuracy for IOP and glaucoma than the 5×10^{-8} cutoff; Gao et al. (2019) observed significant associations between the IOP PRS (weighted) and IOP, with increasing PRS associated with higher IOP. Moreover, the PRS explained an additional 4% of the variation in IOP. They also identified significant associations between the IOP PRS and glaucoma, with study participants in the upper PRS quintiles experiencing greater odds of glaucoma (OR = 6.34) compared to those in the lowest quintile. Overall, the weighted PRS yielded a significant increase ($p = 6.2 \times 10^{-222}$) in the AUC to 0.77 compared to the model using age, sex, body mass index, systolic blood pressure, and type 2 diabetes. Furthermore, they observed similar results for the unweighted PRSs. IOP PRSs were also found to be associated with IOP readings outside clinic office hours, maximum IOP, glaucoma severity, and glaucoma treatment intensity (Qassim et al., 2020a; Qassim et al., 2020b). Gao et al. (2022) further constructed a rare-variant IOP PRS in their whole-exome sequencing study and showed that it is significantly associated with glaucoma in independent individuals.

Mendelian randomization

GWAS results and PRSs are also used in other types of studies, such as MR studies, which observe the causal effects of an exposure

to a specific external factor or a disease outcome based on variation in the population genome. They play an important role in our understanding of how external factors influence the development of a disease in an individual based on their specific genetic makeup. Kim et al. (2021) carried out MR analyses using the UKB dataset and assessed whether genetic loci linked to coffee consumption were associated with IOP. By using a PRS combining 111 IOP genetic variants, they were able to observe the interactions between the cohort's genomes and diets for over 121,000 individuals. They observed that coffee, tea, and caffeine consumption were weakly associated with lower IOP, and that these exposures had no association with glaucoma. However, the association between caffeine intake and IOP was modified by an IOP PRS, such that higher caffeine intake was positively associated with both IOP and glaucoma prevalence, but only among individuals with the highest genetic susceptibility to elevated IOP. Hysi et al. (2020) used variants of IOP as instruments and explored the relationship between refractive error and IOP. They found that IOP predicts a decrease in the spherical equivalent of diopters (more myopic). Choquet et al. (2022) conducted a two-sample MR study to evaluate the nature of the relationship between myopic refractive error and POAG and performed a multivariable MR analysis to adjust for the potential effect of IOP. Han et al. (2020) used a two-sample MR and found evidence of a potential causal inference for the associations of myopia and IOP with retinal detachment.

Genetic association studies of IOP in underrepresented populations

Genetic association studies of IOP in underrepresented populations are rather scarce. Here, underrepresented populations are defined as subgroups that have low representation relative to their numbers in the general population based on the definition described by the National Center for Advancing Translational Sciences of NIH (https://toolkit.ncats.nih.gov/glossary/underrepresented-population/). As such, the following groups are considered underrepresented: African Americans, Hispanics or Latinos, American Indians Alaskan Natives, and Native Hawaiians and other Pacific Islanders. Instead of carrying out ancestry-specific studies, most previous association studies embedded underrepresented populations in studies with a large number of European individuals (Choquet et al., 2017; Gao et al., 2022), possibly due to the smaller sample size of each individual underrepresented cohort. Choquet et al. (2017) used a meta-analysis approach to include underrepresented population samples to increase the overall sample size in their common variant association with IOP analysis. Gao et al. (2022) used a pan-ancestry approach by pooling all samples together and applying mixed-effect models that accounted for both principal components of genetic ancestry and genetic subpopulations in their rare variant analysis. After IOP genetic loci were identified in the overall combined multiethnic meta-analysis or sample, the loci were then explored in individual ethnicity groups (Choquet et al., 2017; Gao et al., 2022). To the best of our knowledge, only one study examined the association between IOP and genetic ancestry in a standalone Latino cohort (Nannini et al., 2016). Using linear regression analyses, Nannini et al. (2016) found that African ancestry was significantly associated with higher IOP in Latinos. After accounting for age, sex, body mass index, systolic blood pressure, central corneal thickness, and type 2 diabetes, this association remained significant. They also found that the association between African ancestry and IOP was modified by a significant interaction with hypertension, such that hypertensive individuals experienced a greater increase in IOP with increasing African ancestry. This study demonstrated for the first time that African ancestry and its interaction with hypertension are associated with higher IOP in Latinos.

Discussion

Since the first success of GWAS in human genetics (Klein et al., 2005), GWASs have become a widely used tool in genetic epidemiology (Gao and Edwards, 2011). These studies have led to the identification of many genetic variants that are associated with a variety of human diseases and traits, including IOP and glaucoma. The use of GWASs has greatly enhanced our ability to search for genetic contributions to complex traits. Due to the need for high statistical power, researchers often employ meta-analysis to combine the results of multiple GWAS studies. The availability of biobank datasets, especially UKB with half a million participants, also propelled genetic studies to another level of discoveries in both common and rare variants. Through ExWASs, large effect-size rare variants for IOP have begun to be unveiled. Such sequencing approaches will become more prevalent in the research world in the years to come. Not only have we seen a much deeper level of biological insights, including pleiotropy, but also have researchers used IOP PRS to help predict glaucoma and genetic instruments for IOP in MR studies for inferring causal relationships with other eye conditions.

Despite all the discoveries that have been made, the majority of the GWASs of IOP were done in individuals of European (95.6%) and Asian (3.1%) descents. Some efforts have been made to include individuals of non-European descent, such as the studies conducted by Choquet et al. (2017); Gao et al. (2022). However, the underrepresented population specific information is still largely unknown. Genetic discoveries in standalone underrepresented population are still in scarcity, with only one Latino-specific genetic association study published so far. Presently, PRSs work mostly in European individuals since most GWASs were done in European samples and do not transfer well to other underrepresented populations. PRS widespread use can create health disparities if this continues (Martin et al., 2019). It would be interesting to compare the discovery of genetic variants associated with a particular trait or disease in a sample of European individuals to that of a sample of individuals of African descent or Latino individuals, with the same sample size, for example, of 100,000 individuals. This comparison could provide insight into potential differences and similarities in the genetic basis of the trait or disease between these populations, which can have implications for the development and application of genetic testing and personalized medicine. Equity, diversity, and inclusion are critically important in all aspects of our life, including genetic research. Efforts to diversity are being made to address the significant imbalance in this field (Denny and Collins, 2021). The All of Us research program, a part of the National Institutes of Health, is working to build an inclusive, diverse database by inviting individuals from all backgrounds to participate (The All of Us Research Program Investigators, 2019). They have over

550,000 enrolled participants, with over 387,000 having completed the first steps to integrate the research program. Over 50% of their participants are from an ethnic minority, and over 80% correspond to a group underrepresented in research.

At the start of a new decade of IOP GWASs, what can we expect to see next? It is possible that GWASs by genotyping arrays will be replaced by GWASs by sequencing as the cost of sequencing continue to decrease. The use of whole-genome sequencing in GWASs is almost certain to yield unexpected discoveries, similar to what agnostic GWASs have already shown. Additionally, advancements in artificial intelligence may transform how we analyze and understand human genetics (Gao et al., 2020). These genetic discoveries are likely to be applied to individual patients of all backgrounds to aid in prevention, diagnosis and treatment.

Author contributions

XG conceived, planned and oversaw the present study. XG and MC wrote the draft of the manuscript and edited it to its final version. HC provided critical feedback on the manuscript and helped in editing it to its final version. AA participated in the overall draft and organization of the manuscript.

Conflict of interest

The authors declare that the research was conducted in the absence of any commercial or financial relationships that could be construed as a potential conflict of interest.

Publisher's note

All claims expressed in this article are solely those of the authors and do not necessarily represent those of their affiliated organizations, or those of the publisher, the editors and the reviewers. Any product that may be evaluated in this article, or claim that may be made by its manufacturer, is not guaranteed or endorsed by the publisher.

References

Allen, N. E., Sudlow, C., Peakman, T., and Collins, R. (2014). UK biobank data: Come and get it. *Sci. Transl. Med.* 6, 224ed4. doi:10.1126/scitranslmed.3008601

Aschard, H., Kang, J. H., Iglesias, A. I., Hysi, P., Cooke Bailey, J. N., Khawaja, A. P., et al. (2017). Genetic correlations between intraocular pressure, blood pressure and primary open-angle glaucoma: A multi-cohort analysis. *Eur. J. Hum. Genet.* 25, 1261–1267. doi:10.1038/ejhg.2017.136

Asefa, N. G., Neustaeter, A., Jansonius, N. M., and Snieder, H. (2019). Heritability of glaucoma and glaucoma-related endophenotypes: Systematic review and meta-analysis. *Surv. Ophthalmol.* 64, 835–851. doi:10.1016/j.survophthal.2019.06.002

Baek, S. U., Kee, C., and Suh, W. (2015). Longitudinal analysis of age-related changes in intraocular pressure in South Korea. *Eye (Lond)* 29, 625–629. doi:10.1038/eye.2015.11

Borrás, T. (2017). The pathway from genes to gene therapy in glaucoma: A review of possibilities for using genes as glaucoma drugs. *Asia Pac J. Ophthalmol. (Phila)* 6, 80–93. doi:10.22608/APO.2016126

Carbonaro, F., Andrew, T., Mackey, D. A., Young, T. L., Spector, T. D., and Hammond, C. J. (2009). Repeated measures of intraocular pressure result in higher heritability and greater power in genetic linkage studies. *Invest. Ophthalmol. Vis. Sci.* 50, 5115–5119. doi:10.1167/iovs.09-3577

Chakraborty, S., Sharma, A., Bagchi, I., Pal, S., Bhattacharyya, C., Gupta, V., et al. (2021). A genomewide association study on individuals with occludable angles identifies potential risk loci for intraocular pressure. *J. Genet.* 100, 69. doi:10.1007/s12041-021-01321-2

Chang, T. C., Congdon, N. G., Wojciechowski, R., Munoz, B., Gilbert, D., Chen, P., et al. (2005). Determinants and heritability of intraocular pressure and cup-to-disc ratio in a defined older population. *Ophthalmology* 112, 1186–1191. doi:10.1016/j.ophtha.2005.03.006

Chen, F., Klein, A. P., Klein, B. E. K., Lee, K. E., Truitt, B., Klein, R., et al. (2015). Exome array analysis identifies CAV1/CAV2 as a susceptibility locus for intraocular pressure. *Investigative Ophthalmol. Vis. Sci.* 56, 544–551. doi:10.1167/iovs.14-15204

Choquet, H., Khawaja, A. P., Jiang, C., Yin, J., Melles, R. B., Glymour, M. M., et al. (2022). Association between myopic refractive error and primary open-angle glaucoma: A 2-sample mendelian randomization study. *JAMA Ophthalmol.* 140, 864–871. doi:10.1001/jamaophthalmol.2022.2762

Choquet, H., Paylakhi, S., Kneeland, S. C., Thai, K. K., Hoffmann, T. J., Yin, J., et al. (2018). A multiethnic genome-wide association study of primary open-angle glaucoma identifies novel risk loci. *Nat. Commun.* 9, 2278. doi:10.1038/s41467-018-04555-4

Choquet, H., Thai, K. K., Yin, J., Hoffmann, T. J., Kvale, M. N., Banda, Y., et al. (2017). A large multi-ethnic genome-wide association study identifies novel genetic loci for intraocular pressure. *Nat. Commun.* 8, 2108. doi:10.1038/s41467-017-01913-6

Civan, M. M., and Macknight, A. D. (2004). The ins and outs of aqueous humour secretion. *Exp. Eye Res.* 78, 625–631. doi:10.1016/j.exer.2003.09.021

Collaborative Normal-Tension Glaucoma Study Group (1998). Comparison of glaucomatous progression between untreated patients with normal-tension glaucoma and patients with therapeutically reduced intraocular pressures. Collaborative Normal-Tension Glaucoma Study Group. *Am. J. Ophthalmol.* 126, 487–497.

Comes, N., Buie, L. K., and Borrás, T. (2011). Evidence for a role of angiopoietin-like 7 (ANGPTL7) in extracellular matrix formation of the human trabecular meshwork: Implications for glaucoma. *Genes. cells.* 16, 243–259. doi:10.1111/j.1365-2443.2010.01483.x

Denny, J. C., and Collins, F. S. (2021). Precision medicine in 2030-seven ways to transform healthcare. *Cell.* 184, 1415–1419. doi:10.1016/j.cell.2021.01.015

The All Of Us Research Program InvestigatorsDenny, J. C., Rutter, J. L., Goldstein, D. B., Philippakis, A., Smoller, J. W., Jenkins, G., et al. (2019). The "all of us" research program. *N. Engl. J. Med.* 381, 668–676. doi:10.1056/NEJMsr1809937

Elliott, M. H., Gu, X., Ashpole, N. E., Griffith, G. L., Boyce, T. M., Tanito, M., et al. (2014). Role of caveolin-1 in intraocular pressure and conventional outflow regulation. *Investigative Ophthalmol. Vis. Sci.* 55, 2888.

Forgetta, V., Manousaki, D., Istomine, R., Ross, S., Tessier, M. C., Marchand, L., et al. (2020). Rare genetic variants of large effect influence risk of type 1 diabetes. *Diabetes* 69, 784–795. doi:10.2337/db19-0831

Gao, X., and Edwards, T. L. (2011). Genome-wide association studies: Where we are heading? *World J. Med. Genet.* 1, 23–35. doi:10.5496/wjmg.v1.i1.23

Gao, X. R., Cebulla, C. M., and Ohr, M. P. (2020). "Chapter 19 - Advancing to precision medicine through big data and artificial intelligence," in *Genetics and genomics of eye disease*. Editor X. R. GAO (Cambridge: Academic Press).

Gao, X. R. (2020). "Chapter 18 - pleiotropy in eye disease and related traits," in *Genetics and genomics of eye disease*. Editor X. R. GAO (Cambridge: Academic Press).

Gao, X. R., Chiariglione, M., and Arch, A. J. (2022). Whole-exome sequencing study identifies rare variants and genes associated with intraocular pressure and glaucoma. *Nat. Commun.* 13, 7376. doi:10.1038/s41467-022-35188-3

Gao, X. R., and Fan, F. (2018). Polygenic risk score is associated with intraocular pressure and improves glaucoma prediction in the UK Biobank cohort. *Investigative Ophthalmol. Vis. Sci.* 59, 779.

Gao, X. R., Huang, H., and Kim, H. (2019). Polygenic risk score is associated with intraocular pressure and improves glaucoma prediction in the UK biobank cohort. *Transl. Vis. Sci. Technol.* 8, 10. doi:10.1167/tvst.8.2.10

Gao, X. R., Huang, H., Nannini, D. R., Fan, F., and Kim, H. (2018). Genome-wide association analyses identify new loci influencing intraocular pressure. *Hum. Mol. Genet.* 27, 2205–2213. doi:10.1093/hmg/ddy111

Gao, X. R., and Huang, H. (2019). PleioNet: A web-based visualization tool for exploring pleiotropy across complex traits. *Bioinformatics* 35, 4179–4180. doi:10.1093/bioinformatics/btz179

Gorlov, I. P., Gorlova, O. Y., Frazier, M. L., Spitz, M. R., and Amos, C. I. (2011). Evolutionary evidence of the effect of rare variants on disease etiology. *Clin. Genet.* 79, 199–206. doi:10.1111/j.1399-0004.2010.01535.x

Han, X., Ong, J. S., An, J., Craig, J. E., Gharahkhani, P., Hewitt, A. W., et al. (2020). Association of myopia and intraocular pressure with retinal detachment in European descent participants of the UK biobank cohort: A mendelian randomization study. *JAMA Ophthalmol.* 138, 671–678. doi:10.1001/jamaophthalmol.2020.1231

Heijl, A., Leske, M. C., Bengtsson, B., Hyman, L., Bengtsson, B., Hussein, M., et al. (2002). Reduction of intraocular pressure and glaucoma progression: Results from the early manifest glaucoma trial. *Arch. Ophthalmol.* 120, 1268–1279. doi:10.1001/archopht.120.10.1268

Huang, L., Chen, Y., Lin, Y., Tam, P. O. S., Cheng, Y., Shi, Y., et al. (2019). Genome-wide analysis identified 17 new loci influencing intraocular pressure in Chinese population. *Sci. China Life Sci.* 62, 153–164. doi:10.1007/s11427-018-9430-2

Hysi, P. G., Cheng, C. Y., Springelkamp, H., Macgregor, S., Bailey, J. N., Wojciechowski, R., et al. (2014). Genome-wide analysis of multi-ancestry cohorts identifies new loci influencing intraocular pressure and susceptibility to glaucoma. *Nat. Genet.* 46, 1126–1130. doi:10.1038/ng.3087

Hysi, P. G., Choquet, H., Khawaja, A. P., Wojciechowski, R., Tedja, M. S., Yin, J., et al. (2020). Meta-analysis of 542,934 subjects of European ancestry identifies new genes and mechanisms predisposing to refractive error and myopia. *Nat. Genet.* 52, 401–407. doi:10.1038/s41588-020-0599-0

Kass, M. A., Heuer, D. K., Higginbotham, E. J., Johnson, C. A., Keltner, J. L., Miller, J. P., et al. (2002). The ocular hypertension treatment study: A randomized trial determines that topical ocular hypotensive medication delays or prevents the onset of primary open-angle glaucoma. *Arch. Ophthalmol.* 120, 701–713. ; discussion 829-30. doi:10.1001/archopht.120.6.701

Khawaja, A. P., Cooke Bailey, J. N., Wareham, N. J., Scott, R. A., Simcoe, M., Igo, R. P., JR., et al. (2018). Genome-wide analyses identify 68 new loci associated with intraocular pressure and improve risk prediction for primary open-angle glaucoma. *Nat. Genet.* 50, 778–782. doi:10.1038/s41588-018-0126-8

Kim, J., Aschard, H., Kang, J. H., Lentjes, M. A. H., Do, R., Wiggs, J. L., et al. (2021). Intraocular pressure, glaucoma, and dietary caffeine consumption: A gene-diet interaction study from the UK biobank. *Ophthalmology* 128, 866–876. doi:10.1016/j.ophtha.2020.12.009

Klein, B. E., Klein, R., and Lee, K. E. (2004). Heritability of risk factors for primary open-angle glaucoma: The beaver dam eye study. *Invest. Ophthalmol. Vis. Sci.* 45, 59–62. doi:10.1167/iovs.03-0516

Klein, B. E., Klein, R., and Linton, K. L. (1992). Intraocular pressure in an American community. The beaver dam eye study. *Invest. Ophthalmol. Vis. Sci.* 33, 2224–2228.

Klein, R. J., Zeiss, C., Chew, E. Y., Tsai, J. Y., Sackler, R. S., Haynes, C., et al. (2005). Complement factor H polymorphism in age-related macular degeneration. *Science* 308, 385–389. doi:10.1126/science.1109557

Kurki, M. I., Karjalainen, J., Palta, P., Sipilä, T. P., Kristiansson, K., Donner, K., et al. (2022). FinnGen: Unique genetic insights from combining isolated population and national health register data. medRxiv, 2022.03.03.22271360.

Lang, G. K. (2007). *Ophthalmology: A pocket textbook atlas*. Stuttgart, New Yok: Thieme.

Lee, S., Emond, M. J., Bamshad, M. J., Barnes, K. C., Rieder, M. J., Nickerson, D. A., et al. (2012a). Optimal unified approach for rare-variant association testing with application to small-sample case-control whole-exome sequencing studies. *Am. J. Hum. Genet.* 91, 224–237. doi:10.1016/j.ajhg.2012.06.007

Lee, S., Wu, M. C., and Lin, X. (2012b). Optimal tests for rare variant effects in sequencing association studies. *Biostatistics* 13, 762–775. doi:10.1093/biostatistics/kxs014

Li, B., and Leal, S. M. (2008). Methods for detecting associations with rare variants for common diseases: Application to analysis of sequence data. *Am. J. Hum. Genet.* 83, 311–321. doi:10.1016/j.ajhg.2008.06.024

Li, Y., and Abecasis, G. R. (2006). Mach 1.0: Rapid haplotype reconstruction and missing genotype inference. *Am. J. Hum. Genet.* S79.

Macarthur, J., Bowler, E., Cerezo, M., Gil, L., Hall, P., Hastings, E., et al. (2017). The new NHGRI-EBI Catalog of published genome-wide association studies (GWAS Catalog). *Nucleic Acids Res.* 45, D896–D901. doi:10.1093/nar/gkw1133

Macgregor, S., Ong, J. S., An, J., Han, X., Zhou, T., Siggs, O. M., et al. (2018). Genome-wide association study of intraocular pressure uncovers new pathways to glaucoma. *Nat. Genet.* 50, 1067–1071. doi:10.1038/s41588-018-0176-y

Machiele, R., Motlagh, M., and Patel, B. C. (2022). *Intraocular pressure*. Treasure Island (FL): StatPearls.

Madsen, B. E., and Browning, S. R. (2009). A groupwise association test for rare mutations using a weighted sum statistic. *PLoS Genet.* 5, e1000384. doi:10.1371/journal.pgen.1000384

Marchini, J., Howie, B., Myers, S., Mcvean, G., and Donnelly, P. (2007). A new multipoint method for genome-wide association studies by imputation of genotypes. *Nat. Genet.* 39, 906–913. doi:10.1038/ng2088

Martin, A. R., Kanai, M., Kamatani, Y., Okada, Y., Neale, B. M., and Daly, M. J. (2019). Clinical use of current polygenic risk scores may exacerbate health disparities. *Nat. Genet.* 51, 584–591. doi:10.1038/s41588-019-0379-x

Martinez-De-La-Casa, J. M., Garcia-Feijoo, J., Fernandez-Vidal, A., Mendez-Hernandez, C., and Garcia-Sanchez, J. (2006). Ocular response analyzer versus Goldmann applanation tonometry for intraocular pressure measurements. *Invest. Ophthalmol. Vis. Sci.* 47, 4410–4414. doi:10.1167/iovs.06-0158

Mcguire, D., Jiang, Y., Liu, M., Weissenkampen, J. D., Eckert, S., Yang, L., et al. (2021). Model-based assessment of replicability for genome-wide association meta-analysis. *Nat. Commun.* 12, 1964. doi:10.1038/s41467-021-21226-z

Nag, A., Venturini, C., Small, K. S., Young, T. L., Viswanathan, A. C., Mackey, D. A., et al. (2014). A genome-wide association study of intra-ocular pressure suggests a novel association in the gene FAM125B in the TwinsUK cohort. *Hum. Mol. Genet.* 23, 3343–3348. doi:10.1093/hmg/ddu050

Nair, K. S., Srivastava, C., Brown, R. V., Koli, S., Choquet, H., Kang, H. S., et al. (2021). GLIS1 regulates trabecular meshwork function and intraocular pressure and is associated with glaucoma in humans. *Nat. Commun.* 12, 4877. doi:10.1038/s41467-021-25181-7

Nannini, D., Torres, M., Chen, Y. D., Taylor, K. D., Rotter, J. I., Varma, R., et al. (2016). African ancestry is associated with higher intraocular pressure in Latinos. *Ophthalmology* 123, 102–108. doi:10.1016/j.ophtha.2015.08.042

Nelson, M. R., Tipney, H., Painter, J. L., Shen, J., Nicoletti, P., Shen, Y., et al. (2015). The support of human genetic evidence for approved drug indications. *Nat. Genet.* 47, 856–860. doi:10.1038/ng.3314

Ojha, P., Wiggs, J. L., and Pasquale, L. R. (2013). The genetics of intraocular pressure. *Semin. Ophthalmol.* 28, 301–305. doi:10.3109/08820538.2013.825291

Ozel, A. B., Moroi, S. E., Reed, D. M., Nika, M., Schmidt, C. M., Akbari, S., et al. (2014). Genome-wide association study and meta-analysis of intraocular pressure. *Hum. Genet.* 133, 41–57. doi:10.1007/s00439-013-1349-5

Pe'er, I., Yelensky, R., Altshuler, D., and Daly, M. J. (2008). Estimation of the multiple testing burden for genomewide association studies of nearly all common variants. *Genet. Epidemiol.* 32, 381–385. doi:10.1002/gepi.20303

Prasanna, G., Li, B., Mogi, M., and Rice, D. S. (2016). Pharmacology of novel intraocular pressure-lowering targets that enhance conventional outflow facility: Pitfalls, promises and what lies ahead? *Eur. J. Pharmacol.* 787, 47–56. doi:10.1016/j.ejphar.2016.03.003

Qassim, A., Mullany, S., Awadalla, M. S., Hassall, M. M., Nguyen, T., Marshall, H., et al. (2020a). A polygenic risk score predicts intraocular pressure readings outside office hours and early morning spikes as measured by home tonometry. *Ophthalmol. Glaucoma* 4, 411–420. doi:10.1016/j.ogla.2020.12.002

Qassim, A., Souzeau, E., Siggs, O. M., Hassall, M. M., Han, X., Griffiths, H. L., et al. (2020b). An intraocular pressure polygenic risk score stratifies multiple primary open-angle glaucoma parameters including treatment intensity. *Ophthalmology* 127, 901–907. doi:10.1016/j.ophtha.2019.12.025

Risch, N., and Merikangas, K. (1996). The future of genetic studies of complex human diseases. *Science* 273, 1516–1517. doi:10.1126/science.273.5281.1516

Sanfilippo, P. G., Hewitt, A. W., Hammond, C. J., and Mackey, D. A. (2010). The heritability of ocular traits. *Surv. Ophthalmol.* 55, 561–583. doi:10.1016/j.survophthal.2010.07.003

Simcoe, M. J., Khawaja, A. P., Mahroo, O. A., Hammond, C. J., Hysi, P. G., Eye, U. K. B., et al. (2020). The role of chromosome X in intraocular pressure variation and sex-specific effects. *Invest. Ophthalmol. Vis. Sci.* 61, 20. doi:10.1167/iovs.61.11.20

Solovieff, N., Cotsapas, C., Lee, P. H., Purcell, S. M., and Smoller, J. W. (2013). Pleiotropy in complex traits: Challenges and strategies. *Nat. Rev. Genet.* 14, 483–495. doi:10.1038/nrg3461

Springelkamp, H., Hohn, R., Mishra, A., Hysi, P. G., Khor, C. C., Loomis, S. J., et al. (2014). Meta-analysis of genome-wide association studies identifies novel loci that influence cupping and the glaucomatous process. *Nat. Commun.* 5, 4883. doi:10.1038/ncomms5883

Springelkamp, H., Iglesias, A. I., Cuellar-Partida, G., Amin, N., Burdon, K. P., Van Leeuwen, E. M., et al. (2015). ARHGEF12 influences the risk of glaucoma by increasing intraocular pressure. *Hum. Mol. Genet.* 24, 2689–2699. doi:10.1093/hmg/ddv027

Springelkamp, H., Iglesias, A. I., Mishra, A., Hohn, R., Wojciechowski, R., Khawaja, A. P., et al. (2017). New insights into the genetics of primary open-angle glaucoma based on meta-analyses of intraocular pressure and optic disc characteristics. *Hum. Mol. Genet.* 26, 438–453. doi:10.1093/hmg/ddw399

Stearns, F. W. (2010). One hundred years of pleiotropy: A retrospective. *Genetics* 186, 767–773. doi:10.1534/genetics.110.122549

Sudlow, C., Gallacher, J., Allen, N., Beral, V., Burton, P., Danesh, J., et al. (2015). UK biobank: An open access resource for identifying the causes of a wide range of complex diseases of middle and old age. *Plos Med.* 12, e1001779. doi:10.1371/journal.pmed.1001779

Tam, V., Patel, N., Turcotte, M., Bossé, Y., Paré, G., and Meyre, D. (2019). Benefits and limitations of genome-wide association studies. *Nat. Rev. Genet.* 20, 467–484. doi:10.1038/s41576-019-0127-1

Tanigawa, Y., Wainberg, M., Karjalainen, J., Kiiskinen, T., Venkataraman, G., Lemmela, S., et al. (2020). Rare protein-altering variants in ANGPTL7 lower

intraocular pressure and protect against glaucoma. *PLoS Genet.* 16, e1008682. doi:10.1371/journal.pgen.1008682

The Blue Mountains Eye Study and The Wellcome Trust Case Control Consortium 2 (2013). Genome-wide association study of intraocular pressure identifies the GLCCI1/ICA1 region as a glaucoma susceptibility locus. *Hum. Mol. Genet.* 22, 4653–4660. doi:10.1093/hmg/ddt293

Van Hout, C. V., Tachmazidou, I., Backman, J. D., Hoffman, J. D., Liu, D., Pandey, A. K., et al. (2020). Exome sequencing and characterization of 49,960 individuals in the UK Biobank. *Nature* 586, 749–756. doi:10.1038/s41586-020-2853-0

Van Koolwijk, L. M., Despriet, D. D., Van Duijn, C. M., Pardo Cortes, L. M., Vingerling, J. R., Aulchenko, Y. S., et al. (2007). Genetic contributions to glaucoma: Heritability of intraocular pressure, retinal nerve fiber layer thickness, and optic disc morphology. *Invest. Ophthalmol. Vis. Sci.* 48, 3669–3676. doi:10.1167/iovs.06-1519

Van Koolwijk, L. M., Ramdas, W. D., Ikram, M. K., Jansonius, N. M., Pasutto, F., Hysi, P. G., et al. (2012). Common genetic determinants of intraocular pressure and primary open-angle glaucoma. *PLoS Genet.* 8, e1002611. doi:10.1371/journal.pgen.1002611

Visscher, P. M., Wray, N. R., Zhang, Q., Sklar, P., Mccarthy, M. I., Brown, M. A., et al. (2017). 10 Years of GWAS discovery: Biology, function, and translation. *Am. J. Hum. Genet.* 101, 5–22. doi:10.1016/j.ajhg.2017.06.005

Vranka, J. A., Kelley, M. J., Acott, T. S., and Keller, K. E. (2015). Extracellular matrix in the trabecular meshwork: Intraocular pressure regulation and dysregulation in glaucoma. *Exp. Eye Res.* 133, 112–125. doi:10.1016/j.exer.2014.07.014

Welter, D., Macarthur, J., Morales, J., Burdett, T., Hall, P., Junkins, H., et al. (2014). The NHGRI GWAS Catalog, a curated resource of SNP-trait associations. *Nucleic Acids Res.* 42, D1001–D1006. doi:10.1093/nar/gkt1229

Willer, C. J., Li, Y., and Abecasis, G. R. (2010). Metal: Fast and efficient meta-analysis of genomewide association scans. *Bioinformatics* 26, 2190–2191. doi:10.1093/bioinformatics/btq340

Wu, M. C., Kraft, P., Epstein, M. P., Taylor, D. M., Chanock, S. J., Hunter, D. J., et al. (2010). Powerful SNP-set analysis for case-control genome-wide association studies. *Am. J. Hum. Genet.* 86, 929–942. doi:10.1016/j.ajhg.2010.05.002

Wu, M. C., Lee, S., Cai, T., Li, Y., Boehnke, M., and Lin, X. (2011). Rare-variant association testing for sequencing data with the sequence kernel association test. *Am. J. Hum. Genet.* 89, 82–93. doi:10.1016/j.ajhg.2011.05.029

Wu, S. Y., and Leske, M. C. (1997). Associations with intraocular pressure in the Barbados eye study. *Arch. Ophthalmol.* 115, 1572–1576. doi:10.1001/archopht.1997.01100160742012

Xu, Z., Hysi, P., and Khawaja, A. P. (2021). Genetic determinants of intraocular pressure. *Annu. Rev. Vis. Sci.* 7, 727–746. doi:10.1146/annurev-vision-031021-095225

Zheng, Y., Xiang, F., Huang, W., Huang, G., Yin, Q., and He, M. (2009). Distribution and heritability of intraocular pressure in Chinese children: The guangzhou twin eye study. *Invest. Ophthalmol. Vis. Sci.* 50, 2040–2043. doi:10.1167/iovs.08-3082

Zhou, W., Nielsen, J. B., Fritsche, L. G., Dey, R., Gabrielsen, M. E., Wolford, B. N., et al. (2018). Efficiently controlling for case-control imbalance and sample relatedness in large-scale genetic association studies. *Nat. Genet.* 50, 1335–1341. doi:10.1038/s41588-018-0184-y

Zhou, W., Zhao, Z., Nielsen, J. B., Fritsche, L. G., Lefaive, J., Gagliano Taliun, S. A., et al. (2020). Scalable generalized linear mixed model for region-based association tests in large biobanks and cohorts. *Nat. Genet.* 52, 634–639. doi:10.1038/s41588-020-0621-6

Zuk, O., Schaffner, S. F., Samocha, K., Do, R., Hechter, E., Kathiresan, S., et al. (2014). Searching for missing heritability: Designing rare variant association studies. *Proc. Natl. Acad. Sci. U. S. A.* 111, E455–E464. doi:10.1073/pnas.1322563111

frontiers | Frontiers in Pediatrics

TYPE Case Report
PUBLISHED 05 May 2023
DOI 10.3389/fped.2023.1147836

OPEN ACCESS

EDITED BY
Denis Plotnikov,
Kazan State Medical University, Russia

REVIEWED BY
Zihan Sun,
University College London, United Kingdom
Jayesh Sheth,
Foundation for Research In Genetics and Endocrinology, India

*CORRESPONDENCE
Fang Lu
lufang@wchscu.cn

SPECIALTY SECTION
This article was submitted to Genetics of Common and Rare Diseases, a section of the journal Frontiers in Pediatrics

RECEIVED 19 January 2023
ACCEPTED 21 March 2023
PUBLISHED 05 May 2023

CITATION
Chen Q and Lu F (2023) Multimodal optical imaging and genetic features of AB variant GM2 gangliosidosis: a case report.
Front. Pediatr. 11:1147836.
doi: 10.3389/fped.2023.1147836

Multimodal optical imaging and genetic features of AB variant GM2 gangliosidosis: a case report

Qin Chen and Fang Lu*

Department of Ophthalmology, West China Hospital, Sichuan University, Chengdu, China

Background: AB variant GM2 gangliosidosis is an extremely rare autosomal recessive lysosomal storage disease. Macular cherry-red spots are the most commonly described ocular sign in this disease. Here, for the first time we report a case of an infant with AB variant GM2 gangliosidosis, along with multimodal optical imaging and genetic testing results.

Case description: A 7-month-old Chinese girl presented to the hospital with nystagmus for 2 months. Her family history for this condition showed negative results, and her parents were not known to be consanguineous. Fundus photography showed a cherry-red spot with a ring of whitish infiltrate surrounding both macula. Fundus fluorescein angiography showed normal retinal circulation and vessels. Optical coherence tomography (OCT) revealed a thickening and increased reflectivity of the inner retinal layers with a shadowing effect on the outer structures. The patient had no obvious neurological symptoms, and the MRI results of the head were normal. The whole-exome genome sequencing results showed that there was a homozygous deletion (chr5: 150639196-150639548) of exon 2 in the *GM2A* gene. Finally, the patient was diagnosed with AB variant GM2 gangliosidosis.

Conclusions: AB variant GM2 gangliosidosis is a rare disease affecting multiple nervous systems. Before the occurrence of typical neurological symptoms, the clinical features of fundus photography and OCT help us diagnose GM2 gangliosidosis.

KEYWORDS

AB variant GM2 gangliosidosis, cherry-red spot, optical coherence tomography, gene, fundus fluorescein angiography (FFA)

Introduction

GM2 gangliosidoses are a group of autosomal recessive lysosomal storage diseases characterized by the accumulation of glycosphingolipids in the nerve cells. According to different causative genes, GM2 gangliosidoses are divided into three subtypes: Tay–Sachs disease (*HEXA* gene), Sandhoff disease (*HEXB* gene), and AB variant GM2 (*GM2A* gene). AB variant GM2 gangliosidosis is a very rare form of disease caused by a lack of the GM2 activator protein. The typical clinical manifestations of GM2 gangliosidoses are neuromotor retardation and regression, hypotonia, and visual impairment (1). Macular cherry-red spots are the most commonly described ocular sign in GM2 gangliosidoses.

However, a full examination of optical coherence tomography (OCT) and fundus fluorescein angiography (FFA) for this specific macular abnormality has not yet been completed. Ophthalmologists can see the various layers of the retina and the vascular

Abbreviations
OCT, optical coherence tomography; FFA, fluorescence fundus angiography; CRAO, central retinal artery occlusion.

systems around the macula using OCT and FFA, which aids in a deeper understanding of macular illness. Here, we provide the findings of OCT, FFA, and genetic testing in a newborn with AB variant GM2 gangliosidosis.

Case description

A 7-month-old Chinese girl presented to the hospital with nystagmus for 2 months. The patient was born at 37 weeks' gestation and weighed 3,400 g. Her growth and development were normal, except that she was unable to sit. Her family history was negative for this condition, and her parents were not known to be consanguineous. An examination of the anterior segment of both her eyes revealed no abnormalities. Color fundus photography (RetCam III, Natus Medical, USA) showed a cherry-red spot with a ring of whitish infiltrate surrounding both macula (**Figures 1A,B**). FFA showed normal retinal circulation and vessels (**Figures 1C,D**). OCT (OPMI LUMERA and RESCAN 700, Carl Zeiss Meditec, AG, Germany) revealed a thickening and increased reflectivity of the inner retinal layers with a shadowing effect on the outer structures. The marked thickening and hyperreflective part was within a 1–2 papillary diameter (PD) area around the fovea. It was difficult to distinguish the inner retinal structure (**Figures 1E,F**). The head MRI of the girl's head revealed no visible anomalies.

A novel homozygous pathogenic variant in GM2A was detected in the whole-exome genome sequencing of the patient. The sequencing results showed that there was a homozygous deletion (Chr5: 150639196-150639548) of exon 2 in the *GM2A* gene, which revealed GM2 activator protein deficiency. The parents of the patient had heterozygous mutations in the same genetic locus (**Figure 2**).

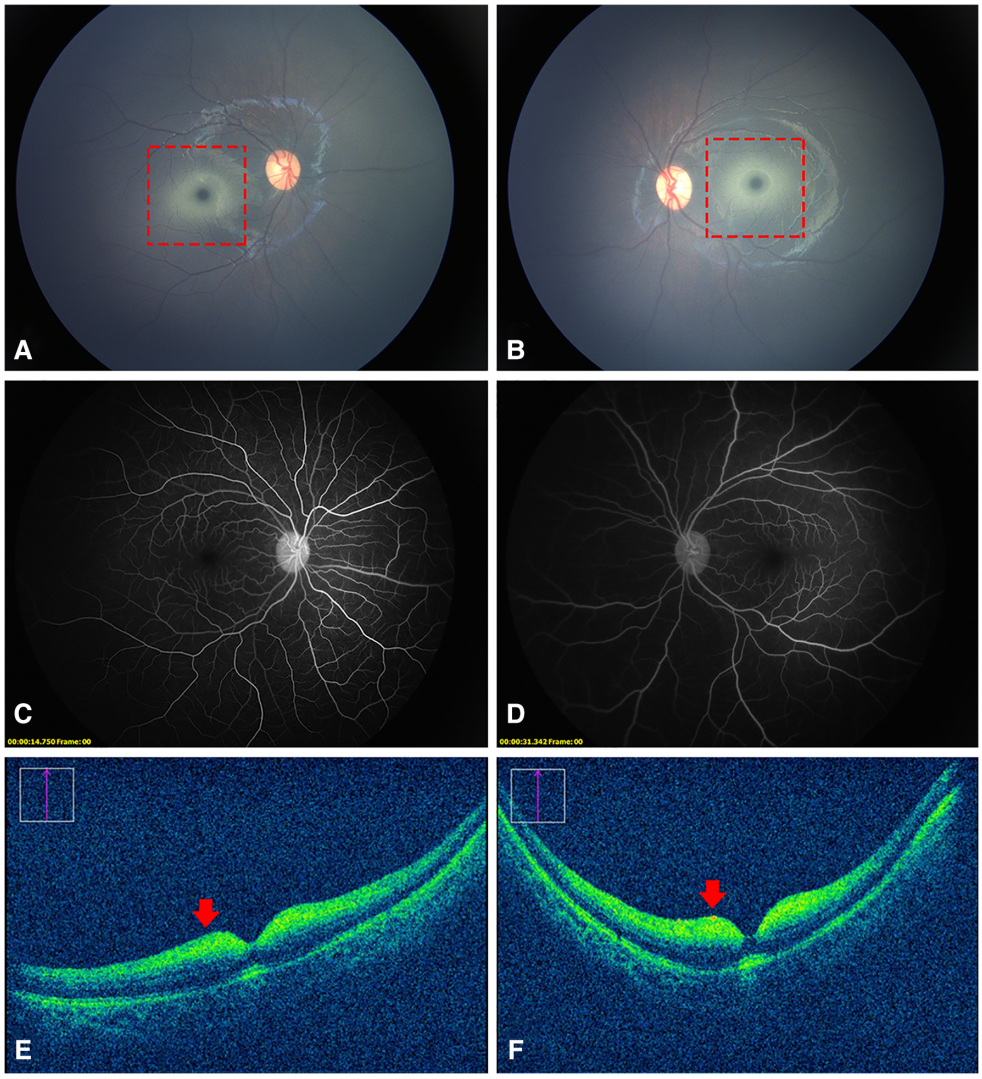

FIGURE 1
Fundus photography, FFA, and OCT images of the patient. (A,B), a cherry-red spot with a ring of whitish infiltrate within a 1–2 PD area surrounding the fovea (dotted red squares). (C,D) normal retinal vessels without obstruction. (E,F) thickened and increased reflectivity of the inner retinal layers with a shadowing effect on the outer structures (red arrows). It was difficult to distinguish the inner retinal structure.

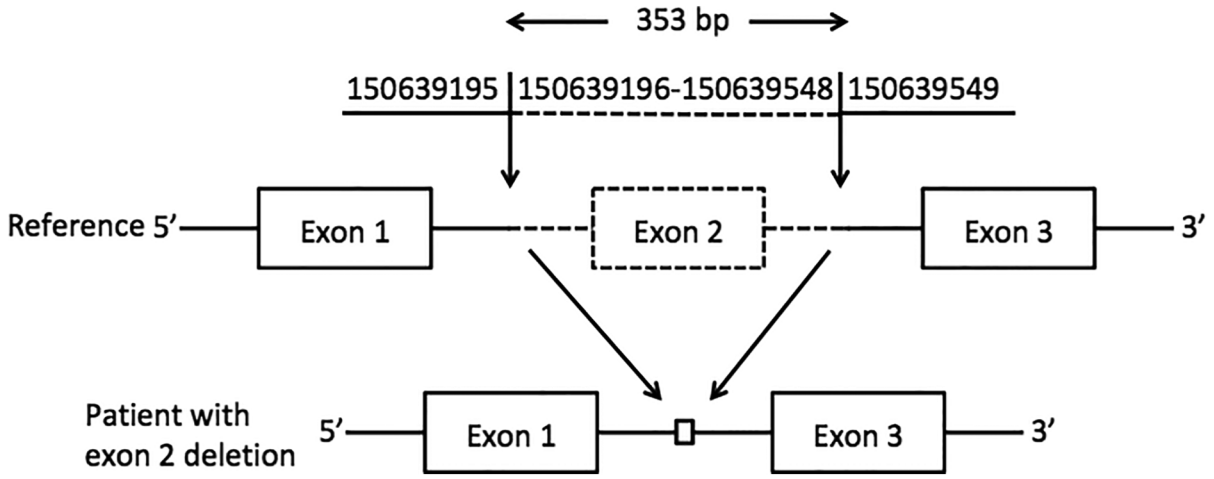

FIGURE 2
Exon 2 deletion in GM2A. A schematic representation of the deletion detected in the GM2A gene. The deleted region is represented by dotted lines, whereas the intact region is represented by solid lines. The downward arrows indicate the breakpoints of the deletion.

Finally, the patient was diagnosed with AB variant GM2 gangliosidosis. One and a half months later, more abnormal findings were reported and these were confined to the nervous system. The girl lost the ability to roll over and hold her bottle. She developed hyperacusis, a heightened sensitivity to sound, and her natural smile lessened. However, there was no effective treatment for this disease.

Discussion

AB variant GM2 gangliosidosis is an extremely rare lysosomal storage disease caused by a deficiency of the GM2 activator protein, which makes an enzyme cofactor for beta-hexosaminidase. No more than 20 cases have been reported thus far (2–4). This disease is not easy to detect by neurologists in the early stage without obvious degenerative changes occurring in the nervous system. This is the first case report from China of AB variant GM2 gangliosidosis, and it was primarily diagnosed by the ophthalmologist. The symptoms and signs of the eyes play a very important role in the early diagnosis of the disease.

The most common clinical optical findings of AB variant GM2 gangliosidosis are cherry-red spots (72%) and nystagmus (22%) (2). Cherry-red spots, or "perifoveal white patch", a term coined by Canadian researchers (5), are caused by the accumulation of glycolipids within the retinal ganglion cell layer of both eyes. Unlike the cherry-red spots formed by the edema of the inner retinal cells as a result of central retinal artery occlusion (CRAO), the perifoveal whitish area of GM2 gangliosidosis, in the patient in this study, was concentrated only in the range of approximately 1–2 PD around the fovea. This abnormal change corresponded to thickened hyperreflective areas on OCT images. FFA did not reveal any occlusion of the retinal vessels or late peripheral vascular leakage. All these indicated that these cherry-red spots were completely different from those resulting from CRAO. In addition to gangliosidosis, this characteristic cherry-red spot is seen in other lysosomal disorders such as Niemann–Pick, metachromatic leukodystrophy, sialidosis, and Farber disease (6).

A review of the literature revealed that this was for the first time OCT and FFA images of GM2 gangliosidosis have been obtained. Similar to other lysosomal disorders, OCT showed hyperreflective inner layers adjacent to the macula and a relative hyporeflectivity of the layers underneath (7). Different from sialidosis, the nerve fiber layer and the border between different inner retina layers was hardly recognizable in our patient. We reasoned that this unique appearance might be explained by prior histology findings. The nerve fiber layer in newborns with GM2 gangliosidosis was described in pathological research as being extremely thin. In addition to the cytoplasm of the retinal ganglion cells filled with large numbers of concentric membranous bodies, there were also a few abnormal vesicular lysosomes in the cells of the inner nuclear layer (8). Moreover, the retinal and OCT structures of infants differed from those of older kids or adults, in which the inner retina cells are more concentrated in the macular area (9). This might also be responsible for the abnormal findings of OCT in our case. Our OCT images could provide valuable clinical experience to better understand the ocular manifestations of this disease.

Conclusions

In summary, AB variant GM2 gangliosidosis is an extremely rare type of lysosomal storage disease affecting multiple neurological systems. Before the occurrence of typical neurological symptoms, the clinical features of fundus photography and OCT help us to diagnose GM2 gangliosidosis early.

Data availability statement

The data presented in the study are deposited in the Sequence Read Archive repository, accession number PRJNA962274.

Ethics statement

The studies involving human participants were reviewed and approved by West China Hospital, Sichuan University. Written informed consent was obtained from the individual(s) and minor (s)' legal guardian/next of kin for the publication of any potentially identifiable images or data included in this article.

Author contributions

QC collected and collated the patient data and wrote the manuscript. FL diagnosed and treated the patient and revised the manuscript. All authors contributed to the article and approved the submitted version.

Conflict of interest

The authors declare that the research was conducted in the absence of any commercial or financial relationships that could be construed as a potential conflict of interest.

Publisher's note

All claims expressed in this article are solely those of the authors and do not necessarily represent those of their affiliated organizations, or those of the publisher, the editors and the reviewers. Any product that may be evaluated in this article, or claim that may be made by its manufacturer, is not guaranteed or endorsed by the publisher.

References

1. Leal AF, Benincore-Flórez E, Solano-Galarza D, Garzón Jaramillo RG, Echeverri-Peña OY, Suarez DA, et al. GM2 gangliosidoses: clinical features, pathophysiological aspects, and current therapies. *Int J Mol Sci*. (2020) 21(17):6213. doi: 10.3390/ijms21176213

2. İnci A, Cengiz Ergin FB, Biberoğlu G, Okur İ, Ezgü FS, Tümer L. Two patients from Turkey with a novel variant in the GM2A gene and review of the literature. *J Pediatr Endocrinol Metab*. (2021) 34(6):805–12. doi: 10.1515/jpem-2020-0655

3. Hall PL, Laine R, Alexander JJ, Ankala A, Teot LA, Lidov HGW, et al. GM2 activator deficiency caused by a homozygous exon 2 deletion in GM2A. *JIMD report*. (2017) 38:61–5. doi: 10.1007/8904_2017_31

4. Sheth J, Datar C, Mistri M, Bhavsar R, Sheth F, Shah K. GM2 gangliosidosis AB variant: novel mutation from India - a case report with a review. *BMC Pediatr*. (2016) 16:88. doi: 10.1186/s12887-016-0626-6

5. Ospina LH, Lyons CJ, McCormick AQ. "Cherry-red spot" or "perifoveal white patch"? *Can J Ophthalmol*. (2005) 40(5):609–10. doi: 10.1016/S0008-4182(05)80054-7

6. Smith NJ, Winstone AM, Stellitano L, Cox TM, Verity CM. GM2 gangliosidosis in a UK study of children with progressive neurodegeneration: 73 cases reviewed. *Dev Med Child Neurol*. (2012) 54(2):176–82. doi: 10.1111/j.1469-8749.2011.04160.x

7. Varela MD, Zein WM, Toro C, Groden C, Johnston J, Huryn LA, et al. A sialidosis type I cohort and a quantitative approach to multimodal ophthalmic imaging of the macular cherry-red spot. *Br J Ophthalmol*. (2021) 105(6):838–43. doi: 10.1136/bjophthalmol-2020-316826

8. Brownstein S, Carpenter S, Polomeno RC, Little JM. Sandhoff's disease (Gm2 gangliosidosis type 2): histopathology and ultrastructure of the eye. *Arch Ophthalmol*. (1980) 98(6):1089–97. doi: 10.1001/archopht.1980.01020031079014

9. Lee H, Proudlock FA, Gottlob I. Pediatric optical coherence tomography in clinical practice—recent progress. *Investig Ophthalmol Vis Sci*. (2016) 57(9):OCT69. doi: 10.1167/iovs.15-18825

frontiers | Frontiers in Genetics

TYPE Original Research
PUBLISHED 07 June 2023
DOI 10.3389/fgene.2023.1113058

OPEN ACCESS

EDITED BY
Jessica Nicole Cooke Bailey,
Case Western Reserve University,
United States

REVIEWED BY
Marie-Hélène Roy-Gagnon,
University of Ottawa, Canada
Jiaxing Wang,
Emory University, United States
Wenjuan Zhuang,
Ningxia Hui Autonomous Region
People's Hospital, China

*CORRESPONDENCE
Hélène Choquet,
Helene.Choquet@kp.org

RECEIVED 01 December 2022
ACCEPTED 25 May 2023
PUBLISHED 07 June 2023

CITATION
Jiang C, Melles RB, Yin J, Fan Q, Guo X, Cheng C-Y, He M, Mackey DA, Guggenheim JA, Klaver C, Consortium for Refractive Error and Myopia (CREAM), Nair KS, Jorgenson E and Choquet H (2023), A multiethnic genome-wide analysis of 19,420 individuals identifies novel loci associated with axial length and shared genetic influences with refractive error and myopia.
Front. Genet. 14:1113058.
doi: 10.3389/fgene.2023.1113058

A multiethnic genome-wide analysis of 19,420 individuals identifies novel loci associated with axial length and shared genetic influences with refractive error and myopia

Chen Jiang[1], Ronald B. Melles[2], Jie Yin[1], Qiao Fan[3,4], Xiaobo Guo[5,6], Ching-Yu Cheng[7], Mingguang He[8,9], David A. Mackey[10], Jeremy A. Guggenheim[11], Caroline Klaver[12], Consortium for Refractive Error and Myopia (CREAM), K. Saidas Nair[13], Eric Jorgenson[14] and Hélène Choquet[1]*

[1]Division of Research, Kaiser Permanente Northern California (KPNC), Oakland, CA, United States, [2]KPNC, Department of Ophthalmology, Redwood City, CA, United States, [3]Centre for Quantitative Medicine, Duke-NUS Medical School, Singapore, Singapore, [4]Ophthalmology and Visual Sciences Academic Clinical Program (Eye ACP), Duke-NUS Medical School, Singapore, Singapore, [5]Department of Statistical Science, School of Mathematics, Sun Yat-Sen University, Guangzhou, China, [6]Southern China Center for Statistical Science, Sun Yat-Sen University, Guangzhou, China, [7]Ocular Epidemiology Research Group, Singapore Eye Research Institute, Singapore, Singapore, [8]State Key Laboratory of Ophthalmology, Zhongshan Ophthalmic Center, Sun Yat-Sen University, Guangzhou, China, [9]Centre for Eye Research Australia; Ophthalmology, Department of Surgery, University of Melbourne, Melbourne, WA, Australia, [10]Lions Eye Institute, Centre for Ophthalmology and Visual Science, University of Western Australia, Perth, WA, Australia, [11]School of Optometry and Vision Sciences, Cardiff University, Cardiff, United Kingdom, [12]Department Ophthalmology, Department Epidemiology, Erasmus Medical Center, Rotterdam, Netherlands, [13]Department of Ophthalmology and Department of Anatomy, School of Medicine, University of California, San Francisco, CA, United States, [14]Regeneron Genetics Center, Tarrytown, NY, United States

Introduction: Long axial length (AL) is a risk factor for myopia. Although family studies indicate that AL has an important genetic component with heritability estimates up to 0.94, there have been few reports of AL-associated loci.

Methods: Here, we conducted a multiethnic genome-wide association study (GWAS) of AL in 19,420 adults of European, Latino, Asian, and African ancestry from the Genetic Epidemiology Research on Adult Health and Aging (GERA) cohort, with replication in a subset of the Consortium for Refractive Error and Myopia (CREAM) cohorts of European or Asian ancestry. We further examined the effect of the identified loci on the mean spherical equivalent (MSE) within the GERA cohort. We also performed genome-wide genetic correlation analyses to quantify the genetic overlap between AL and MSE or myopia risk in the GERA European ancestry sample.

Results: Our multiethnic GWA analysis of AL identified a total of 16 genomic loci, of which 5 are novel. We found that all AL-associated loci were significantly associated with MSE after Bonferroni correction. We also found that AL was genetically correlated with MSE (r_g = −0.83; SE, 0.04; p = 1.95 × 10^{-89}) and myopia (r_g = 0.80; SE, 0.05; p = 2.84 × 10^{-55}). Finally, we estimated the array heritability for AL in the GERA European ancestry sample using LD score regression, and found an overall heritability estimate of 0.37 (s.e. = 0.04).

Discussion: In this large and multiethnic study, we identified novel loci, associated with AL at a genome-wide significance level, increasing substantially our understanding of the etiology of AL variation. Our results also demonstrate an association between AL-associated loci and MSE and a shared genetic basis between AL and myopia risk.

KEYWORDS

GWAS, genetics, single nucleotide polymorphisms (SNPs), axial length, eye biometry, refractive errors, myopia

Introduction

Ocular axial length (AL) is an eye dimension that refers to the distance (in millimeters) from the apex of the anterior corneal (front of the eye) to the retina. AL elongation is a feature of myopia, which is the most common form of refractive error, and several other eye diseases such as retinal tear, retinal detachment, inherited retinal diseases, glaucoma, and myopic macular degeneration (Adams, 1987; Grosvenor, 1988; Arias et al., 2015; Tideman et al., 2016; Tideman et al., 2018; Streho et al., 2019; Rezapour et al., 2021; Fonteh et al., 2022; Foo et al., 2022; Omodaka et al., 2022; Williams et al., 2022; Xu et al., 2022). Moreover, the measurement of AL is generally more precise and reproducible than assessments of refractive/myopia status (Mu et al., 2022). For these reasons, investigation of factors that influence the variation of AL endophenotype is relevant and could provide key insights into the etiology of eye diseases.

AL is predominantly genetically determined, with heritability estimates up to 0.94 (Biino et al., 2005; Dirani et al., 2006; Chen et al., 2007; Paget et al., 2008; Klein et al., 2009; Guggenheim et al., 2013). Although genome-wide association studies (GWAS) have considerably facilitated a wide range of discoveries in the human genetics (Visscher et al., 2017), few GWAS of AL have been reported to date (Fan et al., 2012; Cheng et al., 2013; Miyake et al., 2015; Fuse et al., 2022). Those GWAS were conducted in either European ancestry or in Asian ancestry populations. A recent study (Fan et al., 2020) investigating the genetic basis of corneal curvature identified eight associations with AL in a subset of the Consortium for Refractive Error and Myopia (CREAM) cohorts of European or Asian ancestry. To our knowledge, no studies have yet reported a GWAS of AL in a large and ethnically diverse cohort. It is also unclear what is the shared genetic background between AL, spherical equivalent (that quantifies refractive error), and myopia. Therefore, there is a clear need for research to illuminate the genetic underpinnings of AL.

In this study, we conducted a large multiethnic GWA meta-analysis of AL, including 19,420 individuals from the Genetic Epidemiology Research on Adult Health and Aging (GERA) cohort, with validation of the top associated single nucleotide polymorphisms (SNPs) ($p < 5.0 \times 10^{-8}$) at each locus in 10,851 participants from the CREAM cohorts. We subsequently fine-mapped these AL associations and prioritized causal genes and biological pathways. We then undertook a multiethnic GWA analysis of mean spherical equivalent (MSE) in 72,388 GERA participants and examined associations of lead AL-associated SNPs with MSE. Finally, we investigated the shared genetic effects between AL loci and MSE or myopia.

Methods

GERA cohort and AL measurement

The GERA cohort comprises 110,266 adult men and women who are consented participants in the Research Program on Genes, Environment, and Health, established for members of the Kaiser Permanente Medical Care Plan, Northern California Region (KPNC) (Banda et al., 2015; Kvale et al., 2015). The current study population included 19,420 GERA participants, 18 years and older, who were of non-Hispanic white, Hispanic/Latino, Asian, or African American race/ethnicity, and who had at least one recorded AL measurement on both eyes during the same visit (Table 1). In KPNC, biometry measurements, including AL, are collected using the Haag-Streit Lenstar 900 device prior to cataract surgery. The mean (in millimeters) AL of an individuals' two eyes was used for the analyses. All study procedures were approved by the Institutional Review Board of the Kaiser Foundation Research Institute.

Genotyping and imputation

GERA DNA samples were genotyped at the Genomics Core Facility of the University of California, San Francisco (UCSF) on four ancestry-specific Affymetrix Axiom arrays (Affymetrix, Santa Clara, CA, USA) optimized for individuals of European, Latino, East Asian, and African American ancestry (Hoffmann et al., 2011a; Hoffmann et al., 2011b). Genotype QC (quality control) procedures were performed on an array-wise basis (Kvale et al., 2015), as follows: SNPs with initial genotyping call rate ≥97%, allele frequency difference (≤0.15) between males and females for autosomal markers, and genotype concordance rate (>0.75) across duplicate samples were included.

Imputation was also conducted on an array-wise basis. For imputation, we additionally removed variants with call rates <90%. Genotypes were pre-phased with Eagle (Loh et al., 2016) v2.3.2, and then imputed with Minimac3 (Das et al., 2016) v2.0.1, using two reference panels: variants were preferred if present in the EGA release of the Haplotype Reference Consortium (HRC; n = 27,165; no indels) reference panel (McCarthy et al., 2016), and from the 1000 Genomes Project Phase III release if not (n = 2,504; including indels) (Birney and Soranzo, 2015). As a QC metric, we used the info r^2 from IMPUTE2, which is an estimate of the correlation of the imputed genotype to the true genotype. We considered variants with a good imputation score if $r^2 \geq 0.7$.

TABLE 1 Characteristics of GERA subjects included in the current study by sex, and ethnic group.

		N	AL (mm) Mean ± SD	MSE (diopters), Mean ± SD	Age at 1st AL measurement (years), Mean ± SD
N		19,420	24.07 ± 1.32	−0.38 ± 2.66	75.1 ± 8.7
Myopia					
	Cases	5,448	25.02 ± 1.28	−3.13 ± 2.30	73.0 ± 8.7
	Controls	9,846	23.51 ± 0.93	1.14 ± 1.27	76.3 ± 8.4
Sex	Female	11,501	23.86 ± 1.30	−0.32 ± 2.70	74.5 ± 8.7
	Male	7,919	24.38 ± 1.28	−0.48 ± 2.59	75.9 ± 8.8
Ethnicity	NHW	16,523	24.01 ± 1.26	−0.30 ± 2.59	75.4 ± 8.6
	H/L	1,209	24.01 ± 1.35	0.00 ± 2.52	73.8 ± 9.3
	EAS	1,209	24.88 ± 1.75	−1.94 ± 3.31	72.5 ± 9.4
	AA	479	24.12 ± 1.26	−0.28 ± 2.50	73.4 ± 9.0

Abbreviations: N, number of participants; SD, standard deviation; MSE, mean spherical equivalent; NHW, non-Hispanic white people; H/L, Hispanic/Latinos; EAS, east asians; AA, African-Americans.

GWAS analyses of AL in GERA

Each of the four GERA ethnic groups (non-Hispanic white, Hispanic/Latino, East Asian, and African-American) were first analyzed individually. We performed a linear regression of AL and each SNP using PLINK (Chang et al., 2015) v1.90 (www.cog-genomics.org/plink/1.9/) with the following covariates: age, sex, and ancestry principal components (PCs). The top ten ancestry PCs and the percentage of Ashkenazi (ASHK) ancestry were included as covariates for the non-Hispanic white ethnic group, while the top six ancestry PCs were included for the three other ethnic groups (Banda et al., 2015). The genomic inflation factor λ was calculated for each GWAS analysis to assess inflation due to population stratification (Yang et al., 2011). Data from each genetic variant were modeled using additive dosages to account for the uncertainty of imputation (Huang et al., 2009). The GWAS analyses were also conducted using a recent approach accounting for relatedness that-fits a whole-genome regression model, implemented in REGENIEv2.0.2 (Mbatchou et al., 2021). This new machine-learning method requires only local segments of the genotype matrix to be loaded in memory, making it faster and more efficient in memory use compared to other methods.

We then performed a meta-analysis of AL in GERA by combining the results of the four ethnic groups using the package "meta" of R (https://www.R-project.org) (Balduzzi et al., 2019). Fixed effects and random effects summary estimates were calculated for an additive model. Heterogeneity index, I^2 (0%–100%) and p-value for Cochrane's Q statistic among ethnic groups were assessed. For each locus, the lead SNP was defined as the most significant variant within a 2 Mb window, and novel loci were defined as those that were located over 1 Mb apart from any previously reported locus.

Replication of novel AL-associated loci in CREAM

To test the 5 novel AL-associated SNPs identified in the current study for replication, we evaluated associations in a subset of CREAM participants with AL measurement (Fan et al., 2020). GWAS summary statistics for AL from the study of Fan et al. (Fan et al., 2020), consisting of 10,851 individuals of European and Asian descent from 9 studies, were used for those replication analyses. Among the 5 novel AL-associated SNPs identified in the current study, 2 were available in the CREAM GWAS summary statistics; thus, the Bonferroni threshold was set up at a $p \leq 0.025$ (to account for a total of 2 SNPs tested) for associations that replicated. However, the 5 novel loci were visually inspected by generating regional plots using the European descent CREAM dataset. To generate those regional plots, we used LocusZoom web-based plotting tool (Pruim et al., 2010; Boughton et al., 2021).

COJO (conditional) analysis

To potentially identify independent signals within the 15 identified genomic regions, we performed a multi-SNP-based conditional and joint association analysis (COJO) (Yang et al., 2012), which is implemented in the Genome-wide Complex Trait Analysis (GCTA) integrative tool (Yang et al., 2013). This COJO analysis was conducted on the GERA non-Hispanic white ethnic group GWAS analysis results. To calculate linkage disequilibrium (LD) patterns we used 10,000 random samples from GERA non-Hispanic white ethnic group as a reference panel. For this COJO analysis, a p-value less than 5×10^{-8} was considered significant.

AL array heritability

Array heritability estimate was obtained for AL in GERA non-Hispanic white people (the largest ethnic group of GERA) using LD score regression (Zheng et al., 2017).

Variants prioritization

To prioritize variants within the 15 AL-associated loci identified in the GERA non-Hispanic white ethnic group GWAS analysis, we used a Bayesian approach (CAVIARBF) (Chen et al., 2015). For each of the 15 associated signals, we computed each variant's capacity to explain the

identified signal within a 2 Mb window (±1.0 Mb with respect to the lead SNP). Then, the smallest set of SNPs that included the causal variant with 95% probability (95% credible set) was derived. For this CAVIARBF analysis, we used 10,000 random samples from the GERA non-Hispanic white ethnic group as a reference panel to calculate LD patterns.

VEGAS2 gene-based and pathway analyses

To prioritize genes and biological pathways, we conducted gene-based and pathways association analysis using the Versatile Gene-based Association Study - 2 version 2 (VEGAS2v02) web platform (Mishra and Macgregor, 2015). We first performed a gene-based association analysis on the GERA non-Hispanic white ethnic group GWAS analysis results using the default '-top 100' test that uses all (100%) variants assigned to a gene to compute gene-based *p*-value. We used 1000 Genomes phase 3 European population as the reference panel. As 20,950 genes were tested, the *p*-value adjusted for Bonferroni correction was set as $p < 2.28 \times 10^{-6}$ (0.05/20,950).

Second, we performed a pathway association analysis based on VEGAS2 gene-based *p*-values. We tested enrichment of the genes defined by VEGAS2 in 9,734 pathways or gene-sets derived from the Biosystem's database (https://vegas2.qimrberghofer.edu.au/biosystems20160324.vegas2pathSYM). We adopted the resampling approach to perform this pathway analysis using VEGAS2 derived gene-based *p*-values considering the default '−10 kbloc' parameter as previously described (Iglesias et al., 2018). As 9,734 pathways or gene-sets were tested, the *p*-value adjusted for Bonferroni correction was set as $p < 5.14 \times 10^{-6}$ (0.05/9,734).

Association analysis of lead AL-SNPs with MSE

We evaluated the associations of the 17 lead AL-associated SNPs (sixteen from the multiethnic meta-analysis and an additional one from the non-Hispanic white ethnic group GWA analysis) with MSE by linear regression under an additive model, and adjusting for age, sex, and ancestry PCs. As previously described (Hysi et al., 2020; Choquet et al., 2022), GERA individuals had at least one spherical equivalent value measured during routine eye examinations. Most subjects had multiple measures for both eyes. Spherical equivalent was calculated as the sphere + (cylinder/2). The spherical equivalent was selected from the first documented refraction assessment, and the mean of both eyes was used. After excluding participants with histories of cataract surgery (in either eye), refractive surgery, keratitis or corneal diseases, our GERA sample for this analysis included 72,388 individuals with spherical equivalent measurement from four ethnic groups (Supplementary Table S1). As a note, among those with spherical equivalent measurement, 15,503 (79.8%) were included in the GERA AL sample.

Genetic correlation between AL and MSE or myopia

LD score regressions (Bulik-Sullivan et al., 2015) were conducted, using the LDSC v1.0.1 command line tool (https://github.com/bulik/ldsc), to estimate the genome-wide genetic correlations (r_g) between AL and MSE and between AL and myopia. We used as input data GWAS summary statistics from our previous GWASs of MSE and myopia conducted in the GERA cohort (Choquet et al., 2022) (including 59,094 individuals with RE measurement, and 19,540 myopia cases and 36,487 controls of non-Hispanic white ethnic group). As previously described (Choquet et al., 2022), in GERA, myopia cases were defined as having a MSE ≤ -0.75 diopters (D) and controls as having a MSE > -0.75 D, corresponding to the definition of 'any myopia', as previously used (Hysi et al., 2020). This more myopic threshold (compared to the well-accepted threshold for myopia of MSE ≤ −0.50 D), increases the probability that only "true" myopes are included (Flitcroft et al., 2019).

Results

GERA cohort and AL

The GERA cohort is an unselected cohort of adult members of the KPNC integrated healthcare delivery system, with ongoing longitudinal records from vision examinations. For this study, our GERA sample consisted of 19,420 individuals from 4 ethnic groups (85.1% non-Hispanic white ethnic group, 6.2% Hispanic/Latino, 6.2% East Asian, and 2.5% African American) with a measured AL (Table 1). In our GERA sample, East Asian individuals had higher ALs on average than other groups, consistent with previous studies (Ip et al., 2007; Knight et al., 2012).

Multiethnic genome-wide association study (GWAS) of AL in 19,420 GERA participants

We identified 16 loci that reached genome-wide significance in the GERA meta-analysis, of which 5 were novel: *SLC25A12*, near *BMP3*, *RGR*, *RBFOX1*, and *MYO5B* (Figure 1; Supplementary Table S2; Table 2). The genomic inflation factor, λ, of 1.105, is reasonable for a sample of this size (Yang et al., 2011) (Supplementary Figure S1). Regional plots of the association signals at the 5 novel loci are presented in Supplementary Figure S2. These 16 associations with AL were also examined in each individual ethnic group (Supplementary Table S2) and no other SNPs at the 16 loci identified in the multiethnic GWA meta-analysis reached genome-wide level of significance in East Asians, Hispanic/Latinos, or African Americans from the GERA cohort. While the GWAS results generated using REGENIE (Mbatchou et al., 2021) were similar compared to the results generated using PLINK, we found that *MYO5B* was no longer genome-wide significantly associated with AL using REGENIE (lead SNP rs55754534 *p*-value = 3.0×10^{-7}) (Supplementary Figures S3, S4; Supplementary Table S3). Conducting a GWAS of AL in GERA non-Hispanic white people resulted in the identification of one additional genome-wide significant locus, *PRSS56*, which has been recently reported to be associated with AL in Japanese populations (Fuse et al., 2022) (Supplementary Figures S5, S6; Supplementary Table S4).

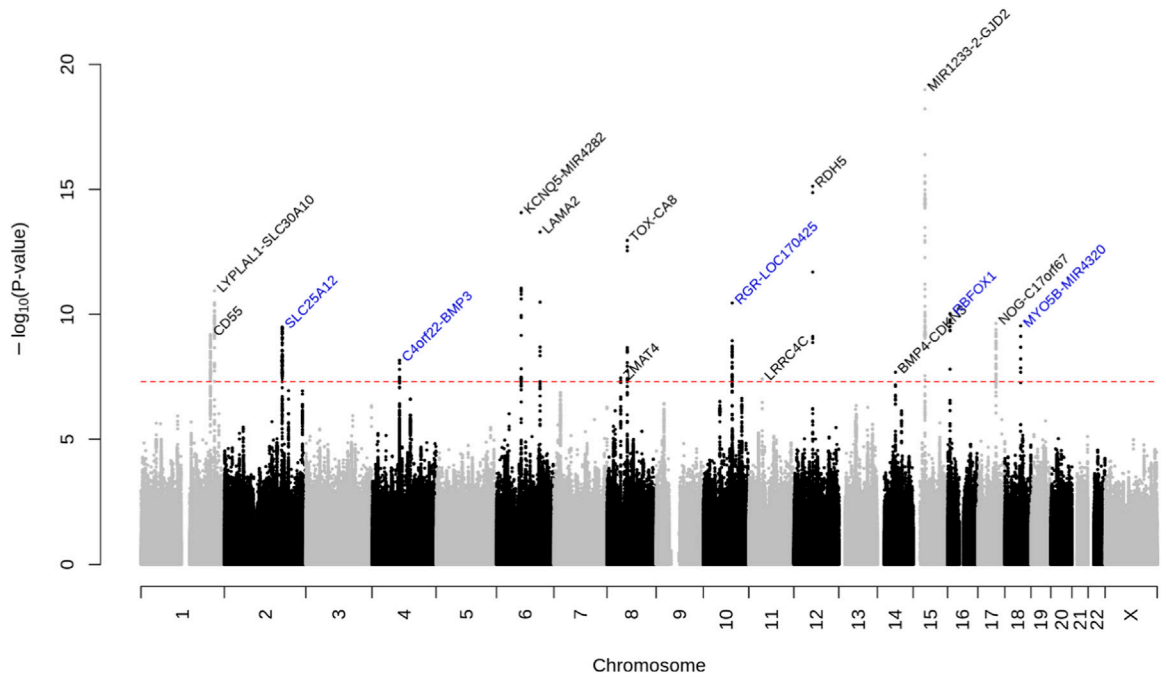

FIGURE 1
Manhattan plot of the multiethnic ancestry GWA meta-analysis of AL in GERA. The *y*-axis represents the -$\log_{10}$(*p*-value); all *p*-values derived from linear regression model are two-sided. The red dotted line represents the threshold of $p = 5.0 \times 10^{-8}$ which is the commonly accepted threshold of adjustments for multiple comparisons in GWAS. Locus names in blue are for the novel loci and the ones in dark are for the previously reported ones.

TABLE 2 Novel AL loci identified in the GERA multiethnic GWA meta-analysis and replication in the CREAM subset.

					Discovery GERA multiethnic meta-analysis				Replication in the (European + Asian ancestry) CREAM subset	
SNP	Chr	Pos	Locus (within or nearest gene)	EA/OA	β (SE)	*P*	*Q*	I^2	β (SE)	*P*
rs57718990	2	172662614	*SLC25A12*	G/T	−0.09 (0.014)	3.26×10^{-10}	0.79	0	NA	NA
rs1353386	4	81947080	*near BMP3*	C/A	−0.10 (0.016)	6.93×10^{-9}	0.41	0	−0.035 (0.015)	0.015
rs140405296	10	86019863	*RGR*	AT/ATT	0.09 (0.013)	3.56×10^{-11}	0.32	14.7	NA	NA
rs58514548	16	7459790	*RBFOX1*	CT/C	0.09 (0.013)	9.46×10^{-11}	0.28	21.1	NA	NA
rs55754534	18	47433745	*MYO5B*	C/G	0.12 (0.018)	2.96×10^{-10}	0.45	0	0.04 (0.019)	0.030

Abbreviations: EA, effect allele; OA, other allele; SE, standard error; I^2, heterogeneity index (0%–100%); and *Q*, *p*-value for Cochrane's Q statistic.

Replication in CREAM dataset

Of the 5 novel lead SNPs, two were available in the CREAM dataset. While lead SNP rs1353386 at *C4orf22-BMP3* replicated at a Bonferroni level of significance ($p \leq 0.025$, 0.05/2 available), SNP rs55754534 at *MYO5B* was nominally associated with AL ($p = 0.030$) in the combined (European and Asian ancestry) CREAM subset (Table 2). In addition, we generated the regional plots at the 5 novel loci using the CREAM European ancestry subset (Supplementary Figure S7), and reported association results for the lead SNPs in CREAM (even if those are different than lead SNPs in GERA) in Supplementary Table S5. Those CREAM results provide evidence of replication at the novel AL identified loci.

Conditional analysis identified additional loci

Conditional (COJO) analysis in the GERA non-Hispanic white ethnic group revealed eight additional independent signals within the identified genomic regions, including at the *CD55*, *LYPLAL1-SLC30A10*, *HAT1*, *PRSS56*, *C4orf22-BMP3*, *RGR-LOC170425*, *RDH5*, and *MYO5B-MIR4320* loci (Supplementary Table S6).

Array heritability for AL

We then estimated the array heritability for AL in the GERA non-Hispanic white ethnic group (the largest group of individuals from GERA) using LD score regression (Zheng et al., 2017), and found an overall heritability estimate of 0.37 (s.e. = 0.04).

Variants prioritization

To prioritize variants within the 15 AL-associated genomic regions identified in the GERA non-Hispanic white ethnic group GWAS analysis, we computed each variant's ability to explain the observed signal and derived the smallest set of variants that included the causal variant with 95% probability (Chen et al., 2015). The 15 credible sets, corresponding to each of the 15 AL-associated loci, contained from one to 74 variants (355 total variants, Supplementary Table S7). Interestingly, two sets included a unique variant (i.e., *KCNQ5-MIR4282* rs7744813, and *LAMA2* rs12193446 with 99.6%, and 99.7% posterior probability of being the causal variants, respectively), suggesting that those variants may be the true causal variants.

Genes and pathways prioritization

To prioritize genes within the 15 AL-associated genomic regions identified in the GERA non-Hispanic white ethnic group GWAS analysis, we performed a gene-based association analysis using the Versatile Gene-based Association Study (VEGAS2v02) integrative tool (Mishra and Macgregor, 2015). We identified 11 significant genes for AL after correcting for multiple testing (Bonferroni correction was set as $p < 2.28 \times 10^{-6}$ (0.05/21,950 genes tested)), including *BMP4*, *PRSS56*, and *RGR* (Supplementary Table S8).

We then conducted a pathway analysis using VEGAS2v02 and based on the gene-based association results to assess enrichment in 9,734 pathways (or gene-sets) derived from the Biosystem's database. We found that pathways involving the cranial skeleton system development as well as the elastic fiber formation were significantly enriched after correcting for multiple testing (Bonferroni correction was set as $p < 5.14 \times 10^{-6}$ (0.05/9,734 pathways tested)) (Supplementary Table S9).

Association of lead AL-SNPs with myopic refractive error

As previous studies have reported that AL is significantly higher in eyes with myopia compared to normal eyes (Adams, 1987; Grosvenor, 1988; Tideman et al., 2018), we evaluated the effect estimates of the 17 AL-SNPs identified in the current study between AL and MSE in GERA. Our GERA MSE sample consisted of 72,388 participants (Supplementary Table S1). All of the 17 AL-associated SNPs were significantly associated with MSE after Bonferroni correction ($p < 0.05/17 = 2.94 \times 10^{-3}$), including 15 at genome-wide level of significance (Supplementary Table S10). The Pearson correlation coefficient between AL effect size (beta) and the MSE effect size (beta) was −0.86 ($p = 1.23 \times 10^{-5}$; Figure 2).

AL shares genetic determinants with RE and myopia

We also performed genome-wide genetic correlation analyses to quantify genetic overlap between AL and MSE or myopia risk in GERA non-Hispanic white people. We found that AL was genetically correlated with MSE ($r_g = -0.83$; SE, 0.04; $p = 1.95 \times 10^{-89}$) and myopia ($r_g = 0.80$; SE, 0.05; $p = 2.84 \times 10^{-55}$). These results suggest considerable shared genetic influences between AL and myopic refractive error.

Discussion

In this study, by conducting a multiethnic GWA meta-analysis across four ethnic groups, we identified 16 genetic loci for AL, of which 5 were not previously identified. In addition, we reported a genome-wide association at *PRSS56* with AL in non-Hispanic white people. We found that all AL-associated loci were significantly associated with myopic refractive error and observed significant shared genetic effects between AL and MSE or myopia. Finally, we prioritized causal variants, genes, and pathways for AL using bioinformatic functional analyses.

Among the novel GWAS-identified associations with AL, our study revealed potential candidate genes, including *SLC25A12, BMP3*, *RGR*, *RBFOX1,* and *MYO5B*, which have all been linked to visual function or eye development and have been implicated in vision disorders (Kiefer et al., 2013; Stambolian et al., 2013; Verhoeven et al., 2013; Hysi et al., 2020). *SLC25A12* encodes the solute carrier family 25 member 12, which is a calcium-binding mitochondrial carrier protein involved in the exchange of aspartate for glutamate across the inner mitochondrial membrane. Mice lacking *Slc25a12* present with an altered vision (Contreras et al., 2016), as *Slc25a12* plays a pivotal role in retina metabolism providing *de novo* synthesis pathway for glutamine, protects glutamate from oxidation, and is required for efficient glucose oxidative metabolism. Interestingly, our lead AL-associated SNP (rs57718990) at *SLC25A12* has been previously reported to be associated with myopia age-of-onset (Wojciechowski and Cheng, 2018). *BMP3* encodes the bone morphogenetic protein 3, which is a secreted ligand of the TGF-β (transforming growth factor-beta) superfamily of proteins. Polymorphisms at *BMP3* have been previously reported to be associated with RE and myopia (Kiefer et al., 2013; Verhoeven et al., 2013; Hysi et al., 2020), retinal detachment (Boutin et al., 2020), and ocular coloboma (Fox et al., 2022), a congenital disorder characterized by gaps in ocular tissues. BMP3 is found to be localized in the corneal keratocytes and has been proposed to be important for producing and maintaining the extracellular matrix of the corneal stroma (Scott et al., 2011). Our study also identified *RGR*, which encodes a retinal G protein coupled receptor that is largely expressed in intracellular membranes of retinal pigment epithelium and Müller cells (Lin et al., 2007; Zhang and Fong, 2018). A recent study has suggested that light-driven visual cycle that depends on RGR contributes to sustained cone

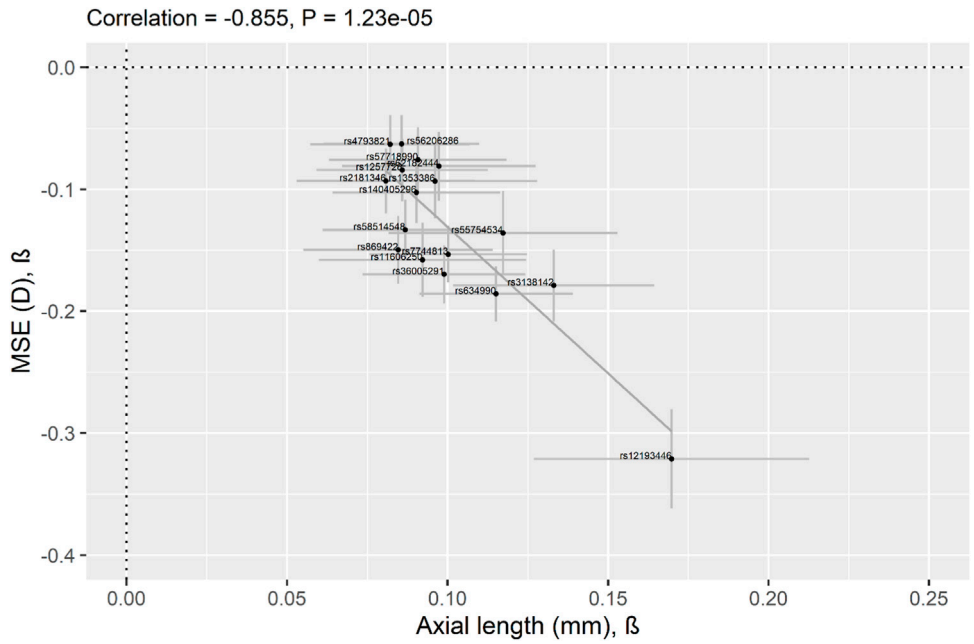

FIGURE 2
Correlation of effect sizes across studies (AL vs. myopic refractive error) for the lead 17 AL-associated lead SNPs identified in the current study. Comparison of regression coefficients for AL in 19,420 GERA participants (*x*-axis) and for MSE in 72,388 GERA participants (*y*-axis). Pearson's correlation coefficient = −0.86. Regression Coefficients (betas) are shown, and 95% confidence intervals (CI) are displayed (the horizontal line for each SNP represents the 95% CI of the AL analysis and the vertical line for each SNP represents the 95% CI of the MSE analysis). The 17 AL-associated lead SNPs are shown as black dots and the solid line indicates the line of best fit through the 17 AL lead SNPs.

vision under daylight conditions (Morshedian et al., 2019). Mutations in this *RGR* gene have been shown to be associated with retinitis pigmentosa (Morimura et al., 1999; Wang et al., 2001) and different forms of retinal diseases (Li et al., 2016). Our study also implicated *RBFOX1* encoding the RNA binding fox-1 homolog 1, which is expressed in retinal ganglion cells and in amacrine cells of mammalian retinas and has a crucial role in visual function and survival of injured retinal ganglion cells in mice (Gu et al., 2022). Polymorphisms at *RBFOX1* have been shown to be associated with pseudoexfoliation syndrome (Zagajewska et al., 2018). Importantly, polymorphisms at both *RGR* and *RBFOX1* have been previously reported to be associated with refractive error and myopia (Kiefer et al., 2013; Stambolian et al., 2013; Verhoeven et al., 2013; Hysi et al., 2020). Our study also identified *MYO5B* that encodes the myosin VB, involved in the MYO5B-Rab10 system which is required for axon development of vertebrate neocortical neurons or zebrafish retinal ganglion cells *in vivo* (Liu et al., 2013).

Our study also reports, for the first time to our knowledge, a genome-wide association at *PRSS56* with AL in European ancestry individuals. Consistently, a recent GWAS in Japanese populations reported *PRSS56* as an AL-associated locus (Fuse et al., 2022). PRSS56 is a serine protease secreted by retinal Müller glia that has previously been implicated in ocular axial growth (Paylakhi et al., 2018; Koli et al., 2021). *PRSS56* mutations are a major cause of nanophthalmos, characterized by severe shortening of ocular axial length and high hyperopia (Gal et al., 2011; Nair et al., 2011; Orr et al., 2011), and polymorphisms at *PRSS56* have been previously reported to be associated with RE and myopia (Kiefer et al., 2013; Verhoeven et al., 2013; Hysi et al., 2020), angle-closure glaucoma (Nair et al., 2011; Jiang et al., 2013), and ocular abnormalities in humans and mice (Labelle-Dumais et al., 2020; Siggs et al., 2020). Using conditional gene targeting strategies in mice, it has been demonstrated that the loss of PRSS56 function in retinal Müller glia results in a shorter ocular axial length compared to those in control animals (Paylakhi et al., 2018). Furthermore, time-specific inactivation of PRSS56 during post-eye opening period in mice have suggested that sustained PRSS56 activity is required for ocular axial growth during stages including when ocular growth is sensitive to visual input (Paylakhi et al., 2018). Interestingly, retinal *Prss56* expression levels are upregulated in response to lens-induced hyperopic defocus that caused ocular axial elongation/myopia in marmosets suggesting a potential of Prss56 in emmetropization, which is avision-guided process ocular growth (Tkatchenko et al., 2018).

Our multiethnic GWAS of AL identified 2 previously reported loci (*ZMAT4* and *BMP4-CDKN3*) that did not reach genome-wide level of significance in our non-Hispanic white GWAS. Interestingly, both *ZMAT4* and *BMP4-CDKN3* have been recently identified as AL-associated loci in a recent GWAS conducted in Japanese individuals (Fuse et al., 2022). Common genetic variants at those *ZMAT4* and *BMP4-CDKN3* loci have been previously reported to be associated with MSE, and high myopia, especially in Asian populations (Yoshikawa et al., 2014; Cheong et al., 2020). More recently, a whole exome sequencing study for refractive error conducted in 51,624 unrelated adults of European ancestry identified novel putative causal variants in the *BMP4* gene (Guggenheim et al., 2022).

In our study, all AL-associated loci were significantly associated with myopic refractive error and we also observed significant genetic correlations between AL and MSE or myopia. Interestingly, a recent

GWAS of corneal curvature, which serves as a proxy for eye size, identified 32 loci and revealed a lack of genetic correlation between eye size and refractive error (Plotnikov et al., 2021). This suggests that genetic variants associated with human eye size are distinct from those conferring susceptibility to myopia. In this recent GWAS of corneal curvature (Plotnikov et al., 2021), the authors also reported significant genetic correlations between corneal curvature and eye size and between eye size and body height. Thus, AL and corneal curvature are two distinct traits and while AL is a relevant endophenotype for refractive error and myopia, corneal curvature reflects more eye size and body height.

Our bioinformatic annotation analyses revealed potential biological pathways involved in AL variation that are relevant to the embryonic cranial skeleton morphogenesis and the elastic fibers formation, consistent with previous works (Ouyang et al., 2019). Overall, the identified genes suggest a role for extracellular matrix remodeling, visual cycle and neuronal development in the determination of AL, similar to those previously suggested to participate in myopia pathogenesis (Kiefer et al., 2013). Follow-up functional experiments utilizing animal models could confirm the involvement of these biological pathways in AL variation and provide insights into the underlying mechanisms of AL-related vision disorders such as myopia.

We recognize potential limitations of our study. First, our study was limited by its restriction to common variants (minor allele frequency ≥1%), which did not allow us to identify lower frequency variants that contribute to variation in AL. Future whole-exome sequencing studies could identify less common variants associated with AL. Second, in our study, we note that the Hispanic/Latino, East Asian, and African American subgroups had smaller sample sizes compared to the non-Hispanic white ethnic group, potentially limiting statistical power to detect some SNP associations in those groups. Future large and ethnically diverse studies will be needed to uncover the genetic architecture of AL in those ethnic groups.

In summary, our large multiethnic GWA meta-analysis provides new insights into the genetic architecture of AL. In addition to expanding the list of AL-associated loci, this study also provides evidence of shared genetic etiology between AL and MSE, or myopia. Altogether, study findings may open new avenues of investigation into eye biometry and its relationship to the risk of vision disorders, such as myopia.

Data availability statement

The multiethnic GERA GWAS summary statistics are available from the NHGRI-EBI GWAS Catalog (https://www.ebi.ac.uk/gwas/downloads/summary-statistics). The GERA genotype data are available upon application to the KP Research Bank (https://researchbank.kaiserpermanente.org/). Pathways or gene-sets were derived from the Biosystem's database which can be accessed through the following link (https://vegas2.qimrberghofer.edu.au/biosystems20160324.vegas2pathSYM).

Ethics statement

The studies involving human participants were reviewed and approved by Institutional Review Board of the Kaiser Foundation Research Institute. The patients/participants provided their written informed consent to participate in this study.

Author contributions

CJ, EJ, and HC conceived and designed the study. EJ was involved in the genotyping and quality control of the GERA cohort. CJ, in collaboration with RM, extracted phenotype data from electronic health records. CJ and JY performed GWAS and post-GWAS analyses. QF, XG, C-YC, MH, DM, JG, and CK provided GWAS replication results from the CREAM dataset and reviewed and revised the manuscript. CJ and HC interpreted the results of analyses and wrote the manuscript with help from RM, KN, and EJ. All authors contributed to the article and approved the submitted version.

Funding

Genotyping of the GERA cohort was funded by a grant from the National Institute on Aging, National Institute of Mental Health, and National Institute of Health Common Fund (RC2AG036607). Support for GERA participant enrollment, survey completion, and biospecimen collection for the Research Program on Genes, Environment and Health was provided by the Robert Wood Johnson Foundation, the Wayne and Gladys Valley Foundation, the Ellison Medical Foundation, and Kaiser Permanente Community Benefit Programs. The study was funded by the National Eye Institute (NEI) (R01EY027004 to HC). KSN is supported by NEI R01EY032666.

Acknowledgments

We are grateful to the Kaiser Permanente Northern California members who have generously agreed to participate in the Kaiser Permanente Research Program on Genes, Environment, and Health.

Conflict of interest

The authors declare that the research was conducted in the absence of any commercial or financial relationships that could be construed as a potential conflict of interest.

Publisher's note

Supplementary material

The Supplementary Material for this article can be found online at: https://www.frontiersin.org/articles/10.3389/fgene.2023.1113058/full#supplementary-material

References

Adams, A. J. (1987). Axial length elongation, not corneal curvature, as a basis of adult onset myopia. *Am. J. Optom. Physiol. Opt.* 64 (2), 150–152. doi:10.1097/00006324-198702000-00012

Arias, L., Caminal, J. M., Rubio, M. J., Cobos, E., Garcia-Bru, P., Filloy, A., et al. (2015). Autofluorescence and axial length as prognostic factors for outcomes of macular hole retinal detachment surgery in high myopia. *Retina* 35 (3), 423–428. doi:10.1097/IAE.0000000000000335

Balduzzi, S., Rucker, G., and Schwarzer, G. (2019). How to perform a meta-analysis with R: A practical tutorial. *Evid. Based Ment. Health* 22 (4), 153–160. doi:10.1136/ebmental-2019-300117

Banda, Y., Kvale, M. N., Hoffmann, T. J., Hesselson, S. E., Ranatunga, D., Tang, H., et al. (2015). Characterizing race/ethnicity and genetic ancestry for 100,000 subjects in the genetic Epidemiology research on adult health and aging (GERA) cohort. *Genetics* 200 (4), 1285–1295. doi:10.1534/genetics.115.178616

Biino, G., Palmas, M. A., Corona, C., Prodi, D., Fanciulli, M., Sulis, R., et al. (2005). Ocular refraction: Heritability and genome-wide search for eye morphometry traits in an isolated Sardinian population. *Hum. Genet.* 116 (3), 152–159. doi:10.1007/s00439-004-1231-6

Birney, E., and Soranzo, N. (2015). Human genomics: The end of the start for population sequencing. *Nature* 526 (7571), 52–53. doi:10.1038/526052a

Boughton, A. P., Welch, R. P., Flickinger, M., VandeHaar, P., Taliun, D., Abecasis, G. R., et al. (2021). LocusZoom.js: Interactive and embeddable visualization of genetic association study results. *Bioinformatics* 37 (18), 3017–3018. doi:10.1093/bioinformatics/btab186

Boutin, T. S., Charteris, D. G., Chandra, A., Campbell, S., Hayward, C., Campbell, A., et al. (2020). Insights into the genetic basis of retinal detachment. *Hum. Mol. Genet.* 29 (4), 689–702. doi:10.1093/hmg/ddz294

Bulik-Sullivan, B. K., Loh, P. R., Finucane, H. K., Ripke, S., Yang, J., et al.Schizophrenia Working Group of the Psychiatric Genomics, et al. (2015). LD Score regression distinguishes confounding from polygenicity in genome-wide association studies. *Nat. Genet.* 47(3), 291–295. doi:10.1038/ng.3211

Chang, C. C., Chow, C. C., Tellier, L. C., Vattikuti, S., Purcell, S. M., and Lee, J. J. (2015). Second-generation PLINK: Rising to the challenge of larger and richer datasets. *GigaScience* 4, 7. doi:10.1186/s13742-015-0047-8

Chen, C. Y., Scurrah, K. J., Stankovich, J., Garoufalis, P., Dirani, M., Pertile, K. K., et al. (2007). Heritability and shared environment estimates for myopia and associated ocular biometric traits: The genes in myopia (GEM) family study. *Hum. Genet.* 121 (3-4), 511–520. doi:10.1007/s00439-006-0312-0

Chen, W., Larrabee, B. R., Ovsyannikova, I. G., Kennedy, R. B., Haralambieva, I. H., Poland, G. A., et al. (2015). Fine mapping causal variants with an approximate bayesian method using marginal test statistics. *Genetics* 200 (3), 719–736. doi:10.1534/genetics.115.176107

Cheng, C. Y., Schache, M., Ikram, M. K., Young, T. L., Guggenheim, J. A., Vitart, V., et al. (2013). Nine loci for ocular axial length identified through genome-wide association studies, including shared loci with refractive error. *Am. J. Hum. Genet.* 93 (2), 264–277. doi:10.1016/j.ajhg.2013.06.016

Cheong, K. X., Yong, R. Y. Y., Tan, M. M. H., Tey, F. L. K., and Ang, B. C. H. (2020). Association of VIPR2 and ZMAT4 with high myopia. *Ophthalmic Genet.* 41 (1), 41–48. doi:10.1080/13816810.2020.1737951

Choquet, H., Khawaja, A. P., Jiang, C., Yin, J., Melles, R. B., Glymour, M. M., et al. (2022). Association between myopic refractive error and primary open-angle glaucoma: A 2-sample mendelian randomization study. *JAMA Ophthalmol.* 140 (9), 864–871. doi:10.1001/jamaophthalmol.2022.2762

Contreras, L., Ramirez, L., Du, J., Hurley, J. B., Satrustegui, J., and de la Villa, P. (2016). Deficient glucose and glutamine metabolism in Aralar/AGC1/Slc25a12 knockout mice contributes to altered visual function. *Mol. Vis.* 22, 1198–1212.

Das, S., Forer, L., Schonherr, S., Sidore, C., Locke, A. E., Kwong, A., et al. (2016). Next-generation genotype imputation service and methods. *Nat. Genet.* 48 (10), 1284–1287. doi:10.1038/ng.3656

Dirani, M., Chamberlain, M., Shekar, S. N., Islam, A. F., Garoufalis, P., Chen, C. Y., et al. (2006). Heritability of refractive error and ocular biometrics: The genes in myopia (GEM) twin study. *Invest. Ophthalmol. Vis. Sci.* 47 (11), 4756–4761. doi:10.1167/iovs.06-0270

Fan, Q., Barathi, V. A., Cheng, C. Y., Zhou, X., Meguro, A., Nakata, I., et al. (2012). Genetic variants on chromosome 1q41 influence ocular axial length and high myopia. *PLoS Genet.* 8 (6), e1002753. doi:10.1371/journal.pgen.1002753

Fan, Q., Pozarickij, A., Tan, N. Y. Q., Guo, X., Verhoeven, V. J. M., Vitart, V., et al. (2020). Genome-wide association meta-analysis of corneal curvature identifies novel loci and shared genetic influences across axial length and refractive error. *Commun. Biol.* 3 (1), 133. doi:10.1038/s42003-020-0802-y

Flitcroft, D. I., He, M., Jonas, J. B., Jong, M., Naidoo, K., Ohno-Matsui, K., et al. (2019). Imi - defining and classifying myopia: A proposed set of standards for clinical and epidemiologic studies. *Invest. Ophthalmol. Vis. Sci.* 60 (3), M20–M30. doi:10.1167/iovs.18-25957

Fonteh, C. N., Patnaik, J. L., Grove, N. C., Lynch, A. M., and Christopher, K. L. (2022). Predictors of pseudophakic retinal tears at a tertiary care academic medical center. *Ophthalmol. Retina* 6 (6), 450–456. doi:10.1016/j.oret.2022.01.010

Foo, L. L., Xu, L., Sabanayagam, C., Htoon, H. M., Ang, M., Zhang, J., et al. (2022). Predictors of myopic macular degeneration in a 12-year longitudinal study of Singapore adults with myopia. *Br. J. Ophthalmol.* 2021, 321046. doi:10.1136/bjophthalmol-2021-321046

Fox, S. C., Widen, S. A., Asai-Coakwell, M., Havrylov, S., Benson, M., Prichard, L. B., et al. (2022). BMP3 is a novel locus involved in the causality of ocular coloboma. *Hum. Genet.* 141 (8), 1385–1407. doi:10.1007/s00439-022-02430-3

Fuse, N., Sakurai, M., Motoike, I. N., Kojima, K., Takai-Igarashi, T., Nakaya, N., et al. (2022). Genome-wide association study of axial length in population-based cohorts in Japan: The tohoku medical megabank organization eye study. *Ophthalmol. Sci.* 2 (1), 100113. doi:10.1016/j.xops.2022.100113

Gal, A., Rau, I., El Matri, L., Kreienkamp, H. J., Fehr, S., Baklouti, K., et al. (2011). Autosomal-recessive posterior microphthalmos is caused by mutations in PRSS56, a gene encoding a trypsin-like serine protease. *Am. J. Hum. Genet.* 88 (3), 382–390. doi:10.1016/j.ajhg.2011.02.006

Grosvenor, T. (1988). High axial length/corneal radius ratio as a risk factor in the development of myopia. *Am. J. Optom. Physiol. Opt.* 65 (9), 689–696. doi:10.1097/00006324-198809000-00001

Gu, L., Kwong, J. M. K., Caprioli, J., and Piri, N. (2022). Visual function and survival of injured retinal ganglion cells in aged Rbfox1 knockout animals. *Cells* 11 (21), 3401. doi:10.3390/cells11213401

Guggenheim, J. A., Clark, R., Cui, J., Terry, L., Patasova, K., Haarman, A. E. G., et al. (2022). Whole exome sequence analysis in 51 624 participants identifies novel genes and variants associated with refractive error and myopia. *Hum. Mol. Genet.* 31 (11), 1909–1919. doi:10.1093/hmg/ddac004

Guggenheim, J. A., Zhou, X., Evans, D. M., Timpson, N. J., McMahon, G., Kemp, J. P., et al. (2013). Coordinated genetic scaling of the human eye: Shared determination of axial eye length and corneal curvature. *Invest. Ophthalmol. Vis. Sci.* 54 (3), 1715–1721. doi:10.1167/iovs.12-10560

Hoffmann, T. J., Kvale, M. N., Hesselson, S. E., Zhan, Y., Aquino, C., Cao, Y., et al. (2011a). Next generation genome-wide association tool: Design and coverage of a high-throughput European-optimized SNP array. *Genomics* 98 (2), 79–89. doi:10.1016/j.ygeno.2011.04.005

Hoffmann, T. J., Zhan, Y., Kvale, M. N., Hesselson, S. E., Gollub, J., Iribarren, C., et al. (2011b). Design and coverage of high throughput genotyping arrays optimized for individuals of East Asian, African American, and Latino race/ethnicity using imputation and a novel hybrid SNP selection algorithm. *Genomics* 98 (6), 422–430. doi:10.1016/j.ygeno.2011.08.007

Huang, L., Wang, C., and Rosenberg, N. A. (2009). The relationship between imputation error and statistical power in genetic association studies in diverse populations. *Am. J. Hum. Genet.* 85 (5), 692–698. doi:10.1016/j.ajhg.2009.09.017

Hysi, P. G., Choquet, H., Khawaja, A. P., Wojciechowski, R., Tedja, M. S., Yin, J., et al. (2020). Meta-analysis of 542,934 subjects of European ancestry identifies new genes and mechanisms predisposing to refractive error and myopia. *Nat. Genet.* 52 (4), 401–407. doi:10.1038/s41588-020-0599-0

Iglesias, A. I., Mishra, A., Vitart, V., Bykhovskaya, Y., Hohn, R., Springelkamp, H., et al. (2018). Cross-ancestry genome-wide association analysis of corneal thickness strengthens link between complex and Mendelian eye diseases. *Nat. Commun.* 9 (1), 1864. doi:10.1038/s41467-018-03646-6

Ip, J. M., Huynh, S. C., Kifley, A., Rose, K. A., Morgan, I. G., Varma, R., et al. (2007). Variation of the contribution from axial length and other oculometric parameters to refraction by age and ethnicity. *Invest. Ophthalmol. Vis. Sci.* 48 (10), 4846–4853. doi:10.1167/iovs.07-0101

Jiang, D., Yang, Z., Li, S., Xiao, X., Jia, X., Wang, P., et al. (2013). Evaluation of PRSS56 in Chinese subjects with high hyperopia or primary angle-closure glaucoma. *Mol. Vis.* 19, 2217–2226.

Kiefer, A. K., Tung, J. Y., Do, C. B., Hinds, D. A., Mountain, J. L., Francke, U., et al. (2013). Genome-wide analysis points to roles for extracellular matrix remodeling, the visual cycle, and neuronal development in myopia. *PLoS Genet.* 9 (2), e1003299. doi:10.1371/journal.pgen.1003299

Klein, A. P., Suktitipat, B., Duggal, P., Lee, K. E., Klein, R., Bailey-Wilson, J. E., et al. (2009). Heritability analysis of spherical equivalent, axial length, corneal curvature, and anterior chamber depth in the Beaver Dam Eye Study. *Arch. Ophthalmol.* 127 (5), 649–655. doi:10.1001/archophthalmol.2009.61

Knight, O. J., Girkin, C. A., Budenz, D. L., Durbin, M. K., Feuer, W. J., and Cirrus, O. C. T. N. D. S. G. (2012). Effect of race, age, and axial length on optic nerve head parameters and retinal nerve fiber layer thickness measured by Cirrus HD-OCT. *Arch. Ophthalmol.* 130 (3), 312–318. doi:10.1001/archopthalmol.2011.1576

Koli, S., Labelle-Dumais, C., Zhao, Y., Paylakhi, S., and Nair, K. S. (2021). Identification of MFRP and the secreted serine proteases PRSS56 and

ADAMTS19 as part of a molecular network involved in ocular growth regulation. *PLoS Genet.* 17 (3), e1009458. doi:10.1371/journal.pgen.1009458

Kvale, M. N., Hesselson, S., Hoffmann, T. J., Cao, Y., Chan, D., Connell, S., et al. (2015). Genotyping informatics and quality control for 100,000 subjects in the genetic Epidemiology research on adult health and aging (GERA) cohort. *Genetics* 200 (4), 1051–1060. doi:10.1534/genetics.115.178905

Labelle-Dumais, C., Pyatla, G., Paylakhi, S., Tolman, N. G., Hameed, S., Seymens, Y., et al. (2020). Loss of PRSS56 function leads to ocular angle defects and increased susceptibility to high intraocular pressure. *Dis. Model Mech.* 13 (5), dmm042853. doi:10.1242/dmm.042853

Li, J., Xiao, X., Li, S., Jia, X., Guo, X., and Zhang, Q. (2016). RGR variants in different forms of retinal diseases: The undetermined role of truncation mutations. *Mol. Med. Rep.* 14 (5), 4811–4815. doi:10.3892/mmr.2016.5847

Lin, M. Y., Kochounian, H., Moore, R. E., Lee, T. D., Rao, N., and Fong, H. K. (2007). Deposition of exon-skipping splice isoform of human retinal G protein-coupled receptor from retinal pigment epithelium into Bruch's membrane. *Mol. Vis.* 13, 1203–1214.

Liu, Y., Xu, X. H., Chen, Q., Wang, T., Deng, C. Y., Song, B. L., et al. (2013). Myosin Vb controls biogenesis of post-Golgi Rab10 carriers during axon development. *Nat. Commun.* 4, 2005. doi:10.1038/ncomms3005

Loh, P. R., Danecek, P., Palamara, P. F., and Fuchsberger, C. (2016). Reference-based phasing using the Haplotype reference Consortium panel. *Nat. Genet.* 48 (11), 1443–1448. doi:10.1038/ng.3679

Mbatchou, J., Barnard, L., Backman, J., Marcketta, A., Kosmicki, J. A., Ziyatdinov, A., et al. (2021). Computationally efficient whole-genome regression for quantitative and binary traits. *Nat. Genet.* 53 (7), 1097–1103. doi:10.1038/s41588-021-00870-7

McCarthy, S., Das, S., Kretzschmar, W., Delaneau, O., Wood, A. R., Teumer, A., et al. (2016). A reference panel of 64,976 haplotypes for genotype imputation. *Nat. Genet.* 48 (10), 1279–1283. doi:10.1038/ng.3643

Mishra, A., and Macgregor, S. (2015). VEGAS2: Software for more flexible gene-based testing. *Twin Res. Hum. Genet.* 18 (1), 86–91. doi:10.1017/thg.2014.79

Miyake, M., Yamashiro, K., Tabara, Y., Suda, K., Morooka, S., Nakanishi, H., et al. (2015). Identification of myopia-associated WNT7B polymorphisms provides insights into the mechanism underlying the development of myopia. *Nat. Commun.* 6, 6689. doi:10.1038/ncomms7689

Morimura, H., Saindelle-Ribeaudeau, F., Berson, E. L., and Dryja, T. P. (1999). Mutations in RGR, encoding a light-sensitive opsin homologue, in patients with retinitis pigmentosa. *Nat. Genet.* 23 (4), 393–394. doi:10.1038/70496

Morshedian, A., Kaylor, J. J., Ng, S. Y., Tsan, A., Frederiksen, R., Xu, T., et al. (2019). Light-driven regeneration of cone visual pigments through a mechanism involving RGR opsin in muller glial cells. *Neuron* 102 (6), 1172–1183. doi:10.1016/j.neuron.2019.04.004

Mu, J., Zeng, D., Fan, J., Liu, M., Zhong, H., Shuai, X., et al. (2022). The accuracy of the axial length and axial length/corneal radius ratio for myopia assessment among Chinese children. *Front. Pediatr.* 10, 859944. doi:10.3389/fped.2022.859944

Nair, K. S., Hmani-Aifa, M., Ali, Z., Kearney, A. L., Ben Salem, S., Macalinao, D. G., et al. (2011). Alteration of the serine protease PRSS56 causes angle-closure glaucoma in mice and posterior microphthalmia in humans and mice. *Nat. Genet.* 43 (6), 579–584. doi:10.1038/ng.813

Omodaka, K., Kikawa, T., Kabakura, S., Himori, N., Tsuda, S., Ninomiya, T., et al. (2022). Clinical characteristics of glaucoma patients with various risk factors. *BMC Ophthalmol.* 22 (1), 373. doi:10.1186/s12886-022-02587-5

Orr, A., Dube, M. P., Zenteno, J. C., Jiang, H., Asselin, G., Evans, S. C., et al. (2011). Mutations in a novel serine protease PRSS56 in families with nanophthalmos. *Mol. Vis.* 17, 1850–1861.

Ouyang, X., Han, Y., Xie, Y., Wu, Y., Guo, S., Cheng, M., et al. (2019). The collagen metabolism affects the scleral mechanical properties in the different processes of scleral remodeling. *Biomed. Pharmacother.* 118, 109294. doi:10.1016/j.biopha.2019.109294

Paget, S., Vitezica, Z. G., Malecaze, F., and Calvas, P. (2008). Heritability of refractive value and ocular biometrics. *Exp. Eye Res.* 86 (2), 290–295. doi:10.1016/j.exer.2007.11.001

Paylakhi, S., Labelle-Dumais, C., Tolman, N. G., Sellarole, M. A., Seymens, Y., Saunders, J., et al. (2018). Muller glia-derived PRSS56 is required to sustain ocular axial growth and prevent refractive error. *PLoS Genet.* 14 (3), e1007244. doi:10.1371/journal.pgen.1007244

Plotnikov, D., Cui, J., Clark, R., Wedenoja, J., Parssinen, O., Tideman, J. W. L., et al. (2021). Genetic variants associated with human eye size are distinct from those conferring susceptibility to myopia. *Invest. Ophthalmol. Vis. Sci.* 62 (13), 24. doi:10.1167/iovs.62.13.24

Pruim, R. J., Welch, R. P., Sanna, S., Teslovich, T. M., Chines, P. S., Gliedt, T. P., et al. (2010). LocusZoom: Regional visualization of genome-wide association scan results. *Bioinformatics* 26 (18), 2336–2337. doi:10.1093/bioinformatics/btq419

Rezapour, J., Bowd, C., Dohleman, J., Belghith, A., Proudfoot, J. A., Christopher, M., et al. (2021). The influence of axial myopia on optic disc characteristics of glaucoma eyes. *Sci. Rep.* 11 (1), 8854. doi:10.1038/s41598-021-88406-1

Scott, S. G., Jun, A. S., and Chakravarti, S. (2011). Sphere formation from corneal keratocytes and phenotype specific markers. *Exp. Eye Res.* 93 (6), 898–905. doi:10.1016/j.exer.2011.10.004

Siggs, O. M., Awadalla, M. S., Souzeau, E., Staffieri, S. E., Kearns, L. S., Laurie, K., et al. (2020). The genetic and clinical landscape of nanophthalmos and posterior microphthalmos in an Australian cohort. *Clin. Genet.* 97 (5), 764–769. doi:10.1111/cge.13722

Stambolian, D., Wojciechowski, R., Oexle, K., Pirastu, M., Li, X., Raffel, L. J., et al. (2013). Meta-analysis of genome-wide association studies in five cohorts reveals common variants in RBFOX1, a regulator of tissue-specific splicing, associated with refractive error. *Hum. Mol. Genet.* 22 (13), 2754–2764. doi:10.1093/hmg/ddt116

Streho, M., Perrenoud, F., Abraham, N., Hawa, K., Puech, M., and Giocanti-Auregan, A. (2019). Predominantly superior retinal tears detected by B-scan ultrasonography. *J. Ophthalmol.* 2019, 7105246. doi:10.1155/2019/7105246

Tideman, J. W. L., Polling, J. R., Vingerling, J. R., Jaddoe, V. W. V., Williams, C., Guggenheim, J. A., et al. (2018). Axial length growth and the risk of developing myopia in European children. *Acta Ophthalmol.* 96 (3), 301–309. doi:10.1111/aos.13603

Tideman, J. W., Snabel, M. C., Tedja, M. S., van Rijn, G. A., Wong, K. T., Kuijpers, R. W., et al. (2016). Association of axial length with risk of uncorrectable visual impairment for Europeans with myopia. *JAMA Ophthalmol.* 134 (12), 1355–1363. doi:10.1001/jamaophthalmol.2016.4009

Tkatchenko, T. V., Troilo, D., Benavente-Perez, A., and Tkatchenko, A. V. (2018). Gene expression in response to optical defocus of opposite signs reveals bidirectional mechanism of visually guided eye growth. *PLoS Biol.* 16 (10), e2006021. doi:10.1371/journal.pbio.2006021

Verhoeven, V. J., Hysi, P. G., Wojciechowski, R., Fan, Q., Guggenheim, J. A., Hohn, R., et al. (2013). Genome-wide meta-analyses of multiancestry cohorts identify multiple new susceptibility loci for refractive error and myopia. *Nat. Genet.* 45 (3), 314–318. doi:10.1038/ng.2554

Visscher, P. M., Wray, N. R., Zhang, Q., Sklar, P., McCarthy, M. I., Brown, M. A., et al. (2017). 10 Years of GWAS discovery: Biology, function, and translation. *Am. J. Hum. Genet.* 101 (1), 5–22. doi:10.1016/j.ajhg.2017.06.005

Wang, Q., Chen, Q., Zhao, K., Wang, L., Wang, L., and Traboulsi, E. I. (2001). Update on the molecular genetics of retinitis pigmentosa. *Ophthalmic Genet.* 22 (3), 133–154. doi:10.1076/opge.22.3.133.2224

Williams, K. M., Georgiou, M., Kalitzeos, A., Chow, I., Hysi, P. G., Robson, A. G., et al. (2022). Axial length distributions in patients with genetically confirmed inherited retinal diseases. *Invest. Ophthalmol. Vis. Sci.* 63 (6), 15. doi:10.1167/iovs.63.6.15

Wojciechowski, R., and Cheng, C. Y. (2018). Involvement of multiple molecular pathways in the genetics of ocular refraction and myopia. *Retina* 38 (1), 91–101. doi:10.1097/IAE.0000000000001518

Xu, C., Feng, C., Han, M., He, J., Zhang, R., Yan, T., et al. (2022). Inverted internal limiting membrane flap technique for retinal detachment due to macular holes in high myopia with axial length ≥ 30 mm. *Sci. Rep.* 12 (1), 4258. doi:10.1038/s41598-022-08277-y

Yang, J., Ferreira, T., Morris, A. P., and Medland, S. E. (2012). Conditional and joint multiple-SNP analysis of GWAS summary statistics identifies additional variants influencing complex traits. *Nat. Genet.* 44(4), 369. doi:10.1038/ng.2213

Yang, J., Lee, S. H., Goddard, M. E., and Visscher, P. M. (2013). Genome-wide complex trait analysis (GCTA): Methods, data analyses, and interpretations. *Methods Mol. Biol.* 1019, 215–236. doi:10.1007/978-1-62703-447-0_9

Yang, J., Weedon, M. N., Purcell, S., Lettre, G., Estrada, K., Willer, C. J., et al. (2011). Genomic inflation factors under polygenic inheritance. *Eur. J. Hum. Genet.* 19 (7), 807–812. doi:10.1038/ejhg.2011.39

Yoshikawa, M., Yamashiro, K., Miyake, M., Oishi, M., Akagi-Kurashige, Y., Kumagai, K., et al. (2014). Comprehensive replication of the relationship between myopia-related genes and refractive errors in a large Japanese cohort. *Invest. Ophthalmol. Vis. Sci.* 55 (11), 7343–7354. doi:10.1167/iovs.14-15105

Zagajewska, K., Piatkowska, M., Goryca, K., Balabas, A., Kluska, A., Paziewska, A., et al. (2018). GWAS links variants in neuronal development and actin remodeling related loci with pseudoexfoliation syndrome without glaucoma. *Exp. Eye Res.* 168, 138–148. doi:10.1016/j.exer.2017.12.006

Zhang, Z., and Fong, H. K. W. (2018). Coexpression of nonvisual opsin, retinal G protein-coupled receptor, and visual pigments in human and bovine cone photoreceptors. *Mol. Vis.* 24, 434–442.

Zheng, J., Erzurumluoglu, A. M., Elsworth, B. L., Kemp, J. P., Howe, L., Haycock, P. C., et al. (2017). LD hub: A centralized database and web interface to perform LD score regression that maximizes the potential of summary level GWAS data for SNP heritability and genetic correlation analysis. *Bioinformatics* 33 (2), 272–279. doi:10.1093/bioinformatics/btw613

frontiers | Frontiers in Genetics

TYPE Original Research
PUBLISHED 09 June 2023
DOI 10.3389/fgene.2023.1161696

OPEN ACCESS

EDITED BY
Denis Plotnikov,
Kazan State Medical University, Russia

REVIEWED BY
Michelle Grunin,
Case Western Reserve University, United States
Ajai Agrawal,
All India Institute of Medical Sciences, India

*CORRESPONDENCE
Maria Pina Concas,
mariapina.concas@burlo.trieste.it

†These authors have contributed equally to this work and share first authorship

RECEIVED 08 February 2023
ACCEPTED 31 May 2023
PUBLISHED 09 June 2023

CITATION
Nardone GG, Spedicati B, Concas MP, Santin A, Morgan A, Mazzetto L, Battaglia-Parodi M and Girotto G (2023), Identifying missing pieces in color vision defects: a genome-wide association study in Silk Road populations. *Front. Genet.* 14:1161696. doi: 10.3389/fgene.2023.1161696

Identifying missing pieces in color vision defects: a genome-wide association study in Silk Road populations

Giuseppe Giovanni Nardone[1†], Beatrice Spedicati[1,2†], Maria Pina Concas[2*], Aurora Santin[1], Anna Morgan[2], Lorenzo Mazzetto[1], Maurizio Battaglia-Parodi[3] and Giorgia Girotto[1,2]

[1]Department of Medicine, Surgery and Health Sciences, University of Trieste, Trieste, Italy, [2]Institute for Maternal and Child Health - IRCCS "Burlo Garofolo", Trieste, Italy, [3]Ophthalmology Department, Vita-Salute San Raffaele University, Milano, Italy

Introduction: Color vision defects (CVDs) are conditions characterized by the alteration of normal trichromatic vision. CVDs can arise as the result of alterations in three genes (*OPN1LW*, *OPN1MW*, *OPN1SW*) or as a combination of genetic predisposition and environmental factors. To date, apart from Mendelian CVDs forms, nothing is known about multifactorial CVDs forms.

Materials and Methods: Five hundred and twenty individuals from Silk Road isolated communities were genotyped and phenotypically characterized for CVDs using the Farnsworth D-15 color test. The CVDs traits Deutan-Protan (DP) and Tritan (TR) were analysed. Genome Wide Association Study for both traits was performed, and results were corrected with a False Discovery Rate linkage-based approach (FDR-p). Gene expression of final candidates was investigated using a published human eye dataset, and pathway analysis was performed.

Results: Concerning DP, three genes: *PIWIL4* (FDR-p: $9.01*10^{-9}$), *MBD2* (FDR-p: $4.97*10^{-8}$) and *NTN1* (FDR-p: $4.98*10^{-8}$), stood out as promising candidates. *PIWIL4* is involved in the preservation of Retinal Pigmented Epithelium (RPE) homeostasis while *MBD2* and *NTN1* are both involved in visual signal transmission. With regards to TR, four genes: *VPS54* (FDR-p: $4.09*10^{-9}$), *IQGAP* (FDR-p: $6{,}52*10^{-10}$), *NMB* (FDR-p: $8.34*10^{-11}$), and *MC5R* (FDR-p: $2.10*10^{-8}$), were considered promising candidates. *VPS54* is reported to be associated with Retinitis pigmentosa; *IQGAP1* is reported to regulate choroidal vascularization in Age-Related Macular Degeneration; *NMB* is involved in RPE homeostasis regulation; *MC5R* is reported to regulate lacrimal gland function.

Discussion: Overall, these results provide novel insights regarding a complex phenotype (i.e., CVDs) in an underrepresented population such as Silk Road isolated communities.

KEYWORDS

color vision defects, Deutan, Protan, Tritan, genome wide association study, genetic isolates, Silk Road, pathway analysis

1 Introduction

Color vision defines an organism's ability to differentiate objects by wavelengths of light that they reflect, emit, or transmit. Many differences exist between animal and human color vision. Human vision is trichromatic, while some animals, such as frogs, fish, marsupials and some types of rodents, can perceive ultraviolet. Birds are believed to possess the most sophisticated visual system among vertebrates, probably perceiving hues of colors inaccessible to humans. In humans, color vision involves several retina and brain mechanisms. In particular, light-absorbing molecules defined as visual pigments, consisting of integral membrane proteins in photoreceptor cells, mediate human vision. The energy carried by photons activates the pigments and eventually starts the photo transduction signal cascade, thus converting the light into an electric signal. Visual pigments reside in two types of photoreceptors, the cone-shaped and rod-shaped cells, and are classified according to the wavelength of maximum light absorption (λ_{max}). Cone photoreceptors contain the three primary visual pigments, the short-wavelength sensitive (S; λ_{max} ~420 nm), the medium-wavelength sensitive (M; λ_{max} ~530 nm), and the long-wavelength sensitive (L; λ_{max} ~560 nm), while rod-shaped cells contain a fourth pigment, called rhodopsin, which mediates vision in dim light conditions and absorbs maximally at λ_{max} ~495 nm (Nathans, 1999). Humans, along with primates, possess three genes encoding for the three primary visual pigments: *OPN1SW*, located on chromosome 7, and *OPN1MW* and *OPN1LW*, both located on chromosome X. Trichromacy arises with the duplication of the *OPN1LW* gene resulting in the formation of the *OPN1MW* gene (Dulai et al., 1999), which confers the ability to discriminate red fruits on a green background. Interestingly, the acquisition of trichromatic vision concurred with the deterioration of the olfactory system in primates (Gilad et al., 2004).

Color Vision Defects (CVDs) are conditions caused by the lack of visual pigments or by their abnormal function. CVDs are divided into congenital and acquired forms and classified based on the affected cone: Deutan affects M-cones causing a defective perception of the red-yellow-green spectrum; Protan affects L-cones causing poor discrimination of the red-green spectrum; and Tritan affects S-cones leading to an alteration in the perception of blue, yellow and orange hues (Hasrod and Rubin, 2016). Congenital CVDs (Deuteranopia, Protanopia, and Tritanopia) are the most characterised forms. They are caused by alterations in: genes coding visual pigments; genes controlling their expression; genes coding components of the phototransduction cascade; genes coding for the α- or β-subunits of the cone cyclic guanosine monophosphate–gated cation channels. Conversely, acquired CVDs arise as a result of ocular, neurologic, or systemic diseases. They can be classified based on the primary disease and the type of color vision alteration encountered (Simunovic, 2016). Moreover, color discrimination ability starts gradually declining from the age of 30. In addition, CVDs can arise during the ageing process, may be influenced by pupil size, crystalline lens coloration, and macular pigment, suggesting the existence of multifactorial forms of CVDs (Ichikawa et al., 2021).

In recent years, Genome-Wide Association Studies (GWAS) proved to be a valid tool in the discovery of novel genes associated with complex diseases and multifactorial traits (Struck et al., 2018). Moreover, it has been proven that GWAS discovery power can be increased by investigating genetic isolates - small communities with reduced genetic variation and environmental homogeneity - offering the possibility to highlight variants underlying complex traits (Girotto et al., 2011). Here, we present the first GWAS analysis investigating multifactorial CVDs in genetic isolates from the Silk Road countries. For centuries, the Silk Road has been a crucial trading route directly linking Europe with Asia. Due to its geographical location and past socio-economic relevance, today, the Silk Road represents a unique collection of populations with admixed ancestries (Mezzavilla et al., 2014), languages and traditions, thus offering the possibility to study rare and unique patterns of genetic variation. Therefore, this study aims to identify novel variants and genes potentially involved in the determination of multifactorial CVDs. To reach this goal, we performed 1) GWAS analyses, 2) evaluation of the expression of candidate genes in a published database, and 3) up-to-date *in silico* pathway construction to evaluate interactions between candidate genes and known genes involved in eye physiology and pathology.

2 Materials and methods

2.1 Cohort characteristics

Eight hundred ninety-three subjects from 20 isolated communities spread across nine Central Asia and Caucasus countries (Afghanistan, Armenia, Azerbaijan, Crimea, Georgia, Kazakistan, Kirghizistan, Tajikistan, Uzbekistan) were recruited during the "Marco Polo" scientific expedition in 2010 (www.marcopolo2010.it). Biological samples, along with information about age, sex, lifestyle, eating habits, profession, and smoking and alcohol consumption, were collected. Moreover, phenotypic information about sensorial abilities and performance, such as hearing thresholds, olfactory performance, and food preferences were collected using several tests and questionnaires. Written informed consent was obtained from all enrolled subjects. The study was conducted in accordance with the Helsinki Declaration, and the research protocol was approved by the ethical committee of IRCCS "Burlo Garofolo" of Trieste, Italy.

2.2 Color vision evaluation

Participants were tested for color discrimination ability using the Farnsworth D-15 saturated color test, administered to all subjects in natural daylight lighting conditions (Oli and Joshi, 2019). Briefly, 15 enumerated colored disks and a reference disk are used in the test. First, subjects select the disk that most closely matches the reference. Then, they select the next color disk matching the previous one and continue until the last disk has been positioned. Scoring is defined by reading the number on the rear of the disk and diagramming the subject's results on a template sheet. Lines crossing the center of the diagram define the type and severity of the CVD (Supplementary Figure S1). To obtain a more precise classification, the tests' results

TABLE 1 Characteristics of the subjects involved in the study, divided by color vision defect.

	All	DP affected	Not affected	All	TR affected	Not affected
N (F)	514 (298)	31 (13)	483 (285)	520 (313)	12 (9)	508 (304)
Age						
Mean	36.4 (36.1)	43.7 (45)	36 (35.7)	36.3 (36.3)	40.1 (37.5)	36.2 (36.2)
SD	15.3 (15.1)	16.8 (21.7)	15 (14.5)	15.1 (14.7)	15.1 (14.7)	15.1 (14.7)
Educational Level - N (F)						
Elementary School	23 (18)	6 (6)	17 (12)	20 (14)	2 (2)	18 (12)
Middle School	59 (36)	4 (0)	55 (36)	58 (38)	1 (1)	57 (37)
High School	251 (146)	13 (5)	238 (141)	263 (159)	8 (5)	255 (154)
University	181 (98)	8 (2)	173 (96)	179 (102)	1 (1)	178 (101)

The number, age, and educational level of analyzed participants is reported; the number, age, and educational level of females is reported in brackets. Age is expressed through mean and standard deviation. Educational level is classified in elementary school, middle school, high school, and university. N: number; F: females; SD: standard deviation; DP: Deutan-Protan; TR: tritan.

interpretation was carried out by a certified ophthalmologist. Individuals were finally classified in Deutan-Protan (DP, 31 cases) and Tritan (TR, 12 cases). All the individuals without color vision alteration were classified as controls.

2.3 Genotyping and imputation

Saliva samples were collected from all enrolled subjects using the Oragene DNA collection kit, and DNA extraction was performed (DNA Genotek, Ontario, Canada). Genotyping was carried out using the Omni Express 700k Illumina Chip, including only samples and sites with call rate ≥0.99 (43,655 variants excluded), Hardy-Weinberg Equilibrium p-value ≥$1*10^{-6}$ (3,153 variants excluded), and minor allele frequency (MAF) ≥ 0.01 (18 variants excluded). Imputation was performed using MINIMAC v4 (Howie et al., 2012) to Haplotype Reference Consortium imputation panel version r1.1 (McCarthy et al., 2016). All data were aligned to the human reference genome build 37 (GRCh37). After imputation, SNPs with Info Score <0.4 (13626943 variants excluded) and MAF <0.01 (40,203 variants excluded) were discarded from statistical analyses. A total of 7783479 SNPs were analysed.

2.4 Genome-wide association studies (GWAS)

GWAS analyses for DP and TR traits were conducted using GEMMA v0.98 software (Zhou and Stephens, 2012). Linear mixed model regressions assuming an additive genetic model were performed. The genomic kinship matrix was used as random effects to take into account relatedness. Covariates included in the analyses were: age, sex, educational level and the first ten principal components (PCs). PCs were calculated from 203,099 genotyped variants using Plink v1.9 (Purcell et al., 2007). Results were then adjusted using a False Discovery Rate (FDR) linkage-based approach adapted from (Chen et al., 2021). Briefly, linkage disequilibrium-based clumping of regression results was performed using Plink v1.9, setting an r^2 threshold of 0.3 and a variant distance of 0.5 Mb. Then, the most significant SNPs of each clump were collected in a new dataset, and FDR calculation was carried out using R (https://www.r-project.org/index.html). For each GWAS, SNPs with an FDR-adjusted p-value (FDR-p) ≤ 1×10^{-5} were annotated with the Variant Effect Predictor tool (VEP) (McLaren et al., 2016) to obtain information on the distance from the closest genes and their functional characteristics (i.e., whether they were contained in an intronic, exonic, or intergenic region). For each SNP, the nearest coding gene in a range of 250 kb was annotated. Long non-coding RNAs (LINC) genes, genes with unknown functions identified with LOC and FAM symbols, and pseudo genes were excluded. Finally, potential candidate genes were selected based on the following criteria:

- FDR-p ≤ $5*10^{-8}$;
- Number of SNPs in linkage with the top SNP ≥ the median of SNPs in linkage for each clump;
- Expression levels in the inquired database;
- Involvement in physiological and/or pathological processes in the eye.

Manhattan and QQplots were generated using R, while heatmap was generated using the ComplexHeatmap R package (Gu et al., 2016).

2.5 Gene expression in eye tissues

The final candidate genes' expression was investigated using a published human eye transcriptome dataset - the "Eye in a Disk" (EiaD) (https://eyeintegration.nei.nih.gov). Briefly, the dataset integrates expression data from GTEx (GTEx Consortium, 2013) and public repositories through the use of a Snakemake-based pipeline to normalise expression values indicated as $\log_2$ [Transcript Per Million (TPM) +1)] and perform quality control. Expression data was extracted from healthy human adult and fetal eye tissues and eye stem cells. For this study, gene expression of candidate genes in the following tissues was investigated: Corneal Endothelium (CE); Corneal Fetal Endothelium (CFE); Corneal Endothelial Stem Cells (CSE); Cornea (Cn); Lens Stem Cell Line (LSC); Fetal Eye Retina (RFE); Retinal Fetal Tissue (RFT); Retinal Ganglion Stem Cells (RGS); Retinal Pigment Epithelium (RPE); Fetal RPE (RPFT); Retina (Rt).

TABLE 2 Selected genes associated with the DP (Deutan-Protan) and TR (Tritan) phenotypes.

Trait	Genes	Top SNP (rs)	HGVS nomenclature	Freq	Beta	StdErr	*p*-value	FDR-p	N° of surrounding SNPs ($p < 1 \times 10^{-4}$)
DP	*PIWIL4*	rs118136100	NC_000011.9: g.94309876G>A	0.983	−0.412	0.061	1.30×10^{-10}	9.01×10^{-9}	2
DP	*NTN1*	rs117797822	NC_000017.10: g.9111250T>C	0.970	−0.304	0.048	1.08×10^{-9}	4.98×10^{-8}	3
DP	*MBD2*	rs17292725	NC_000018.9: g.51880889G>A	0.959	−0.294	0.046	8.06×10^{-10}	4.97×10^{-8}	3
TR	*NMB*	rs145079583	NC_000015.9: g.85195862A>G	0.984	−0.344	0.043	9.45×10^{-14}	8.34×10^{-11}	18
TR	*ATF7IP2*	rs146729070	NC_000016.9: g.10394350C>T	0.981	−0.318	0.043	4.19×10^{-12}	6.52×10^{-10}	2
TR	*IQGAP1*	rs117555778	NC_000015.9: g.91019452C>T	0.975	−0.231	0.031	4.14×10^{-12}	6.52×10^{-10}	6
TR	*NPTN*	rs192430987	NC_000015.9: g.73933216A>C	0.974	−0.243	0.033	4.43×10^{-12}	6.52×10^{-10}	4
TR	*GALNT1*	rs55833596	NC_000018.9: g.33141906C>T	0.983	−0.232	0.034	6.35×10^{-11}	4.09×10^{-9}	2
TR	*VPS54*	rs140150162	NC_000002.11: g.64279003A>C	0.983	−0.237	0.034	6.48×10^{-11}	4.09×10^{-9}	340
TR	*BIN3*	rs73212812	NC_000008.10: g.22532279G>A	0.980	−0.24	0.038	1.14×10^{-9}	2.91×10^{-8}	4
TR	*HTR1B*	rs78752155	NC_000006.11: g.77972985C>T	0.978	−0.227	0.036	1.21×10^{-9}	2.91×10^{-8}	2
TR	*TCIRG1*	rs76912991	NC_000011.9: g.67823868A>G	0.970	−0.174	0.027	6.52×10^{-10}	2.13×10^{-8}	3
TR	*MC5R*	rs77046774	NC_000018.9: g.13825162A>G	0.944	−0.132	0.020	6.17×10^{-10}	2.10×10^{-8}	44
TR	*ATP2B1*	rs117316296	NC_000012.11: g.90338181A>G	0.986	−0.274	0.038	1.70×10^{-11}	1.75×10^{-9}	2
TR	*BBX*	rs116495417	NC_000003.11: g.107567716C>T	0.971	−0.209	0.032	4.01×10^{-10}	1.54×10^{-8}	2
TR	*MDGA2*	rs72680270	NC_000014.8: g.47740920G>T	0.976	−0.219	0.033	3.54×10^{-10}	1.42×10^{-8}	7
TR	*HCN4*	rs191157379	NC_000015.9: g.73500591G>A	0.982	−0.244	0.037	2.95×10^{-10}	1.36×10^{-8}	3
TR	*TPBG*	rs77834841	NC_000006.11: g.83135354C>T	0.976	−0.233	0.035	3.08×10^{-10}	1.36×10^{-8}	4

Trait: DP or TR phenotype found in association with the gene. Genes: closest gene to the top SNP obtained by VEP. Top SNP: most significant SNP; rsIDs are updated to dbSNP build 144; HGVS nomenclature: variant nomenclature according to Human Genome Variation Society recommendations; genomic data is aligned to the GRCh37/hg19 reference sequence. Freq: frequency of the effect allele. Beta: effect from the GWAS analysis. StdErr: standard error of the Beta. *p*-value from GWAS analysis. FDR-p: *p*-value after FDR correction. N° of surrounding SNPs ($p < 1 \times 10^{-4}$): number of SNPs with $p < 1 \times 10^{-4}$ found in linkage with the top SNP.

2.6 Pathway analysis

Finally, the involvement of the candidate genes in eye physiology and pathology was investigated using Qiagen's Ingenuity Pathway Analysis (IPA) from Ingenuity Systems (Redwood City, California, United States; http://www.ingenuity.com). Briefly, a list of promising candidate genes resulting from significant FDR-corrected associations for both traits was uploaded to verify their interaction with a set of genes involved in eye pathologies and physiology using Path Explorer. Finally, interaction maps were generated using IPA's Path Designer. The gene list was obtained by combining manual bibliographic research and IPA databases, including genes involved in cone photoreceptor disorders and cone cell development.

3 Results

3.1 GWAS results

Individuals with missing data regarding age, sex and color vision, or missing genetic data were excluded from the analyses.

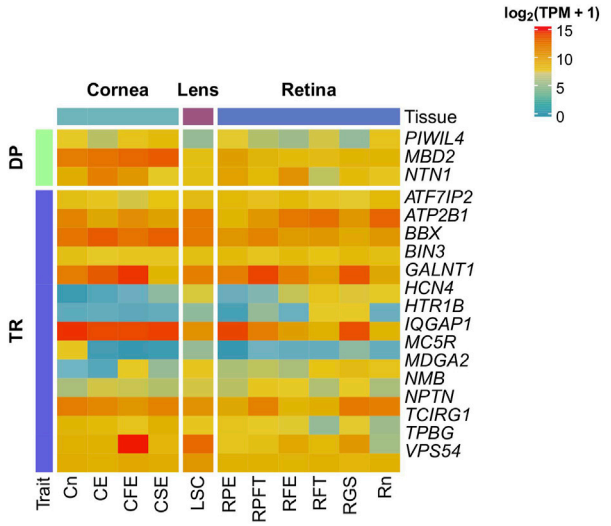

FIGURE 1
Gene expression of candidate genes in the eye. Gene expression of candidate genes was investigated in 11 healthy ocular tissues from Cornea, Lens, and Retina using the Eye on a Disk dataset. Candidate genes are at least weakly expressed in all the tissues. CE, Corneal Endothelium; CFE, Corneal Fetal Endothelium; CSE, Corneal Endothelial Stem Cells; Cn, Cornea; LSE, Lens Stem Cell Line; RFE, Fetal Eye Retina; RFT, Retinal Fetal Tissue; RGS, Retinal Ganglion Stem Cells; RPE, Retinal Pigment Epithelium; RPFT, Fetal RPE; Rt, Retina.

In the GWAS for DP, 514 individuals were included, specifically 31 with DP and 483 without color vision alteration. In the GWAS for TR, 520 subjects were considered, precisely 12 with TR and 508 without color vision alteration. The number, gender, age, and educational level of analyzed participants are reported in Table 1.

Manhattan and QQ plots of GWAS on DP and TR are shown in Supplementary Figure S2. A total of 1,263 associations between SNPs and DP phenotype with $p < 1*10^{-5}$ were detected. Of those, 103 displayed genome-wide significant p-values ($p < 5*10^{-8}$). Regarding TR, 2,968 associations with $p < 1*10^{-5}$ were found; 273 with genome-wide significant p-values. After the FDR correction, 489 variants with FDR-corrected p-values (FDR-p) < $1*10^{-5}$ were retained for DP. Of those, nine showed genome-wide significant FDR-p (Supplementary Table S1). Eight hundred eighty-three variants with FDR-p < $1*10^{-5}$ were retained for the TR trait, 45 with genome-wide significant FDR-p (Supplementary Table S1). All variants showing genome-wide significant FDR-p for both DP and TR were not in linkage-disequilibrium. VEP annotation of the association results for both traits is available in Supplementary Tables S2, S3. Following the selection criteria described in the Materials and Methods section, our analyses allowed the identification of 18 promising candidates, as displayed in Table 2.

After FDR correction, three genes resulted significantly associated with the DP phenotype: *PIWIL4* (top SNP rs118136100, FDR-p = $9.01*10^{-9}$), *MBD2* (top SNP rs17292725, FDR-p = $4.98*10^{-8}$) and *NTN1* (top SNP rs117797822, FDR-p = $4.97*10^{-8}$). Moreover, 15 genes resulted significantly associated with TR, with *NMB* (top SNP rs145079583, FDR-p = $8.34*10^{-11}$), *IQGAP1* (top SNP rs117555778, FDR-p = $6.52*10^{-10}$), *NPTN* (top SNP rs192430987, FDR-p = $6.52*10^{-10}$) and *ATF7IP2* (top SNP rs146729070, FDR-p = $6.52*10^{-10}$) being the most significantly associated genes.

3.2 Expression pattern of the associated genes in the human eye

The expression patterns in the human eye of the three genes for DP and the 15 for TR were investigated using expression data from EiaD and are shown in Figure 1. The corresponding values of $\log_2$ (TPM+1) are fully reported in Supplementary Table S4.

All genes displayed at least a weak expression in all inquired tissues. As regards DP, *NTN1* and *MBD2* showed high expression ($\log_2$ (TPM+1) > 10) throughout all the tissues, especially in corneal tissues. Conversely, *PIWIL4* showed weak expression ($\log_2$ (TPM+1) < 5) in all tissues, excluding corneal tissues, RPE and Rn. Concerning TR, *VPS54*, *BIN3*, *TCIRG1*, *ATF7IP2*, *ATP2B1*, *BBX*, *GALNT1* and *IQGAP1* showed a high expression in all tissues. In contrast, *MC5R*, *MDGA2*, *HTR1B* and *HCN4* showed weak expression in almost all investigated tissues.

3.3 Pathway analysis

Finally, the interaction between the resulting genes for both traits and a set of more than 500 genes involved in eye pathology and physiology was investigated using IPA's Path Explorer. The interaction network is shown in Figure 2. The complete list of genes is reported in Supplementary Table S5.

With the exception of seven genes, *TPBG*, *TCIRG1*, *MDGA2*, *ATF7IP2*, *NTN1*, *MC5R*, and *NMB*, associations with genes involved in eye morphogenesis (formation of the eye, morphology of the eye and retina, morphology of eye cells), physiology (preservation of cone cells, electrophysiology of the eye) and degeneration (retinal dystrophy, retina degeneration, degeneration of the eye) have been found. Concerning DP, *MBD2* was involved in the formation of the eye, interacting both with *HK2* and *HIF1A*, while *PIWIL4* displayed an interaction with *DICER1*, which was involved in retinal degeneration. With regards to TR, *IQGAP1* and *ATP2B1* showed the most complex networks of interaction, interacting both with other candidate genes and with genes involved in all the investigated processes.

4 Discussion

In this study, we performed the first GWAS analyses investigating the molecular determinants of multifactorial forms of CVDs in the rare Silk Road cohort. Our analyses led to the identification of 18 candidate genes. Among them, seven genes proved to be particularly interesting, considering their expression data and pathway analysis results, as described below.

Concerning DP, three genes: *PIWIL4*, *MBD2*, and *NTN1*, were significantly associated after the FDR correction. The *PIWIL4* gene encodes for a protein belonging to the Argonaute family of proteins. Piwi proteins are believed to play a crucial role in spermatogenesis, as their absence leads to male infertility. This gene showed strong

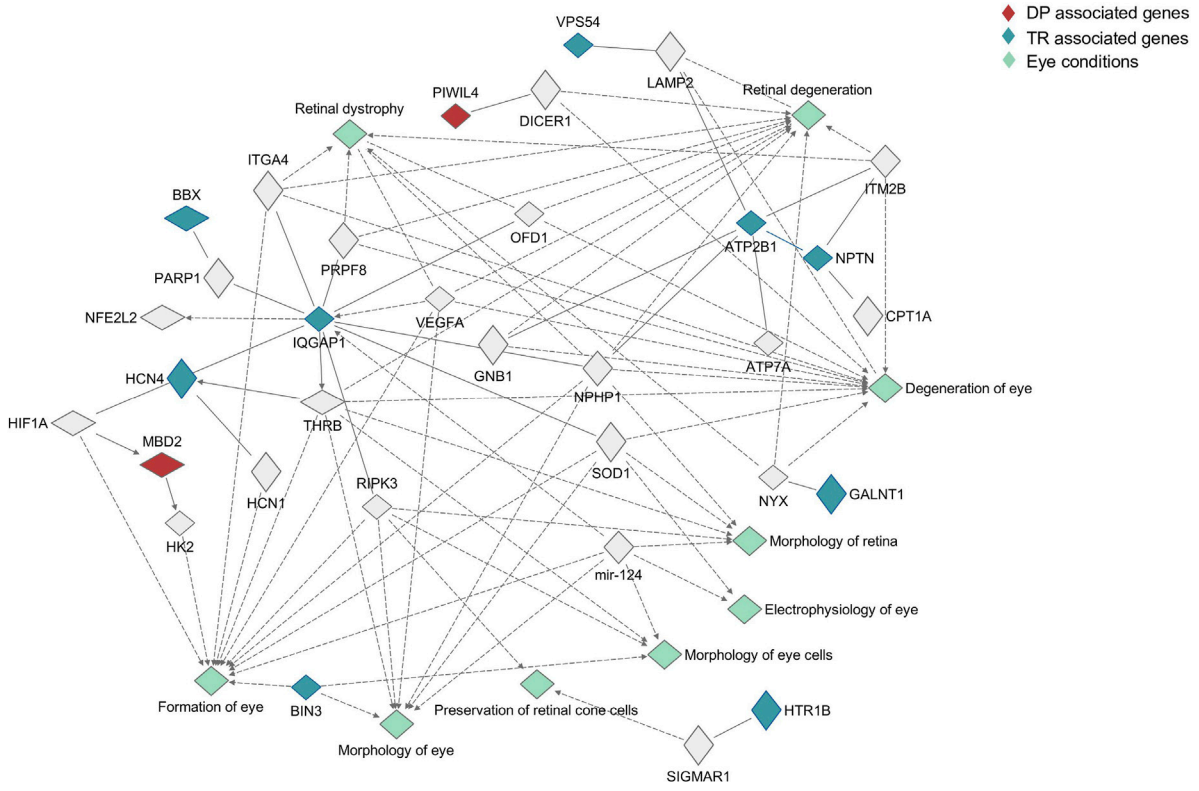

FIGURE 2
Pathway analysis of candidate genes. The role played in the eye by candidate genes was investigated using Ingenuity Pathway analysis, searching for interaction between candidate genes and a list of more than 500 genes involved in eye physiology and pathology. Genes associated with Deutan-Protan (DP) are highlighted in red, while genes associated with Tritan (TR) are highlighted in blue. Eye conditions associated with the interactions are highlighted in aquamarine.

expression values in corneal tissues (Cn, CFE, CSE), in the retinal pigmented epithelium, and in the retina. *PIWIL4* is reported to regulate the expression of Alu RNA in response to oxidative stress, protecting RPE from degeneration (Hwang et al., 2019). Interestingly, the pathway analysis showed *PIWIL4* interaction with *DICER1*, and deficiency of this gene in response to oxidative stress in RPE is reported to lead to the accumulation of Alu RNA and degeneration of the RPE (Kaarniranta et al., 2020), suggesting a role of both *PIWIL4* and *DICER1* in the preservation of RPE. Moreover, *PIWIL4* modulates the expression of tight-junctions proteins in RPE, contributing to the structural integrity of the epithelium (Sivagurunathan et al., 2017).

MBD2 encodes for the methyl-CpG binding domain protein 2, a protein that binds specific methylated sequences, involved in transcription regulation, both repressing and activating the transcription of methylated sites. Moreover, MBD2 encoded protein is associated with many types of cancer, such as breast (Liu et al., 2021), renal (Li et al., 2020), colorectal (Yu et al., 2020) and prostate (Patra et al., 2003). Furthermore, MBD2 is reported to be involved in the T-cells development (Cheng et al., 2021). This gene showed a high expression in all investigated tissues, particularly in corneal tissues. MBD2 protein is reported to mediate apoptosis in retinal ganglion cells (Ge et al., 2020), and possibly play a role in the pathogenesis of age-related macular degeneration (Pan et al., 2014). In addition, our pathway analyses showed a link between MBD2 protein and hexokinase 2 (HK2) protein in the eye's formation process. HK2 protein is reported to have several crucial roles in maintaining photoreceptors' health and functionality (Weh et al., 2020).

NTN1 encodes for Netrin 1, a laminin-related secreted protein involved in axon guidance, cell migration, morphogenesis, angiogenesis, peripheral nerve regeneration and Schwann cell proliferation. NTN1 showed high expression values throughout all inquired tissues, especially in CE, CFE, RFE, and RPE. Although no association between NTN1 and genes involved in eye physiology and pathology was found by the pathway analysis, in the eye, netrin-1 is reported as a key molecule for the growth of axons directed to the optical nerve head (Mann et al., 2004) and for the migration of the glial-precursors from the brain to the retina (Tsai and Miller, 2002).

Notably, all the above genes could play a role in determining the DP phenotype. Alterations in PIWIL4 could lead to RPE degeneration, thus hindering its ability to support photoreceptors and correct color vision. Concerning MBD2 and NTN1, both of these genes play a role in the transmission of the visual signal, acting in retinal ganglion cells and in the optic nerve, respectively. We can therefore hypothesize that defects in these genes could alter the functionality of these tissues leading to an altered color vision.

With regards to TR, among those significantly associated after the FDR correction, four genes - VPS54, IQGAP1, NMB, and MC5R

- stood out as promising candidates, considering the number of SNPs in linkage with the top SNP, their reported role in the eye, and their expression values. VPS54 encodes for a subunit of the GARP complex, a protein complex involved in retrograde transport from early and late endosomes to the trans-Golgi network (TGN). Moreover, VPS54 is reported to be part of RP28, a locus associated with recessive retinitis pigmentosa (Kumar et al., 2004). VPS54 showed a consistent expression in all investigated tissues, and the pathway analysis highlighted its interaction with LAMP2. Loss of function variants in LAMP2 cause Danon disease, a glycogen storage disease also known as X-linked vacuolar cardiomyopathy and myopathy. However, LAMP2 deficiencies are also reported to cause retinopathies and RPE degeneration independently (Kousal et al., 2021) or in association with Danon disease (Fukushima et al., 2020). Interestingly *VPS54* knock-out and the resulting GARP deficiency are reported to alter the formation of lysosomal structures deputed to the accumulation of endolysosomal proteins, including Lamp2 (D'Souza et al., 2019).

IQGAP1 belongs to the IQGAP protein family, a family of scaffold proteins involved in the regulation of several cellular pathways and functions. In particular, the isoform encoded by IQGAP1 interacts with phosphatidylinositol phosphate kinase mediating cell motility and Akt phosphorylation. IQGAP1 showed high expression values throughout all tissues, especially in corneal tissues, in RPE and RGS, and showed a complex network of interactions in the pathway analysis. For instance, IQGAP1 interacts with THRB, a gene encoding for the thyroid hormone receptor (TRβ), and is reported to enhance transcriptional activation of TRβ isoform 2 (Hahm and Privalsky, 2013). The THRB gene is involved in cone photoreceptors' development and function (Deveau et al., 2020). Indeed, THRB is reported to inhibit S opsin expression (Ma and Ding, 2016), and its mutation leads to an imbalance in the distribution of cone types in mice retina (Ng et al., 2001). Moreover, IQGAP1 is reported to regulate retinal neurite growth in chicken retina (Oblander and Brady-Kalnay, 2010) and to play a key role in the regulation of choroidal endothelial cells in the pathogenesis of Age-related Macular Degeneration (Ramshekar et al., 2021).

NMB encodes for neuromedin B, a member of the bombesin-related family of neuropeptides. Neuromedin B is expressed in the central nervous system and in the gastrointestinal tract and is involved in several physiological functions, including regulation of exocrine and endocrine secretions, smooth muscle contraction, feeding, blood pressure, blood glucose, body temperature, and cell growth. NMB showed a moderate expression in all tissues, with higher levels in RPFT, RFE, and RGS. Although no associations between the inquired genes and this gene were highlighted by the pathway analysis, NMB is reported to play a role in the induction of intracellular Ca^{2+} transient and phosphatidylinositol turnover in RPE cells (Kuriyama et al., 1992) and to constitute a marker of chicken retinal ganglion cells (Yamagata et al., 2006).

MC5R belongs to the family of melanocortin receptors, formed by five G-protein coupled receptors involved in a broad spectrum of physiological processes, including regulation of pigmentation, regulation of inflammation, and pain perception. MC5R has a wide peripheral distribution and is involved in many processes such as glucose uptake (Enriori et al., 2016), exocrine gland secretion (Chen et al., 1997) and fatty acids oxidation (An et al., 2007). This gene showed poor expression in all inquired tissues, excluding the corneal tissue, and no associations were found for this gene through the pathway analysis. However, MC5R is reported to protect from uveitis-derived retinal damage by regulating the activation of $CD4^+$ regulatory T cells (Taylor et al., 2006) and to attenuate retinal degeneration in an experimental model of diabetic retinopathy (Rossi et al., 2016). Moreover, MC5R is reported to play a crucial role in the lacrimal gland, maintaining lacrimal function and secretion (Nguyen et al., 2004).

All the above genes proved to be potentially involved in TR determination: defects in *VPS54* could lead to RPE degeneration, thus leading to color vision impairment; alterations in *IQGAP1* can cause cone type imbalances, with a diminished number and functionality of S cones; defects in NMB may alter RPE's ability to regulate fluid homeostasis, resulting in subretinal fluid accumulation and retinal function impairment; alterations in *MC5R* could affect lacrimal gland function leading to dry eye onset and progressive visual impairment.

In conclusion, this study highlighted, for the first time, the association of 15 new genes with the determination of multifactorial forms of CVDs. Notably, seven genes, *PIWIL4*, *MBD2*, *NTN1*, *VPS54*, *IQGAP1*, *NMB*, and *MC5R*, proved to be particularly promising considering their expression in the eye and their known implication in several physiologic and pathologic eye processes. It is worth noting how, in our study, the availability of phenotypic and genotypic data from individuals coming from isolated communities allowed us to enhance the discovery power of GWAS, offering the possibility to capture new and impactful polymorphisms associated with complex traits. Up to date, there are few to no studies investigating complex traits in Silk Road populations. Therefore, with this work, we provide new and insightful information on such underrepresented populations and a natural next step of future research could seek to replicate these findings in different cohorts.

Data availability statement

Publicly available datasets were analyzed in this study. This data can be found here: European Variation Archive (EVA): https://www.ebi.ac.uk/eva/?eva-study=PRJEB60906.

Ethics statement

The studies involving human participants were reviewed and approved by the Ethics Committee of the Institute for Maternal and Child Health—I.R.C.C.S. "Burlo Garofolo" of Trieste (Italy). The patients/participants provided their written informed consent to participate in this study.

Author contributions

MB-P performed the phenotype classification. GGN analysed the data with the support of AS, MPC, BS and LM. GGN and BS wrote the manuscript with the contribution of MPC and AM. GG conceived the study and supervised the project. All authors contributed to the article and approved the submitted version.

Funding

This research was supported by D70-RESRICGIROTTO to GG.

Acknowledgments

The authors wish to thank all the volunteers for their keen participation in the study.

Conflict of interest

The authors declare that the research was conducted in the absence of any commercial or financial relationships that could be construed as a potential conflict of interest.

Publisher's note

All claims expressed in this article are solely those of the authors and do not necessarily represent those of their affiliated organizations, or those of the publisher, the editors and the reviewers. Any product that may be evaluated in this article, or claim that may be made by its manufacturer, is not guaranteed or endorsed by the publisher.

Supplementary material

The Supplementary Material for this article can be found online at: https://www.frontiersin.org/articles/10.3389/fgene.2023.1161696/full#supplementary-material

References

An, J. J., Rhee, Y., Kim, S. H., Kim, D. M., Han, D.-H., Hwang, J. H., et al. (2007). Peripheral effect of α-Melanocyte-stimulating hormone on fatty acid oxidation in skeletal muscle. *J. Biol. Chem.* 282, 2862–2870. doi:10.1074/jbc.M603454200

Chen, W., Kelly, M. A., Opitz-Araya, X., Thomas, R. E., Low, M. J., and Cone, R. D. (1997). Exocrine gland dysfunction in MC5-R-deficient mice: Evidence for coordinated regulation of exocrine gland function by melanocortin peptides. *Cell.* 91, 789–798. doi:10.1016/S0092-8674(00)80467-5

Chen, Z., Boehnke, M., Wen, X., and Mukherjee, B. (2021). Revisiting the genome-wide significance threshold for common variant GWAS. *G3 Genes.|Genomes|Genetics* 11, jkaa056. doi:10.1093/g3journal/jkaa056

Cheng, L., Zhou, K., Chen, X., Zhou, J., Cai, W., Zhang, Y., et al. (2021). Loss of MBD2 affects early T cell development by inhibiting the WNT signaling pathway. *Exp. Cell. Res.* 398, 112400. doi:10.1016/j.yexcr.2020.112400

D'Souza, Z., Blackburn, J. B., Kudlyk, T., Pokrovskaya, I. D., and Lupashin, V. V. (2019). Defects in COG-mediated golgi trafficking alter endo-lysosomal system in human cells. *Front. Cell. Dev. Biol.* 7, 118. doi:10.3389/fcell.2019.00118

Deveau, C., Jiao, X., Suzuki, S. C., Krishnakumar, A., Yoshimatsu, T., Hejtmancik, J. F., et al. (2020). Thyroid hormone receptor beta mutations alter photoreceptor development and function in *Danio rerio* (zebrafish). *PLoS Genet.* 16, e1008869. doi:10.1371/journal.pgen.1008869

Dulai, K. S., von Dornum, M., Mollon, J. D., and Hunt, D. M. (1999). The evolution of trichromatic color vision by opsin gene duplication in new world and old world primates. *Genome Res.* 9, 629–638. doi:10.1101/gr.9.7.629

Enriori, P. J., Chen, W., Garcia-Rudaz, M. C., Grayson, B. E., Evans, A. E., Comstock, S. M., et al. (2016). α-Melanocyte stimulating hormone promotes muscle glucose uptake via melanocortin 5 receptors. *Mol. Metab.* 5, 807–822. doi:10.1016/j.molmet.2016.07.009

Fukushima, M., Inoue, T., Miyai, T., and Obata, R. (2020). Retinal dystrophy associated with Danon disease and pathogenic mechanism through LAMP2-mutated retinal pigment epithelium. *Eur. J. Ophthalmol.* 30, 570–578. doi:10.1177/1120672119832183

Ge, Y., Zhang, R., Feng, Y., and Li, H. (2020). Mbd2 mediates retinal cell apoptosis by targeting the lncRNA mbd2-AL1/miR-188-3p/traf3 Axis in ischemia/reperfusion injury. *Mol. Ther. Nucleic Acids* 19, 1250–1265. doi:10.1016/j.omtn.2020.01.011

Gilad, Y., Wiebe, V., Przeworski, M., Lancet, D., and Pääbo, S. (2004). Loss of olfactory receptor genes coincides with the acquisition of full trichromatic vision in primates. *PLoS Biol.* 2, e5. doi:10.1371/journal.pbio.0020005

Girotto, G., Pirastu, N., Sorice, R., Biino, G., Campbell, H., d'Adamo, A. P., et al. (2011). Hearing function and thresholds: A genome-wide association study in European isolated populations identifies new loci and pathways. *J. Med. Genet.* 48, 369–374. doi:10.1136/jmg.2010.088310

GTEx Consortium (2013). The genotype-tissue expression (GTEx) project. *Nat. Genet.* 45, 580–585. doi:10.1038/ng.2653

Gu, Z., Eils, R., and Schlesner, M. (2016). Complex heatmaps reveal patterns and correlations in multidimensional genomic data. *Bioinformatics* 32, 2847–2849. doi:10.1093/bioinformatics/btw313

Hahm, J. B., and Privalsky, M. L. (2013). Research resource: Identification of novel coregulators specific for thyroid hormone receptor-β2. *Mol. Endocrinol.* 27, 840–859. doi:10.1210/me.2012-1117

Hasrod, N., and Rubin, A. (2016). Defects of colour vision: A review of congenital and acquired colour vision deficiencies. *Afr. Vis. Eye Health* 75, 6. doi:10.4102/aveh.v75i1.365

Howie, B., Fuchsberger, C., Stephens, M., Marchini, J., and Abecasis, G. R. (2012). Fast and accurate genotype imputation in genome-wide association studies through pre-phasing. *Nat. Genet.* 44, 955–959. doi:10.1038/ng.2354

Hwang, Y. E., Baek, Y. M., Baek, A., and Kim, D.-E. (2019). Oxidative stress causes Alu RNA accumulation via PIWIL4 sequestration into stress granules. *BMB Rep.* 52, 196–201. doi:10.5483/BMBRep.2019.52.3.146

Ichikawa, K., Yokoyama, S., Tanaka, Y., Nakamura, H., Smith, R. T., and Tanabe, S. (2021). The change in color vision with normal aging evaluated on standard pseudoisochromatic plates part-3. *Curr. Eye Res.* 46, 1038–1046. doi:10.1080/02713683.2020.1843683

Kaarniranta, K., Pawlowska, E., Szczepanska, J., and Blasiak, J. (2020). DICER1 in the pathogenesis of age-related macular degeneration (AMD) - Alu RNA accumulation versus miRNA dysregulation. *Aging Dis.* 11, 851–862. doi:10.14336/AD.2019.0809

Kousal, B., Majer, F., Vlaskova, H., Dvorakova, L., Piherova, L., Meliska, M., et al. (2021). Pigmentary retinopathy can indicate the presence of pathogenic LAMP2 variants even in somatic mosaic carriers with no additional signs of Danon disease. *Acta Ophthalmol.* 99, 61–68. doi:10.1111/aos.14478

Kumar, A., Shetty, J., Kumar, B., and Blanton, S. H. (2004). Confirmation of linkage and refinement of the RP28 locus for autosomal recessive retinitis pigmentosa on chromosome 2p14-p15 in an Indian family. *Mol. Vis.* 10, 399–402.

Kuriyama, S., Yoshimura, N., Ohuchi, T., Tanihara, H., Ito, S., and Honda, Y. (1992). Neuropeptide-induced cytosolic Ca2+ transients and phosphatidylinositol turnover in cultured human retinal pigment epithelial cells. *Brain Res.* 579, 227–233. doi:10.1016/0006-8993(92)90055-e

Li, L., Li, N., Liu, N., Huo, F., and Zheng, J. (2020). MBD2 correlates with a poor prognosis and tumor progression in renal cell carcinoma. *Onco Targets Ther.* 13, 10001–10012. doi:10.2147/OTT.S256226

Liu, Z., Sun, L., Cai, Y., Shen, S., Zhang, T., Wang, N., et al. (2021). Hypoxia-Induced suppression of alternative splicing of MBD2 promotes breast cancer metastasis via activation of FZD1. *Cancer Res.* 81, 1265–1278. doi:10.1158/0008-5472.CAN-20-2876

Ma, H., and Ding, X.-Q. (2016). Thyroid hormone signaling and cone photoreceptor viability. *Adv. Exp. Med. Biol.* 854, 613–618. doi:10.1007/978-3-319-17121-0_81

Mann, F., Harris, W. A., and Holt, C. E. (2004). New views on retinal axon development: A navigation guide. *Int. J. Dev. Biol.* 48, 957–964. doi:10.1387/ijdb.041899fm

McCarthy, S., Das, S., Kretzschmar, W., Delaneau, O., Wood, A. R., Teumer, A., et al.the Haplotype Reference Consortium (2016). A reference panel of 64,976 haplotypes for genotype imputation. *Nat. Genet.* 48, 1279–1283. doi:10.1038/ng.3643

McLaren, W., Gil, L., Hunt, S. E., Riat, H. S., Ritchie, G. R. S., Thormann, A., et al. (2016). The ensembl variant effect predictor. *Genome Biol.* 17, 122. doi:10.1186/s13059-016-0974-4

Mezzavilla, M., Vozzi, D., Pirastu, N., Girotto, G., d'Adamo, P., Gasparini, P., et al. (2014). Genetic landscape of populations along the Silk Road: Admixture and migration patterns. *BMC Genet.* 15, 131. doi:10.1186/s12863-014-0131-6

Nathans, J. (1999). The evolution and physiology of human color vision: Insights from molecular genetic studies of visual pigments. *Neuron* 24, 299–312. doi:10.1016/S0896-6273(00)80845-4

Ng, L., Hurley, J. B., Dierks, B., Srinivas, M., Saltó, C., Vennström, B., et al. (2001). A thyroid hormone receptor that is required for the development of green cone photoreceptors. *Nat. Genet.* 27, 94–98. doi:10.1038/83829

Nguyen, D. H., Toshida, H., Schurr, J., and Beuerman, R. W. (2004). Microarray analysis of the rat lacrimal gland following the loss of parasympathetic control of secretion. *Physiol. Genomics* 18, 108–118. doi:10.1152/physiolgenomics.00011.2004

Oblander, S. A., and Brady-Kalnay, S. M. (2010). Distinct PTPmu-associated signaling molecules differentially regulate neurite outgrowth on E-, N-, and R-cadherin. *Mol. Cell. Neurosci.* 44, 78–93. doi:10.1016/j.mcn.2010.02.005

Oli, A., and Joshi, D. (2019). Efficacy of red contact lens in improving color vision test performance based on Ishihara, Farnsworth D15, and Martin Lantern Test. *Med. J. Armed Forces India* 75, 458–463. doi:10.1016/j.mjafi.2018.08.005

Pan, J.-R., Wang, C., Yu, Q.-L., Zhang, S., Li, B., and Hu, J. (2014). Effect of Methyl-CpG binding domain protein 2 (MBD2) on AMD-like lesions in ApoE-deficient mice. *J. Huazhong Univ. Sci. Technol. Med. Sci.* 34, 408–414. doi:10.1007/s11596-014-1292-2

Patra, S. K., Patra, A., Zhao, H., Carroll, P., and Dahiya, R. (2003). Methyl-CpG–DNA binding proteins in human prostate cancer: Expression of CXXC sequence containing MBD1 and repression of MBD2 and MeCP2. *Biochem. Biophysical Res. Commun.* 302, 759–766. doi:10.1016/S0006-291X(03)00253-5

Purcell, S., Neale, B., Todd-Brown, K., Thomas, L., Ferreira, M. A. R., Bender, D., et al. (2007). Plink: A tool set for whole-genome association and population-based linkage analyses. *Am. J. Hum. Genet.* 81, 559–575. doi:10.1086/519795

Ramshekar, A., Wang, H., and Hartnett, M. E. (2021). Regulation of Rac1 activation in choroidal endothelial cells: Insights into mechanisms in age-related macular degeneration. *Cells* 10, 2414. doi:10.3390/cells10092414

Rossi, S., Maisto, R., Gesualdo, C., Trotta, M. C., Ferraraccio, F., Kaneva, M. K., et al. (2016). Activation of melanocortin receptors MC1 and MC5 attenuates retinal damage in experimental diabetic retinopathy. *Mediat. Inflamm.* 2016, 7368389. doi:10.1155/2016/7368389

Simunovic, M. P. (2016). Acquired color vision deficiency. *Surv. Ophthalmol.* 61, 132–155. doi:10.1016/j.survophthal.2015.11.004

Sivagurunathan, S., Palanisamy, K., Arunachalam, J. P., and Chidambaram, S. (2017). Possible role of HIWI2 in modulating tight junction proteins in retinal pigment epithelial cells through Akt signaling pathway. *Mol. Cell. Biochem.* 427, 145–156. doi:10.1007/s11010-016-2906-8

Struck, T. J., Mannakee, B. K., and Gutenkunst, R. N. (2018). The impact of genome-wide association studies on biomedical research publications. *Hum. Genomics* 12, 38. doi:10.1186/s40246-018-0172-4

Taylor, A., Kitaichi, N., and Biros, D. (2006). Melanocortin 5 receptor and ocular immunity. *Cell. Mol. Biol. (Noisy-le-Grand, France)* 52, 53–59. doi:10.1170/T708

Tsai, H.-H., and Miller, R. H. (2002). Glial cell migration directed by axon guidance cues. *Trends Neurosci.* 25, 173–175. discussion 175-176. doi:10.1016/s0166-2236(00)02096-8

Weh, E., Lutrzykowska, Z., Smith, A., Hager, H., Pawar, M., Wubben, T. J., et al. (2020). Hexokinase 2 is dispensable for photoreceptor development but is required for survival during aging and outer retinal stress. *Cell. Death Dis.* 11, 422. doi:10.1038/s41419-020-2638-2

Yamagata, M., Weiner, J. A., Dulac, C., Roth, K. A., and Sanes, J. R. (2006). Labeled lines in the retinotectal system: Markers for retinorecipient sublaminae and the retinal ganglion cell subsets that innervate them. *Mol. Cell. Neurosci.* 33, 296–310. doi:10.1016/j.mcn.2006.08.001

Yu, J., Xie, Y., Liu, Y., Wang, F., Li, M., and Qi, J. (2020). MBD2 and EZH2 regulate the expression of SFRP1 without affecting its methylation status in a colorectal cancer cell line. *Exp. Ther. Med.* 20, 242. doi:10.3892/etm.2020.9372

Zhou, X., and Stephens, M. (2012). Genome-wide efficient mixed-model analysis for association studies. *Nat. Genet.* 44, 821–824. doi:10.1038/ng.2310

frontiers | Frontiers in Genetics

TYPE Original Research
PUBLISHED 09 August 2023
DOI 10.3389/fgene.2023.1171217

OPEN ACCESS

EDITED BY
Denis Plotnikov,
Kazan State Medical University, Russia

REVIEWED BY
Irene Kaplow,
Carnegie Mellon University, United States
Ghasemali Garoosi,
Imam Khomeini International University, Iran

*CORRESPONDENCE
Veronique Vitart,
veronique.vitart@ed.ac.uk

RECEIVED 21 February 2023
ACCEPTED 17 July 2023
PUBLISHED 09 August 2023

CITATION
Jiang X, Boutin T and Vitart V (2023), Colocalization of corneal resistance factor GWAS loci with GTEx e/sQTLs highlights plausible candidate causal genes for keratoconus postnatal corneal stroma weakening.
Front. Genet. 14:1171217.
doi: 10.3389/fgene.2023.1171217

Colocalization of corneal resistance factor GWAS loci with GTEx e/sQTLs highlights plausible candidate causal genes for keratoconus postnatal corneal stroma weakening

Xinyi Jiang[1,2], Thibaud Boutin[1] and Veronique Vitart[1]*

[1]MRC Human Genetics Unit, Institute of Genetics and Cancer, University of Edinburgh, Edinburgh, United Kingdom, [2]Centre for Genetics and Molecular Medicine, Institute of Genetics and Cancer, University of Edinburgh, Edinburgh, United Kingdom

Background: Genome-wide association studies (GWAS) for corneal resistance factor (CRF) have identified 100s of loci and proved useful to uncover genetic determinants for keratoconus, a corneal ectasia of early-adulthood onset and common indication of corneal transplantation. In the current absence of studies to probe the impact of candidate causal variants in the cornea, we aimed to fill some of this knowledge gap by leveraging tissue-shared genetic effects.

Methods: 181 CRF signals were examined for evidence of colocalization with genetic signals affecting steady-state gene transcription and splicing in adult, non-eye, tissues of the Genotype-Tissue Expression (GTEx) project. Expression of candidate causal genes thus nominated was evaluated in single cell transcriptomes from adult cornea, limbus and conjunctiva. Fine-mapping and colocalization of CRF and keratoconus GWAS signals was also deployed to support their sharing causal variants.

Results and discussion: 26.5% of CRF causal signals colocalized with GTEx v8 signals and nominated genes enriched in genes with high and specific expression in corneal stromal cells amongst tissues examined. Enrichment analyses carried out with nearest genes to all 181 CRF GWAS signals indicated that stromal cells of the limbus could be susceptible to signals that did not colocalize with GTEx's. These cells might not be well represented in GTEx and/or the genetic associations might have context specific effects. The causal signals shared with GTEx provide new insights into mediation of CRF genetic effects, including modulation of splicing events. Functionally relevant roles for several implicated genes' products in providing tensile strength, mechano-sensing and signaling make the corresponding genes and regulatory variants prime candidates to be validated and their roles and effects across tissues elucidated. Colocalization of CRF and keratoconus GWAS signals strengthened support for shared causal variants but also highlighted many ways into which likely true shared signals could be missed when using readily available GWAS summary statistics.

KEYWORDS

cornea, genome-wide association studies, fine-mapping, colocalization, keratoconus, extracellular matrix, genotype–tissue expression, biomechanics min. 5–max. 8

1 Introduction

The cornea requires specific biomechanical and physical properties to enable a dome-like, transparent, protective, and highly refractive structure necessary for clear vision. Genome-wide association studies (GWASs) have given support to the notion that many genetic determinants of inter-individual variability in quantitative measures of those properties also contribute to disease risk. Identifying the causal variants for these associations and how they exert their effect could thus provide valuable pathogenic insights.

To date, GWAS for central corneal thickness (CCT) and corneal resistance factor (CRF) have proved particularly useful to inform on keratoconus susceptibility. Keratoconus is characterized by postnatal progressive thinning and weakening within the central cornea, manifesting by the surface of the eye adopting an irregular and distorted shape with localized steepening. Alterations in the collagen fibrillar structure constitutive of the corneal stroma underpin these changes (Meek et al., 2005), resulting in visual impairments, from myopia, irregular astigmatism and, in advanced cases, tissue scarring. Transcriptomics and proteomics have provided clues on molecular dysfunctions both in the stromal and epithelial layers of the cornea (Yam et al., 2019), but how they arise remains poorly understood (Davidson et al., 2014). Up to 16 keratoconus risk loci were first identified by testing the effects of variants yielded by CCT GWAS (Lu et al., 2013; Cuellar-Partida et al., 2015; Iglesias et al., 2018; Choquet et al., 2020) in, small, keratoconus case–control cohorts; those variants also associate with CRF (Jiang et al., 2020; Simcoe et al., 2020). A recent multi-ancestry keratoconus GWAS meta-analysis has yielded 36 loci reaching genome-wide significance (Hardcastle et al., 2021), 20 of which overlap with CRF or CCT loci known at the time or since established (He et al., 2022). Leveraging the suspected large contribution of CRF/CCT causal variants to disease risk, additional candidate risk loci (18 novel) have been subsequently extracted from the keratoconus GWAS results not reaching genome-wide significance (He et al., 2022).

Pleiotropy of genetic associations allows to propagate functional insights. Evidencing that causal signals for a trait of interest also underpin mRNA- or protein-level modulations is particularly useful, informing on both causal variants' function and the gene products plausibly mediating impact on trait (Albert and Kruglyak, 2015). With the current lack of GWAS for transcript or protein levels in the directly relevant corneal cells or tissues, we aim to exploit here the notion that a fraction of regulatory variants acts in the same or similar molecular way across multiple tissues in the body, so that effects in corneal cells could be extrapolated from those exerted in non-corneal tissues. Cross-tissues sharing has been extensively studied for the well-characterized catalog of genetic variation affecting steady-state transcript levels in 49 adult, non-ocular, tissues or cells from the Genotype–Tissue Expression (GTEx) consortium (Aguet et al., 2020). That of expression (e)QTLs was shown to be greater for those acting in cis than those acting in trans, and sharing distribution appears U-shaped, with cis-eQTLs discovered in only a few or many tissues (Aguet et al., 2017; Aguet et al., 2020). Regulatory effects sharing has been shown to increase with tissues' similarity, as evaluated from the patterns of gene expression or, inferred, major cell types' composition (Aguet et al., 2020), consistent with sharing of regulatory features across biologically related cell types (Meuleman et al., 2020). We previously reported significant enrichments of CRF GWAS variants in regions bearing hallmarks of regulatory regions in a wide range of tissues and cells, such as in the lungs, heart, skin, and fibroblasts (Jiang et al., 2020). This supports that CRF causal variants located in these regions might also underpin molecular quantitative trait loci (QTLs) detected in GTEx projects. Splicing (s)QTLs could be particularly informative as exerting similar effects across tissues expressing implicated isoforms (Aguet et al., 2020), while shared cis-eQTLs would require cautious interpretation with potential variable magnitude and direction of effects, and target genes nomination across tissues.

We re-analyzed the set of 115 CRF GWAS loci obtained from a single study of 72,301 unrelated UK Biobank participants from White-British ancestry (Jiang et al., 2020) to establish and examine sharing of causal signals with cis-acting GTEx e/sQTLs. This CRF GWAS set is well suited for linkage disequilibrium (LD)–informed fine-mapping, a key step to determine probabilities of causality for variants across loci. As multiple signals can reside at a locus, their identification during the fine-mapping step is increasingly recognized to improve colocalization analysis (Barbeira et al., 2021; Hukku et al., 2021; Wallace, 2021). The CRF loci analyzed here overlap 36 reported keratoconus risk loci, two of which are also Fuchs' endothelial corneal dystrophy (FECD) risk loci, and an additional FECD risk locus, *TCF4*.

Our analysis capitalizes on the latest GTEx release (v8) providing both eQTL and sQTL data and methodologies taking into account locus allelic heterogeneity (Barbeira et al., 2021). Thus, we considerably expand prior investigations which leveraged GTEx, v7, data. One used PrediXcan (Gamazon et al., 2015) to nominate CRF GWAS causal genes based on significant correlations between trait value and genetically predicted gene expression level in skin fibroblast–derived cells, deemed the most relevant (Simcoe et al., 2020). The genetic variants utilized in this type of approach are, however, not necessarily causal for the GWAS of interest, increasing the number of correlated non-causal associations (Wainberg et al., 2019). Another prior investigation used colocalization method which assumed only one causal signal per locus and restricted search to CRF signals with a highly likely causal variant (Jiang et al., 2020). Here, we also further utilize recent release of transcriptome at single-cell resolution for human cornea (Collin et al., 2021) to evaluate nominated candidate genes' expressions in the relevant tissue.

We reasoned that integration of e/sQTLs detected in GTEx tissues, despite the relevant target tissue not being included, could deliver a subset of plausible causal gene and variant candidates for altering corneal resistance. Given accessibility of cornea tissue, these might provide tractable targets for postnatal therapeutic interventions.

2 Results

2.1 Colocalization of CRF GWAS loci with GTEx v8 cis-eQTLs and -sQTLs

Fine-mapping of the analyzed 115 CRF GWAS loci using DAP-G (Wen et al., 2016), to match the method deployed to narrow-down

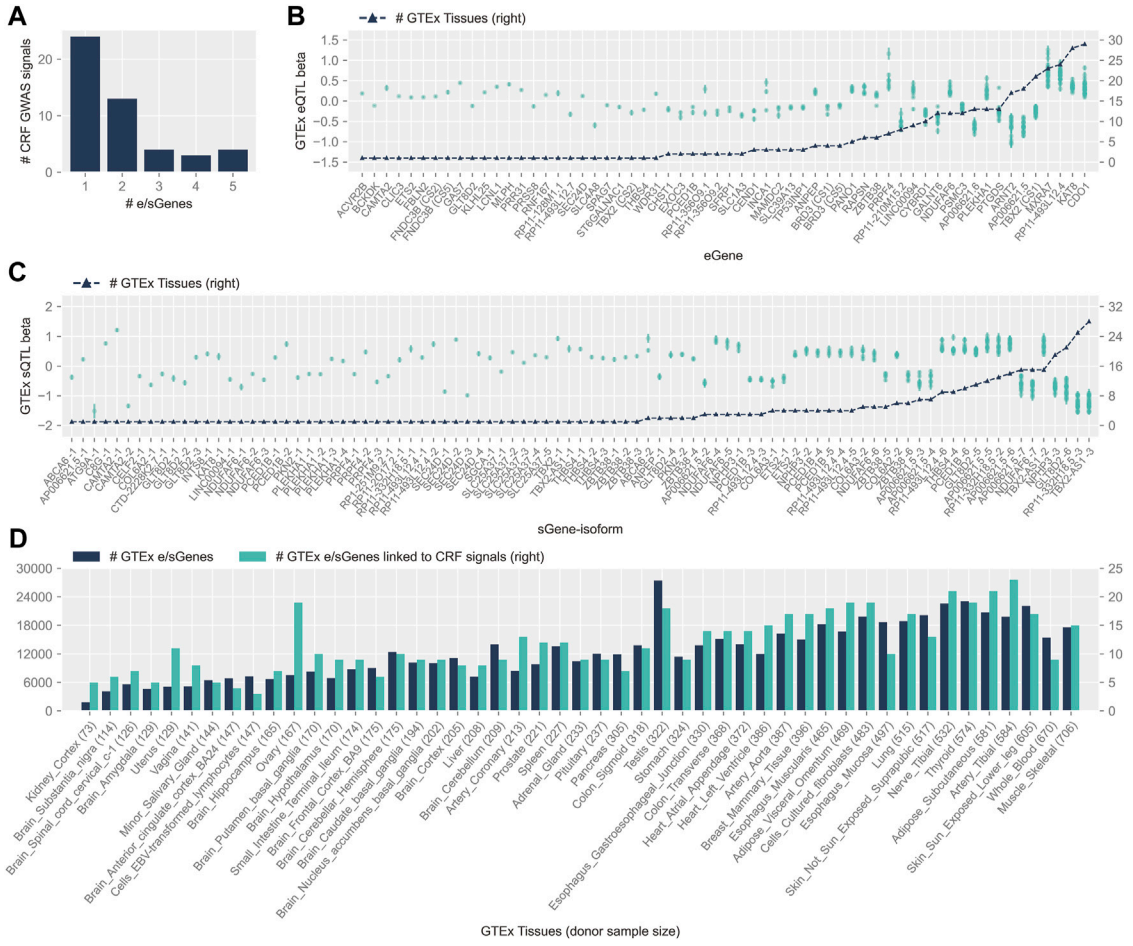

FIGURE 1
Features of colocalizing GTEx v8 cis-e/sQTLs and CRF GWAS signals. **(A)** Distribution of the number of e/sGenes nominated at CRF GWAS signals. **(B)** GTEx cis-eQTL effects (betas), ordered by increasing number of tissues where colocalization with CRF signals was detected (black triangles and scale displayed on right *y*-axis). Effect on mRNA (left *y*-axis scale) is reported for the CRF increasing allele of the lead CRF variant, with standard error of estimate displayed by a bar. Independent signals linked to the same eGene are indicated by unique credible set ID shown in parentheses. **(C)** Same as **(B)** for cis-sQTLs; target sGenes on the *x*-axis are followed by isoform ID (isoform information details can be found in Supplementary Table S3). **(D)** Plots of the number of e/sGenes linked to cis-e/sQTLs from the whole of the GTEx repertoire (dark color) and from the subset colocalizing with CRF GWAS signals (light color), across tissues. The latter are sorted by increasing donor sample size shown in parentheses.

causal variants underpinning eQTLs and sQTLs signals in 49 GTEx tissues (Barbeira et al., 2021), yielded 181 95% credible sets (CS) of causal variants (Supplementary Table S1), with about a third (32%) of the loci harboring multiple signals. These CS matched closely, albeit not perfectly, those obtained previously (Jiang et al., 2020) using FINEMAP (Benner et al., 2016), a different Bayesian method (Supplementary Figure S1). No 95% CS are defined here for CRF locus 11 (closest gene to lead variant *EFEMP1*) and locus 100 (closest gene *ALDH3A1*), the latter also a keratoconus GWAS locus.

Five missense variants with CS posterior inclusion probability (PIP) greater than 99%, located in *ABCA6*, *ADAMST17*, *FBN2*, *GLT8D2*, and *WNT10A*, have previously been discussed (Jiang et al., 2020). Six missense variants with PIP ranging from 0.55% to 22.3% might underlie other associations, based on Combined Annotation Dependent Depletion scores (Kircher et al., 2014) greater than 20, indicating functional impact, at the same (*GLT8D2*, p.M273V) or other (in *COL6A2*, *ITIH3*, *PTPN13*, *WDR31*, and *ZHX3*) loci. The vast majority of the 5,177 candidate causal variants (Supplementary Table S1) is non-coding following variant effect predictor (VEP) (McLaren et al., 2016) annotations: 62% intronic, 15% upstream or downstream genes, and 3% intergenic.

Ninety-nine (55%) of the 181 CRF CS overlapping those defined for cis-e/sQTLs in GTEx tissues were subjected to colocalization analysis (Supplementary Tables S2, S3). The colocalization support obtained from two methods—fastENLOC regional colocalization probability (RCP) and colocalization posterior probability (CLPP)—was highly correlated, with Pearson's R of 0.92 (p-value 3.52×10^{-157}) and 0.87 (p-value 6.83×10^{-96}) for cis-eQTL and cis-sQTL, respectively (Supplementary Figure S2). Forty-eight (26.5%) CRF signals colocalized with GTEx cis-e/sQTL signals, implicating 73 genes (Supplementary Figure S3), with most often one but up to five genes nominated per signal (Figure 1A). Hence, 38 (52%) candidate causal genes are not the nearest gene to the lead variant (with the highest PIP), which include 18 that are not the nearest genes to any variant in CRF CS (*AP006621.6*, *CEND1*, and *PANO1*;

ATG9A; *C8G*, *CLIC3*, *LCNL1*, and *PTGDS*; RP1-251M9.2; *INTS8*; *PCED1B*; *RP11-128M1.1*; *RP11-210M15.2*; *SLC1A3*; *SLC39A13*; *SLC4A8*; *ST6GALNAC1*; *RP11-332H18.5*).

Loci with allelic heterogeneity where independent CS pointed to the same unique target gene strengthen causal gene candidacy. At both CRF loci 81 and 105, along with the CS composed of a highly likely (PIP > 99%) predicted functional coding variant, at respectively *GLT8D2* (pTyr24Cys) and *ABCA6* (p.Cys1359Arg), other sets colocalize with eQTL and sQTL (for *GLT8D2*) or with an sQTL (for *ABCA6*). Two other loci have two CS each co-localizing with eQTLs for the same unique eGene: *FNDC3B* (in different tissues, adipose–visceral omentum, and tibial nerve) and *TBX2* (with effect detected solely in muscle–skeletal tissue for one of the two signals, and the other detected in 20 additional tissues). We have previously highlighted *GLT8D2* and *ABCA6* relevance to cornea biology (Jiang et al., 2020). The former encodes a glycosyltransferase, substrates of which might comprise components of the proteoglycan and glycoprotein–rich extracellular matrix (ECM) of the cornea, and the latter is a top upregulated gene in cultured corneal fibroblasts from granular cornea dystrophy patients (Choi et al., 2010). Fibronectin type III domain containing 3B has an endoplasmic reticulum (ER) membrane location and been implicated in ER and secretory homeostasis (Fucci et al., 2020); zebrafish deficient in its paralog Fndc3a display severe ECM alterations (Liedtke et al., 2019). TBX2 encodes for a T-Box transcription factor 2 that has been implicated in a syndromal cardiovascular and skeletal disorder (Liu et al., 2018).

About half of the colocalizations (58% with eGenes and 56% with sGenes) were found in more than one tissue. For those, the direction of effect on molecular traits for the lead variants' CRF increasing allele was consistent across tissues for all sQTLs and 30 out of 35 (86%) eQTLs (Figures 1B,C). The direction of effects that these variants might have on gene expression in the cornea can thus be advanced with stronger support. Concordant with cis-e/sQTLs detection in GTEx (Aguet et al., 2020), the number of genes linked to colocalizing signals in each tissue was donors' sample size dependent, with a Spearman's correlation of 0.75 (p-value 4.7×10^{-10}). Considering this bias, the cell type heterogeneity within tissues, and the overall small number of colocalizing signals per tissue, the apparent increased sharing of CRF signals with e/sQTLs in the uterus and ovary, and in other diverse tissues such as the heart, blood vessels, and adipose tissues (Figure 1D), can only be tentatively advanced. Of note, the proportion of unique causal signals at the CRF loci colocalizing with GTEx e/sQTLs was greater, although not significant (Fisher exact test p-value = 0.26), for loci reportedly associated with keratoconus (55.6%) than for those loci not associated (37%).

We further utilized the published transposase-accessible chromatin data for two immortalized cell lines derived from human cornea keratocytes (hTK) and cornea epithelial cells (hTCEpi) (Jiang et al., 2020). Most of the e/sGenes implicated as CRF target genes by colocalization (57/73, 78%) have at least one associated candidate causal variant lying in an open chromatin region (OCR) in hTK, mostly, or in hTCEpi cells (Supplementary Figure S3). This supports functional potential in the cornea, particularly in stromal cells, for those causal variant candidates affecting transcription in non-corneal tissues.

2.2 Bioinformatics support for variant causality at CRF loci colocalizing with GTEx sQTLs

Some variants in the CRF CS can be prioritized by our results and genomics input. The lead variant (PIP = 0.538) of the single signal at CRF locus 39, rs13167730, a VEP-annotated splice donor variant, is highly likely to be causal. It is located at the very 5′-end of the differentially excised *THBS4* intron in a splicing event implicated in nine tissues (Figure 2; Table 1), with the CRF increasing G allele associated with increased excision event and more favorable splice donor site [G to T transition −4.751 MMSplice donor score (Cheng et al., 2019)]. No other shared sQTL and CRF causal variant candidate localizes at a canonical intronic dinucleotide acceptor or donor site flanking an implicated splicing event. As previously noted within GTEx data (Aguet et al., 2020), splice donor or acceptor variants represent only a small fraction of sVariants, in line with diverse sequences influencing splicing outside core dinucleotide splice sites (Wang and Burge, 2008). Functional genomic predictions in these intronic and exonic regions are still challenging and driven by machine learning methods such as MMSplice (Cheng et al., 2019). The reference (ref) alleles at five of six putative CRF causal variants localized within 25 bp of a splice junction site highlighted by colocalization with GTEx sQTL show concordant predicted (MMSplice) and observed splicing effect directions (Table 1), supporting causality and mechanism.

Causality for rs786906, located 1 bp away from a canonical acceptor site, is less conclusive. The MMSplice_acceptor score, 0.787, predicts splicing of the *PKN2* intron ending at the acceptor site to be favored by the alternate C allele, but this does not match the allelic effect on the corresponding events observed in GTEx tissues. The frequent effects of sQTLs on more than one splicing event and via mechanisms other than altering splice sites (Garrido-Martin et al., 2021) make functional prioritization of candidate causal variants at this and at the majority of loci colocalizing with sQTLs, distant from implicated splice sites, challenging.

2.3 Colocalization analysis of CRF GWAS loci with keratoconus GWAS loci

Summary statistics for the largest keratoconus GWAS to date (Hardcastle et al., 2021) are from the meta-analysis of multi-ethnic cohorts (36 reported risk loci, ~89% European, 4,669 cases, and 116,547 controls), a situation that might compromise causal signals' fine-mapping and colocalization owing to the potential mixed pattern of LD around causal variants or uneven missing variants across cohorts. Additionally, the keratoconus study size is relatively small, which could prevent good definition of multiple signals at a locus. Nevertheless, surmising that the comparisons of signals obtained in independent CRF and keratoconus GWAS could provide valuable information, we explored here evidence of causal variants sharing at 18 keratoconus GWAS loci, by applying three combinations of different statistical fine-mapping and colocalization methods (Supplementary Tables S4–S7) adopted by the research community.

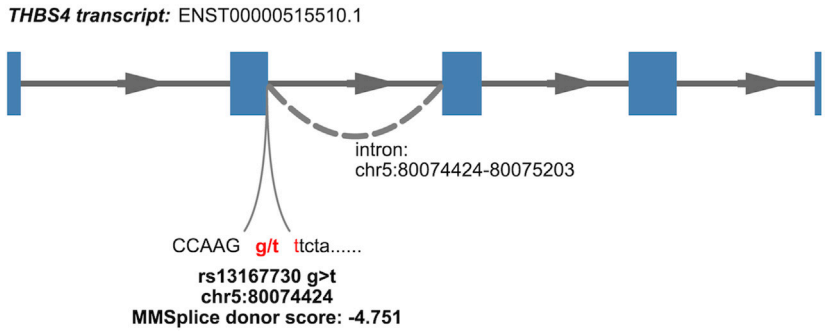

FIGURE 2
Nominated causal variant and mechanism for association at a CRF GWAS signal colocalizing with a THBS4 sQTL (isoform 4, Supplementary Table S3) detected in GTEx v8 tissues. The variant lies within a canonical donor splice site, dinucleotide gt, indicated in red; annotation of isoform is from Ensembl release 108 and GRCh38 coordinates.

Overall, 17 shared GWAS causal signals (within 15 loci) were detected by at least one method, seven of which by all three methods (Table 2). Of note, half of the paired association signals do not pass the criterion we applied with the GTEx data to insure credible colocalization (Table 2), that the intersecting CS variants retain at least 50% PIP of each GWAS signal; sparsity of keratoconus GWAS meta-analysis summary statistics at these loci makes failing it likely.

For five of the "consensus" shared signals, the causal genes could be nominated from colocalization of CRF and GTEx QTLs (Table 2). At the two other "consensus" shared causal signals, near *LINC00970* and *SMAD3*, respectively, at CRF locus 4, also a FECD locus, and locus 90, the very stable fine-mapped CS across methods and independent GWAS (Supplementary Table S4) strengthen causal candidacy of non-coding variants: lead variant rs1200108, with PIP ranging from 0.40 to 0.69, for the former and three variants (rs12913547, rs12912010, and rs12912045) for the latter. The genome-wide enhancer to target map created by activity-by-contact (ABC) model in 131 cell types and tissues (Nasser et al., 2021) does not help in linking rs1200108 to the target gene but the CS variants at locus 90 locate in an enhancer linked to *SMAD3*, based on the ABCmax score (0.033) in transformed *MCF10A* human mammary epithelial cell line.

Overall, the two fine-mapping methods SuSiE and DAP-G return very similar CS, and five colocalizations agreed by both fastENLOC and COLOC, implicating the sGene *SGCA* and the eGene *RP11-128M1.1*.

Colocalizations only detected by DAP-G/fastENLOC (with the closest coding genes *COL5A1* and *IQCH*) appear poorly supported when examining CS overlap, in contrast to those only detected with FINEMAP/CLPP at two loci. At the first locus, the variant with the highest PIP in the solely FINEMAP-defined signal (rs4646785, intronic *ALDH3A1*, *PIP = 0.26*) forms the keratoconus credible set defined by all three fine-mapping methods (PIP >0.95). This most supported causal variant falls in an enhancer linked to *ALDH3A1* by the ABC method (ABCmax = 0.15 in PC-9 cells, derived from human lung carcinoma). This is a very plausible candidate gene encoding for a crystallin protein with an important UV protection role, among others, in the cornea (Estey et al., 2007). At the other locus, the CRF credible set is nearly identical using DAP-G, SuSiE, or FINEMAP (one of four CS at this locus) and colocalized with *COL6A2* sQTL in GTEx tissue.

Colocalization with keratoconus loci was not detected for three CRF loci (54, 56, and 97), with the nearest protein coding genes *NDUFAF6*, *MPDZ*, and *ZNF469*; these loci display well-correlated association patterns (Supplementary Figure S4). The lead SNPs in these three signals are in high LD with many other variants and the association signals strong, making the ranking of the lead variant plausibly highly sensitive to sampling variation.

We also note other undetected but likely shared causal variants at two additional loci. The reported lead keratoconus GWAS variant (rs142493024, p-value = 9×10^{-12}) at locus 35 (Hardcastle et al., 2021) is a low-frequency variant missing from summary statistics, along with the other intronic *COL6A1* variants forming one of four CS delineated at CRF locus 115 by DAP-G (cs1), SuSiE (cs1), and FINEMAP (cs4) (Supplementary Table S4). One of the multiple signals at CRF locus 29 has similarly no paired signal in keratoconus data with unique credible variant rs7635832 (PIP >0.97 by all three fine-mapping methods) missing; shared causal signal is strongly supported by variant rs4894414 in high LD (r^2 = 0.88) with this missing variant forming a keratoconus credible set (PIP>0.95 all fine-mapping methods). The CRF fine-mapped causal variant was not linked to GTEx e/sGene and neither variant at this locus located within enhancers of published ABC catalog (Nasser et al., 2021).

2.4 Main target corneal cell types for CRF GWAS loci

To strengthen support for genes implicated by colocalization with GTEx e/sQTLs participating in corneal phenotypes and provide context for their function, we examined their transcript level in corneal and pericorneal cell types of adult human cornea using a recently released single-cell atlas (Collin et al., 2021). All 59 implicated protein-coding genes and two long non-coding RNA *TBX2-AS1* and LINC00094 (alias BRD3OS) have normalized expression levels equal to or above 1 in at least one cell type (Figure 3). Unsupervised hierarchical clustering based on these levels led to biologically meaningful grouping of cells with separation of stromal, endothelial, and epithelial cells

TABLE 1 CRF credible set variants locating within 25 bp of splice junctions implicated by colocalization of CRF signals with GTEx sQTLs. Variant ID indicates variant chromosome:position in GRCh38 coordinates:reference allele:alternate allele. MMSplice score indicates the predicted change in effect on splicing for the alternate when compared to the reference allele. PIP is the variant posterior inclusion probability to CRF 95% credible set of causal variants.

Variant ID (rsID)	Splicing-increasing allele		PIP (CRF increasing allele)	sGene	Intron excised	Reference transcript	GTEx tissues
	Predicted (MMSplice score)	GTEx					
chr1:88805891:T:C (rs786906)	C (acceptor 0.787)	T	0.1 (T)	*PKN2*	88805672–88805890	ENST00000370521.7 (Exon 11 -> Exon 12)	Pancreas, skin Sun exposed lower leg
						ENST00000370513.9 (Exon 10 -> Exon 11)	
chr4:118816730:T:C (rs3775839)	T (donor intron −0.076)	T	0.05 (C)	*SEC24D*	118815727–118816743	ENST00000506622.5 (Exon6 -> Exon5)	Testis
chr5:80074424:G:T (rs13167730)	G (donor −4.75)	G	0.54 (G)	*THBS4*	80074424–80075203	ENST00000515510.1 (Exon2 -> Exon3)	Adipose subcutaneous, adipose visceral omentum, breast mammary tissue, esophagus gastroesophageal junction, heart left ventricle, muscle skeletal, pituitary, testis, thyroid
chr12:47249150:T:A (rs855157)	A (exon 0.326)	A	0.02 (A)	*PCED1B*	47248302–47249134	Unnamed	Artery tibial, colon sigmoid, artery aorta, artery coronary
				RP11-493L12.4			
chr12:47257447:C:T (rs855175)	T (acceptor 0.142)	T	0.03 (T)	*PCED1B*	47249429–47257461*	Unnamed	Colon sigmoid, lung, artery tibial, breast mammary tissue, adrenal gland, adipose subcutaneous, small intestine terminal ileum, ovary*, artery coronary, spleen
				RP11-493L12.4			
chr12:104021466:C:T (rs11553764)	T (exon 0.163)	T	0.28 (T)	*GLT8D2*	104021492–104029695	Unnamed	Testis
					104021492–104049894	ENST00000360814.8 (Exon2 -> Exon1)	Artery tibial, pituitary
						ENST00000547583.1 (Exon2 -> Exon1)	
chr17:61399054:T:C (rs1476781)	T (exon −0.08)	T	0.16 (C)	*TBX2-AS1*	61393748–61399036	ENST00000590421.1 (Exon2 -> Exon1)	Nerve tibial, pituitary, prostate, adipose subcutaneous, ovary, stomach, spleen, uterus, thyroid, heart left ventricle**
				RP11-332H18.5			

*colocalizing sQTL in the ovary was associated with additional intron, chr12:47249232_47257461, splicing; ** colocalization with the same sQTL was detected in 21 additional GTEx tissues (Supplementary Table S3).

suggesting cell type informative expression (Figure 3). The two corneal stroma cell types, keratocytes and stem cells, clustered tightly together, with high-level co-expression (normalized expression level ≥ 2) of six eGenes or sGenes: *LCNL1*, *CHST1*, *GALNT6*, *THBS4*, *PTGDS*, and *GLT8D2*. The latter three were also marker genes (logFC ≥ 0.25, compared to all remaining cell clusters) for these two cell types (Collin et al., 2021). Two limbal cell types, fibroblasts and stroma keratocytes, were further partitioned together with corneal stroma cells in a stromal cluster showing co-expression (normalized expression ≥ 1) of *COL6A2*, *COL6A3*, and *FNDC3B*. Significant enrichment for candidate CRF e/sGenes expression was found in corneal stromal stem cells and keratocytes among the tested cell types (Figure 4). Considering that GTEx-nominated e/sGenes represent candidate target genes for only a subset, 26.5%, of CRF signals (48 out of 181 GWAS signals), we also performed enrichment analysis using this gene set augmented with the nearest genes for all 181 CRF GWAS signals, and with the nearest genes only (Figure 4). The heuristic "nearest genes to lead SNPs" method for nominating causal genes has been shown on an exemplar data set to have high recall value but lacking in precision (Nasser et al., 2021). Enrichment with the nearest genes was significant in all four stromal cluster cell types, corneal and limbal, with that in corneal cells clearly driven by e/sGenes. Of note, no epithelial cell type shows enrichment whichever gene set was

TABLE 2 CRF and keratoconus GWAS signals colocalizing following at least one of the three methodologies deployed. More information about the CRF locus can be found in Supplementary Table S1 and description of the three combined fine-mapping and colocalization methods, DAP-G–fastENLOC, SuSiE–COLOC, and FINEMAP–CLPP, in the Materials and Methods section, with full results detailed in Supplementary Tables S4–S7. cs id: credible set identifier. Same signal: whether the colocalizing CRF signals found by different methods are likely identical (sum of posterior inclusion probabilities for shared variants across credible sets is larger than 50%); eGenes/sGenes: the genes implicated by GTEx v8 e/sQTL and CRF colocalizing DAP-G–defined signals; no QTL: no GTEx v8 credible sets overlapping with signals; no Coloc: at least one variant has available GTEx v8 QTL information but no significant colocalization was found; NA: no e/sGenes implicated as those were determined using DAP-G–defined credible sets; in red: sum of PIP for variants shared with CRF/keratoconus cs is lower than 50%.

CRF locus	DAP-G–fastENLOC		SuSiE–COLOC		FINEMAP–CLPP		Same signal	Nearest gene (nearest coding gene)	eGenes	sGene
	CRF cs id	Kerato cs id	CRF cs id	Kerato cs id	CRF cs id	Kerato cs id				
4	1	1	1	1	1	1	TRUE	*LINC00970* (*ATP1B1*)	no QTL	no QTL
6	1	1	1	1	\	\	TRUE	*C1orf132 (CD34)*	no Coloc	no Coloc
29	3	3	3	5	\	\	TRUE	*TMEM212*	no QTL	no QTL
	2	2	2	2	1	2	TRUE	*TMEM212*	*FNDC3B*	no QTL
36	2	1	1	1	\	\	FALSE	*RP11-94D20.1* (*MOCS2*)	no QTL	no QTL
60	4	1	\	\	\	\	\	*RP11-473E2.4* (*COL5A1*)	no QTL	no QTL
61	1	1	1	1	1	1	TRUE	*LCN12*	PTGDS, PRR31, LCNL1, CLIC3	C8G
69	1	1	1	1	1	1	TRUE	*CMB9-55F22.1* (*PDDC1*)	*CEND1*, *PANO1*, *AP006621.5*, *AP006621.6*	*AP006621.5*
77	1	1	1	1	1	1	TRUE	*GALTN6*	*SLC4A8*, *GALNT6*	no QTL
83	1	1	1	1	\	\	TRUE	*FOXO1*	no Coloc	no QTL
90	1	1	1	1	1	1	TRUE	*SMAD3*	no QTL	no QTL
	2	2	\	\	\	\	\	*IQCH*	no Coloc	no Coloc
98	1	1	1	1	1	1	TRUE	*CAMTA2*	*CAMTA2*, *RNF167*, *SPAG7*, *INCA1*	*CAMTA2*
100	\	\	\	\	1	1	\	*ALDH3A1*	NA	NA
103	1	1	1	1	\	\	TRUE	*SGCA*	no Coloc	*SGCA*
112	1	1	1	1	\	\	TRUE	*STK35*	*RP11-128M1.1*	no QTL
115	\	\	\	\	1	1	\	*COL6A2*	no Coloc	*COL6A2*

10.3389/fgene.2023.1171217

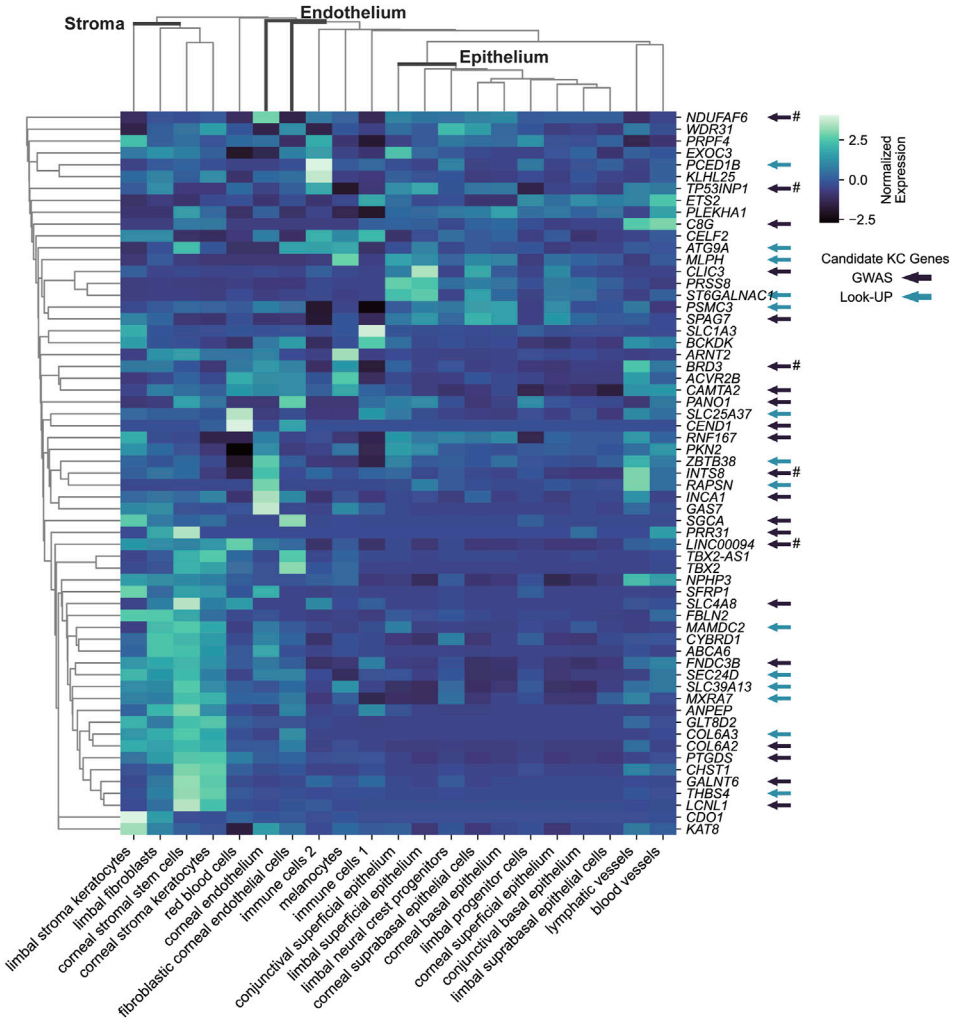

FIGURE 3
Transcriptional expression level for CRF candidate target e/sGenes across cell types of the human adult cornea cell atlas. Subset of keratoconus candidate causal genes is indicated by arrow: in dark colors, those implicated by keratoconus GWAS; in light colors, those implicated by associations using CRF or CCT associated variants (look up). # indicates that there is no evidence that the CRF and keratoconus overlapping GWAS signals are the same from colocalization analysis. Unsupervised clustering based on normalized expression levels from Collin et al (2021) analysis was performed using the *clustermap* function in python package *seaborn* v0.12.2.

tested, while some enrichment in endothelial cells is detected but not strong enough to reach significance. The stronger gene sets enrichment in corneal stromal cells when e/sGenes complement the nearest genes list and the contrasted difference in enrichment magnitude between corneal and limbal keratocytes for the nearest genes (small) and e/sGenes (large) (Figure 4) suggest selection bias in causal genes nomination from regulatory signals detected in GTEx tissues.

Conditional enrichment analysis was performed to investigate whether the significant enrichment in a given cell type is independent of that in other cell types (Supplementary Figure S5). For CRF-identified e/sGenes, no significant enrichment remains when either corneal stroma keratocytes or stem cells are conditioned on, indicating that enrichment is largely driven by a shared set of expressed genes. A hint of genes specifically enriched in the contributing stem cells is notable but enrichment does not reach significance. For the same gene set with the nearest genes added, the enrichments detected in corneal stroma keratocytes and stem cells show similar dependency, in line with these enrichments being driven by identified e/sGenes. Conditional analyses also confirmed limbal stromal keratocytes and fibroblast enrichments detected with this gene set are driven mostly by genes distinct from those driving corneal stromal cell types' enrichment. Of note, the two limbal cell types enriched do not show complete dependency and a significant enrichment in limbal fibroblast remains after conditioning on limbal stromal keratocytes expression.

The top 10% ranked genes based on cell-specificity metrics for each individual cell type are listed in Supplementary Table S8.

3 Discussion

Using the GTEx data, a resource combining dense genotyping data with molecular traits uniformly acquired across tissues collected post-mortem (Aguet et al., 2017), we obtained from colocalizing CRF and cis e/s-QTL signals both gene products that

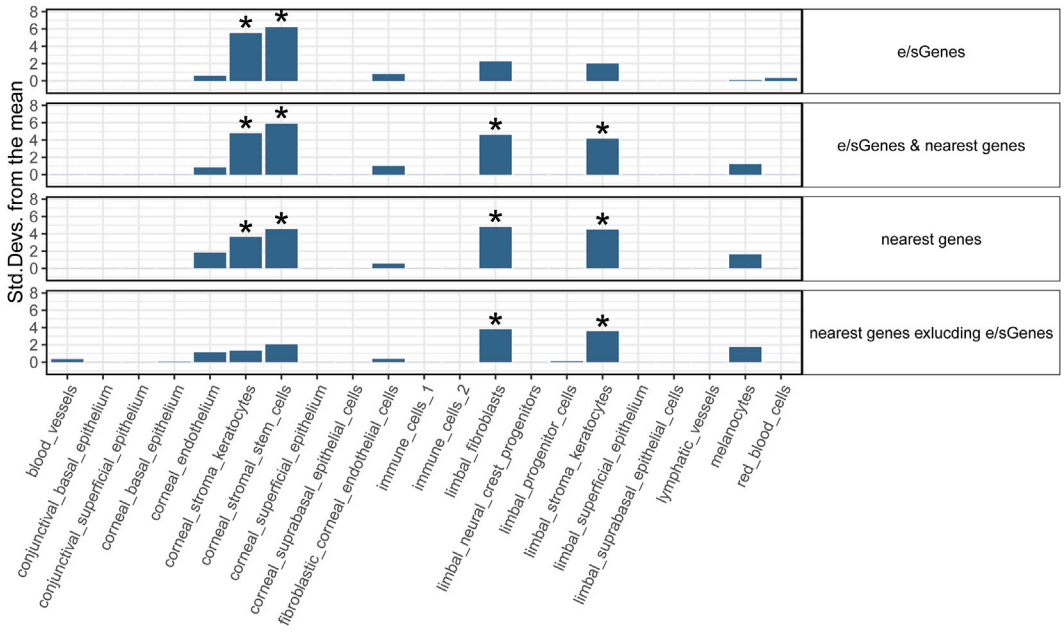

FIGURE 4
Cell type enrichment of CRF candidate target genes in human adult cornea. Four target gene sets are tested: 1) e/sGenes: e/sGenes nominated by colocalization of CRF and GTEx v8 QTL signals, 2) e/sGenes & nearest genes: e/sGenes and the nearest genes to lead variants of CRF fine-mapped signals, if not already e/sGenes, 3) nearest genes, and 4) nearest genes excluding nominated e/sGenes. *y*-axis: the number of standard deviations from the mean expression level was found to be in the target gene set, relative to the mean expression level from bootstrap-generated gene sets, sampled without replacement from data set gene list. *: significant enrichment (Benjamini–Hochberg corrected q-value ≤ 0.05).

could participate in phenotypic outcome and the nature, and potentially the identity, of causative variants. This approach to nominate plausible causal genes, despite their absence in GTEx of the target tissue in which they most likely mediate the effect on phenotype, was vindicated by experimental follow-up in a recent investigation of bone mineral density associations (Al-Barghouthi et al., 2022). Here, its potential value is supported by several lines of evidence.

The analysis of cornea single-cell transcriptomic profiles showed that the expression of the identified CRF target genes is enriched in cells from the corneal stroma. This is in line with the abundant highly organized collagenous ECM produced by these cells, being a major determinant of the biomechanical properties of the cornea (Yang et al., 2022). Indeed, 13 of the 73 GTEx-nominated genes encode for core matrisome constituents (*COL6A2*, *COL6A3*, and *FBLN2*), glycosylation and sulfation enzymes that are likely to affect proteoglycans and glycoproteins–rich ECM (keratan sulfotransferase *CHST1*, *ST6GALNAC1*, *GLT8D2*, and *GALNT6*), an endoplasmic reticulum to Golgi export component (*SEC24D*) involved in procollagen trafficking (Lu et al., 2022), a component of the sarcoglycan complex anchoring cells to the ECM (*SGCA*), and ECM remodeling actors and regulators (*LINC0094*, *MXRA7*, *THBS4*, and *SFRP1*) (Subramanian and Schilling, 2014; Wang et al., 2020; Piipponen et al., 2022; Shen et al., 2023). An additional eGene, the zinc transporter encoding gene *SLC39A13*, is mutated in spondylodysplastic Ehlers–Danlos syndrome (OMIM 612350), a rare syndrome with multi-tissues manifestations: skeletal dysplasia, blue sclera, muscular hypotonia, and ocular impairments that include myopia and keratoconus. The ECM plays essential structural and physiological roles in all tissues, in health and disease (Frantz et al., 2010) and tissue sharing of gene products impacting on its, tissue-diverse, composition indicated by a wide range of systemic manifestations in inherited monogenic connective and musculoskeletal tissue disorders (Callewaert et al., 2008; Voermans et al., 2008).

Our results leveraging genetic control of gene expression in tissues other than the cornea suggest some level of regulatory instructions sharing for ECM-concerned genes across tissues. The gene encoding sarcoglycan A is an interesting target gene considering that the closest coding gene at an intergenic unresolved signal in CRF locus 82 encodes for another subunit of the sarcoglycan complex, SGCG, and both SGCA and SGCG are known to bind, in the muscles, to the ECM component biglycan (Rafii et al., 2006) that is encoded by the closest gene to a strong CRF signal reported on the X chromosome (Simcoe et al., 2020), not analyzed here. Biglycan also interacts with type VI collagen (Wiberg et al., 2002), strongly causally implicated in CRF determination by our present analysis and that of rare coding variants (van Hout et al., 2020) and both implicated in regulating ECM stiffness and maximal load (Leiphart et al., 2021). The anchoring of cells to the ECM via bridging interactions is thought to play a critical role in mechanosensing and signaling, processes that have not been previously highlighted in the context of CRF or keratoconus GWAS interpretations but recognized important players in cornea biology (Yang et al., 2022), and potential drivers of keratoconus pathology (Dou et al., 2022). Among its multiple roles, *THBS4* has been shown to influence trafficking of sarcoglycans in myocytes (Brody et al., 2018), but the function of

the specific isoform modulated by causal splicing variant highlighted by our study remains to be determined. *PLEKH1*, also known as *TAPP1*, encoded by an implicated eGene, is one plausible effector of signals transduced by sarcoglycans' associated macromolecular complexes as recruited by syntrophins, adapter proteins, in fibroblasts (Hogan et al., 2004); it also interacts with cytoplasmic tyrosine phosphatase *PTPN13* (Kimber et al., 2003), implicated by a credible set coding variant (pE1630K).

The fraction of all CRF-associated causal variant and gene candidates exposed here are likely relevant to more than one tissue and involved in homeostatic rather than (or as well as) developmental processes. These are important considerations for the identification of potential therapeutic targets for postnatal interventions. Many CRF GWAS variants show associations with other traits and diseases and significant genetic correlations reported with ocular and, at lower strength, non-ocular traits such as blood pressure and respiratory capacity (Simcoe et al., 2020). Colocalization would enable transfer of knowledge and hypothesis on causal mechanisms across these traits and diseases. Combined genomic and fine-mapping evidence have well established that the majority of GWAS signals reside in putative enhancer regions, but the relative lack of their colocalization with detected eQTL, even when target tissues are surveyed, has been much remarked upon (Connally et al., 2022). Assuming false negative results from colocalization and power are minor or non-issues, the most obvious explanation is that the right cellular context is not interrogated or masked in bulk RNA analysis of heterogeneous tissues. The genes causally implicated by colocalizing CRF and GTEx e/sQTLs appear biologically relevant, but our enrichment analyses show them to be skewed toward those expressed in two corneal stromal cell types when compared to the, larger, set of genes nearest to signals. These show significant enrichments in two additional, limbal, cell types, which indicates an inherent bias in the representation of cell types (or states) in the GTEx data resource and/or plausible higher specificity of genetic regulation of implicated genes expressed in the limbal cell types. The current and future growing focus on cataloging molecular traits' associations in specific cellular contexts should help unmask some missed regulatory links between variants and genes (van der Wijst et al., 2020; Balliu et al., 2021; Neavin et al., 2021).

It has been argued that eQTL mapping efforts might, however, never fully evidence all missing cis regulatory GWAS hits as GWAS and eQTL detections operate under different premises (Mostafavi et al., 2022). For example, variants with small effect on the transcript level of genes that are tightly regulated and critical during development have little power to be detected by eQTL analysis, yet are likely to have a strong effect on the phenotype. This might be the case for the candidate coding genes previously highlighted as strongly supported by their role in Mendelian cornea and/or connective tissue disorders (Iglesias et al., 2018; He et al., 2022) which are notably absent from the e/sGenes; they are *UBIAD1* (CRF locus 1 cs1) implicated in Schnyder corneal dystrophy (OMIM 121800), *DCN* (CRF locus 79), *TGFB2* (CRF locus 7 cs1), *SMAD3* (CRF locus 90), *COL5A1* (locus 60 cs2, cs3, and cs4), *ZNF469* (CRF locus 97 cs1) implicated in stromal cornea dystrophy (OMIM 610048), Loeys–Dietz syndrome types 4 (OMIM 614816) and 3 (OMIM 613795), and classical Ehlers–Danlos (OMIM 130000) and Brittle cornea (OMIM 229200) syndromes, and all are potential keratoconus susceptibility genes. All, but *TGFB2*, are the closest coding genes to lead variants (highest PIP in CS), and for all, the lead variants are located 13–590 kb [median 92.5 kb] away from their promoter, in putative enhancer regions. One of these enhancers affecting *SMAD3* is the most supported in transformed cells subjected to tamoxifen treatment (Ji et al., 2018) among a wide range of cells surveyed using the ABC method (Nasser et al., 2021), supporting that some of the enhancers and associated variants might be revealed only under specific challenges. In the adult corneal and pericorneal tissues' single-cell transcriptomics data examined, *ZNF469* and *COL5A1* showed high specificity of expression (>60%) in the limbal stroma keratocytes, a cell type (or state) not significantly enriched in target genes implicated by colocalization with GTEx e/sQTLs. The non-detection of highly likely target genes as eGenes could thus be due to non-representation in GTEx of cell types/states in which variants exert their effects. It remains to be seen whether or not they will be detected in future eQTL efforts or by other means, and how specific in time, space, and environment their regulatory function might be.

Other limitations of our and similar studies lie in the means to ascertain that causal variants are shared, i.e., colocalization of fine-mapped signals, as both statistical fine-mapping and colocalization have limitations (Hukku et al., 2021; Wallace, 2021). Regions with multiple causal signals that are physically close and in some level of LD, which fine-mapping algorithms might resolve differently, requirements for LD reference matching summary statistics and consequences of insufficiently powered studies or missing data for the proper enumeration of CS to be compared, the choice of prior probability of colocalization for Bayesian methods are all influencing parameters. Methods to identify errors or heterogeneity in GWAS summary statistic (Chen et al., 2021) could have been deployed to remove problematic markers or loci but missing data would remain a major problem. Increasing availability of whole genome sequences for large data sets on which well-powered GWAS can be performed, such as that of a quantitative measure like CRF in the UK Biobank, will make those GWAS the best suited for colocalization analyses.

We noted some variations in the eQTL colocalization results between our current and previous analyses of the subset of CRF loci; while the analysis should have improved by taking into account the locus heterogeneity in both data sets and GTEx analysis being more powered in v8 than in v7, the more stringent criteria that we applied to ensure credible colocalization and differences in methodology all contributed to this variation and missed potentially true shared signals. *GLT8D1*, for example, is biologically supported by another glycosyltransferase *GLT8D2* being implicated at another locus by two independent causal signals. The CRF signal passed thresholds for colocalization with *GLT8D1* eQTL in both methods applied in our current study but failed the additional criterion introduced.

In conclusion, despite pitfalls and restricted search space, the insight gained from integrating CRF GWAS with cis e/sQTL from non-corneal tissues represented in GTEx v8 provided many functional pointers, for 26.5% of CRF signals, guiding prioritization for experimental validation. The subset of CRF associations highlighted is biased but therapeutically interesting as genetic effects detected in GTEx and expression of nominated genes in the adult cornea suggest entry points into homeostatic, rather than the less targetable developmental, processes.

4 Materials and methods

4.1 Colocalization of CRF GWAS signals with GTEx v8 cis e/s-QTLs

Readily available fine-mapping results for cis-e/sQTLs signals for all v8 GTEx tissues were downloaded from the public repository at https://zenodo.org/record/3517189#.Y-0UwcfP2Ul.

Fine-mapping of causal signals at CRF GWAS loci was identically performed, using DAP-G (Wen et al., 2016). LD information was calculated by plink v1.90b4 (Chang et al., 2015) option *--r* using the CRF GWAS sample of 72, 301 unrelated UK Biobank participants of White-British ancestry (Jiang et al., 2020). The 95% CS were constructed using the script get_credible_set.pl (https://github.com/xqwen/dap/tree/master/utility) following DAP-G run with parameter *-msize* set to 5. Colocalization of causal signals was performed using fastENLOC v2.0 (Wen et al., 2017) with default parameters, which returns both a single variant colocalization probability (SCP) and a regional colocalization probability. The required annotation files (VCF format) for GTEx v8 e/sQTL DAP-G results were prepared using an in-house python script (https://github.com/xinyixinyijiang/CRF_GTExv8_KC) combining information from available {tissue}.variants_pip.txt.gz and {tissue}.clusters.txt.gz files (https://zenodo.org/record/3517189#.Y-0UwcfP2Ul). CRF GWAS variants' IDs were formatted to match the GTEx v8 variant ID (format: chromosome_position_ref_alt_build) in build GRCh38, using pyliftover v0.4 (https://github.com/konstantint/pyliftover), lifting coordinates from the genome build GRCh37 to GRCh38. We used GTEx_Analysis_v8_sQTL_groups.tar.gz from the GTEx data portal (https://gtexportal.org/home/datasets) for mapping the sQTL introns to the corresponding genes. The signal colocalization posterior probability (CLPP) (Hormozdiari et al., 2016) was calculated using the DAP-G fine-mapping results with the formula described in Gay et al. (2020):

$$\mathrm{CLPP} = 1 - \prod_{i=1}^{K} (1 - \mathrm{PIP}_{GWAS,i} \times \mathrm{PIP}_{QTL,i}),$$

where K is the number of common variants between GWAS and QTL overlapping CS, and PIP is the posterior inclusion probability of variants to each credible set of causal variants.

The thresholds for colocalization were set to 0.01 and 0.1 for CLPP and fastENLOC RCP, respectively, following Gay et al. (2020) and Barbeira et al. (2021), and we used the union of these methods to declare colocalization. Higher thresholds of 0.1 and 0.5, respectively, for CLPP and fastENLOC indicate strongly supported colocalizations. After visual inspections of the colocalizing signals using LocusCompare (Liu et al., 2019), the two quality criteria were added to filter out dubious colocalization results: i) GTEx cis-e/sQTLs with the false discovery rate (FDR) larger than 5% and ii) CRF-e/sQTLs paired signals not encompassing the important contributing variants to original signals in their intersect (those for which the sum of PIPs for overlapping variants was lower than 0.5 in either study).

4.2 Colocalization with keratoconus GWAS

With no standard or exact way to conduct statistical fine-mapping and colocalization, we deployed the most currently adopted algorithms and practices, all of which account for potential multiple independent GWAS signals within a single genomic region.

Three Bayesian fine-mapping methods, which differ in the priors used, and in the approach taken to compute posterior inclusion probabilities: DAP-G (Wen et al., 2016), SuSiE (Zou et al., 2022), and FINEMAP (Benner et al., 2016) were paired, respectively, with fastENLOC v2.0 (Wen et al., 2017), COLOC v5.1.0 (Wallace, 2021), and CLPP (Gay et al., 2020). The keratoconus GWAS summary statistics was downloaded from Supplementary Data 15 of Hardcastle et al. (2021). LD information was derived from the CRF GWAS sample. Of note, DAP-G and SuSiE do not always return a credible set of causal variants, while FINEMAP does.

For fastEnLOC, the CRF GWAS DAP-G fine-mapping results (Section 4.1) were used. The same DAP-G pipeline was used to generate keratoconus GWAS fine-mapping results, which were summarized into VCF format by the script summarize_dap2enloc.pl (https://github.com/xqwen/fastenloc/tree/master/src) and provided to fastENLOC using the -eqtl command. FastENLOC was executed with the default settings.

For SuSiE and FINEMAP fine-mapping, performed for both CRF and keratoconus GWAS, LD information was calculated using the LDSTORE v2.0 (Benner et al., 2017) with default parameters. The COLOC package was run with the functions *runsusie* (for fine-mapping) and *coloc.susie* (for colocalization) with all parameters set to default. For CLPP, we used the CRF fine-mapping results obtained with FINEMAP, previously published (Jiang et al., 2020). The keratoconus GWAS fine-mapping results for CLPP were generated using FINEMAP with option *–sss* and the variant priors extracted from PolyFun (approach 1 implemented in the function extract_snpvar.py), which uses the precomputed prior causal probabilities based on 15 UK Biobank traits meta-analysis (Weissbrod et al., 2020).

4.3 Nearest gene identification

The nearest gene of each CRF fine-mapped variant is identified using the function "closest-features" in the software BEDOPS v2.4.41 (Neph et al., 2012), with the argument "--closest --dist". The same gene annotation for GTEx v8, GENCODE v26, was downloaded from the GTEx data portal, transferred to bed file format (function gtf2bed), sorted (function sort-bed), and used for finding the nearest gene or protein-coding gene.

4.4 Human adult cornea cell type enrichment

The human adult cornea singe-cell expression matrix based on RNA-seq and metadata were downloaded from http://retinalstemcellresearch.co.uk/CorneaCellAtlas (i.e., with cell type annotations kept as per the authors' analysis (Collin et al., 2021)). These data were input into the R package expression weighted cell type enrichment (EWCE) v1.5.7 as a cell type data set (CTD) (Skene and Grant, 2016). When creating the CTD data, this software calculates for each gene a cell type specificity metric that represents the proportion of the average transcript level in cells of a particular cell type relative to the average across all cells. This measure is

thus independent of the expression level, and genes with low expression that might appear highly cell specific are removed (Skene and Grant, 2016). The EWCE function bootstrap_enrichment_test was used for calculating enrichment metrics, using 10,000 repetitions, and the options genelistSpecies and sctSpecies were set to "human". The "controlledCT" option in bootstrap_enrichment_test was used for conditional analysis. To generate reproducible results, the random seed for the bootstrap was set to 1.

Data availability statement

The data sets used in this study can be found in online repositories. The names of the repositories can be found in Material and Methods section and in CRF and Keratoconus GWAS publications (Jiang et al., 2020; Hardcastle et al., 2021). The codes used for this study can be found in the GitHub repository https://github.com/xinyixinyijiang/CRF_GTExv8_KC. The data sets generated are fully presented in Supplementary Material.

Author contributions

VV conceived the project and supervised analyses together with TB. XJ performed the analysis and wrote the first draft of the manuscript. All authors contributed to the article and approved the submitted version.

Funding

XJ was sponsored by the Centre for Genomic and Experimental Medicine, University of Edinburgh, and Institute for Molecular Medicine Finland, University of Helsinki, joint PhD program in Human Genomics. VV and TB were supported by an MRC University Unit Program grant (MC_UU_00007/10) (QTL in Health and Disease). VV was further supported by MRC University Unit transition program MC_UU_00035/15.

Acknowledgments

The authors thank Ayellet V. Segrè and Andrew Hamel affiliated with the Broad Institute of Harvard and MIT for helpful discussions regarding the colocalization analysis with GTEx v8 data. The authors would like to express their gratitude to Andrew Papanastasiou, cross-disciplinary fellow at the University of Edinburgh, and currently at the CRUK Beatson Institute, for answering their questions on the human adult cornea scRNAseq data analysis.

Conflict of interest

The authors declare that the research was conducted in the absence of any commercial or financial relationships that could be construed as a potential conflict of interest.

Publisher's note

Supplementary material

The Supplementary Material for this article can be found online at: https://www.frontiersin.org/articles/10.3389/fgene.2023.1171217/full#supplementary-material

References

Aguet, F., Brown, A. A., Castel, S. E., Davis, J. R., He, Y., Jo, B., et al. (2017). Genetic effects on gene expression across human tissues. *Nature* 550, 204–213. doi:10.1038/NATURE24277

Aguet, F., Barbeira, A. N., Bonazzola, R., Brown, A., Castel, S. E., Jo, B., et al. (2020). The GTEx Consortium atlas of genetic regulatory effects across human tissues. *Sci. (1979)* 369, 1318–1330. doi:10.1126/science.aaz1776

Al-Barghouthi, B. M., Rosenow, W. T., Du, K. P., Heo, J., Maynard, R., Mesner, L., et al. (2022). Transcriptome-wide association study and eQTL colocalization identify potentially causal genes responsible for human bone mineral density GWAS associations. *Elife* 11, e77285. doi:10.7554/ELIFE.77285

Albert, F. W., and Kruglyak, L. (2015). The role of regulatory variation in complex traits and disease. *Nat. Rev. Genet.* 16, 197–212. doi:10.1038/NRG3891

Balliu, B., Carcamo-Orive, I., Gloudemans, M. J., Nachun, D. C., Durrant, M. G., Gazal, S., et al. (2021). An integrated approach to identify environmental modulators of genetic risk factors for complex traits. *Am. J. Hum. Genet.* 108, 1866–1879. doi:10.1016/J.AJHG.2021.08.014

Barbeira, A. N., Bonazzola, R., Gamazon, E. R., Liang, Y., Park, Y. S., Kim-Hellmuth, S., et al. (2021). Exploiting the GTEx resources to decipher the mechanisms at GWAS loci. *Genome Biol.* 22, 49–24. doi:10.1186/s13059-020-02252-4

Benner, C., Spencer, C. C. A., Havulinna, A. S., Salomaa, V., Ripatti, S., and Pirinen, M. (2016). Finemap: Efficient variable selection using summary data from genome-wide association studies. *Bioinformatics* 32, 1493–1501. doi:10.1093/BIOINFORMATICS/BTW018

Benner, C., Havulinna, A. S., Järvelin, M. R., Salomaa, V., Ripatti, S., and Pirinen, M. (2017). Prospects of fine-mapping trait-associated genomic regions by using summary statistics from genome-wide association studies. *Am. J. Hum. Genet.* 101, 539–551. doi:10.1016/J.AJHG.2017.08.012

Brody, M. J., Vanhoutte, D., Schips, T. G., Boyer, J. G., Bakshi, C. v., Sargent, M. A., et al. (2018). Defective flux of thrombospondin-4 through the secretory pathway impairs cardiomyocyte membrane stability and causes cardiomyopathy. *Mol. Cell. Biol.* 38, e00114-18. doi:10.1128/MCB.00114-18

Callewaert, B., Malfait, F., Loeys, B., and de Paepe, A. (2008). Ehlers-Danlos syndromes and Marfan syndrome. *Best. Pract. Res. Clin. Rheumatol.* 22, 165–189. doi:10.1016/J.BERH.2007.12.005

Chang, C. C., Chow, C. C., Tellier, L. C. A. M., Vattikuti, S., Purcell, S. M., and Lee, J. J. (2015). Second-generation PLINK: Rising to the challenge of larger and richer datasets. *Gigascience* 4, 7. doi:10.1186/s13742-015-0047-8

Chen, W., Wu, Y., Zheng, Z., Qi, T., Visscher, P. M., Zhu, Z., et al. (2021). Improved analyses of GWAS summary statistics by reducing data heterogeneity and errors. *Nat. Commun.* 12, 7117. doi:10.1038/S41467-021-27438-7

Cheng, J., Nguyen, T. Y. D., Cygan, K. J., Çelik, M. H., Fairbrother, W. G., Avsec, Ž., et al. (2019). MMSplice: Modular modeling improves the predictions of genetic variant effects on splicing. *Genome Biol.* 20, 48–15. doi:10.1186/s13059-019-1653-z

Choi, S., Yoo, Y. M., Kim, B. Y., Kim, T., Cho, H., Ahn, S. Y., et al. (2010). Involvement of TGF-{beta} receptor- and integrin-mediated signaling pathways in the pathogenesis

of granular corneal dystrophy II. *Invest. Ophthalmol. Vis. Sci.* 51, 1832–1847. doi:10.1167/IOVS.09-4149

Choquet, H., Melles, R. B., Yin, J., Hoffmann, T. J., Thai, K. K., Kvale, M. N., et al. (2020). A multiethnic genome-wide analysis of 44,039 individuals identifies 41 new loci associated with central corneal thickness. *Commun. Biol.* 3, 301. doi:10.1038/S42003-020-1037-7

Collin, J., Queen, R., Zerti, D., Bojic, S., Dorgau, B., Moyse, N., et al. (2021). A single cell atlas of human cornea that defines its development, limbal progenitor cells and their interactions with the immune cells. *Ocul. Surf.* 21, 279–298. doi:10.1016/J.JTOS.2021.03.010

Connally, N., Nazeen, S., Lee, D., Shi, H., Stamatoyannopoulos, J., Chun, S., et al. (2022). The missing link between genetic association and regulatory function. *Elife* 11, e74970. doi:10.7554/ELIFE.74970

Cuellar-Partida, G., Springelkamp, H., Lucas, S. E. M., Yazar, S., Hewitt, A. W., Iglesias, A. I., et al. (2015). WNT10A exonic variant increases the risk of keratoconus by decreasing corneal thickness. *Hum. Mol. Genet.* 24, 5060–5068. doi:10.1093/HMG/DDV211

Davidson, A. E., Hayes, S., Hardcastle, A. J., and Tuft, S. J. (2014). The pathogenesis of keratoconus. *Eye (Lond)* 28, 189–195. doi:10.1038/EYE.2013.278

Dou, S., Wang, Q., Zhang, B., Wei, C., Wang, H., Liu, T., et al. (2022). Single-cell atlas of keratoconus corneas revealed aberrant transcriptional signatures and implicated mechanical stretch as a trigger for keratoconus pathogenesis. *Cell. Discov.* 8, 66. doi:10.1038/S41421-022-00397-Z

Estey, T., Piatigorsky, J., Lassen, N., and Vasiliou, V. (2007). ALDH3A1: A corneal crystallin with diverse functions. *Exp. Eye Res.* 84, 3–12. doi:10.1016/J.EXER.2006.04.010

Frantz, C., Stewart, K. M., and Weaver, V. M. (2010). The extracellular matrix at a glance. *J. Cell. Sci.* 123, 4195–4200. doi:10.1242/JCS.023820

Fucci, C., Resnati, M., Riva, E., Perini, T., Ruggieri, E., Orfanelli, U., et al. (2020). The interaction of the tumor suppressor FAM46C with p62 and FNDC3 proteins integrates protein and secretory homeostasis. *Cell. Rep.* 32, 108162. doi:10.1016/J.CELREP.2020.108162

Gamazon, E. R., Wheeler, H. E., Shah, K. P., Mozaffari, S. V., Aquino-Michaels, K., Carroll, R. J., et al. (2015). A gene-based association method for mapping traits using reference transcriptome data. *Nat. Genet.* 47, 1091–1098. doi:10.1038/NG.3367

Garrido-Martín, D., Borsari, B., Calvo, M., Reverter, F., and Guigó, R. (2021). Identification and analysis of splicing quantitative trait loci across multiple tissues in the human genome. *Nat. Commun.* 12 (1), 727. doi:10.1038/s41467-020-20578-2

Gay, N. R., Gloudemans, M., Antonio, M. L., Abell, N. S., Balliu, B., Park, Y., et al. (2020). Impact of admixture and ancestry on eQTL analysis and GWAS colocalization in GTEx. *Genome Biol.* 21 (1), 233. doi:10.1186/s13059-020-02113-0

Hardcastle, A. J., Liskova, P., Bykhovskaya, Y., McComish, B. J., Davidson, A. E., Inglehearn, C. F., et al. (2021). A multi-ethnic genome-wide association study implicates collagen matrix integrity and cell differentiation pathways in keratoconus. *Commun. Biol.* 4 (1), 266. doi:10.1038/s42003-021-01784-0

He, W., Han, X., Ong, J. S., Hewitt, A. W., MacKey, D. A., Gharahkhani, P., et al. (2022). Association of novel loci with keratoconus susceptibility in a multitrait genome-wide association study of the UK Biobank database and Canadian longitudinal study on aging. *JAMA Ophthalmol.* 140, 568–576. doi:10.1001/JAMAOPHTHALMOL.2022.0891

Hogan, A., Yakubchyk, Y., Chabot, J., Obagi, C., Daher, E., Maekawa, K., et al. (2004). The phosphoinositol 3,4-bisphosphate-binding protein TAPP1 interacts with syntrophins and regulates actin cytoskeletal organization. *J. Biol. Chem.* 279, 53717–53724. doi:10.1074/JBC.M410654200

Hormozdiari, F., van de Bunt, M., Segrè, A. v., Li, X., Joo, J. W. J., Bilow, M., et al. (2016). Colocalization of GWAS and eQTL signals detects target genes. *Am. J. Hum. Genet.* 99, 1245–1260. doi:10.1016/J.AJHG.2016.10.003

Hukku, A., Pividori, M., Luca, F., Pique-Regi, R., Im, H. K., and Wen, X. (2021). Probabilistic colocalization of genetic variants from complex and molecular traits: Promise and limitations. *Am. J. Hum. Genet.* 108, 25–35. doi:10.1016/J.AJHG.2020.11.012

Iglesias, A. I., Mishra, A., Vitart, V., Bykhovskaya, Y., Höhn, R., Springelkamp, H., et al. (2018). Cross-ancestry genome-wide association analysis of corneal thickness strengthens link between complex and Mendelian eye diseases. *Nat. Commun.* 9 (1), 1864. doi:10.1038/s41467-018-03646-6

Ji, Z., He, L., Rotem, A., Janzer, A., Cheng, C. S., Regev, A., et al. (2018). Genome-scale identification of transcription factors that mediate an inflammatory network during breast cellular transformation. *Nat. Commun.* 9, 2068. doi:10.1038/S41467-018-04406-2

Jiang, X., Dellepiane, N., Pairo-Castineira, E., Boutin, T., Kumar, Y., Bickmore, W. A., et al. (2020). Fine-mapping and cell-specific enrichment at corneal resistance factor loci prioritize candidate causal regulatory variants. *Commun. Biol.* 3 (1), 762. doi:10.1038/s42003-020-01497-w

Kimber, W. A., Deak, M., Prescott, A. R., and Alessi, D. R. (2003). Interaction of the protein tyrosine phosphatase PTPL1 with the PtdIns(3,4)P2-binding adaptor protein TAPP1. *Biochem. J.* 376, 525–535. doi:10.1042/BJ20031154

Kircher, M., Witten, D. M., Jain, P., O'roak, B. J., Cooper, G. M., and Shendure, J. (2014). A general framework for estimating the relative pathogenicity of human genetic variants. *Nat. Genet.* 46, 310–315. doi:10.1038/NG.2892

Leiphart, R. J., Pham, H., Harvey, T., Komori, T., Kilts, T. M., Shetye, S. S., et al. (2021). Coordinate roles for collagen VI and biglycan in regulating tendon collagen fibril structure and function. *Matrix Biol. Plus* 13, 100099. doi:10.1016/J.MBPLUS.2021.100099

Liedtke, D., Orth, M., Meissler, M., Geuer, S., Knaup, S., Köblitz, I., et al. (2019). ECM alterations in Fndc3a (Fibronectin Domain Containing Protein 3A) deficient zebrafish cause temporal fin development and regeneration defects. *Sci. Rep.* 9, 13383. doi:10.1038/s41598-019-50055-w

Liu, N., Schoch, K., Luo, X., Pena, L. D. M., Bhavana, V. H., Kukolich, M. K., et al. (2018). Functional variants in TBX2 are associated with a syndromic cardiovascular and skeletal developmental disorder. *Hum. Mol. Genet.* 27, 2454–2465. doi:10.1093/HMG/DDY146

Liu, B., Gloudemans, M. J., Rao, A. S., Ingelsson, E., and Montgomery, S. B. (2019). Abundant associations with gene expression complicate GWAS follow-up. *Nat. Genet.* 51, 768–769. doi:10.1038/s41588-019-0404-0

Lu, Y., Vitart, V., Burdon, K. P., Khor, C. C., Bykhovskaya, Y., Mirshahi, A., et al. (2013). Genome-wide association analyses identify multiple loci associated with central corneal thickness and keratoconus. *Nat. Genet.* 45, 155–163. doi:10.1038/NG.2506

Lu, C. L., Ortmeier, S., Brudvig, J., Moretti, T., Cain, J., Boyadjiev, S. A., et al. (2022). Collagen has a unique SEC24 preference for efficient export from the endoplasmic reticulum. *Traffic* 23, 81–93. doi:10.1111/TRA.12826

McLaren, W., Gil, L., Hunt, S. E., Riat, H. S., Ritchie, G. R. S., Thormann, A., et al. (2016). The Ensembl variant effect predictor. *Genome Biol.* 17 (1), 122. doi:10.1186/S13059-016-0974-4

Meek, K. M., Tuft, S. J., Huang, Y., Gill, P. S., Hayes, S., Newton, R. H., et al. (2005). Changes in collagen orientation and distribution in keratoconus corneas. *Invest. Ophthalmol. Vis. Sci.* 46, 1948–1956. doi:10.1167/IOVS.04-1253

Meuleman, W., Muratov, A., Rynes, E., Halow, J., Lee, K., Bates, D., et al. (2020). Index and biological spectrum of human DNase I hypersensitive sites. *Nature* 584, 244–251. doi:10.1038/S41586-020-2559-3

Mostafavi, H., Spence, J. P., Naqvi, S., and Pritchard, J. K. (2022). Limited overlap of eQTLs and GWAS hits due to systematic differences in discovery. *bioRxiv*, 491045. doi:10.1101/2022.05.07.491045

Nasser, J., Bergman, D. T., Fulco, C. P., Guckelberger, P., Doughty, B. R., Patwardhan, T. A., et al. (2021). Genome-wide enhancer maps link risk variants to disease genes. *Nature* 593, 238–243. doi:10.1038/s41586-021-03446-x

Neavin, D., Nguyen, Q., Daniszewski, M. S., Liang, H. H., Chiu, H. S., Wee, Y. K., et al. (2021). Single cell eQTL analysis identifies cell type-specific genetic control of gene expression in fibroblasts and reprogrammed induced pluripotent stem cells. *Genome Biol.* 22, 76. doi:10.1186/S13059-021-02293-3

Neph, S., Kuehn, M. S., Reynolds, A. P., Haugen, E., Thurman, R. E., Johnson, A. K., et al. (2012). Bedops: High-performance genomic feature operations. *Bioinformatics* 28, 1919–1920. doi:10.1093/BIOINFORMATICS/BTS277

Piipponen, M., Riihilä, P., Knuutila, J. S., Kallajoki, M., Kähäri, V. M., and Nissinen, L. (2022). Super enhancer-regulated LINC00094 (SERLOC) upregulates the expression of MMP-1 and MMP-13 and promotes invasion of cutaneous squamous cell carcinoma. *Cancers (Basel)* 14, 3980. doi:10.3390/CANCERS14163980

Rafii, M. S., Hagiwara, H., Mercado, M. L., Seo, N. S., Xu, T., Dugan, T., et al. (2006). Biglycan binds to alpha- and gamma-sarcoglycan and regulates their expression during development. *J. Cell. Physiol.* 209, 439–447. doi:10.1002/JCP.20740

Shen, Y., Ning, J., Zhao, L., Liu, W., Wang, T., Yu, J., et al. (2023). Matrix remodeling associated 7 proteins promote cutaneous wound healing through vimentin in coordinating fibroblast functions. *Inflamm. Regen.* 43, 5. doi:10.1186/S41232-023-00256-8

Simcoe, M. J., Khawaja, A. P., Hysi, P. G., and Hammond, C. J.UK Biobank Eye and Vision Consortiu; m (2020). Genome-wide association study of corneal biomechanical properties identifies over 200 loci providing insight into the genetic etiology of ocular diseases. *Hum. Mol. Genet.* 29, 3154–3164. doi:10.1093/HMG/DDAA155

Skene, N. G., and Grant, S. G. N. (2016). Identification of vulnerable cell types in major brain disorders using single cell transcriptomes and expression weighted cell type enrichment. *Front. Neurosci.* 10, 16. doi:10.3389/fnins.2016.00016

Subramanian, A., and Schilling, T. F. (2014). Thrombospondin-4 controls matrix assembly during development and repair of myotendinous junctions. *Elife* 3, e02372. doi:10.7554/ELIFE.02372

van der Wijst, M. G. P., de Vries, D. H., Groot, H. E., Trynka, G., Hon, C. C., Bonder, M. J., et al. (2020). The single-cell eQTLGen consortium. *Elife* 9, e52155. doi:10.7554/ELIFE.52155

van Hout, C. v., Tachmazidou, I., Backman, J. D., Hoffman, J. D., Liu, D., Pandey, A. K., et al. (2020). Exome sequencing and characterization of 49,960 individuals in the UK Biobank. *Nature* 586, 749–756. doi:10.1038/S41586-020-2853-0

Voermans, N. C., Bönnemann, C. G., Huijing, P. A., Hamel, B. C., van Kuppevelt, T. H., de Haan, A., et al. (2008). Clinical and molecular overlap between myopathies and inherited connective tissue diseases. *Neuromuscul. Disord.* 18, 843–856. doi:10.1016/J.NMD.2008.05.017

Wainberg, M., Sinnott-Armstrong, N., Mancuso, N., Barbeira, A. N., Knowles, D. A., Golan, D., et al. (2019). Opportunities and challenges for transcriptome-wide association studies. *Nat. Genet.* 51, 592–599. doi:10.1038/S41588-019-0385-Z

Wallace, C. (2021). A more accurate method for colocalisation analysis allowing for multiple causal variants. *PLoS Genet.* 17, e1009440. doi:10.1371/JOURNAL.PGEN.1009440

Wang, Z., and Burge, C. B. (2008). Splicing regulation: From a parts list of regulatory elements to an integrated splicing code. *RNA* 14, 802–813. doi:10.1261/RNA.876308

Wang, H., Liu, Y., Liang, X., Yang, G., Liu, Y., Li, F., et al. (2020). Effects of Secreted frizzled-related protein 1 on inhibiting cardiac remodeling. *Eur. Rev. Med. Pharmacol. Sci.* 24, 6270–6278. doi:10.26355/EURREV_202006_21525

Weissbrod, O., Hormozdiari, F., Benner, C., Cui, R., Ulirsch, J., Gazal, S., et al. (2020). Functionally informed fine-mapping and polygenic localization of complex trait heritability. *Nat. Genet.* 52, 1355–1363. doi:10.1038/s41588-020-00735-5

Wen, X., Lee, Y., Luca, F., and Pique-Regi, R. (2016). Efficient integrative multi-SNP association analysis via deterministic approximation of posteriors. *Am. J. Hum. Genet.* 98, 1114–1129. doi:10.1016/j.ajhg.2016.03.029

Wen, X., Pique-Regi, R., and Luca, F. (2017). Integrating molecular QTL data into genome-wide genetic association analysis: Probabilistic assessment of enrichment and colocalization. *PLoS Genet.* 13, e1006646. doi:10.1371/JOURNAL.PGEN.1006646

Wiberg, C., Heinegård, D., Wenglén, C., Timpl, R., and Mörgelin, M. (2002). Biglycan organizes collagen VI into hexagonal-like networks resembling tissue structures. *J. Biol. Chem.* 277, 49120–49126. doi:10.1074/JBC.M206891200

Yam, G. H. F., Fuest, M., Zhou, L., Liu, Y. C., Deng, L., Chan, A. S. Y., et al. (2019). Differential epithelial and stromal protein profiles in cone and non-cone regions of keratoconus corneas. *Sci. Rep.* 9, 2965. doi:10.1038/S41598-019-39182-6

Yang, S., Zhang, J., Tan, Y., and Wang, Y. (2022). Unraveling the mechanobiology of cornea: From bench side to the clinic. *Front. Bioeng. Biotechnol.* 10, 953590. doi:10.3389/FBIOE.2022.953590

Zou, Y., Carbonetto, P., Wang, G., and Stephens, M. (2022). Fine-mapping from summary data with the "sum of single effects" model. *PLoS Genet.* 18, e1010299. doi:10.1371/JOURNAL.PGEN.1010299

Frontiers in Genetics

Highlights genetic and genomic inquiry relating to all domains of life

The most cited genetics and heredity journal, which advances our understanding of genes from humans to plants and other model organisms. It highlights developments in the function and variability of the genome, and the use of genomic tools.

Discover the latest Research Topics

See more →

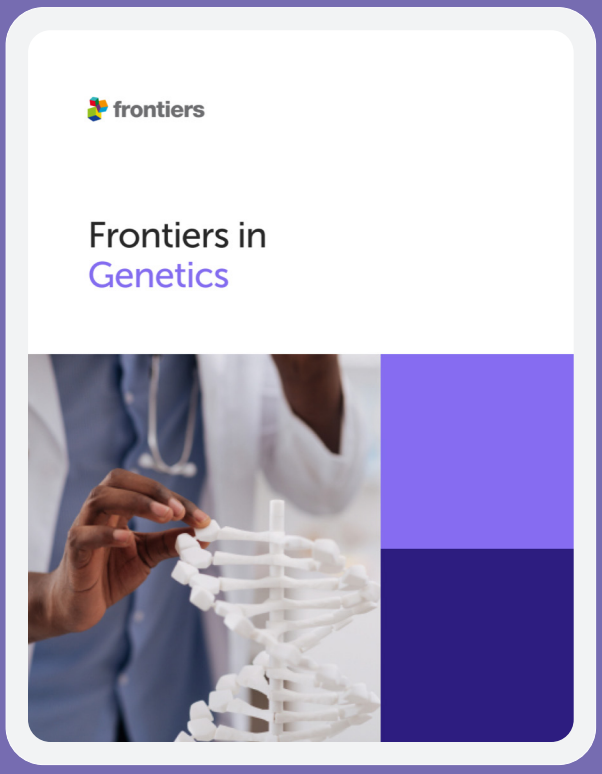

Frontiers

Avenue du Tribunal-Fédéral 34
1005 Lausanne, Switzerland
frontiersin.org

Contact us

+41 (0)21 510 17 00
frontiersin.org/about/contact